

Synthesis and Characterization of Ru(II) Complexes as Potential Catalysts in Olefin Hydroarylation

Evan Elizabeth Joslin
Atlanta, GA

B.A. Chemistry, Agnes Scott College, 2008

A Dissertation presented to the Graduate Faculty
of the University of Virginia in Candidacy for the Degree of
Doctor of Philosophy

Department of Chemistry

University of Virginia
July 2013

ABSTRACT

JOSLIN, EVAN E. Synthesis and Characterization of Ru(II) Complexes as Potential Catalysts in Olefin Hydroarylation. (Under the direction of Professor T. Brent Gunnoe).

The production of alkyl arenes from benzene and simple olefins is a continually growing market. However, current acid base technologies (i.e., Friedel-Crafts & Zeolites) have significant drawbacks. For example, Friedel-Crafts alkylation of arenes exhibits extensive polyalkylation, and thus requires an additional high temperature transalkylation process to increase the selectivity for monoalkylated products. Furthermore, Friedel Crafts is selective for the Markovnikov addition products when α -olefins are employed. Additionally, the ability to recycle the catalyst is impossible due to degradation during product isolation. Our strategy is to use transition metal catalysts for olefin hydroarylation that proceeds via an alternative mechanism which combines both olefin insertion and C–H activation which could potentially overcome these challenges.

Extension to previous studies conducted by our group on a series of complexes with the motif TpRu(L)Ph(NCMe) [Tp = hydridotris(pyrazolyl)borate, L= neutral two electron donor] were investigated. These studies demonstrated that an electron poor metal center was needed to strike promote olefin insertion over olefin C–H activation. Therefore, the electron donating properties of $\text{P}(\overline{\text{OCH}_2})_2(\text{OCCH}_3)$ where explored using cyclic voltammetry of a variety of Ru(II) complexes contain a wide range of phosphites and phosphines. It was determined that the metal center is less electron rich with $\text{P}(\overline{\text{OCH}_2})_2(\text{OCCH}_3)$ than L = PMe_3 , $\text{P}(\text{OCH}_2)_3\text{CEt}$, PPh_3 , and P(OMe)_3 ; however, the metal center is still more electron rich than when L = CO. The Ru(II) complex

$\text{TpRu}[\text{P}(\text{OCH}_2)_2(\text{OCCH}_3)](\text{NCMe})\text{Ph}$ has been synthesized and isolated. This complex was shown to be both capable of activating C–H bonds and an active catalyst for ethylene hydrophenylation.

Additionally, rather than varying the electron density of the metal center via the neutral two electron ligand one could alter the electron density by replacing the anionic Tp ligand with neutral analogues, such as tri(pyrazolyl)alkanes. Complexes with tris(pyrazolyl)alkanes were synthesized, characterized and tested for olefin hydrophenylation the results of these experiments will be discussed herein.

ACKNOWLEDGMENTS

I would first like to thank all my professors from the Agnes Scott Chemistry Department who helped me learn the fundamentals of chemistry and show me how much I enjoyed the subject and guided me to pursue it. In particular, Dr. Venable who gave me the opportunity to do research in his inorganic lab and helped me realize that I would rather go to graduate school rather than medical school. I would also like to thank Dr. Venable for all the encouragement during the last five years when I started to wonder if I would be able to complete this long road.

Thank you to all the staff of the Chemistry Department at UVA for making my time here have more laughs and be a lot less stressful. In particular thanks to Danny and the stockroom guys for helping me with the groups purchase and for all the sports talk. Thanks to Jeff Ellena for helping me all the times that I “broke” the NMR or need help running a new experiment. Thanks to Dr. Tom Cundari and Claire at the University of North Texas for all the calculations to help support my experimental data. Additionally, thank you to Dr. Sabat for looking at all my lousy crystals and being willing to try to solve them even when there was thought to be no hope. Finally, thank you to Dr. Bill Myers for all the discussions and mass spect. data collected.

I would also like to thank my committee members, Dr. Dean Harman, Dr. Robert Davis, and Dr. James Marshall. Thank you for taking the time out of your busy schedules to read my dissertation, annual reports, and to answer my questions. Additionally, Dean thank you for all your helpful suggestions in both research and teaching and allowing me to shadow you while you taught.

Thanks to all my Agnes Scott friends (Jaxen, Aly, Diana, Diane, and Dana) and to all my Virginia friends (there are just too many to name, I am bound to forget one) for hanging in with me these last five years even in times when it seemed like I had fallen off the face of the earth. In particular, thank you to Scott Donald for all the conversations, pep me ups, laughs and tennis games. I hope you are planning to have guest in California because I am coming to VISIT! Additionally, thanks to all my teammates during intramurals, kickball, Saturday basketball or any other activity I am missing. Without these breaks from chemistry I wouldn't have been able to make it through!

To my fellow Gunnoers, thank you for all the memories. Samantha, thank you for always being there and listening to all my crazy stories no matter how busy you are and always making me smile with your squeal. I have enjoyed all the football games that we have attended (maybe one day Virginia will win more). Brad, from our times in Brent office (because of course you lost rock, paper, scissors to Joanna!) to both of us finishing up it has been a great rollercoaster. Even though there have been times that I find you more annoying than some of my own sibling (e.g., candidacy exam time) you can always make me laugh and have answered all my questions and I am extremely thankful. Joanna, thank you for all the girl power talks that we had my first four years and helping to encourage me to continue on. To the current members of the Gunnoe group: JJ, Steve, Kathleen, Mike, Tristan, Ben, Shaun, Zuming, George, Ted, Bridget, Anna, Tomas, Nate, Michael thanks for all the memories and of course the most important thing make sure to keep the Gunnoe group superior to the Harman group! To past members: Brandon, Tamara, Jeremy, Mark, Sam, Zorida, Max and Chong thanks for those enjoyable

moments in lab and certain ones in particular thanks for helping me learn how to be a scientist and how not to blow myself up in lab, I couldn't have done it without all your help.

Coach Brent thanks for all the support during these last five years. Thank you for always pushing me and helping me understand that I can do more than I think. Thank you for your patience as a teacher. Your optimism, enthusiasm, and passion for science helped me in the times when I thought that my chemistry would never work. Thank you for letting me coach basketball with you the past two seasons. It has been so much fun to see Leah and the other girls start to understand basketball and improve. I have greatly enjoyed all of our talks on how to teach 3rd/4th girls basketball along with all our times talking about running. I know you can make that 6-minute mile you just have to run it on an outside track rather than an indoor one—less turning is the key! Thanks for everything and I could not be happy for picking you to be my advisor in graduate school.

A huge thanks to Shawn Fahl and his family for all their love and support. Shawn, thank you for all the times of talking me down when I thought things could not get worse and for encouraging me to continue. Thank you for putting up with all my quarks no matter how crazy they might be. Thanks for the smiles, laughs and terrific memories so far, from me throwing the EMPTY beer can at you, to the Huskey Research Exhibition, all the sporting events to Paris I could not have found someone more supportive and who I enjoy spending time with anywhere.

Finally and the most important thank you to my family for always believing in me and encouraging me that I can do most anything I put my mind to. Mom and Dad, you are

the most terrific parents that any one could ask for, I could not have been luckier. Thank you for always believing in me and encouraging me to continue. Thank you for all the phone calls and visits to Charlottesville when I needed a distraction. Love you more!

TABLE OF CONTENTS

LIST OF SCHEMES.....	IX
LIST OF FIGURES.....	XII
LIST OF TABLES.....	XVII

1. Introduction	1
1.1. Current Methods for Industrial Synthesis of Alkyl Arenes.....	2
1.1.1. Friedel-Crafts Catalysts	2
1.1.2. Zeolite Catalysts	5
1.2. Transition Metal Catalyzed C–C Bond Forming Reactions.....	9
1.3. Transition Metal Mediated C–H Activation for the Synthesis of Alkyl Arenes	12
1.4. Examples of Transition Metal Catalysts for Olefin Hydroarylation	15
1.4.1. Transition Metal C–H Activation by an Acid Catalyzed Pathway	15
1.4.2. Non-Acid Catalyzed Transition Metal Promoted C–H Activation of Unactivated Olefins.....	16
1.5. Summary and Thesis Aims	34
1.6. References.....	36
 2. Structural and Electronic Properties of Ru(II) Complexes Containing	 41
2.1. Introduction.....	41
2.2. Results and Discussion.....	44
2.2.1. Synthesis of $\text{P}(\text{OCH}_2)_2(\text{OCCH}_3)$	44
2.2.2. Synthesis and Characterization of $\text{TpRu}(\text{L})(\text{PPh}_3)\text{Cl}$ Complexes	45
2.2.3. Synthesis and Characterization of $(\eta^6\text{-C}_6\text{H}_6)\text{Ru}(\text{L})\text{Cl}_2$ Complexes.....	52
2.2.4. Synthesis and Characterization of $(\eta^6\text{-}p\text{-cymene})\text{Ru}(\text{L})\text{Cl}_2$ Complexes.	59
2.2.5. Calculations: Bicyclic Phosphite π -Acidity.....	68
2.3. Conclusions.....	71
2.4. Experimental Section.....	72
2.5. References.....	84
 3. Aromatic C–H Activation and Catalytic Hydroarylation of Ethylene Using $\text{TpRu}[\text{P}(\text{OCH}_2)_2(\text{OCCH}_3)](\text{NCMe})\text{Ph}$	 89
3.1. Introduction.....	89
3.2. Results and Discussion.....	91
3.2.1. Synthesis of $\text{TpRu}[\text{P}(\text{OCH}_2)_2(\text{OCCH}_3)](\text{NCMe})\text{Ph}$	91
3.2.2. Stoichiometric Benzene Activation	99
3.2.3. Catalytic Hydrophenylation of Ethylene by $\text{TpRu}[\text{P}(\text{OCH}_2)_2(\text{OCCH}_3)](\text{NCMe})\text{Ph}$ (4)	103

3.2.4. Catalytic Hydroarylation by $\text{TpRu}[\text{P}(\text{OCH}_2)_2(\text{OCCH}_3)](\text{NCMe})\text{Ph}$ (4) using Ethylbenzene and Ethylene.....	109
3.2.5. Attempted Hydrophenylation of Monosubstituted Olefins.....	110
3.2.6. DFT Calculations of Ethylene Hydrophenylation by $\text{TpRu}[\text{P}(\text{OCH}_2)_2(\text{OCCH}_3)](\text{NCMe})\text{Ph}$	110
3.2.7. Comparison of $\text{TpRu}(\text{L})(\text{NCMe})\text{Ph}$ Catalysts.....	113
3.3. Summary and Conclusions	118
3.4. Experimental	119
3.5. References.....	128
 4. Catalytic Decomposition Pathway for $\text{TpRu}(\text{CO})(\text{NCMe})\text{Ph}$	130
4.1. Introduction.....	130
4.2. Results and Discussion.....	132
4.2.1. Kinetics of Decomposition of $\text{TpRu}(\text{CO})(\text{NCMe})\text{Ph}$ in THF	132
4.2.2. Competing Decomposition Reactions: Dependence on Ethylene Concentration.....	133
4.2.3. Competing Deactivation Pathways: Dependence on Catalyst Loading.....	136
4.3. Conclusions.....	137
4.4. Experimental	138
4.5. References.....	141
 5. Synthesis and Characterization of (L)Ru(II) complexes (L = neutral 6-electron donor) for Olefin Hydroarylation.....	142
5.1. Introduction.....	142
5.2. Results and Discussion.....	145
5.2.1. Synthesis of $(\eta^6\text{-}p\text{-cymene})\text{Ru}(\text{L})\text{PhBr}$	145
5.2.2. Olefin hydrophenylation using $(\eta^6\text{-}p\text{-cymene})\text{Ru}(\text{L})\text{PhBr}$	152
5.2.3. Synthesis of $\{[\text{C}(\text{pz})_4]\text{Ru}[\text{P}(\text{OCH}_2)_3\text{Cet}]\text{Ph}(\text{NCMe})\}[\text{Y}]$ Complexes	153
5.2.4. Synthesis of $\{[\text{HC}(\text{pz}')_3]\text{Ru}[\text{P}(\text{OCH}_2)_3\text{Cet}]\text{Ph}(\text{NCMe})\}[\text{Y}]$ Complexes ($\text{pz}' = 3,5\text{-dimethyl-pyrazolyl}$ and $\text{Y} = \text{Br}, \text{BAR}'_4, \text{BF}_4$ or PF_6).....	157
5.2.5. Attempted Synthesis of $\{[\text{C}(\text{pz})_4]\text{Ru}[\text{P}(\text{OCH}_2)_3\text{Cet}]\text{Ph}(\text{NCMe})\}[\text{BAR}'_4]$	162
5.3. Conclusions.....	175
5.4. Experimental Section.....	176
5.5. Acknowledgements for High-Resolution Mass Spectroscopy Data.....	193
5.6. References.....	193
 6. Summary and Future Outlook	196
6.1. Olefin Hydroarylation with $\text{TpRu}(\text{L})\text{Ph}(\text{NCMe})$	196
6.2. Olefin Hydroarylation with Ru(II) Complex contain neutral 6-electron donor ligands.	199
6.3. Onward to Rhodium	200
6.4. References.....	202

LIST OF SCHEMES

CHAPTER 1

Scheme 1.1. Alkyl arenes produced from benzene and olefins.	2
Scheme 1.2. Overall reaction for Friedel-Crafts alkylation.	3
Scheme 1.3. Mechanism for Friedel-Crafts alkylation reaction.	3
Scheme 1.4. Mechanism for Friedel-Crafts alkylation reaction with α -olefins.	5
Scheme 1.5. Product shape selectivity of <i>p</i> -xylene is favorable due to pore size restrictions.	6
Scheme 1.6. General reaction scheme for cross-coupling reactions utilizing palladium.	10
Scheme 1.7. Proposed Heck cross coupling mechanism.	11
Scheme 1.8. General olefin hydroarylation reaction.	12
Scheme 1.9. Cycle for transition metal catalyzed olefin hydroarylation.	13
Scheme 1.10. Potential competing side reactions for olefin hydroarylation.	14
Scheme 1.11. Proposed catalytic cycle for addition of arenes to alkynes.	17
Scheme 1.12. Proposed mechanism for ethylene hydrophenylation with (dmpp)Pt.	19
Scheme 1.13. Proposed mechanism for the formation of diethylbenzene by $[(^t\text{bpy})\text{Pt}(\text{Ph})(\text{THF})][\text{BAR}'_4]$	21
Scheme 1.14. <i>Trans-Cis</i> isomerization of $(\text{acac})_2\text{Ir}(\text{Ph})\text{L}$ ($\text{L} = \text{H}_2\text{O}$ or $\text{C}_5\text{H}_5\text{N}$).	22
Scheme 1.15. Proposed Olefin Hydroarylation Catalytic Cycle by $\text{TpRu}(\text{L})(\text{NCMe})(\text{R})$	27
Scheme 1.16. Allyl formation through C–H olefin activation for $\text{TpRu}(\text{L})$ complexes.	29
Scheme 1.17. Competition between ethylene C–H activation and ethylene insertion.	29
Scheme 1.18. Regioselective of α -olefin hydroarylation.	30
Scheme 1.19. Olefin coordination inhibited due to steric bulk of $\text{P}(\text{pyr})_3$	31
Scheme 1.20. Intramolecular C–H activation of $\text{TpRu}[\text{P}(\text{pyr})_3](\text{NCMe})\text{Ph}$ to yield $\text{TpRu}\{\kappa^2\text{-P,C-P}(\text{pyr})_2(\text{NC}_4\text{H}_9)\text{NCMe}$	31
Scheme 1.21. Calculated Gibbs Free Energy (kcal/mol) for benzene C–H activation by $\text{TpRu}(\text{L})(\text{NCMe})\text{Ph}$ [$\text{L} = \text{CO}$, $\text{P}(\text{OCH}_2)_3\text{CEt}$, PMe_3 and $\text{P}(\text{pyr})_3$].	34

CHAPTER 2

Scheme 2.1. Comparison of acyclic and bicyclic phosphites based on the hinge effect.	42
Scheme 2.2. Synthesis of $\text{P}(\text{OCH}_2)_2(\text{OCCH}_3)$ (1).	45
Scheme 2.3. Synthesis of $\text{TpRu}[\text{P}(\text{OCH}_2)_2(\text{OCCH}_3)](\text{PPh}_3)\text{Cl}$ (2).	46
Scheme 2.4. Synthesis of $(\eta^6\text{-C}_6\text{H}_6)\text{Ru}(\text{L})\text{Cl}_2$ ($\text{L} = \text{PMe}_3$, $\text{P}(\text{OCH}_2)_3\text{CEt}$ and $\text{P}(\text{OCH}_2)_2(\text{OCCH}_3)$).	53
Scheme 2.5. Synthesis of $(\eta^6\text{-p-cymene})\text{Ru}(\text{L})\text{Cl}_2$ ($\text{L} = \text{P}(\text{OCH}_2)_3\text{CEt}$, $\text{P}(\text{OCH}_2)_2(\text{OCCH}_3)$, $\text{P}(\text{OMe})_3$, and PPh_3).	59
Scheme 2.6. Proposed mechanism for exchange reaction of L with $\text{P}(\text{OMe})_3$ to form $(\eta^6\text{-p-cymene})\text{Ru}[\text{P}(\text{OMe})_3]\text{Cl}_2$ in CDCl_3 at 60°C	68

CHAPTER 3

Scheme 3.1. Ethylene C–H activation vs ethylene insertion in olefin hydroarylation cycle.	90
Scheme 3.2. Synthesis of $[(\eta^6\text{-}p\text{-cymene})\text{Ru}[\text{P}(\text{OCH}_2)_2(\text{OCCH}_3)]\text{Br}_2$ (1).	92
Scheme 3.3. Synthesis of $[(\eta^6\text{-}p\text{-cymene})\text{Ru}[\text{P}(\text{OCH}_2)_2(\text{OCCH}_3)]\text{PhBr}$.	94
Scheme 3.4. Synthesis of $\text{TpRu}[\text{P}(\text{OCH}_2)_2(\text{OCCH}_3)](\text{NCMe})\text{Ph}$ (4).	96
Scheme 3.5 Proposed mechanism for benzene C–H activation by $\text{TpRu}(\text{L})(\text{NCMe})\text{Ph}$.	100
Scheme 3.6. Stoichiometric C–D benzene of complex 4 .	101
Scheme 3.7. Proposed Catalytic Cycle for the Hydrophenylation of Ethylene using $\text{TpRu}(\text{L})(\text{NCMe})_3\text{Ph}$ [$\text{L} = \text{CO}$, $\text{P}(\text{OCH}_2)_3\text{CEt}$ or $\text{P}(\text{OCH}_2)_2(\text{OCCH}_3)$].	104
Scheme 3.8. $\text{TpRu}[\text{P}(\text{OCH}_2)_2(\text{OCCH}_3)](\eta^3\text{-C}_3\text{H}_4\text{Me})$ (5) and minor products caused by multiple ethylene insertions.	107
Scheme 3.9. Formation of 1,3- and 1,4-diethylbenzene.	110
Scheme 3.10. Calculated Gibbs free energies (kcal/mol) for hydrophenylation of ethylene by $\text{TpRu}[\text{P}(\text{OCH}_2)_2(\text{OCCH}_3)](\text{NCMe})\text{Ph}$.	111
Scheme 3.11. Calculated Gibbs free energies (kcal/mol) for ethylene hydrophenylation catalytic cycle by $\text{TpRu}(\text{L})(\text{NCMe})\text{Ph}$ [$\text{L} = \text{CO}$, PMe_3 , $\text{P}(\text{OCH}_2)_3\text{CEt}$, $\text{P}(\text{pyr})_3$ and $\text{P}(\text{OCH}_2)_2(\text{OCCH}_3)$].	115
Scheme 3.12. Calculated Gibbs Free Energies (kcal/mol) for benzene C–H activation and formation of ethylbenzene by $\text{TpRu}(\text{L})(\eta^2\text{-C}_2\text{H}_4)(\text{CH}_2\text{CH}_2\text{Ph})$.	117

CHAPTER 4

Scheme 4.1. Proposed catalytic cycle for olefin hydroarylation with $\text{TpRu}(\text{II})$ complexes.	134
Scheme 4.2. Competing deactivation pathways during catalysis for $\text{TpRu}(\text{CO})(\text{NCMe})\text{Ph}$.	138

CHAPTER 5

Scheme 5.1. Synthesis of $(\eta^6\text{-}p\text{-cymene})\text{Ru}(\text{L})\text{Br}_2$ [$\text{L} = \text{P}(\text{OCH}_2)_3\text{CEt}$ (1) or PMe_3 (3)].	146
Scheme 5.2. Synthesis of $(\eta^6\text{-}p\text{-cymene})\text{Ru}(\text{L})\text{PhBr}$ [$\text{L} = \text{P}(\text{OCH}_2)_3\text{CEt}$ (2) or PMe_3 (4)].	149
Scheme 5.3. Synthesis of $(\kappa^3\text{-}N, C^5, N)\text{C}(\text{pz})_4\text{Ru}[\text{P}(\text{OCH}_2)_3\text{CEt}](\text{NCMe})\text{Br}$ (6).	156
Scheme 5.4. C–H activation of 5-position of the Tp pyrazolyl ring in $\text{TpIr}(\text{PPh}_3)(\text{C}_2\text{H}_4)$.	157
Scheme 5.5. Synthesis of $\{[\text{HC}(\text{pz}')_3]\text{Ru}[\text{P}(\text{OCH}_2)_3\text{CEt}]\text{Ph}(\text{NCMe})\}[\text{Br}]$ (7).	158
Scheme 5.6. Synthesis of $\{[\text{HC}(\text{pz}')_3]\text{Ru}[\text{P}(\text{OCH}_2)_3\text{CEt}]\text{Ph}(\text{NCMe})\}[\text{BAR}'_4]$ (8).	161
Scheme 5.7. Synthesis of $[\text{C}(\text{pz})_4]\text{Ru}(\text{PPh}_3)\text{Cl}_2$ (9).	163
Scheme 5.8. Synthesis of $[\kappa^2\text{-C}(\text{pz})_4]\text{Ru}[\text{P}(\text{OCH}_2)_3\text{CEt}]\text{Cl}_2$ and $[\kappa^3\text{-C}(\text{pz})_4]\text{Ru}[\text{P}(\text{OCH}_2)_3\text{CEt}]\text{Cl}_2$ (10).	164

Scheme 5.9. Synthesis of $\{[C(pz)_4]Ru[P(OCH_2)_3CEt]Cl(NCMe)\}[Cl]$ (11).	166
Scheme 5.10. Synthesis of $\{[C(pz)_4]Ru[P(OCH_2)_3CEt]Cl(NCMe)\}[BAr'_4]$ (12).	167
Scheme 5.11. Synthesis of $\{[C(pz)_4]Ru[P(OCH_2)_3CEt](OTf)(NCMe)\}[BAr'_4]$ (13).	170
Scheme 5.12. Synthesis of $\{[C(pz)_4]Ru[P(OCH_2)_3CEt](Me)(NCMe)\}[BAr'_4]$ (14).	173
Scheme 5.13. Synthesis of $\{[(N,C^5,N)C(pz)_4]Ru[P(OCH_2)_3CEt[(NCMe)_2]\}[BAr'_4]$ (15).	174

LIST OF FIGURES

CHAPTER 1

Figure 1.1. Depiction of a ZSM-5 zeolite catalyst (A) Structure looking from the top at Zeolite channels (B) Looking side on at zeolite material- four pores are marked for orientation (a,b,c and d). Copyright 2009 Wiley. Used with permission from Macquarrie, D. J., Industrial Friedel-Crafts Chemistry, <i>Catalytic Asymmetric Friedel-Crafts Alkylations</i> , Wiley-VCH.....	7
Figure 1.2. Depiction of a Y zeolite. Copyright 2010 Wiley. Used with permission from Broach, R.W. Zeolite Types and Structures, <i>Zeolites in Industrial Separation and Catalysis</i> , Wiley-VCH.....	9
Figure 1.3. (dmpp)Pt catalyst precursors for olefin hydroarylation.....	18
Figure 1.4. [^t bpy]Pt(Ph)L][BAR' ₄] catalyst for olefin hydroarylation.....	20
Figure 1.5. bis-acac- <i>O,O</i> -Ir(III) (acac = acetylacetonato or 2,4-pentanedione) and bis-hfac- <i>O,O</i> -Rh(III) (hfac- <i>O,O</i> = b-diketonate κ^2 - <i>O,O</i> -1,1,1,5,5,5-hexafluoroacetylacetonate) complexes for olefin hydroarylation of benzene.....	22
Figure 1.6. Catalyst design motif for Ru(II) complexes for olefin hydroarylation.....	24
Figure 1.7. TpRu(L)Ph(NCMe) catalyst first examined for olefin hydroarylation.....	25
Figure 1.8. Electronics and cone angles for TpRu(L)(NCMe)Ph.....	25
Figure 1.9. C–H activation transition state, “oxidative hydrogen migration”.	28

CHAPTER 2

Figure 2.1. Tolman’s method for measuring cone angle for phosphines/phosphites	41
Figure 2.2. Anticipated impact of O–P–O bond angle of σ^* (P–O) orbital energy and, hence, $d\pi$ -to- σ^* back bonding.	43
Figure 2.3. Examples of bicyclic phosphites.....	44
Figure 2.4. ¹ H NMR spectrum of TpRu[P(OCH ₂) ₂ (OCCH ₃)](PPh ₃)Cl (2) in CDCl ₃	46
Figure 2.5. ¹³ C NMR spectrum of TpRu[P(OCH ₂) ₂ (OCCH ₃)](PPh ₃)Cl (2) in CDCl ₃	47
Figure 2.6. ORTEP of TpRu[P(OCH ₂) ₂ (OCCH ₃)](PPh ₃)Cl (2) (50% probability with hydrogen atoms omitted)	49
Figure 2.7. Calculation of cone angles using crystallographic data	50
Figure 2.8. ¹ H NMR spectrum of TpRu[P(OMe) ₃](PPh ₃)Cl (5) in CDCl ₃	51
Figure 2.9. ¹³ C NMR spectrum of TpRu[P(OMe) ₃](PPh ₃)Cl (5) in CDCl ₃	51
Figure 2.10. ¹ H NMR spectrum of (η^6 -C ₆ H ₆)Ru(PMe ₃)Cl ₂ (8) in CDCl ₃	53
Figure 2.11. ¹³ C NMR spectrum of (η^6 -C ₆ H ₆)Ru(PMe ₃)Cl ₂ (8) in CDCl ₃	53
Figure 2.12. ¹ H NMR spectrum of (η^6 -C ₆ H ₆)Ru[P(OCH ₂) ₃ CEt]Cl ₂ (9) in DMSO.	54
Figure 2.13. ¹³ C NMR spectrum of (η^6 -C ₆ H ₆)Ru[P(OCH ₂) ₃ CEt]Cl ₂ (9) in DMSO.	54
Figure 2.14. ¹ H NMR spectrum of (η^6 -C ₆ H ₆)Ru[P(OCH ₂) ₂ (OCCH ₃)]Cl ₂ (11) in CD ₂ Cl ₂	55
Figure 2.15. ¹³ C NMR spectrum of (η^6 -C ₆ H ₆)Ru[P(OCH ₂) ₂ (OCCH ₃)]Cl ₂ (11) in CD ₂ Cl ₂	55

Figure 2.16. ORTEP diagram of $(\eta^6\text{-C}_6\text{H}_6)\text{Ru}[\text{P}(\text{OCH}_2)_2(\text{OCCH}_3)]\text{Cl}_2$ (11) (50% probability with hydrogen atoms omitted).....	56
Figure 2.17. ^1H NMR spectrum of $(\eta^6\text{-}p\text{-cymene})\text{Ru}[\text{P}(\text{OCH}_2)_3\text{CEt}]\text{Cl}_2$ (12) in CDCl_3 . 60	
Figure 2.18. ^{13}C NMR spectrum of $(\eta^6\text{-}p\text{-cymene})\text{Ru}[\text{P}(\text{OCH}_2)_3\text{CEt}]\text{Cl}_2$ (12) in CDCl_3 . 60	
Figure 2.19. ^1H NMR spectrum of $(\eta^6\text{-}p\text{-cymene})\text{Ru}[\text{P}(\text{OCH}_2)_2(\text{OCCH}_3)]\text{Cl}_2$ (13) in CDCl_3	61
Figure 2.20. ^{13}C NMR spectrum of $(\eta^6\text{-}p\text{-cymene})\text{Ru}[\text{P}(\text{OCH}_2)_2(\text{OCCH}_3)]\text{Cl}_2$ (13) in CDCl_3	61
Figure 2.21. ORTEP of $(\eta^6\text{-}p\text{-cymene})\text{Ru}[\text{P}(\text{OCH}_2)_3\text{CEt}]\text{Cl}_2$ (12) (50% probability with hydrogen atoms omitted)	63
Figure 2.22. Representative kinetic plots for the exchange reaction of L in $(\eta^6\text{-}p\text{-cymene})\text{Ru}(\text{L})\text{Cl}_2$ [L = $\text{P}(\text{OCH}_2)_2(\text{OCCH}_3)$, $\text{P}(\text{OCH}_2)_3\text{CEt}$ or PPh_3] complexes with $\text{P}(\text{OMe})_3$ (40 equivalents relevant to concentration of Ru complex) in CDCl_3 at 60 °C.....	65
Figure 2.23. Plot of k_{obs} versus concentration of PPh_3 for the exchange of PPh_3 with $\text{P}(\text{OMe})_3$ upon reaction of $(\eta^6\text{-}p\text{-cymene})\text{Ru}(\text{PPh}_3)\text{Cl}_2$ (15) with excess $\text{P}(\text{OMe})_3$ in CDCl_3 at 60 °C.	67
Figure 2.24. Plot of k_{obs} versus concentration of $\text{P}(\text{OMe})_3$ for the exchange of PPh_3 with $\text{P}(\text{OMe})_3$ upon reaction of $(\eta^6\text{-}p\text{-cymene})\text{Ru}(\text{PPh}_3)\text{Cl}_2$ (15) with excess $\text{P}(\text{OMe})_3$ in CDCl_3 at 60 °C.	67
Figure 2.25. Rate law for exchange reaction of L in $(\eta^6\text{-}p\text{-cymene})\text{Ru}(\text{L})\text{Cl}_2$ [L = $\text{P}(\text{OCH}_2)_2(\text{OCCH}_3)$, $\text{P}(\text{OCH}_2)_3\text{CEt}$ or PPh_3] complexes with $\text{P}(\text{OMe})_3$ to form $(\eta^6\text{-}p\text{-cymene})\text{Ru}[\text{P}(\text{OMe})_3]\text{Cl}_2$ in CDCl_3 at 60 °C.....	68
Figure 2.26. Orientations of $\text{P}(\text{OMe})_3$ ligand defined by the torsion Au-P-O-Me (viewed along the Au-P bond) that were modeled using DFT calculations.	70

CHAPTER 3

Figure 3.1. ^1H NMR spectrum of $(\eta^6\text{-}p\text{-cymene})\text{Ru}[\text{P}(\text{OCH}_2)_2(\text{OCCH}_3)]\text{Br}_2$ (1) in CDCl_3	93
Figure 3.2. ^{13}C NMR spectrum of $(\eta^6\text{-}p\text{-cymene})\text{Ru}[\text{P}(\text{OCH}_2)_2(\text{OCCH}_3)]\text{Br}_2$ (1) in CDCl_3	93
Figure 3.3. ^1H NMR spectrum of $(\eta^6\text{-}p\text{-cymene})\text{Ru}[\text{P}(\text{OCH}_2)_2(\text{OCCH}_3)](\text{Ph})\text{Br}$ (2) in CDCl_3	94
Figure 3.4. ^{13}C NMR spectrum of $(\eta^6\text{-}p\text{-cymene})\text{Ru}[\text{P}(\text{OCH}_2)_2(\text{OCCH}_3)](\text{Ph})\text{Br}$ (2) in CDCl_3	95
Figure 3.5. ^1H NMR spectrum of $(\text{NCMe})_3\text{Ru}[\text{P}(\text{OCH}_2)_2(\text{OCCH}_3)]\text{PhBr}$ (3) in CD_3CN	96
Figure 3.6. ^1H NMR spectrum of $\text{TpRu}[\text{P}(\text{OCH}_2)_2(\text{OCCH}_3)](\text{NCMe})\text{Ph}$ (4) in C_6D_6	97

Figure 3.7. ^{13}C NMR spectrum of $\text{TpRu}[\text{P}(\text{OCH}_2)_2(\text{OCCH}_3)](\text{NCMe})\text{Ph}$ (4) in C_6D_6 ...	97
Figure 3.8. ORTEP of $\text{TpRu}[\text{P}(\text{OCH}_2)_2(\text{OCCH}_3)](\text{NCMe})\text{Ph}$ (4) (50% probability, hydrogen atoms omitted for clarity)	98
Figure 3.9. Representative plot of C–D activation of C_6D_6 by $\text{TpRu}[\text{P}(\text{OCH}_2)_2(\text{OCCH}_3)](\text{NCMe})\text{Ph}$ (4) in C_6D_6 at 60 °C monitored by ^1H NMR spectroscopy ($k_{\text{obs}} = 7.0(2) \times 10^{-6} \text{ s}^{-1}$, $R^2 = 0.99$). The plot shows relative amount of protio-phenyl ligand (integrated against an internal standard) of 4 as a function of time.	102
Figure 3.10. Linear fit for plot of k_{obs} ($\times 10^{-5}, \text{ s}^{-1}$) values vs. Ru(III/II) potentials (vs. NHE, V) for the C–D activation of C_6D_6 by $\text{TpRu}(\text{L})(\text{NCMe})\text{Ph}$ at 60 °C with 0.065 mmol of added NCMe ($R^2 = 0.92$, $m = -1.29 \text{ s}^{-1}\text{V}^{-1}$).	103
Figure 3.11. Comparison of catalytic hydrophenylation of ethylene by complex 4 (90 °C) at variable ethylene pressures.	105
Figure 3.12. Comparison of catalytic hydrophenylation of ethylene by complex 4 (15 psi & 90 °C) through 4 h with minimal decomposition of catalyst present ($R^2 = 0.99$ when trendline is forced through 0,0).	105
Figure 3.13. Comparison of catalytic hydrophenylation of ethylene by complex 4 at 15 psi of ethylene and variable temperature.	106
Figure 3.14. ^1H NMR spectrum of $\text{TpRu}[\text{P}(\text{OCH}_2)_2(\text{OCCH}_3)](\eta^3\text{-C}_3\text{H}_4\text{Me})$ (5) in C_6D_6	108
Figure 3.15. ^{13}C NMR spectrum of $\text{TpRu}[\text{P}(\text{OCH}_2)_2(\text{OCCH}_3)](\eta^3\text{-C}_3\text{H}_4\text{Me})$ (5) in C_6D_6	108
Figure 3.16. Low-Resolution Mass Spectrometry of $\text{TpRu}[\text{P}(\text{OCH}_2)_2(\text{OCCH}_3)](\eta^3\text{-C}_3\text{H}_4\text{Me})$ (5) in C_6D_6 from $m/z = 490$ to 600.	109
Figure 3.17. Transition state for benzene C–H activation (TS2, Scheme 3.10) by $\text{TpRu}(\text{L})(\text{NCMe})\text{Ph}$. See Table 3.3 for calculated distances.	112
Figure 3.18. Plot of TOF vs. Ru(III/II) potential for catalytic hydrophenylation of ethylene by $\text{TpRu}(\text{L})(\text{NCMe})\text{Ph}$ ($\text{L} = \text{P}(\text{OCH}_2)_3\text{CEt}$, $\text{P}(\text{OCH}_2)_2(\text{OCCH}_3)$ or CO) using 0.025 mol % of catalyst, 15 psi of ethylene at 90 °C. TOF calculated after 4 hours of reaction ($R^2 = 0.97$).	117

CHAPTER 4

Figure 4.1. First order plot of $\ln([\text{TpRu}(\text{CO})(\text{NCMe})\text{Ph}])$ vs time determined from ^1H NMR spectroscopy (using the internal standard HMDS) for the decomposition of $\text{TpRu}(\text{CO})(\text{NCMe})\text{Ph}$ in $\text{THF-}d_8$ at 75 °C.	133
Figure 4.2. Second order plot of the $[\text{TpRu}(\text{CO})(\text{NCMe})\text{Ph}]^{-1}$ vs time ($R^2 = 0.98$) determined from ^1H NMR spectroscopy (using the internal standard HMDS) for the decomposition of $\text{TpRu}(\text{CO})(\text{NCMe})\text{Ph}$ in $\text{THF-}d_8$ at 75 °C.	133
Figure 4.3. Comparison of catalytic hydrophenylation of ethylene at various pressures (1 atm, 25 and 50 psi) by $\text{TpRu}(\text{CO})(\text{NCMe})\text{Ph}$ at 0.01 mol% Ru and 90 °C.	135

Figure 4.4. Comparison of catalytic hydrophenylation of ethylene at various Ru mol % loadings (0.001 – 0.3 mol %) by $\text{TpRu}(\text{CO})\text{Ph}(\text{NCMe})$ at 1 atm and 90 °C.	137
--	-----

CHAPTER 5

Figure 5.1. Examples of some scorpionate ligands.....	142
Figure 5.2. Comparison of experimental Ru(III/II) (V vs NHE) potentials for $\text{TpRu}(\text{L})\text{Ph}(\text{NCMe})$ to predicted Ru(III/II) (V vs NHE) potentials for $\text{EpRu}(\text{L})\text{Ph}(\text{NCMe})$	144
Figure 5.3. ^1H NMR spectrum of $(\eta^6\text{-}p\text{-cymene})\text{Ru}[\text{P}(\text{OCH}_2)_3\text{CEt}]\text{Br}_2$ (1) in CDCl_3 ..	146
Figure 5.4. ^{13}C NMR spectrum of $(\eta^6\text{-}p\text{-cymene})\text{Ru}[\text{P}(\text{OCH}_2)_3\text{CEt}]\text{Br}_2$ (1) in CDCl_3 ..	147
Figure 5.5. ^1H NMR spectrum of $(\eta^6\text{-}p\text{-cymene})\text{Ru}(\text{PMe}_3)\text{Br}_2$ (3) in CDCl_3	147
Figure 5.6. ^{13}C NMR spectrum of $(\eta^6\text{-}p\text{-cymene})\text{Ru}(\text{PMe}_3)\text{Br}_2$ (3) in CDCl_3	148
Figure 5.7. ORTEP of $(\eta^6\text{-}p\text{-cymene})\text{Ru}[\text{P}(\text{OCH}_2)_3\text{CEt}]\text{PhBr}$ (2) (35% probability with hydrogen atoms omitted)	149
Figure 5.8. ^1H NMR spectrum of $(\eta^6\text{-}p\text{-cymene})\text{Ru}[\text{P}(\text{OCH}_2)_3\text{CEt}]\text{PhBr}$ (2) in CDCl_3	150
Figure 5.9. ^{13}C NMR spectrum of $(\eta^6\text{-}p\text{-cymene})\text{Ru}[\text{P}(\text{OCH}_2)_3\text{CEt}]\text{PhBr}$ (2) in CDCl_3	150
Figure 5.10. ORTEP of $(\eta^6\text{-}p\text{-cymene})\text{Ru}(\text{PMe}_3)\text{PhBr}$ (4) (35% probability with hydrogen atoms omitted)	151
Figure 5.11. ^1H NMR spectrum of $(\eta^6\text{-}p\text{-cymene})\text{Ru}(\text{PMe}_3)\text{PhBr}$ (4) in CDCl_3	151
Figure 5.12. ^{13}C NMR spectrum of $(\eta^6\text{-}p\text{-cymene})\text{Ru}(\text{PMe}_3)\text{PhBr}$ (4) in CDCl_3	152
Figure 5.13. ^1H NMR spectrum of $(\text{NCMe})_3\text{Ru}[\text{P}(\text{OCH}_2)_3\text{CEt}]\text{PhBr}$ (5) in CD_3CN	154
Figure 5.14. The reaction of $(\eta^6\text{-}p\text{-cymene})\text{Ru}[\text{P}(\text{OCH}_2)_3\text{CEt}]\text{PhBr}$ (2) and $\text{C}(\text{pz})_4$ in NCMe at 90 °C.....	155
Figure 5.15. ^1H NMR spectrum of $(\kappa^3\text{-}N, C^5, N)\text{C}(\text{pz})_4\text{Ru}[\text{P}(\text{OCH}_2)_3\text{CEt}](\text{NCMe})\text{Br}$ (6) in CD_2Cl_2	156
Figure 5.16. ^{13}C NMR spectrum of $(\kappa^3\text{-}N, C^5, N)\text{C}(\text{pz})_4\text{Ru}[\text{P}(\text{OCH}_2)_3\text{CEt}](\text{NCMe})\text{Br}$ (6) in CD_2Cl_2	157
Figure 5.17. ^1H NMR spectrum of $\{[\text{HC}(\text{pz}')_3]\text{Ru}[\text{P}(\text{OCH}_2)_3\text{CEt}]\text{Ph}(\text{NCMe})\}[\text{Br}]$ (7) in CD_2Cl_2	159
Figure 5.18. ^{13}C NMR spectrum for $\{[\text{HC}(\text{pz}')_3]\text{Ru}[\text{P}(\text{OCH}_2)_3\text{CEt}]\text{Ph}(\text{NCMe})\}[\text{Br}]$ (7) in CD_2Cl_2	159
Figure 5.19. ^1H NMR spectrum of $\{[\text{HC}(\text{pz}')_3]\text{Ru}[\text{P}(\text{OCH}_2)_3\text{CEt}]\text{Ph}(\text{NCMe})\}[\text{BAr}'_4]$ (8) in CD_2Cl_2	161
Figure 5.20. ^{13}C NMR spectrum of $\{[\text{HC}(\text{pz}')_3]\text{Ru}[\text{P}(\text{OCH}_2)_3\text{CEt}]\text{Ph}(\text{NCMe})\}[\text{BAr}'_4]$ (8) in CD_2Cl_2	162
Figure 5.21. ^1H NMR spectrum of $[\text{C}(\text{pz})_4]\text{Ru}(\text{PPh}_3)\text{Cl}_2$ (9) in CDCl_3	163
Figure 5.22. ^{13}C NMR spectrum of $[\text{C}(\text{pz})_4]\text{Ru}(\text{PPh}_3)\text{Cl}_2$ (9) in CDCl_3	163
Figure 5.23. ^1H NMR spectrum of $[\text{C}(\text{pz})_4]\text{Ru}[\text{P}(\text{OCH}_2)_3\text{CEt}]\text{Cl}_2$ (10) in CD_2Cl_2	165
Figure 5.24. ^{13}C NMR spectrum of $[\text{C}(\text{pz})_4]\text{Ru}[\text{P}(\text{OCH}_2)_3\text{CEt}]\text{Cl}_2$ (10) in CD_2Cl_2	165
Figure 5.25. ^1H NMR spectrum of $\{[\text{C}(\text{pz})_4]\text{Ru}[\text{P}(\text{OCH}_2)_3\text{CEt}]\text{Cl}(\text{NCMe})\}[\text{Cl}]$ (11) in CD_2Cl_2	166

Figure 5.26. ^{13}C NMR spectrum of $\{[\text{C}(\text{pz})_4]\text{Ru}[\text{P}(\text{OCH}_2)_3\text{CEt}]\text{Cl}(\text{NCMe})\}[\text{Cl}]$ (11) in CD_2Cl_2 .	167
Figure 5.27. ORTEP of $\{[\text{C}(\text{pz})_4]\text{Ru}[\text{P}(\text{OCH}_2)_3\text{CEt}]\text{Cl}(\text{NCMe})\}[\text{BAr}'_4]$ (12) (35% probability with hydrogen atoms and BAr'_4 omitted)	168
Figure 5.28. ^1H NMR spectrum of $\{[\text{C}(\text{pz})_4]\text{Ru}[\text{P}(\text{OCH}_2)_3\text{CEt}]\text{Cl}(\text{NCMe})\}[\text{BAr}'_4]$ (12) in CD_2Cl_2 .	169
Figure 5.29. ^{13}C NMR spectrum of $\{[\text{C}(\text{pz})_4]\text{Ru}[\text{P}(\text{OCH}_2)_3\text{CEt}]\text{Cl}(\text{NCMe})\}[\text{BAr}'_4]$ (12) in CD_2Cl_2 .	169
Figure 5.30. ^1H NMR spectrum of $\{[\text{C}(\text{pz})_4]\text{Ru}[\text{P}(\text{OCH}_2)_3\text{CEt}](\text{OTf})(\text{NCMe})\}[\text{BAr}'_4]$ (13) in CD_2Cl_2 .	171
Figure 5.31. ^{13}C NMR spectrum of $\{[\text{C}(\text{pz})_4]\text{Ru}[\text{P}(\text{OCH}_2)_3\text{CEt}](\text{OTf})(\text{NCMe})\}[\text{BAr}'_4]$ (13) in CD_2Cl_2 .	171
Figure 5.32. ^1H NMR spectrum of $\{[\text{C}(\text{pz})_4]\text{Ru}[\text{P}(\text{OCH}_2)_3\text{CEt}](\text{Me})(\text{NCMe})\}[\text{BAr}'_4]$ (14) in C_6D_6 .	173
Figure 5.33. ^1H NMR spectrum of $\{[(N, C^5, N)\text{C}(\text{pz})_4]\text{Ru}[\text{P}(\text{OCH}_2)_3\text{CEt}](\text{NCMe})_2\}[\text{BAr}'_4]$	174
Figure 5.34. ^{13}C NMR spectrum of $\{[(N, C^5, N)\text{C}(\text{pz})_4]\text{Ru}[\text{P}(\text{OCH}_2)_3\text{CEt}](\text{NCMe})_2\}[\text{BAr}'_4]$ (15) in C_6D_6 .	175

CHAPTER 6

Figure 6.1. MSM supported $\text{TpRu}(\text{CO})(\text{NCMe})\text{Ph}$.	197
Figure 6.2. Examples of tris(pyrazolyl)alkanes.	199
Figure 6.3. Calculated ΔG^\ddagger (kcal/mol) for benzene C–H activation via a two-step reaction for $\text{M} = \text{Rh}$ or Pt .	201
Figure 6.4. Potential $\text{Rh}(\text{I})$ catalyst for olefin hydroarylation.	201

LIST OF TABLES

CHAPTER 1

Table 1.1. Olefin hydroarylation with $\text{TpRu}(\text{CO})(\text{NCMe})\text{Ph}$ as catalyst (unless otherwise noted, reaction conditions are 90 °C, 25 psi of gas, 0.1 mol% of Ru, 4h. ^a 50 equiv. based on Ru, after 6h).	26
Table 1.2. Calculated $\text{DG}^\ddagger_{\text{insertion}}$ (kcal/mol) for ethylene insertion and $\text{DG}^\ddagger_{\text{CH activation}}$ (kcal/mol) of ethylene for $\text{TpRu}(\text{L})(\eta^2\text{-C}_2\text{H}_4)\text{Ph}$ complexes.	33

CHAPTER 2

Table 2.1. Coupling constants observed for the ligand in the ^1H NMR spectrum of $\text{TpRu}[\text{P}(\text{OCH}_2)_2(\text{OCCH}_3)](\text{PPh}_3)\text{Cl}$ (2).	47
Table 2.2. Selected Crystallographic Data for $\text{TpRu}(\text{PPh}_3)[\text{P}(\text{OCH}_2)_2(\text{OCCH}_3)]\text{Cl}$ (2), $(\eta^6\text{-C}_6\text{H}_6)\text{Ru}[\text{P}(\text{OCH}_2)_2(\text{OCCH}_3)]\text{Cl}_2$ (11) and $(\eta^6\text{-p-cymene})\text{Ru}[\text{P}(\text{OCH}_2)_2(\text{OCCH}_3)]\text{Cl}_2$ (12).	49
Table 2.3. Ru(III/II) potentials for $\text{TpRu}(\text{L})(\text{PPh}_3)\text{Cl}$ complexes. Data from cyclic voltammetry in NCMe with reversible potentials ($E_{1/2}$) reported vs NHE (in V). ...	51
Table 2.4. Ru(III/II) potentials for $(\eta^6\text{-C}_6\text{H}_6)\text{Ru}(\text{L})\text{Cl}_2$ complexes. Data from cyclic voltammetry in NCMe with potentials reported vs NHE (in V).	58
Table 2.5. Comparison of bond lengths from crystallographic data for $(\eta^6\text{-p-cymene})\text{Ru}(\text{L})\text{Cl}_2$ complexes.	63
Table 2.6. Ru(III/II) potentials for $(\eta^6\text{-p-cymene})\text{Ru}(\text{L})\text{Cl}_2$ complexes. Data from cyclic voltammetry in NCMe with potentials reported vs NHE (in V).	64
Table 2.7. Data from DFT calculations of $\text{P}(\text{OCH}_2)_2(\text{OCCH}_3)$ (1), $\text{P}(\text{OMe})_3$, $\text{P}(\text{OCH}_2)_3\text{CEt}$ and PF_3 .	70

CHAPTER 3

Table 3.1. Selective Crystallographic Data for $\text{TpRu}[\text{P}(\text{OCH}_2)_2(\text{OCCH}_3)](\text{NCMe})\text{Ph}\cdot\text{CH}_2\text{Cl}_2$ (4).	99
Table 3.2. Ru(III/II) Potentials and Rate Constants for the Activation of C_6D_6 at 60 °C by $\text{TpRu}(\text{L})(\text{NCMe})\text{Ph}$.	102
Table 3.3. Calculated Distances (Å) for C–H Activation Transition State (TS2, Scheme 3.10) for $\text{TpRu}(\text{L})(\text{NCMe})\text{Ph}$ (see Figure 3.17 for labels).	112
Table 3.4. Comparison of TON and TOF for Ethylbenzene Production from Catalytic Hydrophenylation of Ethylene by $\text{TpRu}(\text{L})(\text{NCMe})\text{Ph}$ Complexes.	113
Table 3.5. Calculated $\text{DG}^\ddagger_{\text{insertion}}$ (kcal/mol) for Ethylene Insertion (TS1, Scheme 3.10) and $\text{DG}^\ddagger_{\text{CH activation}}$ (kcal/mol) of ethylene for $\text{TpRu}(\text{L})(\eta^2\text{-C}_2\text{H}_4)\text{Ph}$ Complexes. ...	116
Table 3.6. Allyl Coupling Diagram for $\text{TpRu}[\text{P}(\text{OCH}_2)_2(\text{OCCH}_3)](\eta^3\text{-C}_3\text{H}_4\text{Me})$ (5).	127

CHAPTER 4

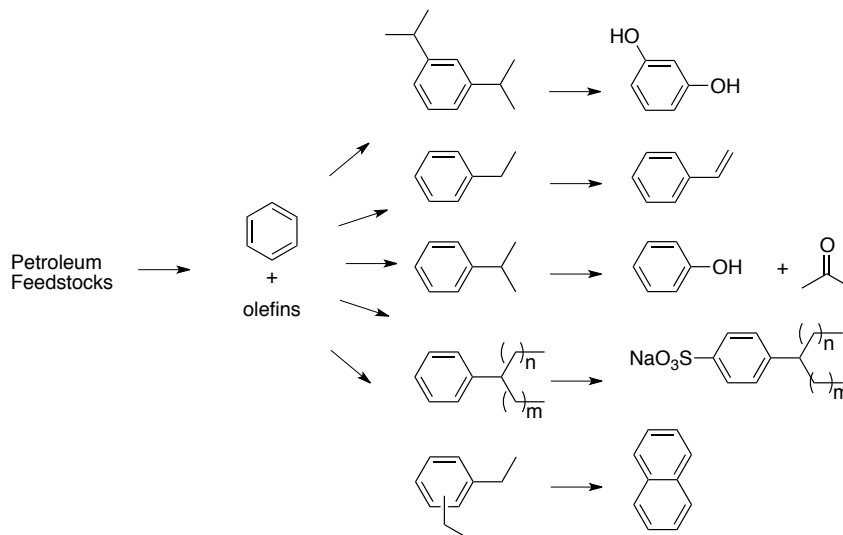
Table 4.1. Comparison of TON and TOF for Ethylbenzene Production from Catalytic Hydrophenylation of Ethylene by TpRu(L)(NCMe)Ph Complexes.	132
Table 4.2. Comparison of $\text{TpRu(CO)}(\eta^3\text{-C}_3\text{H}_4\text{Me})$ yield during catalysis at 0.01 mol % Ru at varying pressures of ethylene at 90 °C.	136
Table 4.3. Comparison of $\text{TpRu(CO)}(\eta^3\text{-C}_3\text{H}_4\text{Me})$ concentration during catalysis as a function of catalyst loading.....	137

CHAPTER 5

Table 5.1. Selected Crystallographic Data for $(\eta^6\text{-}p\text{-cymene})\text{Ru}[\text{P}(\text{OCH}_2)_3\text{CEt}]\text{PhBr}$ (2), and $(\eta^6\text{-}p\text{-cymene})\text{Ru}(\text{PMe}_3)\text{PhBr}$ (4)	152
Table 5.2. Selected Crystallographic Data for $\{[\text{C}(\text{pz})_4]\text{Ru}[\text{P}(\text{OCH}_2)_3\text{CEt}]\text{Cl}(\text{NCMe})\}[\text{BAR}'_4]$ (12).	168
Table 5.3. Attempted alkylation of $\{[\text{C}(\text{pz})_4]\text{Ru}[\text{P}(\text{OCH}_2)_3\text{CEt}]\text{Cl}(\text{NCMe})\}[\text{BAR}'_4]$ (12).	170
Table 5.4. Attempted alkylation of $\{[\text{C}(\text{pz})_4]\text{Ru}[\text{P}(\text{OCH}_2)_3\text{CEt}](\text{OTf})(\text{NCMe})\}[\text{BAR}'_4]$ (13).....	172

1. Introduction

The use of transition metal catalysts to provide less energy-intensive and more atom economical synthetic pathways for the production of substituted aromatic substrates has recently become an area of increased attention. As the demand continues to grow in the United States and throughout the world for plastics, elastomers, detergents, pharmaceuticals, and other materials derived from simple aromatic precursors more efficient ways to produce these commodities is needed (Scheme 1.1).¹⁻⁵ Benzene, toluene, and xylene from petroleum feedstock serve as the chemical building blocks to these desired compounds. As a result of their widespread use, the demand for these three chemicals is substantial. For example, in 2004, the world demand for benzene was 36.4×10^6 t (t = tonnes), and the demand is expected to continue to increase 4%–6% per year.⁴ The United States was the second largest consumer of benzene with 9.7×10^6 t consumed in 2004. Approximately 75% of benzene is converted to alkyl arenes.^{4,6} In particular, the worldwide consumption of ethylbenzene has continued to increase as the demand for plastics and elastomers rises. In 2004, the United States produced approximately 5.1×10^6 t of ethylbenzene, of which approximately 99% was converted to styrene. Approximately 65% of styrene is used to synthesize polystyrene.^{3,4}



Scheme 1.1. Alkyl arenes produced from benzene and olefins.

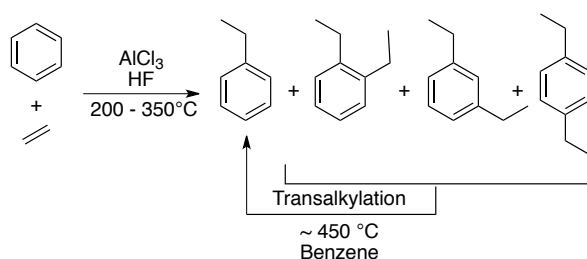
With the increasing demand for benzene derivatives and new government environmental restrictions (i.e., The United States Clean Air Act), older, more conventional methods, (i.e., Friedel-Crafts alkylation, *vide infra*) must be improved and alternative industrial methods for the production of alkyl arenes must be developed. In addition, new catalyst technologies can provide routes to new compounds that are not currently accessible.

1.1. Current Methods for Industrial Synthesis of Alkyl Arenes

1.1.1. Friedel-Crafts Catalysts

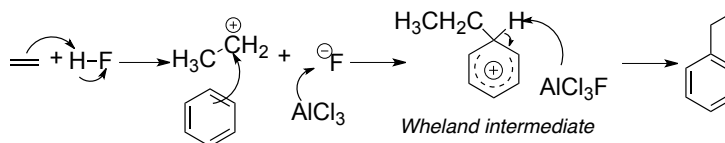
In the late 1870s, Charles Friedel and James M. Crafts discovered that aromatic rings (e.g., benzene) can be functionalized with alkyl-halides (i.e., MeCl) in the presence of an aluminum halide (e.g., AlCl₃). This was a prominent discovery since alkyl-halides by themselves are not sufficiently electrophilic to react with the functionally inert C–H

bond in benzene (BDE = ~ 110 kcal/mol) or other aromatic substrates to produce alkyl arenes.⁷⁻¹¹ Later, it was found that alkenes (e.g., ethylene), in the presence of a Lewis acid (often in combination with a Brønsted acid, e.g., HF) could perform a similar reaction (Scheme 1.2). The ability to functionalize C–H bonds of benzene provided an opportunity to manipulate some of the basic building blocks from fossil resources to produce value-added chemicals.



Scheme 1.2. Overall reaction for Friedel-Crafts alkylation.

The Friedel-Crafts mechanism is considered an electrophilic aromatic substitution reaction (Scheme 1.3).^{6,8,10-15} The reaction proceeds by initial protonation of the alkene by the Brønsted acid to produce a carbocation. The electrons from the benzene ring subsequently attack the carbocation to form a new C–C bond and yield a Wheland intermediate. Finally, the $[\text{AlCl}_3\text{X}]^-$ deprotonates the Wheland intermediate generating the desired alkyl arene and regenerating the starting Brønsted and Lewis acids.

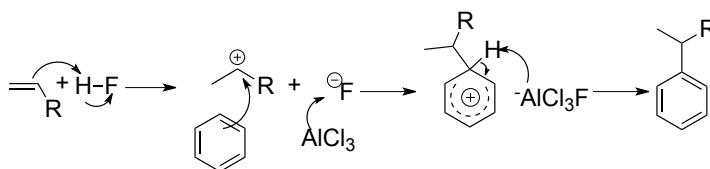


Scheme 1.3. Mechanism for Friedel-Crafts alkylation reaction.

Starting in the 1930s, the majority of the ethylbenzene was produced from ethylene and benzene using Friedel-Crafts alkylation in the presence of an $\text{AlCl}_3\text{-HCl}$ catalyst under mild temperatures and pressures ($160\text{ }^\circ\text{C}$ and $\sim 1\text{ atm}$).^{4,8,13} However, due to the nature of the mechanism many drawbacks arise. One significant drawback is polyalkylation to produce di/tri-substituted ethylbenzenes, which inherently limits the purity of the final reaction solution. Polyalkylation is a result of the ethylbenzene product being more reactive than the starting material by approximately 2–5 times.⁸ To increase the yield of ethylbenzene the di/tri-substituted benzenes are reacted with benzene in a transalkylation process (Scheme 1.2); however, this process is energy intensive.⁸ Additionally, since the reaction occurs in the liquid phase, it therefore requires the use of non-corrosive vessels, which can be costly. Additional drawbacks include the production of stoichiometric amounts of halogenated waste as a result of the inability to recycle the catalyst due to neutralization during product workup. Later, to be more environmentally friendly, industries started to substitute HF for AlCl_3 primarily because of the volatility of HF enables it to be reused and recycled more readily.⁵ However, the use of HF as a catalyst still suffers from drawback such as extreme toxicity if a leak in the production stream occurs.

Due to the formation of a carbocation, when α -olefins are used the Markovnikov (i.e., branched) species is obtained (Scheme 1.4). Historically, highly branched alkyl arenes were used in detergents; however, their slow decomposition rate led to pollution of water sources causing industry to implement the use of “linear” alkyl arene sulfonates

starting in the 1960s (Scheme 1.1). A linear alkyl benzene is defined as a molecule with the chemical formula of $C_6H_5C_nH_{2n+1}$ where $n = 10 - 14$.¹³ This increase in demand for linear alkyl arenes has caused alternative processes to be explored and developed (see Section 1.1.2).^{8,12} Another drawback of Friedel-Crafts alkylation is that in the presence of aromatic substrates containing electron-withdrawing substituents the reaction does not proceed, thus limiting the substrate scope.



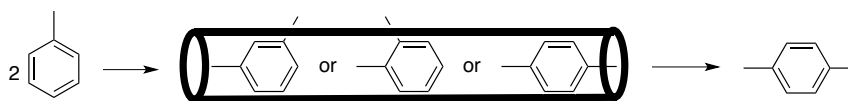
Scheme 1.4. Mechanism for Friedel-Crafts alkylation reaction with α -olefins.

1.1.2. Zeolite Catalysts

Due to the drawbacks with liquid phase Friedel-Crafts catalysis, alternative techniques have been developed. One way to improve the drawbacks of waste production (e.g., salt formation), low yields, corrosion of the reaction vessel and formation of polyalkylated species in the production of alkyl arenes is the use of solid supports. The first use of solid support was in the 1940s when amorphous silica-alumina gel was employed enabling the reaction to occur in the gas phase.^{13,16} This technology quickly evolved, and the use of zeolite catalyst was first explored on the industrial scale in 1976 by Mobil-Badger.^{13,17-20} Today, zeolites are one of the most utilized catalyst for heterogeneous catalysis.^{2,21}

Zeolites are surfaces that consist of porous crystalline aluminosilicates and are constructed most commonly using SiO_4^{4-} and AlO_4^{5-} ; however, they also can be made using other elements such as boron, gallium, iron or titanium.^{4,22} Zeolites are beneficial to industry because of their wide range of properties including the ability to vary pore size, which can control selectivity, high surface area, high thermal and hydrothermal stability, and the ability to vary the chemical properties of the active sites which can increase selectivity.^{2,23}

As stated above, one of the advantages of zeolites is the ability to vary the pore size and control selectivity based on size and or shape. There are three main ways that the effects of pore shape can influence selectivity: 1) Reactant shape selectivity, which involves biasing one reaction over a competing side reaction by using size exclusion toward the entrance to the pore. 2) Product shape selectivity, which biases which product is released from the pore dependent on the size (Scheme 1.5). 3) Transition state selectivity, where one transition state is favored because of the geometry of the pore.^{4,24} The pores of zeolites are typically well defined and range from 0.5–1 nm in diameter.⁵ Additionally, zeolites can have different orientations of the pores such as zig-zag or straight.



Scheme 1.5. Product shape selectivity of *p*-xylene is favorable due to pore size restrictions.²⁴

In 1976, the first zeolite catalyst for the production of ethylbenzene, known as ZSM-5, was developed (Figure 1.1).^{3,4,6,13,14,23,25} ZSM-5 zeolite is one of the three widely used industrial catalysts, the other two are zeolite Y and zeolite A.²² ZSM-5 zeolites are constructed of five rings with channels connecting them, which are straight and zigzag ten-ring channels yielding an orthorhombic space group. Due to their high Si:Al ratios ($\geq 10:1$) these zeolites are hydrophobic and organophilic.²² Using ZSM-5 aromatic alkylation is carried out in the gas phase. Under a constant ethylene stream the catalyst is active between 40 - 60 days, after which regeneration is necessary due to coke deposits in the pores.²⁶ The reaction is conducted under high temperatures (390–450 °C) and pressures (1.5 to 2 MPa).⁴ Polyalkylated species are recycled back into the original reactor vessel and undergo transalkylation.

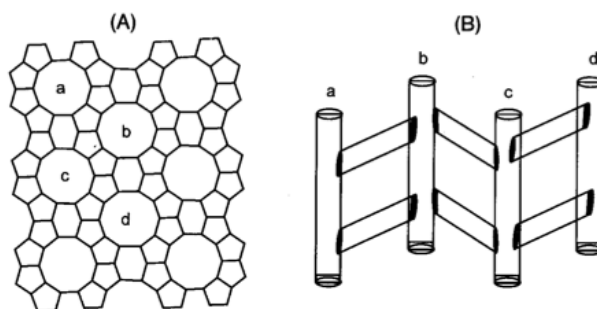


Figure 1.1. Depiction of a ZSM-5 zeolite catalyst (A) Structure looking from the top at Zeolite channels (B) Looking side on at zeolite material- four pores are marked for orientation (a,b,c and d). Copyright 2009 Wiley. Used with permission from Macquarrie, D. J., Industrial Friedel-Crafts Chemistry, *Catalytic Asymmetric Friedel-Crafts Alkylations*, Wiley-VCH.⁵

Approximately 10 years later two new zeolite systems were developed, which moved the transalkylation reaction to a separate reactor. Lummus-UOP modified the

ZSM-5 zeolites to form Zeolite Y. Zeolite Y is a three dimension 12 ring pore system which forms large cavities called “supercages” (Figure 1.2). As a result they could run the alkylation and transalkylation reaction in the liquid phase and could reduce the temperature for the reaction (~ 270 °C) with 3.8 MPa of ethylene. Due to the reduced temperature compared to catalysis with ZSM-5 zeolites the overall energy consumption is decreased, which increases the lifetime of the catalyst. Higher selectivity for the desired monoalkylated products is also observed for the liquid phase reaction.³ Around the same time, Mobil-Badger reported a third generation manufacturing ethylbenzene process using ZSM-5. Similar to the Lummus-UOP process, transalkylation occurs in a separate reactor allowing for an increase in zeolite cycle life to approximately three years. Later in the mid-1990s, three more heterogeneous zeolite catalysts were used. These included CDtech ED (1994) and the Lummus-UOP-EBONE (1996) (EBZ-500 zeolite), both of which conduct alkylation and transalkylation in the liquid phase, and the Mobil’s EBMAX process (1995) that uses MCM-22 based zeolite catalyst where the reaction occurs in a mix phase reactor with alkylation in the liquid phase and transalkylation in the vapor phase. However, the reaction was later changed to a liquid phase reaction.^{3,5} Currently, technology continues to improve. Mobil has been awarded 33 licenses for ethylbenzene Zeolite technology.^{21,23}

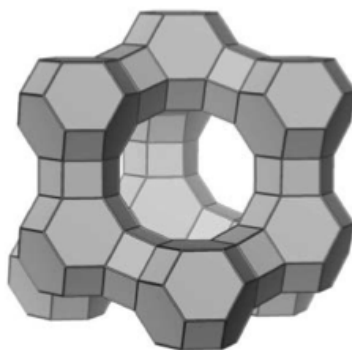
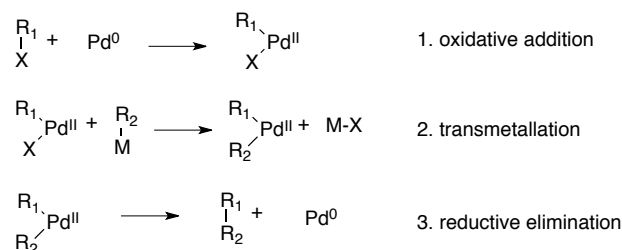


Figure 1.2. Depiction of a Y zeolite. Copyright 2010 Wiley. Used with permission from Broach, R.W. Zeolite Types and Structures, *Zeolites in Industrial Separation and Catalysis*, Wiley-VCH.²²

1.2. Transition Metal Catalyzed C–C Bond Forming Reactions

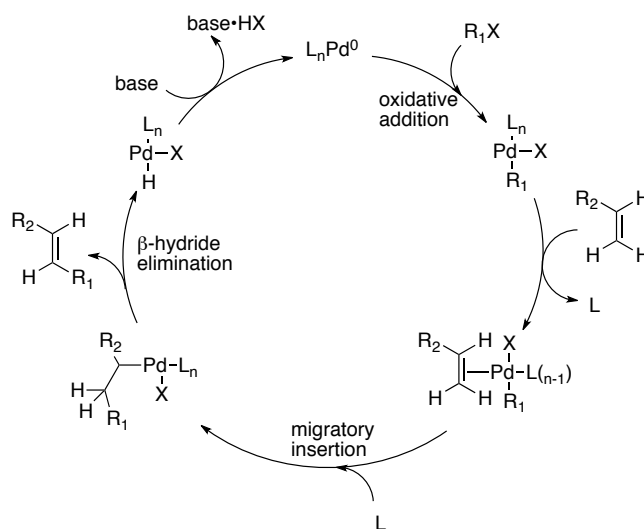
Carbon–Carbon bond forming reactions are important and are incorporated by the petrochemical industry to convert hydrocarbons derived from natural gas or petroleum into higher-value molecules as well as by synthetic organic chemistry for the preparation of complex molecules.²⁷⁻³² A wide range of transition metals have been used to promote C–C bond formation. The most widely used transition metal is palladium, but coupling reactions also occur in the presence of copper, nickel, rhodium, or cobalt.³³ These C–C bonding forming reactions (i.e., Suzuki, Negishi, Stille, and Sonogashira), sometimes termed cross-coupling reactions, typically involve three distinct steps 1) carbon-halide oxidative addition 2) transmetallation and 3) reductive elimination (Scheme 1.6).³³



Scheme 1.6. General reaction scheme for cross-coupling reactions utilizing palladium.

Although there are many variations of C–C coupling reactions, three important cross coupling processes include Negishi (mid 1970's), Stille (late 1970s), Suzuki (early 1980s) and Heck (mid 1970's) reactions. The 2010 Nobel Prize in Chemistry, was jointly awarded to Heck, Suzuki and Negishi.³⁴⁻³⁶ The most common Pd catalyst is Pd(PPh₃)₄; however, Pd(II) salts such as PdCl₂(PPh₃)₂ or Pd(OAc)₂ can also be employed with PPh₃ since the Pd(II) species is reduced to Pd(0) *in situ*.^{27,37} The Negishi reaction occurs between aryl zinc reagents and aryl halides or triflates. The reaction is tolerant to many functional groups including esters, amines, ketones and aldehydes.²⁷ Stille incorporated aryl-stannanes rather than aryl-zincs, which led to increased tolerance to functional groups. The reaction conditions are typically mild; however, a major drawback is the toxicity of organotin reagents.^{32,38} Another variations of late transition metal catalyzed C–C cross coupling is the Suzuki-Miyaura reaction. This reaction uses boronic acids with aryl-halides, arylboranes or boronic acid esters. However, all of these coupling reactions suffer from the need for halogenated/activated substrates, which result in halogenated waste and a stoichiometric organometallic reagent.³⁹

Another important cross coupling reaction is the Heck reaction, which functions by a different catalytic cycle than the cross coupling reactions discussed above. The Heck reaction does incorporate a transmetallation step. The proposed catalytic cycle involves an initial alkyl halide oxidative addition to Pd(0) to produce a Pd(II) complex (Scheme 1.7). Subsequent olefin coordination and migratory insertion leads to an intermediate Pd-alkyl species. The desired product is released from the metal center after the β -hydride elimination step. Reductive elimination of HX, which is captured by a base, regenerates the Pd(0) catalyst. These reactions are conducted in polar solvents at temperatures of 100-140 °C. The majority of Heck reactions incorporate phosphorous-based palladium complexes; however, many studies have looked at different palladium catalysts such as those ligated with NHC.^{38,40} One major reason for the research on alternative palladium catalysts is because the phosphorous palladium catalysts are toxic, air sensitive and expensive.³⁸

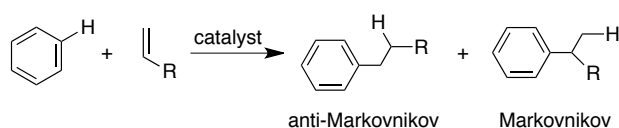


Scheme 1.7. Proposed Heck cross coupling mechanism.³⁸

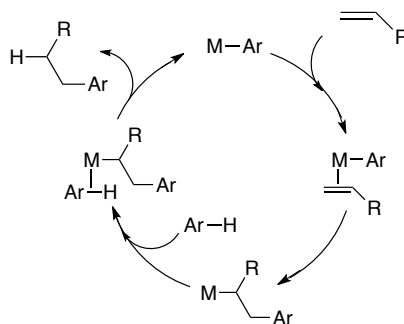
Although cross coupling reactions are valuable to synthetic chemists, application to industrial scale processes is difficult. For example, the production of halogenated waste is a hindrance.⁴¹ Additionally, the use of large amounts of Pd that give relatively low turnover numbers is an issue. Finally, the inability to recycle the catalyst efficiently is an issue.⁴¹

1.3. Transition Metal Mediated C–H Activation for the Synthesis of Alkyl Arenes

Transition metal mediated non-Friedel-Crafts olefin hydroarylation (Scheme 1.8) is generally believed to proceed through the mechanism shown in Scheme 1.9. The cycle proceeds via η^2 -coordination of the olefin to the metal center, followed by olefin insertion into the M–aryl bond, which generates an open coordination site. Arene coordination is followed by C–H activation, and alkyl arene dissociation regenerates the starting catalyst.⁴²⁻⁴⁶



Scheme 1.8. General olefin hydroarylation reaction.



Scheme 1.9. Cycle for transition metal catalyzed olefin hydroarylation.

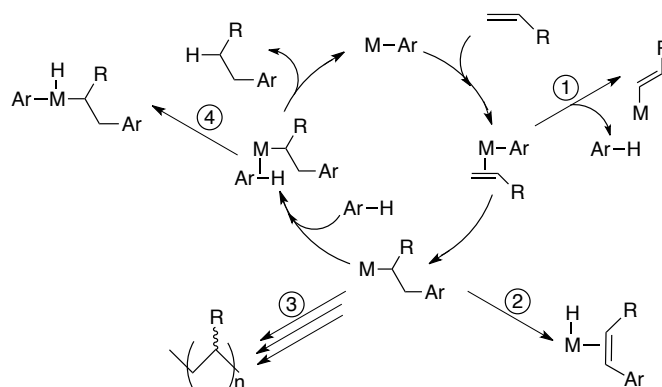
Examples of catalytic metal-mediated C–H functionalization of aromatic substrates have increased substantially in recent years.⁴⁷⁻⁶⁰ Although several transition metal catalysts for olefin hydroarylation using substrates functionalized with heteroatomic groups are known,^{55,57,61-66} examples of transition metal catalysts that convert unactivated hydrocarbons (e.g., benzene, ethylene or propene) to alkyl or vinyl arenes are relatively rare.⁶⁷⁻⁷¹ Catalysts based on ruthenium, iridium and platinum complexes have been utilized to promote olefin hydroarylation using simple hydrocarbons.^{42-45,56,62,67-70,72-76}

There are multiple potential benefits of olefin hydroarylation that proceeds by the cycle shown in Scheme 1.9.

1. Transition metal catalyzed olefin hydroarylation of α -olefins could afford selectivity for linear products (Scheme 1.8).
2. Selectivity for mono-alkyl arenes might be achieved, which is not possible with Friedel-Crafts catalyst since the products formed in the reactions are typically ~5 times more reactive than the starting materials.⁸

3. Regioselectivity for dialkyl arenes is possible. In contrast, Friedel-Crafts catalysts are not selective for a second alkylation of benzene. The lack of selectivity for Friedel-Crafts alkylation is due the poor directing ability of an alkyl group.
4. Direct oxidative olefin hydroarylation (potentially with O_2) to give vinyl arenes such as styrene could provide a direct synthesis of styrene from benzene and ethylene.

A substantial challenge to developing transition metal catalysis for olefin hydroarylation is avoiding potential competing side reactions. Four undesirable reactions include: 1. C–H activation of the olefin, 2. β -hydride elimination from the M–alkyl species (note: desirable if vinyl arenes are the target), 3. olefin oligomerization/polymerization and 4. irreversible oxidative addition (Scheme 1.10).



Scheme 1.10. Potential competing side reactions for olefin hydroarylation.

Considering these side reactions can provide some guidance to catalyst design. In order to have a catalyst that readily inserts the olefin into the metal-phenyl bond a less electron rich metal center is desired due to decreased backbonding between the metal and

olefin π^* orbitals. However, if the metal center is too electron deficient, such as a d^0 complex, oligomerization/polymerization could compete with arene C–H activation leading to deactivation of the catalyst. Avoiding β -hydride elimination is likely to be a challenge. Thus, if alkyl arenes are desired, the most viable strategy is to suppress olefin displacement and render β -hydride elimination reversible. Finally, if the metal center is too electron rich, irreversible oxidative addition could occur.^{45,59}

1.4. Examples of Transition Metal Catalysts for Olefin Hydroarylation

1.4.1. Transition Metal C–H Activation by an Acid Catalyzed Pathway

Tilley and coworkers have reported olefin hydroarylation using [2-(2-pyridyl)indole]Pt(Cl)(C₂H₄).⁷² Attempted catalysis using [2-(2-pyridyl)Pt(Cl)(C₂H₄) in benzene with norbornene resulted in no reaction. Yet, the addition of 1 equiv. AgOTf at elevated temperatures (115 °C) for 20 h, produced *exo*-phenylnorbornane. The use of AgBF₄ allowed a lower temperature (80 °C) and increased the yield of the reaction with a 92% yield after 2 h versus a 79% yield after 20 hours in the case of AgOTf. These data suggest that the Ag salt is not just a chloride abstraction agent but potentially also increases the rate of hydrophenylation. Catalysis with ethylene and benzene to produce ethylbenzene was not successful, and only ethylene polymerization occurred. Upon further examination of the mechanism, it is believed that the reaction proceeds through an acid-catalyzed mechanism.⁷²

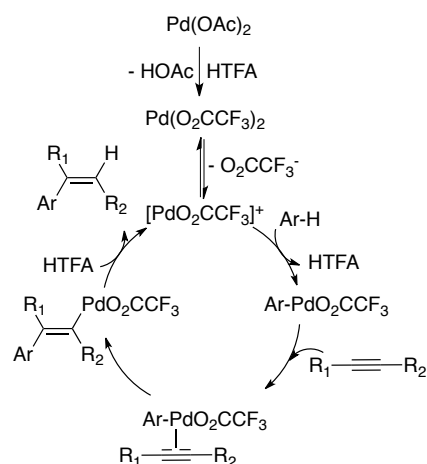
Recently, Tilley, Bergman and coworkers published a mechanistic study on olefin hydroarylation for (COD)Pt(OTf)₂ and ('bpy)PtOTf₂ ('bpy = 4,4'-di-*tert*-butyl-2,2'-

bipyridyl).⁶² Norborene was initially studied, and the best yield (41%) was obtained using 9-fold excess of benzene at 110 °C for 5 h. Additionally, hydroarylation of cyclic alkenes was studied. The reaction of a 9-fold excess of benzene at 100 °C for 24 h with cyclohexene produced cyclohexylbenzene in 36% yield, but dicyclohexylbenzene (21% yield) was also observed. It was found that Pt(COD)(OTf)₂ and (bpy)Pt(OTf)₂ could achieve olefin hydroarylation with the best yield being obtained from the reaction between cyclohexene and mesitylene; but the reaction is catalyzed by HOTf rather than by Pt.

1.4.2. Non-Acid Catalyzed Transition Metal Promoted C–H Activation of Unactivated Olefins

The ability to produce alkyl benzenes through olefin hydroarylation using a transition metal as catalyst in the presence of an acid source is well documented in the literature.⁵⁶ Fujiwara and coworkers have extensively studied Pd complexes for aromatic C–H functionalization.^{61,77,78} For example, in 2000, Pt (PtCl₂/AgOAc) and Pd (Pd(OAc)₂) catalysts for regio- and stereoselective addition of arenes to alkynes and alkenes in trifluoroacetic acid (HTFA) were reported by Fujiwara and coworkers⁶¹ It was found that both Pt(II) and Pd(II) were more active than RhCl₃/3AgOAc, RuCl₃/3AgOAc and Ni(OAc)₂. Although no detailed mechanistic studies were conducted since the reaction is being conducted in HTFA, it was proposed that [Pd(O₂CCF₃)]⁺ is generated *in situ* and is the active catalyst. This cationic species is proposed to undergo electrophilic metalation with the arene to form a σ-aryl-Pd complex, Ar–PdO₂CCF₃. Then an η²-alkyne-Pd

complex is formed. Insertion of the alkyne into the Ar–Pd bond and protonation by HTFA forms the product and regenerates the catalyst (Scheme 1.11).



Scheme 1.11. Proposed catalytic cycle for addition of arenes to alkynes.

To survey the versatility of $\text{PtCl}_2/\text{AgOAc}$ and $\text{Pd}(\text{OAc})_2$ as catalysts, the addition of a variety of arenes to substituted alkynes was studied.⁶¹ Using more electron-donating groups on the arene improves the yield of reactions with bulky molecules. One major advantage observed was the chemoselectivity for substrates with traditionally reactive functional groups on the arene ($-\text{OH}$, $-\text{Br}$, $-\text{CHO}$ or vinyl groups) and alkynes ($-\text{CHO}$, $-\text{COMe}$, $-\text{CO}_2\text{H}$, $-\text{CO}_2\text{Et}$, $-\text{CO}_2\text{Me}$) and the reaction predominantly yields *cis* product. Furthermore, $\text{Pd}(\text{II})$ was found to be a more active than $\text{Pt}(\text{II})$; however, $\text{Pt}(\text{II})$ was longer lived, gave higher yields, exhibited better selectivity and fewer by-products such as products from multiple alkyne insertions or coupling of two arenes.

Goldberg and co-workers reported in 2008 that $[\text{dmpp}]\text{Pt}(\text{SMe}_2)\text{Ph}$ and $[(\text{dmpp})\text{PtMe}_3]$ (dmpp = 3,5-dimethyl-2-(2-pyridyl)pyrrolide) are capable of catalytic olefin hydroarylation of unactivated substrates (Figure 1.3).⁶⁸ The reaction of ethylene and benzene in the presence of either $[\text{dmpp}]\text{Pt}(\text{SMe}_2)\text{Ph}$ or $[(\text{dmpp})\text{PtMe}_3]$ at $\sim 100^\circ\text{C}$ resulted in 36 and 26 TON of ethylbenzene, respectively. When propylene was used under similar conditions, the Markovnikov product was formed over the anti-Markovnikov product in approximately an 85:15 ratio for both Pt catalysts.

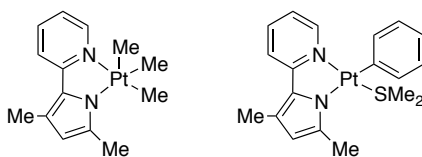
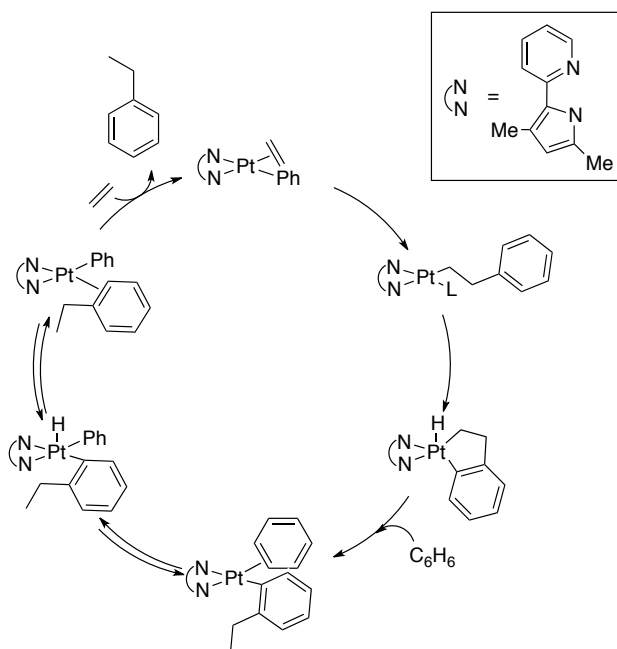


Figure 1.3. $(\text{dmpp})\text{Pt}$ catalyst precursors for olefin hydroarylation.

The mechanism of olefin hydroarylation with the $(\text{dmpp})\text{Pt}$ catalyst is not likely a Friedel-Crafts reaction. Evidence against a Friedel-Crafts pathway includes formation of the linear product for reactions with α -olefins (although not selectively) and selectivity for the functionalization of *meta* and *para* positions when substituted arenes were used. Friedel-Crafts reactions generally are not selective for dialkylation. The proposed catalytic cycle is shown in Scheme 1.12. The reaction is initiated with the formation of a phenyl-ethylene complex, which is followed by olefin insertion into the $\text{Pt}-\text{Ph}$ bond. Cyclometalation results in the formation of a five-coordinated platinum species. Reductive elimination and solvent coordination yields a four coordinate Pt^{II} species with

coordinated ethylbenzenyl. This complex is likely in rapid equilibrium with a 5-coordinate hydride species, which was determined using isotopic studies. The isotopic studies yielded a significant amount of deuterium incorporation (D_0 – D_6) into the ethylbenzene fragment when reactions were performed in a 1:1 solution of C_6D_6 : C_6H_6 under ethylene pressure. The catalytic cycle is completed by coordination of ethylene and dissociation of ethylbenzene (Scheme 1.12).



Scheme 1.12. Proposed mechanism for ethylene hydrophenylation with (dmpp)Pt.

Recently, our group has published that $[(^i\text{bpy})\text{Pt}(\text{Ph})\text{L}][\text{BAr}'_4]$ ($\text{L} = \text{NCMe}$, NC_3F_5 or THF and $\text{Ar}' = 3,5\text{-bis(trifluoromethyl)phenyl}$) is capable of catalyzing olefin hydroarylation.^{70,73}

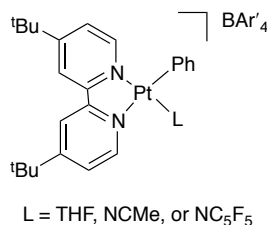
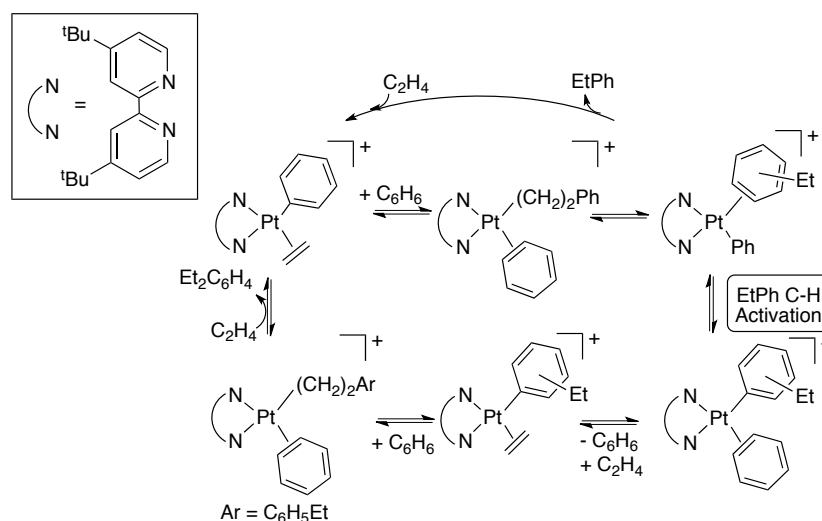


Figure 1.4. [(^tbpy)Pt(Ph)L][BAr'₄] catalyst for olefin hydroarylation.

Catalytic reactions with [(^tbpy)Pt(Ph)(THF)][BAr'₄] (0.025 mol % relative to benzene) in benzene under 0.1 MPa of ethylene at 100 °C for 16 h yielded 53 TON of ethylbenzene and approximately 11 total TON of diethylbenzenes with an *ortho:meta:para* ratio of 1:2.6:1.6. Replacing the THF with NCMc or NC₅F₅ inhibited the rate of the reaction most likely due to the stronger interaction between the metal and the ligand. For example, only 21 TON and 20 TON of ethylbenzene were observed after 16 hours for the *N*-donor ligands respectively, with diethylbenzene also being observed. Upon further studying the impact of temperature and ethylene pressure on catalysis, it was found that increasing temperature increases the rate of olefin insertion and that increased ethylene pressures inhibits catalysis.

Further mechanistic studies were conducted to elucidate the cause of a relatively large quantity of polyalkylated benzene species that are formed. This was of particular interest since, as stated above, a major drawback to Friedel-Crafts catalysis is the production of polyalkylated species and the need of high temperatures for subsequent transalkylation. It is proposed that the production of dialkylated benzene using [(^tbpy)Pt(Ph)(THF)][BAr'₄] as the catalyst is a result of a second aromatic C–H activation competing with ethylbenzene dissociation (Scheme 1.13). Currently, alternative platinum

catalysts are being synthesized in our laboratories to investigate the structure and activity relationship of platinum catalysts with similar motifs on olefin hydroarylation.



Scheme 1.13. Proposed mechanism for the formation of diethylbenzene by $[(t\text{Bu-bpy})\text{Pt}(\text{Ph})(\text{THF})][\text{BAr}'_4]$.

In 2000, Periana and coworkers reported catalytic hydroarylation of olefins using the dinuclear complex, $\text{Ir}(\mu\text{-acac-O,O,C}^3)(\text{acac-O,O})(\text{acac-C}^3)]_2$ (acac = acetylacetonato or 2,4-pentanedione) (Figure 1.5).⁷⁹ When reactions were performed with $\text{Ir}(\mu\text{-acac-O,O,C}^3)(\text{acac-O,O})(\text{acac-C}^3)]_2$ in the presence of benzene and 1.96 MPa of ethylene at 180 °C, 455 TO of ethylbenzene were observed after 3 h. When the reaction was performed with 0.78 MPa of propylene at 180 °C for 20 minutes formation of *n*-propylbenzene and cumene was observed in a 61:39 ratio with 13 total TOs.^{44,79} In 2002,

Periana and coworkers reported that mononuclear Ir(III) catalyst with acac ligands are also active (Figure 1.5).⁶⁹

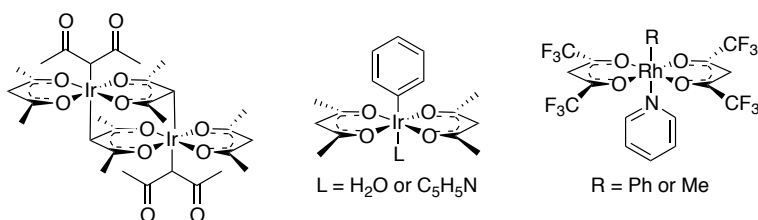
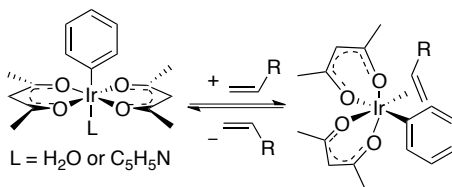


Figure 1.5. bis-acac-*O,O*-Ir(III) (acac = acetylacetonato or 2,4-pentanedione) and bis-hfac-*O,O*-Rh(III) (hfac-*O,O* = β -diketonate κ^2 -*O,O*-1,1,1,5,5,5-hexafluoroacetylacetonate) complexes for olefin hydroarylation of benzene.

Upon reaction of the mononuclear Ir complexes with propylene under similar reaction conditions as the dinuclear complex $\text{Ir}(\mu\text{-acac-}O,O,C^3)(\text{acac-}O,O)(\text{acac-}C^3)]_2$ the same 61:39 linear to branched ratio was observed. For catalysis using $(\text{acac})_2\text{Ir(Ph)L}$ ($L = \text{H}_2\text{O}$ or $\text{C}_5\text{H}_5\text{N}$) it has been proposed that the initial step in the catalytic process is *trans* to *cis* isomerization of the Ph and “L” (Scheme 1.14) followed by olefin coordination and insertion into the Ir–Ph bond. Subsequent coordination of benzene, C–H activation and coordination of another equivalent of olefin to release the product and regenerate the active catalyst completes the catalytic cycle.^{44,69}



Scheme 1.14. *Trans-Cis* isomerization of $(\text{acac})_2\text{Ir(Ph)L}$ ($L = \text{H}_2\text{O}$ or $\text{C}_5\text{H}_5\text{N}$).

Periana and coworkers reported a rhodium catalyst as an extension of their bis-Ir-acac system.⁸⁰ Due to calculations showing that the rate of olefin insertion can be enhanced with a less- π basic metal center, they replaced the $-\text{CH}_3$ groups of acac with the strongly electron-withdrawing perfluoromethyl groups (Figure 1.5).^{42,45} Attempts to make the *cis*-(*hfac-O,O*)₂Ir(Ph)(py) analog were unsuccessful; *trans*-(*hfac-O,O*)₂Rh(CH₃)(py) and *trans*-(*hfac-O,O*)₂Rh(Ph)(py) (*hfac-O,O* = β -diketonate κ^2 -*O,O*-1,1,1,5,5,5-hexafluoroacetylacetonate) were isolated. Heating *trans*-(*hfac-O,O*)₂Rh(CH₃)(py) in benzene or mesitylene (1,3,5-trimethylbenzene) at 190 °C lead to the formation of *cis*-(*hfac-O,O*)₂Rh(R)(py) (R = phenyl or ethyl-3,5-dimethylbenzene) with release of methane, which demonstrates that *trans*-(*hfac-O,O*)₂Rh(CH₃)(py) is capable of activating sp^2 and sp^3 C–H bonds. To study if *cis*-(*hfac-O,O*)₂Rh(CH₃)(py) is capable of catalytic C–H activation, the complex was placed in a 1:1 mixture of toluene-*d*₈ and C₆H₆ at 190 °C. The reaction yielded a rate of H/D exchange of $2.0 \times 10^{-3} \text{ s}^{-1}$, which is approximately the same rate (taking in consideration the difference in reaction conditions) as the *cis*-(*acac-O,O*)₂Ir(Ph)(py). Reacting benzene and styrene in the presence of *cis*-(*hfac-O,O*)₂Rh(Ph)(py) at 90 °C lead to stoichiometric amounts of the anti-Markovnikov product dihydrostilbene; however, at longer reaction times polystyrene was formed. Thus, olefin insertion is too facile leading to multiple insertions to generate polymeric product. Catalytic activity with other olefins, e.g., ethylene, was not studied due to the poor activity of *cis*-(*hfac-O,O*)₂Rh(Ph)(py) with benzene and styrene.

Our group has published a series of Ru(II) catalysts for olefin hydroarylation through a mechanism involving metal mediated C–H activation (Scheme 1.15).^{43,46,71,81,82} A main objective of these studies was to look at the effects of sterics and electronics on catalysis. The catalyst are TpRu(L)(NCMe)Ph (Tp = hydridotris(pyrazolyl)borate; L = CO, PMe_3 , P(pyr)_3 , and $\text{P(OCH}_2)_3\text{CEt}$; pyr = *N*-pyrrolyl). Thus the catalyst motif uses a neutral two-electron donor ligand, L, which allows tuning of steric and electronic properties. Additionally, a labile ligand in the equatorial plane is needed so when the catalyst precursor is placed in the presence of an olefin, ligand dissociation and olefin coordination can occur to initiate the catalytic cycle (Figure 1.6). Finally, the κ^3 -coordinated Tp ligand was used. The facial coordination mode restricts orientation for the R–group and the ethylene to a *cis* conformation, which is need for olefin insertion and C–H activation.

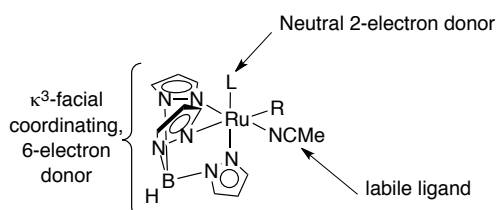


Figure 1.6. Catalyst design motif for Ru(II) complexes for olefin hydroarylation.

Synthetic targets TpRu(L)(NCMe)Ph (Tp = hydridotris(pyrazolyl)borate; L = CO, PMe_3 , P(pyr)_3 , and $\text{P(OCH}_2)_3\text{CEt}$; pyr = *N*-pyrrolyl) are shown in Figure 1.7 and Figure 1.8.

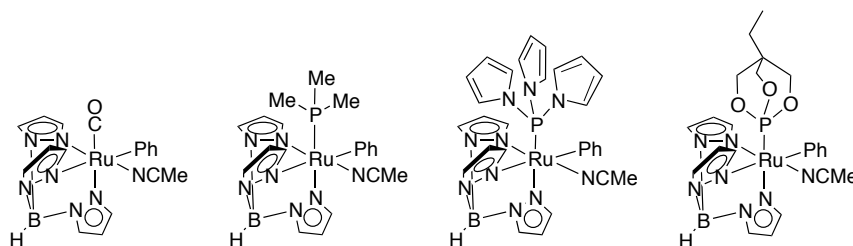
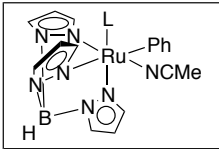


Figure 1.7. TpRu(L)Ph(NCMe) catalyst first examined for olefin hydroarylation.




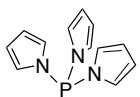
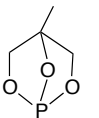
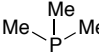
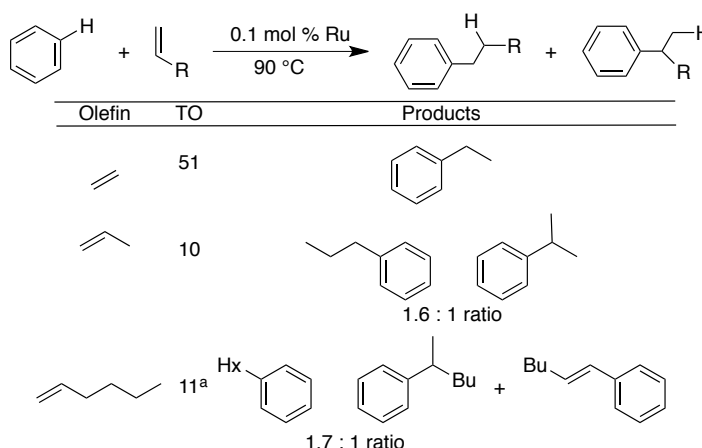
Ligand				
$E_{1/2}$ (V) (vs NHE)	1.03	0.82	0.69	0.29
Cone Angle ($^{\circ}$)	95	145	101	118

Figure 1.8. Electronics and cone angles for TpRu(L)(NCMe)Ph ^{83,84}

The first catalyst for olefin hydroarylation developed in our group was TpRu(CO)(NCMe)Ph .^{71,85} This catalyst is to our knowledge the most active transition metal catalyst for olefin hydroarylation proceeding through a mechanism that involves C–H activation and olefin insertion. At 0.1 mol% Ru, 25 psi of ethylene and 90 °C, 51 turnovers (TO) of ethylbenzene were observed after 4 hours with a total of 77 TO after 24 h before catalyst deactivation to NMR silent materials. When propylene (25 psi) was used as the olefin with 0.1 mol % Ru at 90 °C both cumene and *n*-propylbenzene were observed in a 1:1.6 ratio (Table 1.1). The selectivity for *n*-propylbenzene over cumene supports a non-Friedel-Crafts mechanism. In addition, the reaction of benzene and 1-

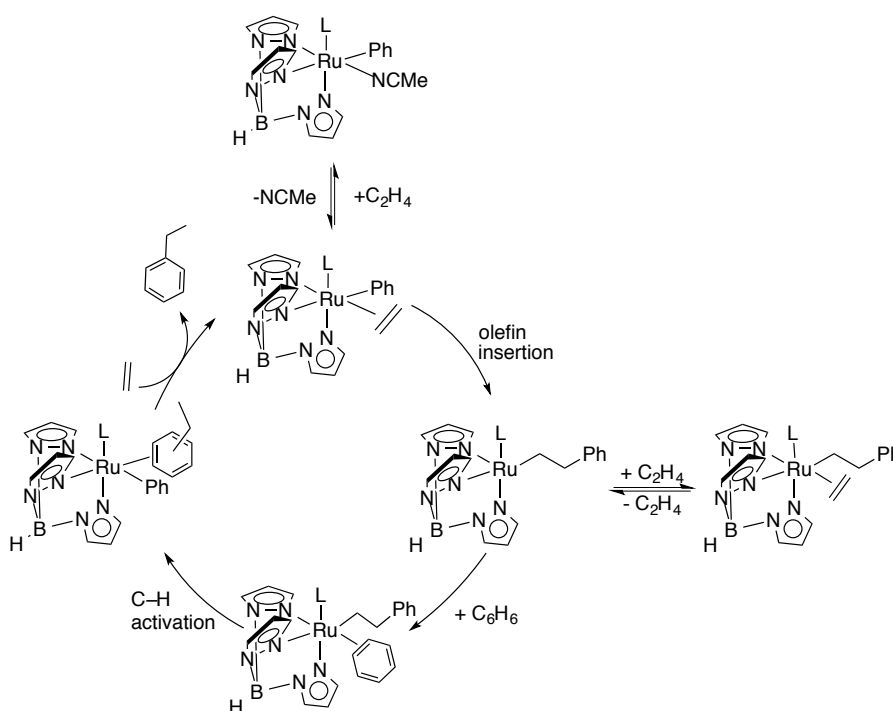
hexene at 90 °C with 1 mol % of Ru catalyst) yielded only 2-phenylhexane and 1-phenylhexane in a 1:1.6 ratio demonstrating catalyst selectivity for the linear product over the branch and no evidence for isomerization of hexene to yield the internal 3-phenylhexane.

Table 1.1. Olefin hydroarylation with $\text{TpRu}(\text{CO})(\text{NCMe})\text{Ph}$ as catalyst (unless otherwise noted, reaction conditions are 90 °C, 25 psi of gas, 0.1 mol% of Ru, 4h. ^a50 equiv. based on Ru, after 6h).



Experimental and computational studies performed by Prof. Thomas Cundari at University of North Texas support the mechanism depicted in Scheme 1.15.⁷¹ Initial, NCMe dissociation followed by olefin coordination forms the catalytic active species. Olefin insertion into the Ru–Ph bond followed by coordination of ethylene leads to formation of a phenethyl/ethylene species (the proposed catalytic resting state). Dissociation of ethylene and subsequent coordination of benzene and C–H activation through what is considered a “oxidative hydrogen migration” transition state,^{42,45} similar

to σ -bond metathesis with non- d^0 metals (Figure 1.9), leads to formation of the alkylated species. Replacement of ethylbenzene with ethylene regenerates the active catalyst. Kinetic isotope studies were completed. Monitoring the product isotopic distribution (i.e., $M_w = 111$ vs 112) for catalytic reactions using a 1:1 solution of $C_6H_6:C_6D_6$ under ethylene pressure lead to a kinetic isotopic effect (KIE) of 2.1(1). Additionally, the KIE for stoichiometric benzene activation by $TpRu(CO)(NCMe)Me$ to produce $TpRu(CO)(NCMe)Ph$ was studied. A KIE of 2.5(5) was determined, which is in agreement with the catalytic benzene activation KIE demonstrating that benzene C–H bond activation is the rate-limiting step of the catalytic cycle.



Scheme 1.15. Proposed Olefin Hydroarylation Catalytic Cycle by $TpRu(L)(NCMe)(R)$.

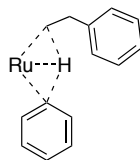
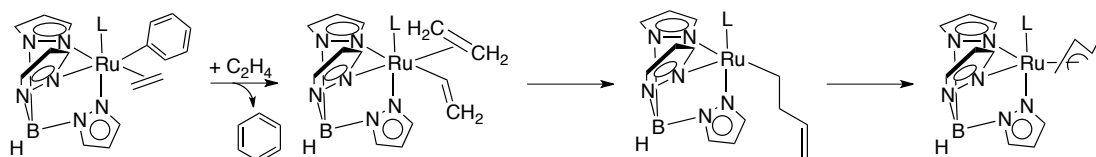


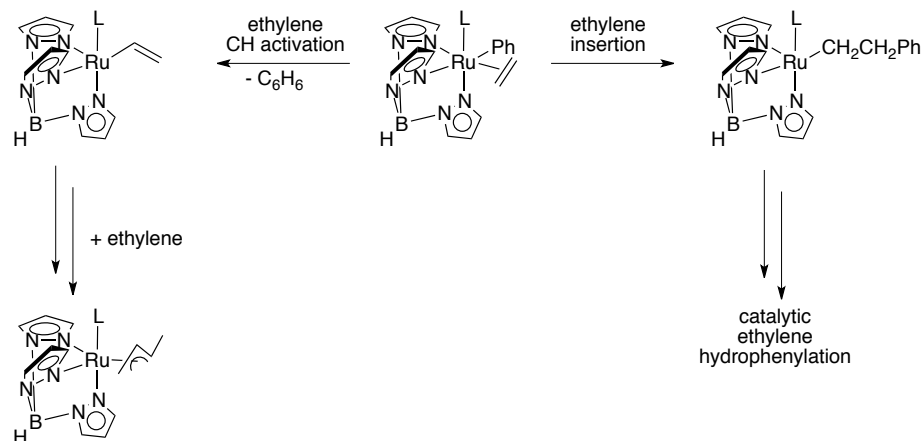
Figure 1.9. C–H activation transition state, “oxidative hydrogen migration”.

To study the effect of increased electron density at the metal center, $\text{TpRu}(\text{PMe}_3)(\text{NCMe})\text{Ph}$ was synthesized and probed for benzene C–H activation as well as catalytic ethylene hydrophenylation.⁸² This complex does not catalyze olefin hydroarylation. Under extreme olefin hydroarylation conditions (0.100 mol % Ru, 180 °C and 800 psi of ethylene) the reaction yields only 3.6 TO of ethylbenzene in 12 h with 2.5 TO of styrene; however, $\text{TpRu}(\text{PMe}_3)(\text{NCMe})\text{Ph}$ is not stable under these conditions; therefore, another species is accomplishing the production of ethylbenzene and styrene.

The increased electron density on the metal center of $\text{TpRu}(\text{PMe}_3)(\text{NCMe})\text{Ph}$ was found to increase the barrier to olefin insertion and cause the ethylene C–H activation to compete with ethylene insertion. Ethylene C–H activation yields a vinyl species upon which a subsequent equivalent of ethylene could coordinate and insert into the $\text{Ru}-\text{C}_{\text{vinyl}}$ bond. Isomerization of the species leads to an η^3 -allyl complex, $\text{TpRu}(\text{PMe}_3)(\eta^3-\text{C}_3\text{H}_4\text{Me})$. This complex has been shown to be inactive in catalyzing olefin hydroarylation (Scheme 1.17, Scheme 1.16). Therefore for $\text{TpRu}(\text{L})(\text{NCMe})\text{Ph}$ catalyst, if the metal center is too electron-rich olefin insertion is inhibited and the rate of olefin C–H activation competes with olefin insertion.

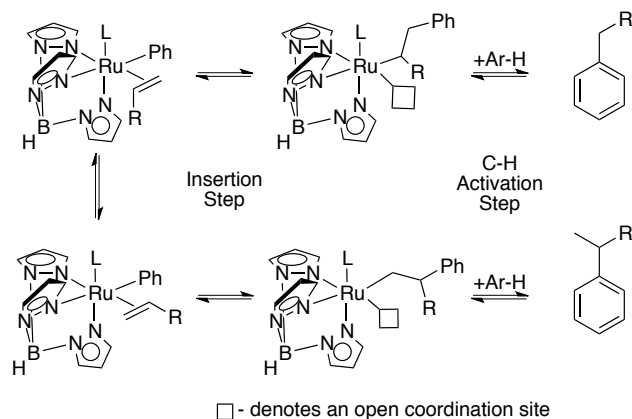


Scheme 1.16. Allyl formation through C–H olefin activation for TpRu(L) complexes.



Scheme 1.17. Competition between ethylene C–H activation and ethylene insertion.

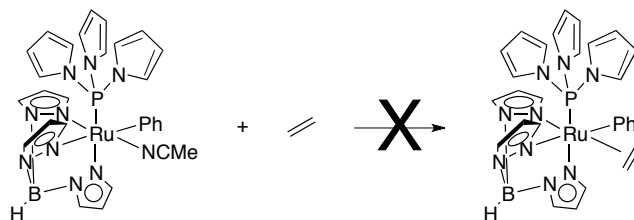
As stated above, $\text{TpRu(PMe}_3\text{)(NCMe)Ph}$ was found to be too electron-donating and unable to accomplish catalytic olefin hydroarylation; furthermore, the less electron rich complex TpRu(CO)(NCMe)Ph is capable of olefin hydroarylation (TON 77 after 24 h). Thus, we sought a phosphite/phosphine that would be similar in electron donating ability as CO. Studies have shown that tris-*N*-pyrrolyl $[\text{P(pyr)}_3]$ phosphine has a similar overall donating ability as CO.⁸⁴ $\text{TpRu[P(pyr)}_3\text{](NCMe)Ph}$ was synthesized and tested to determine if steric bulk would help control the regioselectivity of hydroarylation when α -olefins were employed while having a metal center that was similar in electron density as the CO (Scheme 1.18).⁸¹



Scheme 1.18. Regioselective of α -olefin hydroarylation.

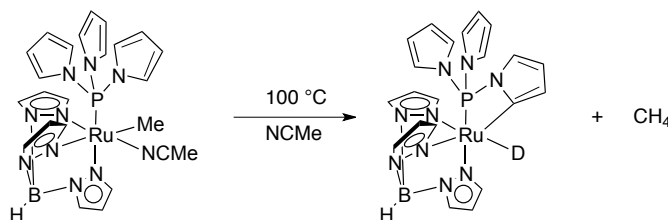
TpRu[P(pyr)₃](NCMe)Ph is not a catalyst for olefin hydroarylation. Upon examining a wide range of temperatures (90 °C – 180 °C) and pressures of ethylene (15 psi – 700 psi), production of ethylbenzene was not observed until 80 psi of ethylene at 120 °C (0.2 TO of ethylbenzene). Under 100 psi of ethylene at 180 °C near stoichiometric amounts of ethylbenzene were produced. TpRu[P(pyr)₃](NCMe)Ph is not stable under these conditions. Due to the lack of catalytic activity observed with TpRu[P(pyr)₃](NCMe)Ph, reactions were conducted to determine if the steric bulk of the P(pyr)₃ was inhibiting catalytic activity. TpRu[P(pyr)₃](NCMe)Ph was placed in an THF-*d*₈ under 80 psi of ethylene at 60 °C for 5 days. The formation of TpRu[P(pyr)₃](η^2 -C₂H₄)Ph was not observed. Hence, it is speculated that the steric bulk of the P(pyr)₃ ligand inhibits ethylene coordination (Scheme 1.19). DFT calculations performed by Dr. Cundari's group at the University of North Texas support the experimental results. Calculations showed that coordination of ethylene to TpRu[P(pyr)₃]Ph is less favorable

than both $\text{TpRu}(\text{CO})\text{Ph}$ and $\text{TpRu}(\text{PMe}_3)\text{Ph}$ by 8.9 kcal/mol and 5.1 kcal/mol, respectively.



Scheme 1.19. Olefin coordination inhibited due to steric bulk of $\text{P}(\text{pyr})_3$.

Intramolecular C–H activation of one pyrrolyl ring of the $\text{P}(\text{pyr})_3$ was also observed under certain conditions with $\text{TpRu}[\text{P}(\text{pyr})_3](\text{NCMe})\text{Me}$. Heating $\text{TpRu}[\text{P}(\text{pyr})_3](\text{NCMe})\text{Me}$ in C_6H_6 lead to the production of $\text{TpRu}[\text{P}(\text{pyr})_3](\text{NCMe})\text{Ph}$, CH_3D and an insoluble NMR inactive species. Similar to $\text{TpRu}(\text{CO})(\text{NCMe})\text{Me}$, the addition of NCMe to the reaction of $\text{TpRu}[\text{P}(\text{pyr})_3](\text{NCMe})\text{Me}$ in C_6D_6 inhibited decomposition; but, it also lead to the formation of a new species (minor), $\text{TpRu}\{\kappa^2\text{-P,C,P-P}(\text{pyr})_2(\text{NC}_4\text{H}_3)\}\text{NCMe}$, due to intramolecular C–H activation of the 2-position of the pyrrolyl (Scheme 1.20).



Scheme 1.20. Intramolecular C–H activation of $\text{TpRu}[\text{P}(\text{pyr})_3](\text{NCMe})\text{Ph}$ to yield $\text{TpRu}\{\kappa^2\text{-P,C-P}(\text{pyr})_2(\text{NC}_4\text{H}_3)\}\text{NCMe}$.

For accessible CH bonds [e.g., P(OMe)_3 or PPh_3], intramolecular CH activation and cyclometallation of the phosphite can inhibit catalysis. Thus, we initially probed $\text{TpRu[P(OMe)}_3\text{](NCMe)R}$; however, cyclometallation of the phosphite inhibited catalysis.⁸⁶ Therefore, the neutral bicyclic phosphite $\text{P(OCH}_2\text{)}_3\text{CEt}$ was explored since the cyclic structure of $\text{P(OCH}_2\text{)}_3\text{CEt}$ would prohibit cyclometallation. Furthermore, it is less donating than PMe_3 and less bulky than P(pyr)_3 ; however, since the ligand is more sterically bulk than CO it was hypothesized that regioselectivity with α -olefins could be achieved.

Under optimal catalyst conditions (0.1 mol %, 90 °C and 10 psi of ethylene) $\text{TpRu[P(OCH}_2\text{)}_3\text{CEt](NCMe)Ph}$ gives 10 TO of ethylbenzene after 28 h. Increasing the pressure of ethylene (e.g., 50 psi) decreases the TO which indicates an inverse dependence on ethylene concentration that is consistent with the proposed mechanism shown in Scheme 1.15. Unfortunately, relatively rapid catalyst deactivation through formation of $\text{TpRu[P(OCH}_2\text{)}_3\text{CEt](}\eta^3\text{-C}_3\text{H}_4\text{Me)}$ was observed. Thus, $\text{TpRu[P(OCH}_2\text{)}_3\text{CEt](NCMe)Ph}$ is too electron-rich and olefin C–H activation is competitive with olefin insertion.

The Gibbs free energies of each step of the catalytic cycle for TpRu(L)(NCMe)Ph were examined using DFT calculations {B3LYP/CEP-31G(d) level of theory} (Scheme 1.21). According to both calculations and experimental results there is a direct correlation between steric bulk of L and the ΔG for ethylene coordination and insertion. For example, the ΔG s for ethylene coordination are negative when $\text{L} = \text{CO}$ (–7.9 kcal/mol),

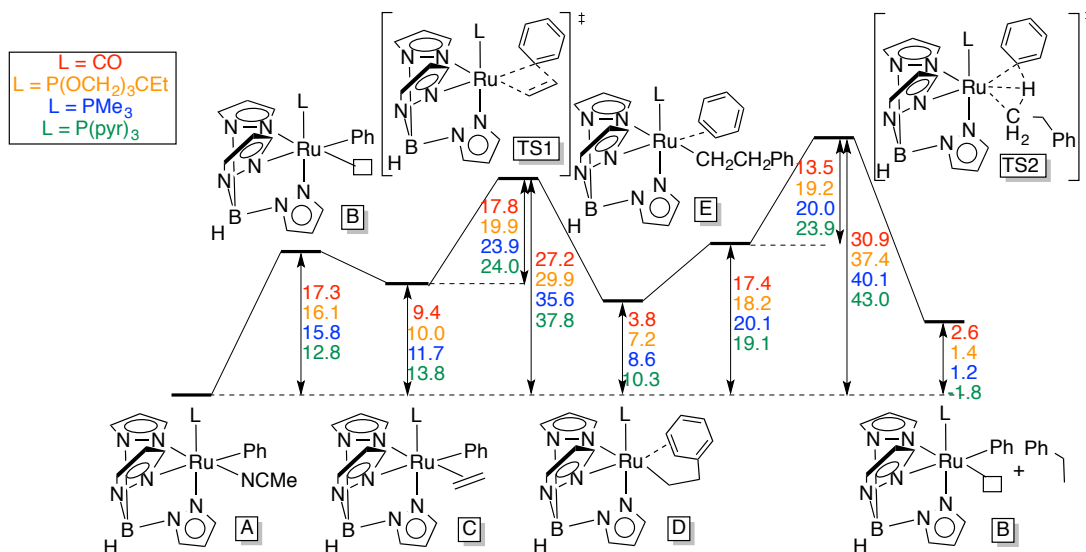
PMe_3 (−4.1 kcal/mol) or $\text{P}(\text{OCH}_2)_3\text{CEt}$ (−6.1 kcal/mol); however, $\text{L} = \text{P}(\text{pyr})_3$ ethylene coordination is overall endergonic at +1 kcal/mol.⁴³

To understand the propensity of $\text{TpRu}(\text{L})(\text{NCMe})\text{Ph}$ ($\text{L} = \text{PMe}_3$ or $\text{P}(\text{OCH}_2)_3\text{CEt}$) to form $\text{TpRu}(\text{L})(\eta^3\text{-C}_3\text{H}_4\text{Me})$, $\Delta\Delta G^\ddagger$ s for ethylene C–H activation and ethylene insertion from $\text{TpRu}(\text{L})(\eta^2\text{-C}_2\text{H}_4)\text{Ph}$ were calculated. Calculations demonstrate a clear trend. As the electron density of the metal center increases, the $\Delta\Delta G^\ddagger$ for ethylene C–H activation and ethylene insertion decrease. When $\text{L} = \text{PMe}_3$ the difference in energies ($\Delta\Delta G^\ddagger$) is 3.1 kcal/mol; whereas, $\text{L} = \text{CO}$ has a significantly larger $\Delta\Delta G^\ddagger$ at 8.6 kcal/mol (Table 1.2).

Table 1.2. Calculated $\Delta G^\ddagger_{\text{insertion}}$ (kcal/mol) for ethylene insertion and $\Delta G^\ddagger_{\text{CH activation}}$ (kcal/mol) of ethylene for $\text{TpRu}(\text{L})(\eta^2\text{-C}_2\text{H}_4)\text{Ph}$ complexes.

L	$\Delta G^\ddagger_{\text{insertion}}$ of C_2H_4	$\Delta G^\ddagger_{\text{C-H activation}}$ of C_2H_4	$\Delta\Delta G^\ddagger$
PMe_3	23.9	27.0	3.1
$\text{P}(\text{pyr})_3$	23.2	28.6	5.4
$\text{P}(\text{OCH}_2)_3\text{CEt}$	20.1	27.3	7.4
CO	26.4	17.8	8.6

Furthermore, calculations show that the rate limiting step for ethylene hydrophenylation is the benzene C–H activation step, which is consistent with experimental results.⁴⁶ However, the calculated $\Delta\Delta G^\ddagger$ for ethylene insertion ($\Delta\Delta G^\ddagger$ of ~6.2 kcal/mol) is larger than the $\Delta\Delta G^\ddagger$ for benzene C–H activation (~4.4 kcal/mol) as the ligand L is varied (Scheme 1.21). Therefore, varying the donor ability of L has a greater impact on the rate of olefin insertion compared to the rate of benzene C–H activation.



Scheme 1.21. Calculated Gibbs Free Energy (kcal/mol) for benzene C–H activation by TpRu(L)(NCMe)Ph [L = CO, P(OCH₂)₃CEt, PMe₃ and P(pyr)₃].

1.5. Summary and Thesis Aims

Through the studies of the TpRu(L)(NCMe)Ph (L = CO, PMe₃, P(pyr)₃, and P(OCH₂)₃CEt) complexes, a few important trends were observed. 1) If the ancillary ligand is too sterically bulky (e.g. P(pyr)₃ cone angle 145°), olefin coordination is inhibited and the catalytic olefin hydroarylation cannot be accessed. 2) Metal centers which are too electronic rich, cause olefin C–H activation to become competitive with olefin insertion and lead to the formation of a TpRu(L)(η³-C₃H₄Me). 3) The ancillary ligand's electron influence is relatively small on the activation barrier for benzene C–H activation (with more electron-donating ligands), slightly reducing the free energy of activation; however, steric influence can have a substantial effect on the rate of olefin insertion vs. C–H activation.

Presented herein is an extension of the previous work on olefin hydroarylation using Ru(II) metal centers. Chapter 2 discusses the studies of the bicyclic phosphite ligand $\text{P}(\overline{\text{OCH}_2})_2(\text{OCCH}_3)$ coordinated to Ru(II). This ligand is predicted to be less electron donating but sterically similar to $\text{P}(\text{OCH}_2)_3\text{CEt}$ and was hoped to lead to a better TpRu(II) olefin hydroarylation catalyst. Chapter 3 delineates the use of $\text{P}(\overline{\text{OCH}_2})_2(\text{OCCH}_3)$ in synthesis of the Ru(II) catalyst $\text{TpRu}[\text{P}(\overline{\text{OCH}_2})_2(\text{OCCH}_3)](\text{NCMe})\text{Ph}$ and its ability to catalyze olefin hydroarylation compared to the previously reported $\text{TpRu}(\text{L})(\text{NCMe})\text{Ph}$ [$\text{L} = \text{CO}$, PMe_3 , $\text{P}(\text{pyr})_3$, and $\text{P}(\text{OCH}_2)_3\text{CEt}$] complexes. Chapter 4 describes a more in-depth study of our $\text{TpRu}(\text{CO})(\text{NCMe})\text{Ph}$ catalyst, and the effects of catalyst loading and ethylene concentration on olefin hydroarylation. As studies with the TpRu(II) catalyst have shown that the electron density of the metal center has more of an impact on olefin insertion versus C–H activation, a more electron poor system was sought. Thus, Chapter 5 discusses the synthesis and screening of other neutral six-electron-donor motifs including $(\eta^6\text{-}p\text{-cymene})\text{Ru}(\text{L})\text{PhBr}$ [$\text{L} = \text{P}(\text{OMe})_3$ or $\text{P}(\text{OCH}_2)_3\text{CEt}$], $\text{C}(\text{pz})_4\text{Ru}[\text{P}(\text{OCH}_2)_3\text{CEt}](\text{NCMe})\text{R}[\text{BAr}^+_4]$ ($\text{C}(\text{pz})_4 = \kappa^3\text{-}N,N,N\text{-tetrakis}(1\text{-pyrazolyl})\text{methane}$) and $\text{HC}(\text{pz}'_3)\text{Ru}[\text{P}(\text{OCH}_2)_3\text{CEt}](\text{NCMe})\text{Ph}$ ($\text{pz}' = 3,5\text{-dimethylpyrazole}$) for catalytic hydroarylation.

1.6. References

- (1) Somorjai, G. A.; Rioux, R. M. *Catal. Today* **2005**, *100*, 201.
- (2) Corma, A. *Chem. Rev.* **1997**, *97*, 2373.
- (3) Gerzeliev, I. M.; Khadzhiev, S. N.; Sakharova, I. E. *Petrol Chem+* **2011**, *51*, 39.
- (4) Perego, C.; Pollesel, P. In *Advances in Nanoporous Materials*; Stefan, E., Ed.; Elsevier: 2010; Vol. 1, p 97.
- (5) Macquarrie, D. J. In *Catalytic Asymmetric Friedel–Crafts Alkylations*; Wiley-VCH: 2009, p 271.
- (6) Perego, C.; Ingallina, P. *Green Chem.* **2004**, *6*, 274.
- (7) Brown, H. C.; Pearsall, H. W.; Eddy, L. P.; Wallace, W. J.; Grayson, M.; Nelson, K. L. *Industrial & Engineering Chemistry* **1953**, *45*, 1462.
- (8) Olah, G. A.; Molnar, A. *Hydrocarbon Chemistry*; 2nd ed.; Wiley-Interscience: New York, 2003.
- (9) You, S.-L.; Cai, Q.; Zeng, M. *Chem. Soc. Rev.* **2009**, *38*, 2190.
- (10) Roberts, R. M.; Khalaf, A. A. *Friedel-Crafts Alkylation Chemistry: A Century of Discovery*; Marcel Dekker, Inc. : New York, 1984.
- (11) Corma, A.; Garcia, H. *Chem. Rev.* **2003**, *103*, 4307.
- (12) Kocal, J. A.; Vora, B. V.; Imai, T. *Appl. Catal., A* **2001**, *221*, 295.
- (13) Perego, C.; Ingallina, P. *Catal. Today* **2002**, *73*, 3.
- (14) Degnan, T. F.; Smith, C. M.; Venkat, C. R. *Appl. Catal., A* **2001**, *221*, 283.
- (15) Cejka, J.; Wichterlova, B. *Catal. Rev.* **2002**, 375.
- (16) O'Kelly, A. A.; Kellett, J., III; Plucker, J. J. *Ind. Eng. Chem.* **1947**, *39*, 154.
- (17) Fechete, I.; Wang, Y.; Védrine, J. C. *Catal. Today* **2012**, *189*, 2.
- (18) Haag, W. O. *Catalysis by Zeolites – Science and Technology*; Elsevier, 1994; Vol. 84.

- (19) O'Connor, C. T.; Van Steen, E.; Dry, M. E. *New Catalytic Applications of Zeolites for Petrochemicals*; Elsevier, 1996; Vol. 102.
- (20) Weitkamp, J. *New Directions in Zeolite Catalysis*; Elsevier, 1991; Vol. 65.
- (21) Tanabe, K.; Hölderich, W. F. *Appl. Catal., A* **1999**, *181*, 399.
- (22) Broach, R. W. In *Zeolites in Industrial Separation and Catalysis*; Wiley-VCH: 2010, p 27.
- (23) Martínez, C.; Corma, A. *Coord. Chem. Rev.* **2011**, *255*, 1558.
- (24) Degnan, T. F. *J. Catal.* **2003**, *216*, 32.
- (25) Kulprathipanja, S. *Zeolites in Industrial Separation and Catalysis*; John Wiley & Sons.
- (26) Guisnet, M.; Ribeiro, F. R. *Deactivation and Regeneration of Zeolite Catalysts*; Imperial College Press: London, 2011.
- (27) Stanforth, S. P. *Tetrahedron* **1998**, *54*, 263.
- (28) Negishi, E.-I.; Anastasia, L. *Chem. Rev.* **2003**, *103*, 1979.
- (29) Beletskaya, I. P.; Cheprakov, A. V. *Chem. Rev.* **2000**, *100*, 3009.
- (30) Corbet, J.-P.; Mignani, G. *Chem. Rev.* **2006**, *106*, 2651.
- (31) Shen, H. C. *Selected Applications of Transition Metal-Catalyzed Carbon-Carbon Cross-Coupling Reactions in the Pharmaceutical Industry*; John Wiley & Sons, Inc., 2012.
- (32) Caron, S.; Ghosh, A.; Gut Ruggeri, S.; Ide, N. D.; Nelson, J. D.; Ragan, J. A. *Selected Metal-Mediated Cross-Coupling Reactions*; John Wiley & Sons, Inc., 2011.
- (33) Carey, F. A.; Sundberg, R. J. *Advanced Organic Chemistry*; 5th ed.; Springer, 2007.
- (34) Negishi, E.-i. *Angew. Chem. Int. Ed.* **2011**, *50*, 6738.
- (35) Colacot, T. J. *Platinum Met. Rev.* **2011**, *55*, 84.
- (36) Lipshutz, B. H.; Taft, B. R.; Abela, A. R.; Ghorai, S.; Krasovskiy, A.; Duplais, C. *Platinum Met. Rev.* **2012**, *56*, 62.

- (37) Miyaura, N.; Suzuki, A. *Chem. Rev.* **1995**, *95*, 2457.
- (38) Fortman, G. C.; Nolan, S. P. *Chem. Soc. Rev.* **2011**, *40*, 5151.
- (39) Kuhl, N.; Hopkinson, M. N.; Wencel-Delord, J.; Glorius, F. *Angew. Chem. Int. Ed.* **2012**, *51*, 10236.
- (40) Fu, G. C. *Acc. Chem. Res.* **2008**, *41*, 1555.
- (41) Cornils, B.; Herrmann, W. A. In *Applied Homogeneous Catalysis with Organometallic Compounds*; Wiley-VCH Verlag GmbH: 2008, p 599.
- (42) Oxgaard, J.; Periana, R. A.; Goddard, W. A. *J. Am. Chem. Soc.* **2004**, *126*, 11658.
- (43) Foley, N. A.; Lee, J. P.; Ke, Z. F.; Gunnoe, T. B.; Cundari, T. R. *Acc. Chem. Res.* **2009**, *42*, 585.
- (44) Oxgaard, J.; Muller, R. P.; Goddard, W. A.; Periana, R. A. *J. Am. Chem. Soc.* **2004**, *126*, 352.
- (45) Oxgaard, J.; Goddard, W. A. *J. Am. Chem. Soc.* **2004**, *126*, 442.
- (46) Foley, N. A.; Ke, Z. F.; Gunnoe, T. B.; Cundari, T. R.; Petersen, J. L. *Organometallics* **2008**, *27*, 3007.
- (47) Lewis, J. C.; Bergman, R. G.; Ellman, J. A. *Acc. Chem. Res.* **2008**, *41*, 1013.
- (48) Colby, D. A.; Bergman, R. G.; Ellman, J. A. *Chem. Rev.* **2010**, *110*, 624.
- (49) Engle, K. M.; Mei, T.-S.; Wasa, M.; Yu, J.-Q. *Acc. Chem. Res.* **2012**, *45*, 788.
- (50) Chen, X.; Engle, K. M.; Wang, D.-H.; Yu, J.-Q. *Angew. Chem. Int. Ed.* **2009**, *48*, 5094.
- (51) Neufeldt, S. R.; Sanford, M. S. *Acc. Chem. Res.* **2012**, *45*, 936.
- (52) Daugulis, O.; Do, H.-Q.; Shabashov, D. *Acc. Chem. Res.* **2009**, *42*, 1074.
- (53) Hartwig, J. F. *Acc. Chem. Res.* **2011**, *45*, 864.
- (54) Hickman, A. J.; Sanford, M. S. *ACS Catalysis* **2011**, *1*, 170.

- (55) Baxter, R. D.; Sale, D.; Engle, K. M.; Yu, J.-Q.; Blackmond, D. G. *J. Am. Chem. Soc.* **2012**, *134*, 4600.
- (56) Goj, L. A.; Gunnoe, T. B. *Curr. Org. Chem.* **2005**, *9*, 671.
- (57) Ritleng, V.; Sirlin, C.; Pfeffer, M. *Chem. Rev.* **2002**, *102*, 1731.
- (58) Nadres, E. T.; Daugulis, O. *J. Am. Chem. Soc.* **2011**, *134*, 7.
- (59) Lin, B. L.; Bhattacharyya, K. X.; Labinger, J. A.; Bercaw, J. E. *Organometallics* **2009**, *28*, 4400.
- (60) Sevov, C. S.; Hartwig, J. F. *J. Am. Chem. Soc.* **2013**, *135*, 2116.
- (61) Jia, C.; Piao, D.; Oyamada, J.; Lu, W.; Kitamura, T.; Fujiwara, Y. *Science* **2000**, *287*, 1992.
- (62) Bowring, M. A.; Bergman, R. G.; Tilley, T. D. *Organometallics* **2011**, *30*, 1295.
- (63) Jia, C. G.; Kitamura, T.; Fujiwara, Y. *Acc. Chem. Res.* **2001**, *34*, 633.
- (64) Kakiuchi, F.; Murai, S. *Acc. Chem. Res.* **2002**, *35*, 826.
- (65) Colby, D. A.; Bergman, R. G.; Ellman, J. A. *Chem Rev* **2010**, *110*, 624.
- (66) Kubota, A.; Emmert, M. H.; Sanford, M. S. *Org Lett* **2012**, *14*, 1760.
- (67) Andreatta, J. R.; McKeown, B. A.; Gunnoe, T. B. *J. Organomet. Chem.* **2011**, *696*, 305.
- (68) Luedtke, A. T.; Goldberg, K. I. *Angew. Chem., Int. Ed.* **2008**, *47*, 7694.
- (69) Periana, R. A.; Liu, X. Y.; Bhalla, G. *Chem. Commun.* **2002**, 3000.
- (70) McKeown, B. A.; Foley, N. A.; Lee, J. P.; Gunnoe, T. B. *Organometallics* **2008**, *27*, 4031.
- (71) Lail, M.; Bell, C. M.; Conner, D.; Cundari, T. R.; Gunnoe, T. B.; Petersen, J. L. *Organometallics* **2004**, *23*, 5007.
- (72) Karshtedt, D.; Bell, A. T.; Tilley, T. D. *Organometallics* **2004**, *23*, 4169.
- (73) McKeown, B. A.; Gonzalez, H. E.; Friedfeld, M. R.; Gunnoe, T. B.; Cundari, T. R.; Sabat, M. *J. Am. Chem. Soc.* **2011**, *133*, 19131.

- (74) Karshtedt, D.; McBee, J. L.; Bell, A. T.; Tilley, T. D. *Organometallics* **2006**, 25, 1801.
- (75) Jones, W. D.; Maguire, J. A.; Rosini, G. P. *Inorg. Chim. Acta* **1998**, 270, 77.
- (76) Cucciolito, M. E.; D'Amora, A.; Tuzi, A.; Vitagliano, A. *Organometallics* **2007**, 26, 5216.
- (77) Jia, C. G.; Lu, W. J.; Oyamada, J.; Kitamura, T.; Matsuda, K.; Irie, M.; Fujiwara, Y. *J. Am. Chem. Soc.* **2000**, 122, 7252.
- (78) Jia, C. G.; Lu, W. J.; Kitamura, T.; Fujiwara, Y. *Org Lett* **1999**, 1, 2097.
- (79) Matsumoto, T.; Taube, D. J.; Periana, R. A.; Taube, H.; Yoshida, H. *J. Am. Chem. Soc.* **2000**, 122, 7414.
- (80) Tenn III, W. J.; Conley, B. L.; Bischof, S. M.; Periana, R. A. *J. Organomet. Chem.* **2011**, 696, 551.
- (81) Foley, N. A.; Lail, M.; Gunnoe, T. B.; Cundari, T. R.; Boyle, P. D.; Petersen, J. L. *Organometallics* **2007**, 26, 5507.
- (82) Foley, N. A.; Lail, M.; Lee, J. P.; Gunnoe, T. B.; Cundari, T. R.; Petersen, J. L. *J. Am. Chem. Soc.* **2007**, 129, 6765.
- (83) Tolman, C. A. *Chem. Rev.* **1977**, 77, 313.
- (84) Moloy, K. G.; Petersen, J. L. *J. Am. Chem. Soc.* **1995**, 117, 7696.
- (85) Lail, M.; Arrowood, B. N.; Gunnoe, T. B. *J. Am. Chem. Soc.* **2003**, 125, 7506.
- (86) *Unpublished results from a former Gunnoe group member.*

2. Structural and Electronic Properties of Ru(II) Complexes Containing $\text{P}(\text{OCH}_2)_2(\text{OCCH}_3)$.

2.1. Introduction

Phosphorous-based compounds offer a wide range of steric properties and basicities due to the variety of accessible substituents,¹⁻¹⁶ and many phosphorous-based compounds bind strongly to transition metals. As a result of their coordinating ability and highly tunable stereoelectronic character, phosphorous-based compounds are among the most heavily utilized class of ligands in coordination chemistry and homogeneous catalysis.^{1-3,5-7,9,16-19} Several studies have quantified the steric and donor properties of a wide range of phosphorous-based ligands.^{6,8,10-16,20-22} For example, the classic work by Tolman established the comparison of the steric properties of phosphorus ligands using cone angles.⁶ The donor abilities of phosphorous ligands have been studied using CO absorption energies for metal carbonyl complexes with phosphorous ligands [*e.g.*, $\text{Ni}(\text{CO})_3\text{L}$ where L = phosphite, phosphine, etc.].⁶

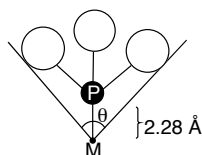
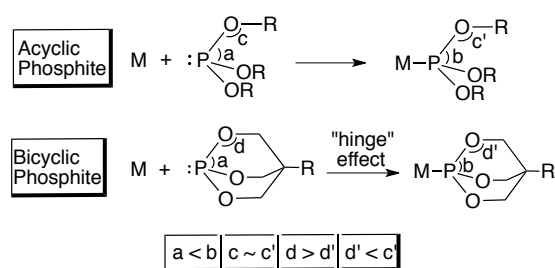


Figure 2.1. Tolman's method for measuring cone angle for phosphines/phosphites.⁶

Bicyclic phosphites have been investigated and compared to acyclic phosphites. In general, the steric profiles of bicyclic phosphites are constrained relative to acyclic compounds, and cyclic phosphites exhibit reduced basicity relative to acyclic phosphites.

Verkade has proposed the “hinge” effect to explain the influence of the bicyclic phosphites’ rigidity on basicity (Scheme 2.1).^{3,23-26} Uncoordinated phosphites adopt a trigonal pyramidal geometry, while coordination (or protonation) of the phosphite results in a shift toward tetrahedral geometry. Upon coordination to a metal center, the O–P–O and the P–O–C angles of an acyclic phosphite can adjust independently. But, reorganization of bicyclic phosphites upon metal ligation is more restricted because adjustment of the O–P–O angle influences the P–O–C angle. For coordinated phosphites, bicyclic phosphites exhibit a smaller P–O–C angle compared to the acyclic phosphites (*i.e.*, $d' < c'$ in Scheme 2.1). Verkade has proposed that these changes result in a reduction of the *p*-orbital overlap between O and P, which increases the positive charge on the P atom and decreases the basicity relative to acyclic phosphites. Thus, the donor ability of bicyclic phosphites is reduced relative to related acyclic phosphites.^{27,28}



Scheme 2.1. Comparison of acyclic and bicyclic phosphites based on the hinge effect.

The hinge effect looks at the influence of the *p*-orbital; however, another orbital that can contribute to the π -acidity of phosphites is the vacant P–O σ^* orbital, which has

been proposed to play a role in $d\pi$ -to-P orbital back-bonding.¹ Specifically with the bicyclic phosphites, the energy level of the σ^* orbital can be related to the O–P–O bond angles. As the O–P–O angle is constrained the overlap between the metal and the P–O σ -orbitals decreases which raises the energy of the σ -orbital lowers the energy of the P–O σ^* . The decrease energy of the P–O σ^* provides better overlap with the metal $d\pi$ orbitals. As a result, more electron density can be donated from the metal center to the ligand decreasing the electron density on the metal center (Figure 2.2).

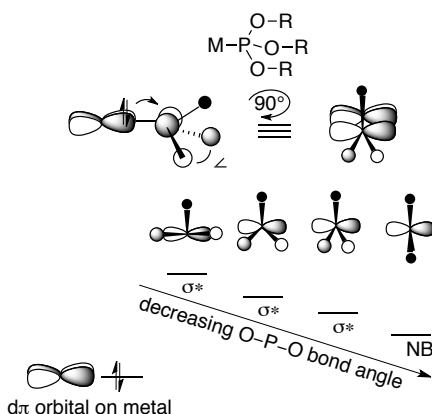


Figure 2.2. Anticipated impact of O–P–O bond angle of σ^* (P–O) orbital energy and, hence, $d\pi$ -to- σ^* back bonding.

A few bicyclic phosphites have been prepared and studied, and similar to acyclic phosphorous-based ligands their steric and donor properties are variable (Figure 2.3).^{6,29} While several examples of transition metal complexes with bicyclic phosphite ligands are known, including nickel, cobalt, iron, chromium, molybdenum and tungsten complexes,^{2-4,30-32} however to our knowledge, no example of a structurally characterized transition

metal complex with $\text{P}(\overline{\text{OCH}_2})_2(\text{OCCH}_3)$ (1) (4-methyl-2,6,7-trioxa-1-

phosphabicyclo[2,2,1]heptane) is known. The structure of the phosphate $\text{O}=\text{P}(\overline{\text{OCH}_2})_2(\text{OCCH}_3)$ has been reported.²⁹ Verkade *et al.* have studied a variety of polycyclic phosphorous compounds including their coordination to transition metals.^{2,3,24,27,29,30} Based on trends in basicity, it is anticipated that **1** would be less donating to metal centers than the more commonly studied bicyclic phosphite $\text{P}(\text{OCH}_2)_3\text{CEt}$.²⁸

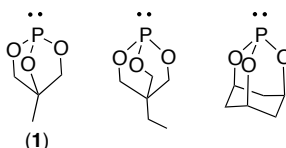


Figure 2.3. Examples of bicyclic phosphites.

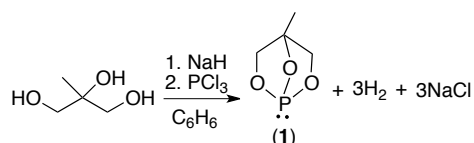
Phosphorous-based ligands are generally considered good donor ligands; however, we felt that phosphite **1** might provide a relatively weakly donating phosphorus-based ligand. In order to study phosphite **1** and compare its donor ability to other phosphorous-based ligands as well as other non-phosphorous based ligands (e.g., CO), we sought suitable transition metal systems that would allow the coordination of several phosphorous-based ligands.

2.2. Results and Discussion

2.2.1. Synthesis of $\text{P}(\overline{\text{OCH}_2})_2(\text{OCCH}_3)$

The preparation of **1** from 2-methyl-1,2,3-propanetriol has been reported.³³ Our attempts to synthesize and cleanly isolate **1** using this procedure were not successful. In addition, using alternate procedures reported for similar bicyclic phosphorous species did

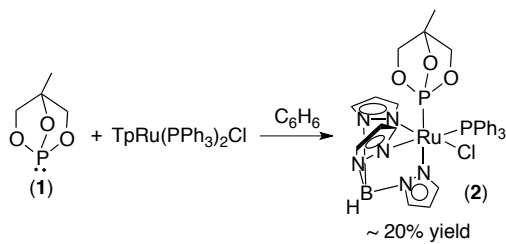
not result in the clean isolation of **1**.^{24,30,34,35} Thus, we developed a modified procedure that involves the *in situ* generation and subsequent reaction of **1** without isolation.^{36,37} The reaction of 2-methyl-1,2,3-propanediol with 3 equivalents of NaH followed by addition of PCl₃ leads to the formation of compound **1**, as evidenced by a single resonance at 115 ppm in the ³¹P NMR spectrum (Scheme 2.2).



Scheme 2.2. Synthesis of $\text{P}(\text{OCH}_2)_2(\text{OCCH}_3)$ (**1**).

2.2.2. Synthesis and Characterization of $\text{TpRu}(\text{L})(\text{PPh}_3)\text{Cl}$ Complexes

The addition of $\text{TpRu}(\text{PPh}_3)_2\text{Cl}$ to a benzene solution of **1** followed by reflux results in the formation of $\text{TpRu}[\text{P}(\text{OCH}_2)_2(\text{OCCH}_3)](\text{PPh}_3)\text{Cl}$ (**2**) (Scheme 2.3). For **2**, the methylene hydrogen atoms are diastereotopic as indicated by three resonances (one missing due to coincidental overlap) due to the two CH₂ groups (3.93, 3.45, 3.50 ppm) with ²J_{HH} = 8 Hz and ³J_{HP} between 8 Hz and 3.6 Hz. Furthermore, a ⁴J_{HH} of 1.4 Hz is observed for two of the methylene hydrogen atoms (Figure 2.4, Figure 2.5, Table 2.1). The observation of 9 unique Tp resonances is also consistent with an asymmetric complex.



Scheme 2.3. Synthesis of $\text{TpRu}[\text{P}(\text{OCH}_2)_2(\text{OCCH}_3)](\text{PPh}_3)\text{Cl}$ (**2**).

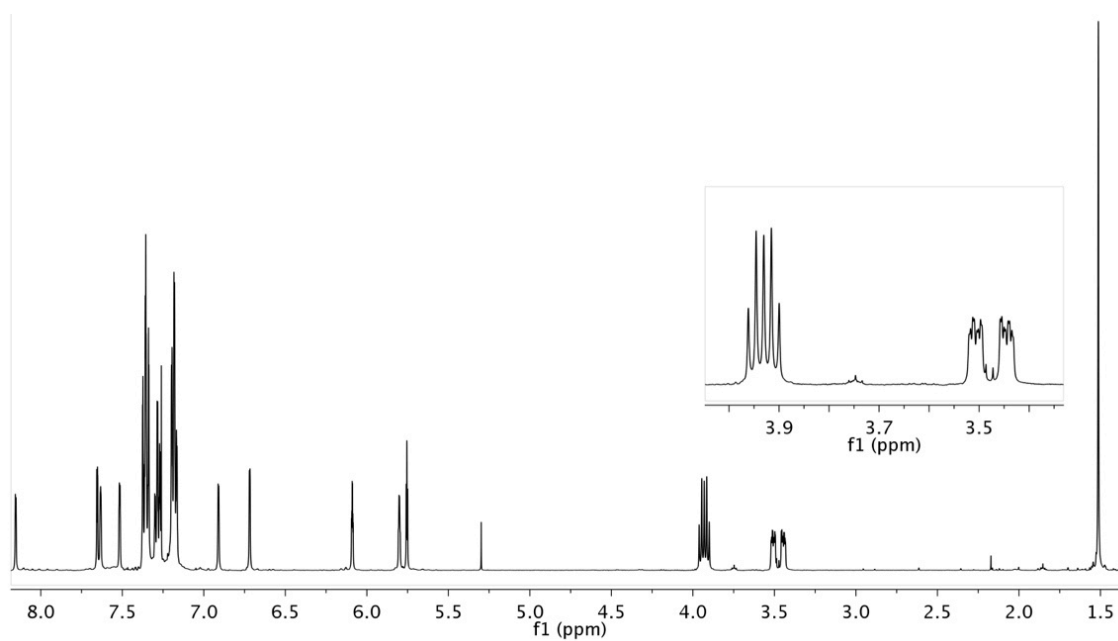


Figure 2.4. ^1H NMR spectrum of $\text{TpRu}[\text{P}(\text{OCH}_2)_2(\text{OCCH}_3)](\text{PPh}_3)\text{Cl}$ (**2**) in CDCl_3 .

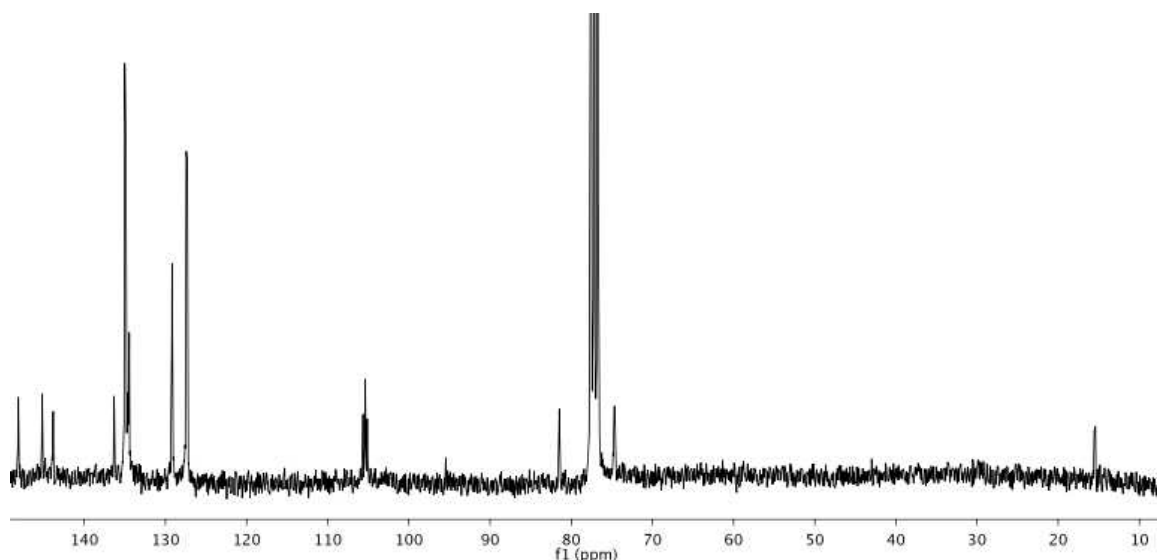
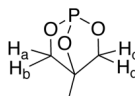


Figure 2.5. ^{13}C NMR spectrum of $\text{TpRu}[\text{P}(\text{OCH}_2)_2(\text{OCCH}_3)](\text{PPh}_3)\text{Cl}$ (**2**) in CDCl_3 .

Table 2.1. Coupling constants observed for the $\text{P}(\text{OCH}_2)_2(\text{OCCH}_3)$ ligand in the ^1H NMR spectrum of $\text{TpRu}[\text{P}(\text{OCH}_2)_2(\text{OCCH}_3)](\text{PPh}_3)\text{Cl}$ (**2**).

		$^2J_{\text{HH}}$	$^3J_{\text{HP}}$	$^4J_{\text{HH}}$
	H _a	8.0 Hz ^b	8.0 Hz	- ^a
	H _b	8.0 Hz ^b	3.6 Hz	1.4 Hz
	H _c	8.0 Hz	8.0 Hz	- ^a
	H _d	8.0 Hz	3.6 Hz	1.4 Hz

^a A third coupling constant was not resolved for these resonances. ^b $^2J_{\text{HaHb}}$. ^c $^2J_{\text{HcHd}}$.

An X-ray diffraction study was performed on a crystal of complex **2** (Figure 2.6, Table 2.2). A search of the Cambridge Structural Database revealed no other examples of structures with phosphite **1**. We have previously reported the structure of $\text{TpRu}[\text{P}(\text{OCH}_2)_3\text{CEt}](\text{PPh}_3)\text{Cl}$ (**3**).³¹ The $\text{Ru}-\text{P}_{\text{phosphite}}$ bond lengths for complexes **2** and **3**

are 2.191(1) Å and 2.2025(8) Å respectively. Thus, phosphite **1** exhibits a slightly shorter Ru–P_{phosphite} bond distance than P(OCH₂)₃CEt. The average P_{phosphite}–O bond distance for complex **2** is 1.627(3) Å, whereas complex **3** has a shorter average P_{phosphite}–O bond length of 1.605(2) Å. The longer P–O bond distances for **1** [compared to P(OCH₂)₃CEt] are anticipated if ligand **1** functions as a better π -acid than P(OCH₂)₃CEt and the dp-backbonding involves the P–O σ^* orbitals.¹ Complex **2** exhibits one larger [100.2(1)°] and two smaller [94.6(1)° and 95.0(1)°] O–P–O bond angles. The O2–P1–Ru angle in complex **2** is 126.2(1)°, whereas the O3–P1–Ru and O1–P1–Ru angles are 116.80(1)° and 118.49(1)°. The O3–P_{phosphite}–Ru angles [118.33(9)°, 113.34(9)° and 118.79(9)°] of **3** are similar to the same angles with O1 and O3 of complex **2**. For the C_{phosphite}–O–P_{phosphite} angles, complex **2** has one angle smaller than the other two [97.5(2)° vs. 107.3(2)° and 107.4(2)°]. For complex **3**, all the angles for C_{phosphite}–O–P_{phosphite} are similar at 116.9(2)°, 115.8(2)° and 116.5(2)°. Thus, the C_{phosphite}–O–P_{phosphite} angles of **2** are smaller than **3**, which is consistent with a more pronounced “hinge” effect for **1** compared to P(OCH₂)₃CEt. Cone angles were calculated from crystallographic data for the phosphite ligands of complexes **2** and **3**. Using the P1–Ru–O angles and the van der Waals radius for oxygen, the cone angle for complex **2** was determined to be 104°, whereas complex **3** is slightly larger at 108° (Figure 2.7). Those cone angles cannot be directly compared to Tolman’s published cone angles since the M–P bond length in the crystallographic data was not adjusted to be 2.28 Å.¹⁴ The cone angle of P(OMe)₃ is 107°.

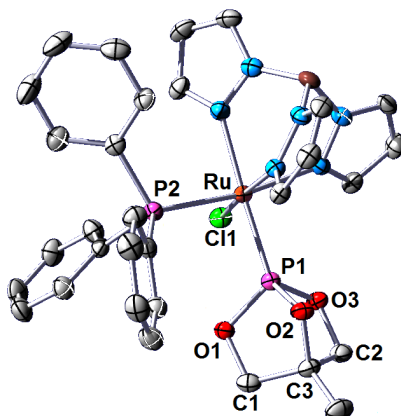


Figure 2.6. ORTEP of $\text{TpRu}[\text{P}(\text{OCH}_2)_2(\text{OCCH}_3)](\text{PPh}_3)\text{Cl}$ (**2**) (50% probability with hydrogen atoms omitted.). Selected bond lengths (Å): Ru–P1, 2.191(1); Ru–P2, 2.342(1); P–O1, 1.627(3); P–O2, 1.632(3); P–O3, 1.620(3). Selected bond angles (°): P1–Ru–P2, 94.1(4); O3–P1–O1, 100.2(1); O3–P1–O2, 94.6(1); O1–P1–O2, 95.0(1); O1–P1–Ru, 118.5(1); O2–P1–Ru, 126.2(1); O3–P1–Ru, 116.8(1); C1–O1–P1, 107.3(2); C3–O2–P1, 97.5(2); C2–O3–P1, 107.4(2).

Table 2.2. Selected Crystallographic Data for $\text{TpRu}(\text{PPh}_3)[\text{P}(\text{OCH}_2)_2(\text{OCCH}_3)]\text{Cl}$ (**2**), $(\eta^6\text{-C}_6\text{H}_6)\text{Ru}[\text{P}(\text{OCH}_2)_2(\text{OCCH}_3)]\text{Cl}_2$ (**11**) and $(\eta^6\text{-}p\text{-cymene})\text{Ru}[\text{P}(\text{OCH}_2)_2(\text{OCCH}_3)]\text{Cl}_2$ (**12**).

	complex 2 •CH ₂ Cl ₂	complex 11 •(CHCl ₃) ₂	complex 12 •(CH ₂ Cl ₂) ₂
empirical formula	C ₃₂ H ₃₄ BCl ₃ N ₆ O ₃ P ₂ Ru	C ₁₂ H ₁₅ Cl ₈ O ₃ PRu	C ₁₈ H ₂₉ Cl ₆ O ₃ PRu
Fw	830.82	622.88	638.15
cryst syst	monoclinic	monoclinic	monoclinic
space group	<i>P</i> 2 ₁ / <i>c</i>	<i>P</i> 2 ₁ / <i>c</i>	<i>P</i> 2 ₁ / <i>n</i>
<i>a</i> , Å	14.5126(3)	10.219(1)	10.7611(3)
<i>b</i> , Å	13.5883(3)	10.518(1)	10.4473(3)
<i>c</i> , Å	17.8390(4)	20.162(2)	22.4999(6)
<i>b</i> , deg	93.643(1)	99.416(1)	99.312(1)
<i>V</i> , Å ³	3510.8(1)	2137.9(4)	2496.2(1)
<i>Z</i>	4	4	4
<i>D</i> _{calcd} , mg/m ³	1.572	1.935	1.698
<i>R</i> 1, <i>wR</i> 2 (<i>I</i> > 2(<i>I</i>))	0.0346, 0.0994	0.0492, 0.1298	0.0253, 0.0965
GOF	0.833	1.056	0.863

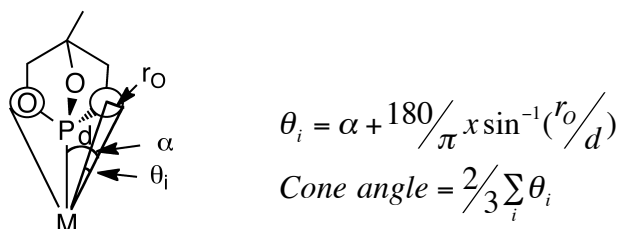


Figure 2.7. Calculation of cone angles using crystallographic data.¹⁴

In addition to **2** and **3**, $\text{TpRu}(\text{PMe}_3)(\text{PPh}_3)\text{Cl}$ (**4**) and $\text{TpRu}[\text{P}(\text{OMe})_3](\text{PPh}_3)\text{Cl}$ (**5**).³⁸ $\text{TpRu}[\text{P}(\text{OMe})_3](\text{PPh}_3)$ (**5**) were synthesized and isolated in the same manner as complexes **2** and **3** by refluxing in C_6H_6 . The ^1H NMR spectrum shows a doublet at 3.24 ppm with a coupling constant of $^3J_{\text{HP}} = 10.3$ Hz for the coordinated $\text{P}(\text{OMe})_3$ ligand (Figure 2.8, Figure 2.9). The relative donor-ability of **1** [compared to PMe_3 , $\text{P}(\text{OMe})_3$ and $\text{P}(\text{OCH}_2)_3\text{CEt}$] was probed by comparing the $\text{Ru}(\text{III}/\text{II})$ redox potentials of $\text{TpRu}(\text{L})(\text{PPh}_3)\text{Cl}$ [$\text{L} = \text{P}(\text{OCH}_2)_2(\text{OCCH}_3)$ (**2**), $\text{P}(\text{OCH}_2)_3\text{CEt}$ (**3**), PMe_3 (**4**) and $\text{P}(\text{OMe})_3$ (**5**)] complexes (Table 2.3).^{31,38} The $\text{Ru}(\text{III}/\text{II})$ potentials indicate the following trend in overall donor ability: $\text{PMe}_3 > \text{P}(\text{OMe})_3 > \text{P}(\text{OCH}_2)_3\text{CEt} > \mathbf{1}$. The $\text{Ru}(\text{III}/\text{II})$ potentials of complexes **2** and **3** differ by 0.13 V (1.08 V and 0.95 V, respectively) with the potential of **2** positive compared to the potential of **3**, thus supporting the hypothesis that ligand **1** is less donating overall than $\text{P}(\text{OCH}_2)_3\text{CEt}$.

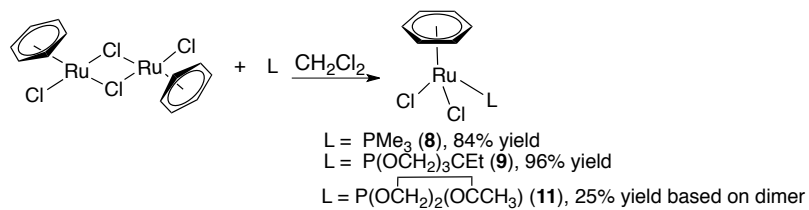
Table 2.3. Ru(III/II) potentials for TpRu(L)(PPh₃)Cl complexes. Data from cyclic voltammetry in NCMe with reversible potentials (E_{1/2}) reported vs NHE (in V).

Chemical structures of the complexes are shown in Figure 1. The complexes are all of the type $\text{Ru}(\text{PPh}_3)_2\text{Cl}(\text{L})$, where L is a 1,3,5-trisubstituted-1H-pyrazole-4-borane derivative. The complexes are all of the type $\text{Ru}(\text{PPh}_3)_2\text{Cl}(\text{L})$, where L is a 1,3,5-trisubstituted-1H-pyrazole-4-borane derivative. The complexes are all of the type $\text{Ru}(\text{PPh}_3)_2\text{Cl}(\text{L})$, where L is a 1,3,5-trisubstituted-1H-pyrazole-4-borane derivative.

Ligand	$E_{1/2}$
(2)	1.08
(3)	0.95
(5)	0.88
(4)	0.75

2.2.3. Synthesis and Characterization (η^6 -C₆H₆)Ru(L)Cl₂ Complexes

To gain further insight into the donor ability of **1**, we prepared a series of (η^6 -C₆H₆)Ru(L)Cl₂ complexes [L = PPh₃ (**6**), P(OMe)₃ (**7**), PMe₃ (**8**), P(OCH₂)₃CEt (**9**), CO (**10**) and P(OCH₂)₂(OCCH₃) (**11**)].³⁹⁻⁴⁵ Our main reasons for selecting this ligand set are the literature precedent and the ease of synthesis. The syntheses of complexes **6**, **7** and **10** have been previously reported.^{39,40} Complexes **8**, **9** and **11** were synthesized by stirring commercially available [(η^6 -C₆H₆)Ru(Cl)(μ -Cl)]₂ with excess L in dichloromethane (Scheme 2.4). ¹H NMR spectroscopy of (η^6 -C₆H₆)Ru(PMe₃)Cl₂ (**8**) shows a singlet for the η^6 -coordinated benzene and a distinct doublet at 1.65 ppm with a ²J_{HP} of 11.4 Hz for PMe₃ (Figure 2.10, Figure 2.11). Complex **9** differs from complexes **8** and **11** in that it lacks solubility in dichloromethane and thus precipitates during synthesis. Similar to complex **8**, the ¹H NMR spectrum of (η^6 -C₆H₆)Ru[P(OCH₂)₃CEt] Cl₂ (**9**) has a singlet for the coordinated η^6 -benzene. A doublet is also observed for the methylene groups of the phosphite, with the ethyl-tail of the phosphite, P(OCH₂)₃CEt, giving the characteristic quartet and triplet (Figure 2.12, Figure 2.13). The ¹H NMR spectrum of complex **11** shows a singlet for coordinated η^6 -benzene. Additionally, the methylene hydrogen atoms of the phosphite are diastereotopic, similar to complex **2**, and give us two distinct resonances, a triplet and a doublet; while a singlet is observed for the methyl group (Figure 2.14, Figure 2.15).



Scheme 2.4. Synthesis of $(\eta^6\text{-C}_6\text{H}_6)\text{Ru}(\text{L})\text{Cl}_2$ ($\text{L} = \text{PMe}_3$, $\text{P}(\text{OCH}_2)_3\text{CEt}$ and $\text{P}(\text{OCH}_2)_2(\text{OCCH}_3)$).

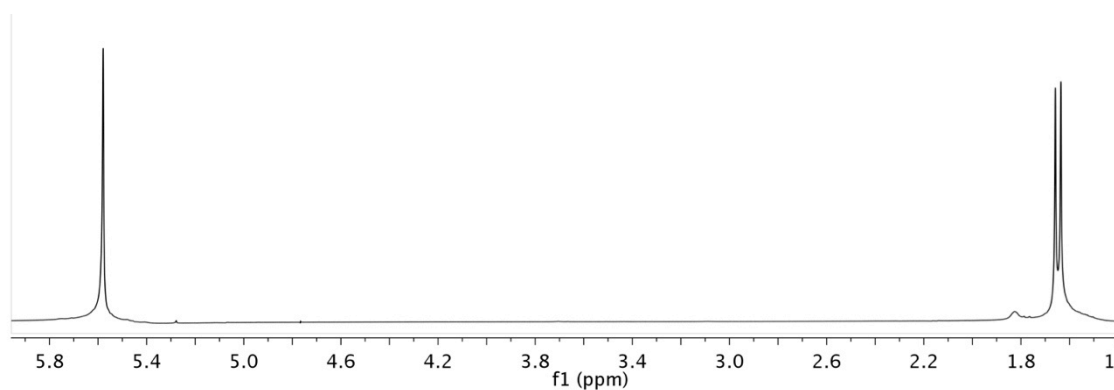


Figure 2.10. ^1H NMR spectrum of $(\eta^6\text{-C}_6\text{H}_6)\text{Ru}(\text{PMe}_3)\text{Cl}_2$ (**8**) in CDCl_3 .

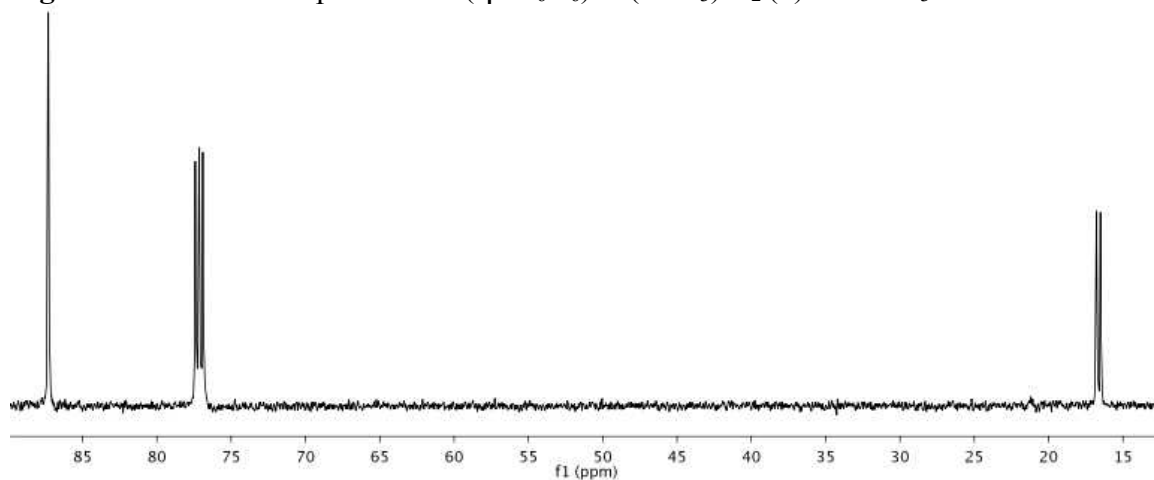


Figure 2.11. ^{13}C NMR spectrum of $(\eta^6\text{-C}_6\text{H}_6)\text{Ru}(\text{PMe}_3)\text{Cl}_2$ (**8**) in CDCl_3 .

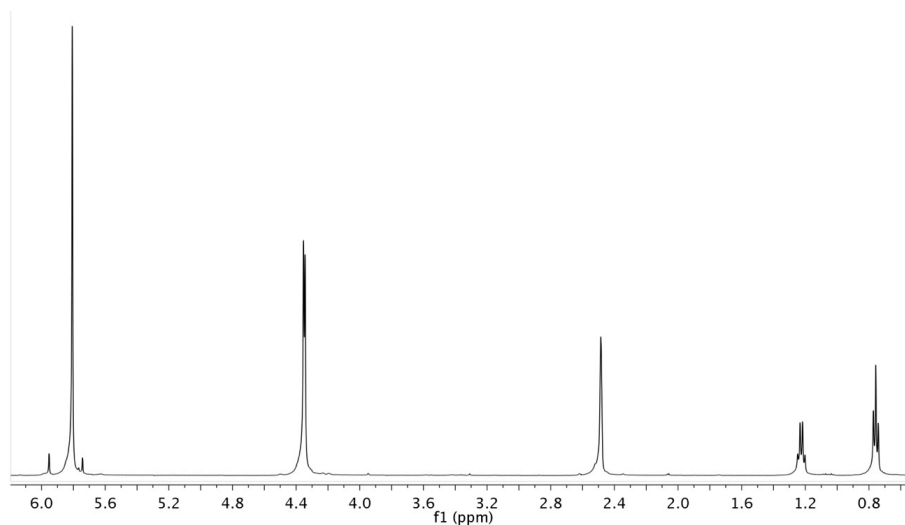


Figure 2.12. ^1H NMR spectrum of $(\eta^6\text{-C}_6\text{H}_6)\text{Ru}[\text{P}(\text{OCH}_2)_3\text{CEt}]\text{Cl}_2$ (**9**) in DMSO.

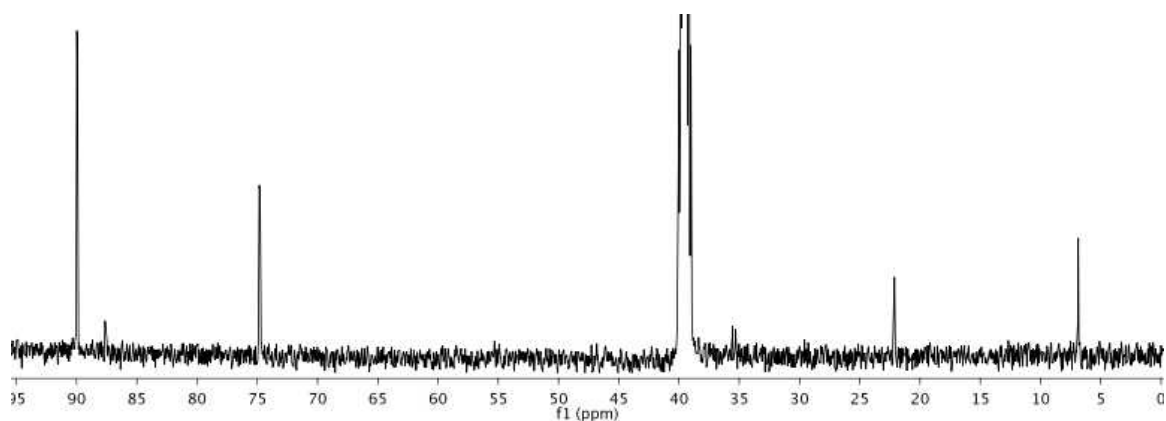


Figure 2.13. ^{13}C NMR spectrum of $(\eta^6\text{-C}_6\text{H}_6)\text{Ru}[\text{P}(\text{OCH}_2)_3\text{CEt}]\text{Cl}_2$ (**9**) in DMSO.

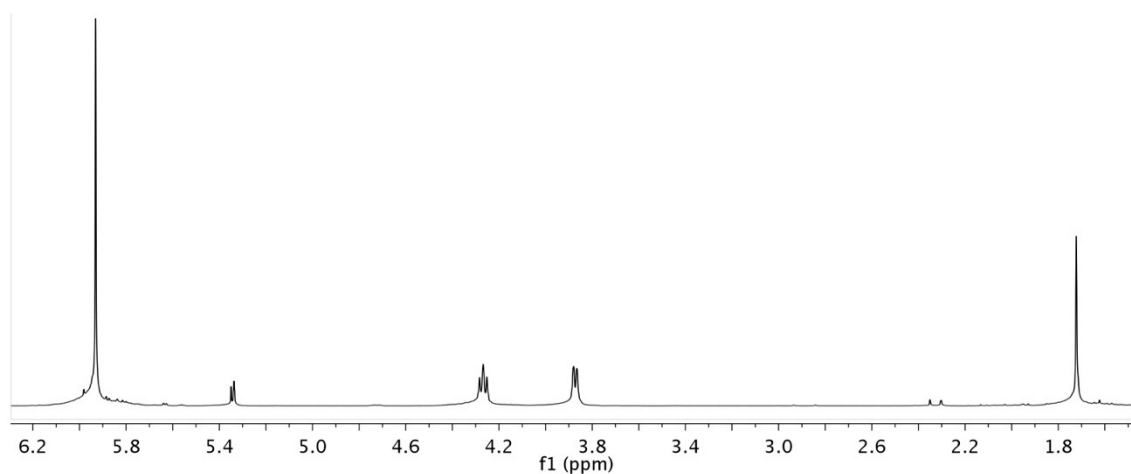


Figure 2.14. ^1H NMR spectrum of $(\eta^6\text{-C}_6\text{H}_6)\text{Ru}[\text{P}(\text{OCH}_2)_2(\text{OCCH}_3)]\text{Cl}_2$ (**11**) in CD_2Cl_2 .

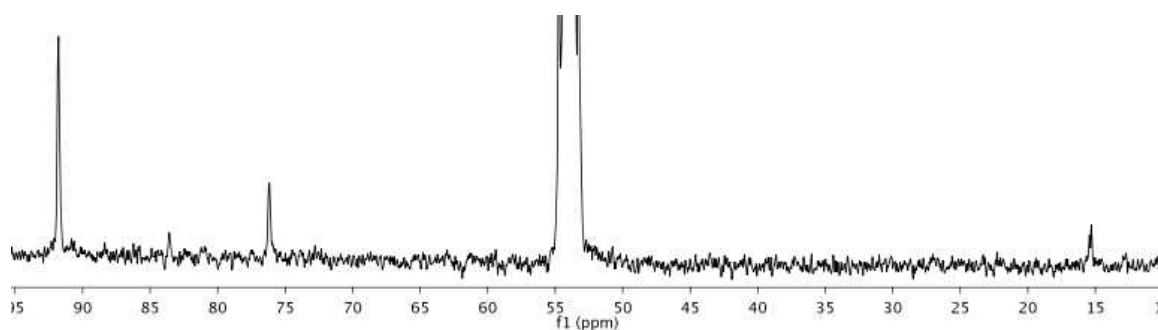


Figure 2.15. ^{13}C NMR spectrum of $(\eta^6\text{-C}_6\text{H}_6)\text{Ru}[\text{P}(\text{OCH}_2)_2(\text{OCCH}_3)]\text{Cl}_2$ (**11**) in CD_2Cl_2 .

A single crystal of **11** suitable for an X-ray diffraction study was grown (Figure 2.16). The phosphite ligand of **11** has features that are similar to complex **2**. For example, there are one larger $[102.5(1)^\circ]$ and two smaller $[95.77(9)^\circ$ and $96.38(1)^\circ]$ O–P–O bond angles which is a consequence of the removal of the methylene group from one of the tethered arms. The C3–O1–P1 angle $[96.89(1)^\circ]$ is substantially smaller by approximately 10° than the other two C–O–P angles, which are 106° . The cone angle of

$\overline{\text{P}(\text{OCH}_2)_2(\text{OCCH}_3)}$ calculated from the structure of complex **11** is 104° , which is identical to that determined using the structure of complex **2**. The average P–O bond distances for **11** [1.613(2) Å] are longer than those for the $\text{P}(\text{OCH}_2)_3\text{CEt}$ complex **3** [1.605(2) Å], but not as long as those of complex **2** [1.627(3) Å]. Table 2.4 shows some comparative geometric data of complexes **2**, **11** and the previously reported complex $(\eta^6\text{-C}_6\text{H}_6)\text{Ru}[\text{P}(\text{OMe})_3]\text{Cl}_2$ (**7**).⁴¹

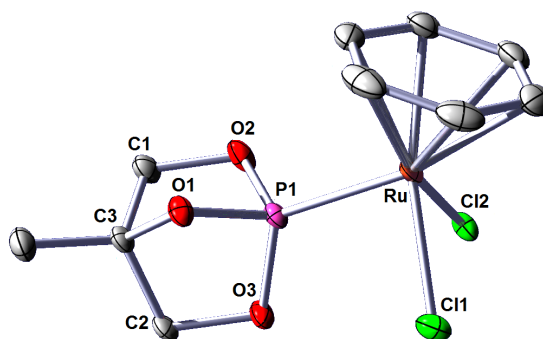


Figure 2.16. ORTEP diagram of $(\eta^6\text{-C}_6\text{H}_6)\text{Ru}[\overline{\text{P}(\text{OCH}_2)_2(\text{OCCH}_3)}]\text{Cl}_2$ (**11**) (50% probability with hydrogen atoms omitted.) Selected bond lengths (Å): Ru–P1, 2.2453(7); P1–O1, 1.615(2); P1–O2, 1.616(2), P1–O3, 1.607(2); Avg. $\text{C}_{(\text{C}_6\text{H}_6)}\text{--Ru}$, 2.198(1). Selected bond angles ($^\circ$): O1–P1–O2, 95.77(9); O3–P1–O1, 96.38(1); O3–P1–O2 102.5(1); Cl1–Ru–Cl2, 87.33(2); P1–Ru–Cl1, 88.66(2); P1–Ru–Cl2, 84.03(2); C3–O1–P1 96.89(1); C1–O2–P1 106.58(1); C2–O3–P1 106.24(1).

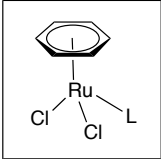

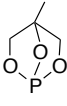
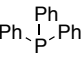
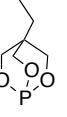
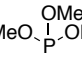
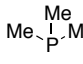
Table 2.4. Selected bond lengths and angles comparing $\text{TpRu}[\text{P}(\text{OCH}_2)_2(\text{OCCH}_3)](\text{PPh}_3)\text{Cl}$ (**2**), $(\eta^6\text{-C}_6\text{H}_6)\text{Ru}(\text{PMe}_3)\text{Cl}_2$ (**7**) and $(\eta^6\text{-C}_6\text{H}_6)\text{Ru}[\text{P}(\text{OCH}_2)_2(\text{OCCH}_3)]\text{Cl}_2$ (**11**). The structure of **7** has been previously reported.⁴¹

Complex	O–P–O (°)	C–O–P (°)	O–P–Ru (°)	P–O (Å)
2	100.2(1)	97.5(2)	118.5(1)	1.627(3)
	94.6(1)	107.3(2)	126.2(1)	1.632(3)
	95.0(1)	107.4(2)	116.8(1)	1.620(3)
7	107.0(2)	123.1(3)	111.2(1)	1.565(3)
	98.7(2)	131.4(3)	123.4(1)	1.569(3)
	97.5(2)	119.4(3)	115.7(1)	1.594(3)
11	102.5(1)	96.89(1)	121.20(7)	1.615(2)
	95.77(9)	106.58(1)	120.98(6)	1.616(2)
	96.38(1)	106.24(1)	115.31(8)	1.607(2)

The $(\eta^6\text{-C}_6\text{H}_6)\text{Ru}(\text{L})\text{Cl}_2$ complexes were studied using cyclic voltammetry to determine if a similar trend observed for the $\text{TpRu}(\text{L})(\text{PPh}_3)\text{Cl}$ complexes held true for a broader range of phosphites/phosphines with the metal center containing $\text{P}(\text{OCH}_2)_2(\text{OCCH}_3)$ is the least electron rich. For $(\eta^6\text{-C}_6\text{H}_6)\text{Ru}^{\text{II}}$ complexes, irreversible $\text{Ru}(\text{III}/\text{II})$ potentials are often observed (Table 2.4), possibly due to dissociation of the benzene ligand in the oxidized $\text{Ru}(\text{III})$ state.⁴⁴ For the $(\eta^6\text{-C}_6\text{H}_6)\text{Ru}(\text{L})\text{Cl}_2$ complexes studied herein, some complexes exhibit quasi-reversible $\text{Ru}(\text{III}/\text{II})$ potentials while others have chemically irreversible potentials. In order to standardize comparisons, we use $E_{\text{p,a}}$ and $E_{\text{p,c}}$ in the discussions below. The carbonyl complex $(\eta^6\text{-C}_6\text{H}_6)\text{Ru}(\text{CO})\text{Cl}_2$ (**10**), with $E_{\text{p,a}} = +1.78$ V (vs NHE), was used as a benchmark to compare the donor ability of **1** because of the known strong π -acidity of the CO ligand. The $E_{\text{p,a}}$ for complex **11** (1.50 V) is 0.28 V more negative than the $E_{\text{p,a}}$ for the CO complex **10**, indicating that the phosphite **1** is more donating than CO. Consistent with the $\text{TpRu}(\text{L})(\text{PPh}_3)\text{Cl}$ complexes,

the Ru(III/II) potentials for the $(\eta^6\text{-C}_6\text{H}_6)\text{Ru}(\text{L})\text{Cl}_2$ complexes indicate the following trend in overall donating ability: PMe_3 (complex **8**) > $\text{P}(\text{OMe})_3$ (complex **7**) > $\text{P}(\text{OCH}_2)_3\text{CEt}$ (complex **6**) \approx PPh_3 (complex **9**) > $\text{P}(\text{OCH}_2)_2(\text{OCCH}_3)$ (complex **11**) > CO (complex **10**). Of the phosphines and phosphites studied, complex **11** yields a metal center with the most positive potential with $E_{\text{p,a}} = 1.50$ V.

Table 2.4. Ru(III/II) potentials for $(\eta^6\text{-C}_6\text{H}_6)\text{Ru}(\text{L})\text{Cl}_2$ complexes. Data from cyclic voltammetry in NCMe with potentials reported vs NHE (in V).

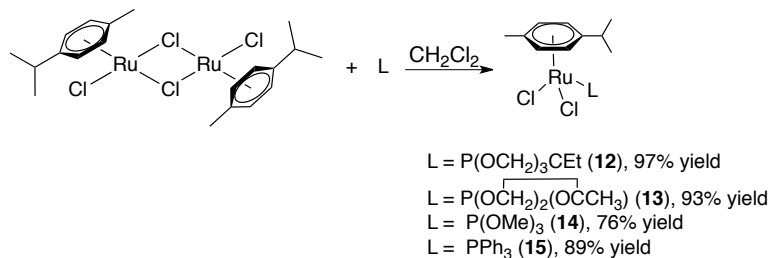
						
Ligand	 (10)	 (11)	 (6)	 (9)	 (7)	 (8)
$E_{\text{p,a}}$	1.78	1.50*	1.40*	1.39	1.34*	1.24*
$E_{\text{p,c}}$	-0.50	-0.99	-1.07 -0.85	-1.09	-0.94 (n = 2)	-1.25

* Denotes quasi-reversible potential, $E_{1/2}$ is reported in experimental section.

In addition to the Ru(III/II) potentials, a cathodic wave ($E_{\text{p,c}}$) is observed for each $(\eta^6\text{-C}_6\text{H}_6)\text{Ru}(\text{L})\text{Cl}_2$ complex (Table 2.4). The $\text{P}(\text{OMe})_3$ complex **7** displays a two-electron reduction at -0.94 V.⁴⁶ Two one-electron reductions are observed for complex **6**, at $E_{\text{p,a}} = -0.85$ V and -1.07 V. All of the other complexes exhibit one single-electron reduction. As the electron density of the metal center decreases, one would expect the $E_{\text{p,c}}$ to become less negative. Indeed, complexes **10** and **11** have the least negative reduction potentials, -0.50 V and -0.99 V, respectively.

2.2.4. Synthesis and Characterization of (η^6 -*p*-cymene)Ru(L)Cl₂ Complexes.

Another group of metal complexes containing phosphites/phosphines is (η^6 -*p*-cymene)Ru(L)Cl₂.^{5,47-49} Similar to the (η^6 -C₆H₆)Ru(L)Cl₂, the complexes (η^6 -*p*-cymene)Ru[P(OCH₂)₃CEt]Cl₂ (**12**), (η^6 -*p*-cymene)Ru[P(OCH₂)₂(OCCH₃)]Cl₂ (**13**), (η^6 -*p*-cymene)Ru[P(OMe)₃]Cl₂ (**14**) and (η^6 -*p*-cymene)Ru(PPh₃)Cl₂ (**15**) were synthesized by the reaction of [(η^6 -*p*-cymene)Ru(Cl)(μ -Cl)]₂ with excess L in dichloromethane (Scheme 2.5). The ¹H NMR spectrum of the bicyclic phosphite, complex **12**, displays 2 doublets (each 2H) for the CH groups of the *p*-cymene ligand. Upfield of the CH group of the *p*-cymene, the distinct septet for the CH of the isopropyl group is observed. The methyl group of the *p*-cymene is observed as a singlet upfield at approximately 2.2 ppm with the doublet from the isopropyl CH₃ groups overlapping with the quartet of the phosphite. Similar to the (η^6 -C₆H₆)Ru[P(OCH₂)₃CEt]Cl₂ species, the phosphite yields a doublet for the methylene hydrogens and a quartet and triplet for the ethyl-group (Figure 2.17, Figure 2.18). The ¹H NMR spectrum of complex **13** displays similar resonances for the *p*-cymene ligand (Figure 2.19, Figure 2.20).



Scheme 2.5. Synthesis of (η^6 -*p*-cymene)Ru(L)Cl₂ (L = P(OCH₂)₃CEt, P(OCH₂)₂(OCCH₃), P(OMe)₃, and PPh₃).

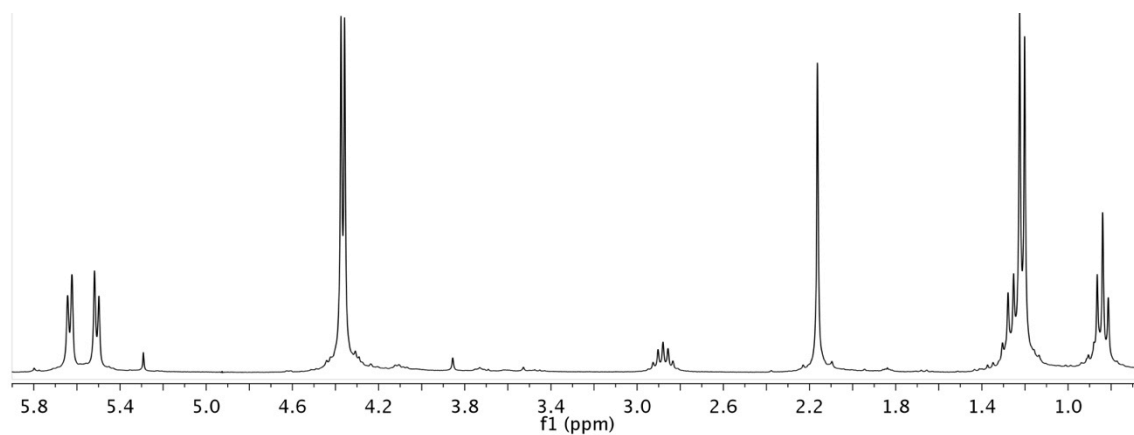


Figure 2.17. ^1H NMR spectrum of $(\eta^6\text{-}p\text{-cymene})\text{Ru}[\text{P}(\text{OCH}_2)_3\text{CEt}]\text{Cl}_2$ (**12**) in CDCl_3 .

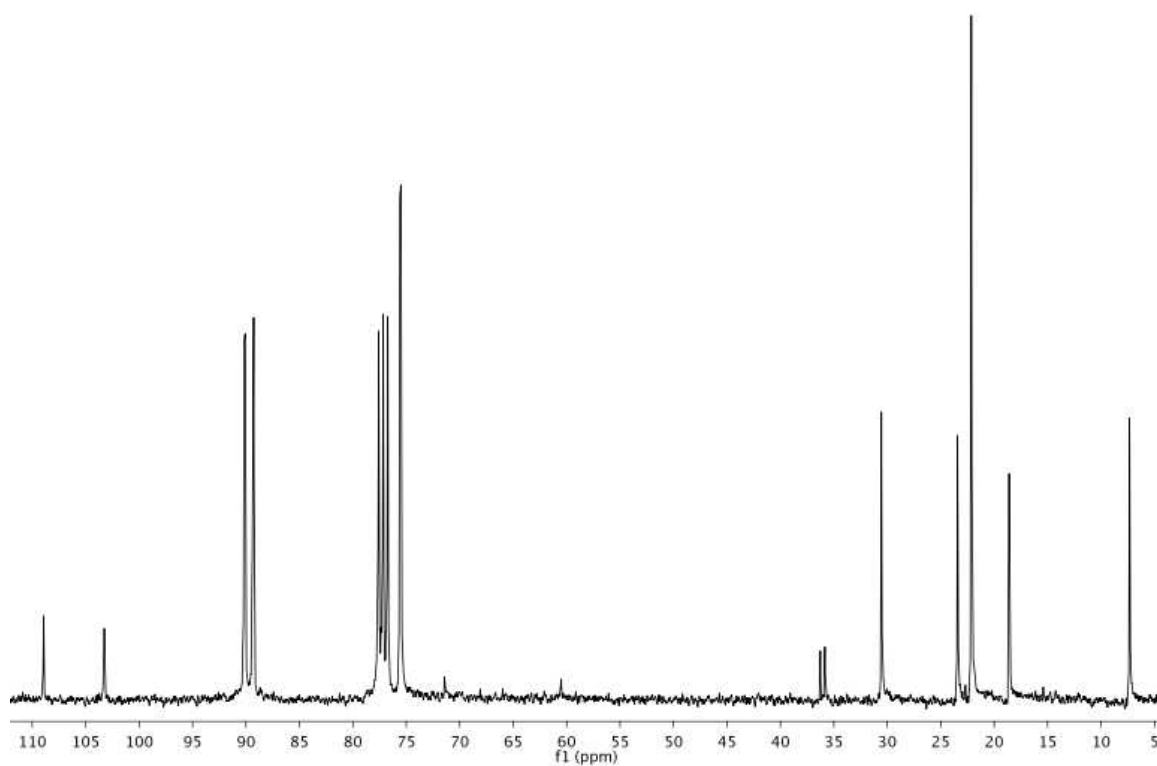


Figure 2.18. ^{13}C NMR spectrum of $(\eta^6\text{-}p\text{-cymene})\text{Ru}[\text{P}(\text{OCH}_2)_3\text{CEt}]\text{Cl}_2$ (**12**) in CDCl_3 .

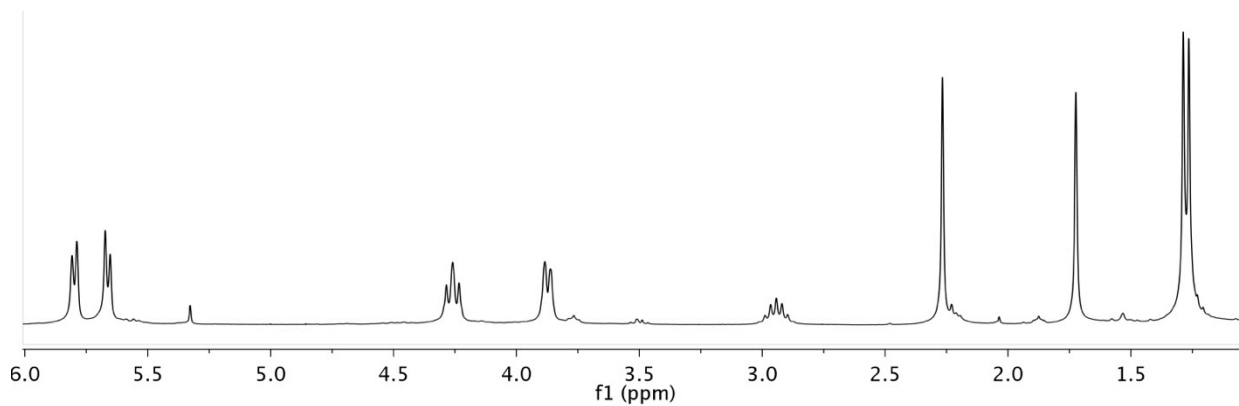


Figure 2.19. ^1H NMR spectrum of $(\eta^6\text{-}p\text{-cymene})\text{Ru}[\text{P}(\text{OCH}_2)_2(\text{OCCH}_3)]\text{Cl}_2$ (**13**) in CDCl_3 .

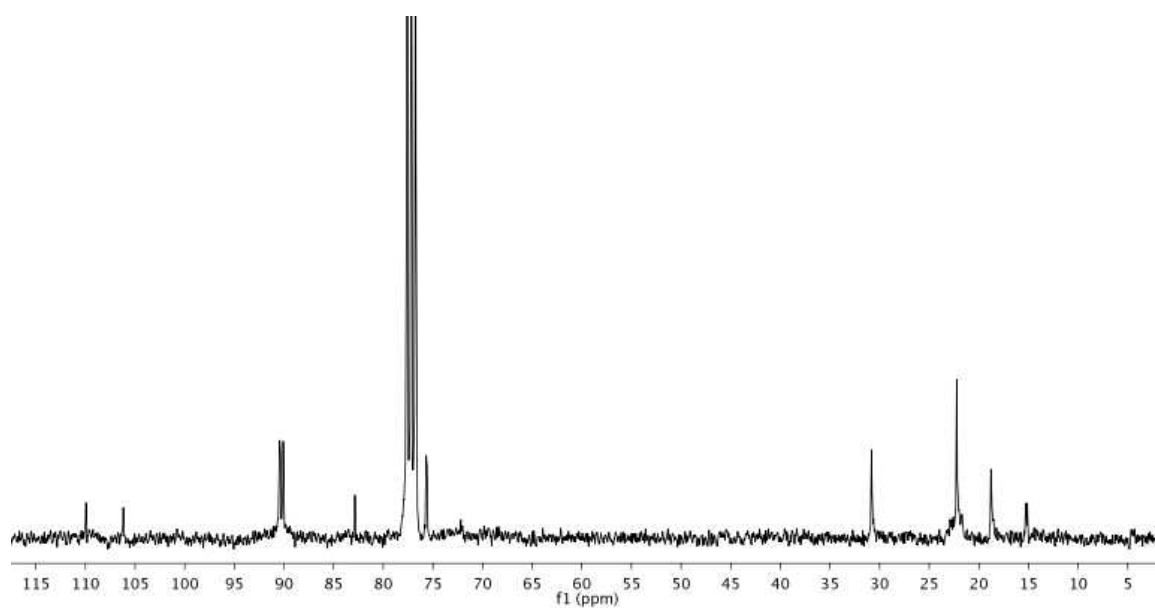


Figure 2.20. ^{13}C NMR spectrum of $(\eta^6\text{-}p\text{-cymene})\text{Ru}[\text{P}(\text{OCH}_2)_2(\text{OCCH}_3)]\text{Cl}_2$ (**13**) in CDCl_3 .

A single crystal suitable for X-ray diffraction was grown of complex **12** (Figure 2.21). Using previously reported data for $(\eta^6\text{-}p\text{-cymene})\text{Ru}[\text{P}(\text{OCH}_2)_3\text{CEt}]\text{Cl}_2$ [L = $\text{P}(\text{OCH}_2)_3\text{CEt}$ (**12**), $\text{P}(\text{OPh})_3$, PPh_3 (**15**), $\text{P}(\text{NC}_4\text{H}_4)_3$],^{5,47,49} the Ru–P bond distance increases with the following trend $\text{P}(\text{OCH}_2)_3\text{CEt}$ (**12**) < $\text{P}(\text{OPh})_3$ < PPh_3 (**15**) < $\text{P}(\text{NC}_4\text{H}_4)_3$ (Table 2.5). When comparing the O–P–O bond angles of complexes $\text{TpRu}[\text{P}(\overline{\text{OCH}_2)_2(\text{OCCH}_3)}](\text{PPh}_3)\text{Cl}$ (**2**), $(\eta^6\text{-C}_6\text{H}_6)\text{Ru}[\text{P}(\overline{\text{OCH}_2)_2(\text{OCCH}_3)}]\text{Cl}_2$ (**11**), and $(\eta^6\text{-}p\text{-cymene})\text{Ru}[\text{P}(\text{OCH}_2)_3\text{CEt}]\text{Cl}_2$ (**12**), the removal of the methylene group from $\text{P}(\text{OCH}_2)_3\text{CEt}$ to form phosphite **1**, $\text{P}(\overline{\text{OCH}_2)_2(\text{OCCH}_3)}$, results in a substantial decrease in the O–P–O bond angle where the methylene group is removed by approximately 5° for complexes **2** and **11**. The Ru–P bond length for $(\eta^6\text{-}p\text{-cymene})\text{Ru}[\text{P}(\text{OCH}_2)_3\text{CEt}]\text{Cl}_2$ (**12**) [2.2529(4) Å] is longer than that for $\text{TpRu}[\text{P}(\overline{\text{OCH}_2)_2(\text{OCCH}_3)}](\text{PPh}_3)\text{Cl}$ (**2**) [2.191(1) Å] and $(\eta^6\text{-C}_6\text{H}_6)\text{Ru}[\text{P}(\overline{\text{OCH}_2)_2(\text{OCCH}_3)}]\text{Cl}_2$ (**11**) [2.2453(7) Å]. Additionally, the average P–O bond lengths for complex **2** [1.627(3) Å] and **11** [1.613(2) Å] are longer than for complex **12** [1.597(2) Å], consistent with phosphite **1** being a better π -acid than $\text{P}(\text{OCH}_2)_3\text{CEt}$.

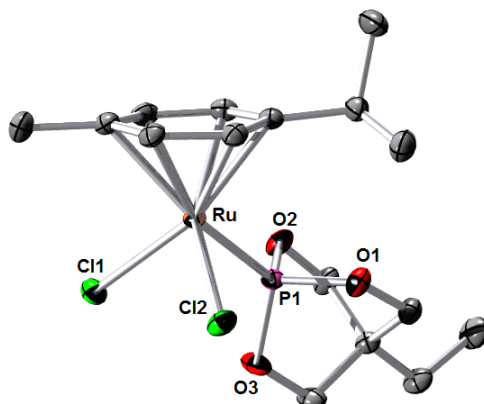
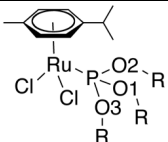


Figure 2.21. ORTEP of $(\eta^6\text{-}p\text{-cymene})\text{Ru}[\text{P}(\text{OCH}_2)_3\text{CEt}]\text{Cl}_2$ (**12**) (50% probability with hydrogen atoms omitted.) Selected bond lengths (Å): Ru–P1, 2.2529(4); P1–O1, 1.599(1); P1–O2, 1.599(1), P1–O3, 1.594(1). Selected bond angles (°): O3–P1–O2, 102.82(6); O3–P1–O1, 102.37(6); O2–P1–O1, 102.31(6); Cl(1)–Ru–Cl2, 88.59(1); P1–Ru–Cl1, 88.10(1); P1–Ru–Cl2, 83.91(1).

Table 2.5. Comparison of bond lengths from crystallographic data for $(\eta^6\text{-}p\text{-cymene})\text{Ru}(\text{L})\text{Cl}_2$ complexes.

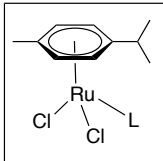
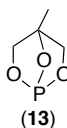
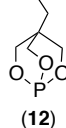
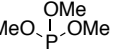
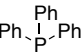
				
Ligand “L”	Ru–P(Å)	P–O1 (Å)	P–O2 (Å)	P–O3 (Å)
PPh ₃	2.3438(6)	– ^a	– ^a	– ^a
P(OCH ₂) ₃ CEt	2.2529(4)	1.599(1)	1.599(1)	1.594(1)
P(NC ₄ H ₉) ₃	2.396(2)	– ^a	– ^a	– ^a
P(OPh) ₃	2.2642(8)	1.596(2)	1.607(2)	1.584(2)

^a No oxygen atom in P-based ligand.

The $(\eta^6\text{-}p\text{-cymene})\text{Ru}(\text{L})\text{Cl}_2$ complexes **12–15** were studied using cyclic voltammetry (Table 2.6). It was determined that the least electron density on the metal center is observed for complex **13** containing $\text{P}(\text{OCH}_2)_2(\text{OCCH}_3)$ with quasi-reversible Ru(III/II) wave at $E_{1/2} = 1.44$ V, and $E_{p,c} = -1.05$ V. This observation is consistent with

data collected for the $(\eta^6\text{-C}_6\text{H}_6)\text{Ru}(\text{L})\text{Cl}_2$ systems (see above). Intriguingly, both metal centers containing cyclic phosphites (complex **12** and **13**) are less electron-rich than the acyclic phosphites, unlike the $\eta^6\text{-C}_6\text{H}_6$ systems in which the bicyclic phosphite, $\text{P}(\text{OCH}_2)_3\text{CEt}$ and PPh_3 are basically identical. Unlike the $(\eta^6\text{-C}_6\text{H}_6)\text{Ru}(\text{L})\text{Cl}_2$ systems, all of the $\eta^6\text{-}p\text{-cymene}$ systems show reversible waves. The same trend as shown with $\text{TpRu}(\text{PPh}_3)_2\text{Cl}$ and $(\eta^6\text{-C}_6\text{H}_6)\text{Ru}(\text{L})\text{Cl}_2$ complexes of the metal center being the least electron rich with $\text{L} = \overline{\text{P}(\text{OCH}_2)_2(\text{OCCH}_3)}$ and the most electron rich with the phosphines studied is apparent using both $E_{1/2}$ and $E_{p,a}$ for the $(\eta^6\text{-}p\text{-cymene})\text{Ru}(\text{L})\text{Cl}_2$ complexes.

Table 2.6. Ru(III/II) potentials for $(\eta^6\text{-}p\text{-cymene})\text{Ru}(\text{L})\text{Cl}_2$ complexes. Data from cyclic voltammetry in NCMe with potentials reported vs NHE (in V).

				
Ligand	 (13)	 (12)	 (14)	 (15)
$E_{p,a}$	1.47*	1.35*	1.30*	$E_{1/2} = 1.25$
$E_{p,c}$	-1.05	-1.23	-1.21	-1.25

* Denotes quasi-reversible potential, $E_{1/2}$ is reported in experimental section.

Kinetic Studies for Phosphine/Phosphite Exchange. As a final probe of the properties of **1** as a ligand, we compared the rate of ligand exchange using $\text{P}(\text{OMe})_3$ for $(\eta^6\text{-}p\text{-cymene})\text{Ru}(\text{L})\text{Cl}_2$ complexes [$\text{L} = \mathbf{1}$, $\text{P}(\text{OCH}_2)_3\text{CEt}$ and PPh_3]. The exchange rates

were determined under pseudo-first-order conditions by monitoring (^1H NMR spectroscopy) the disappearance of $(\eta^6\text{-}p\text{-cymene})\text{Ru}(\text{L})\text{Cl}_2$ in the presence of excess $\text{P}(\text{OMe})_3$ to form $(\eta^6\text{-}p\text{-cymene})\text{Ru}[\text{P}(\text{OMe})_3]\text{Cl}_2$. In all cases the reaction proceeded to quantitative conversion. Figure 2.22 displays plots of concentration of Ru complex vs time for **12**, **13** and **15**. The k_{obs} values for each reaction were determined by fitting the plots to first-order decays, which gives the following relative k_{obs} magnitudes: $(\eta^6\text{-}p\text{-cymene})\text{Ru}(\text{PPh}_3)\text{Cl}_2$ (**15**) [$k_{\text{obs}} = 0.0045(3) \text{ s}^{-1}$] > $(\eta^6\text{-}p\text{-cymene})\text{Ru}[\text{P}(\text{OCH}_2)_2(\text{OCCH}_3)]\text{Cl}_2$ (**13**) [$k_{\text{obs}} = 0.0030(1) \text{ s}^{-1}$] >> $(\eta^6\text{-}p\text{-cymene})\text{Ru}[\text{P}(\text{OCH}_2)_3\text{CEt}]\text{Cl}_2$ (**12**) [$k_{\text{obs}} = 8.5(6) \times 10^{-5} \text{ s}^{-1}$].

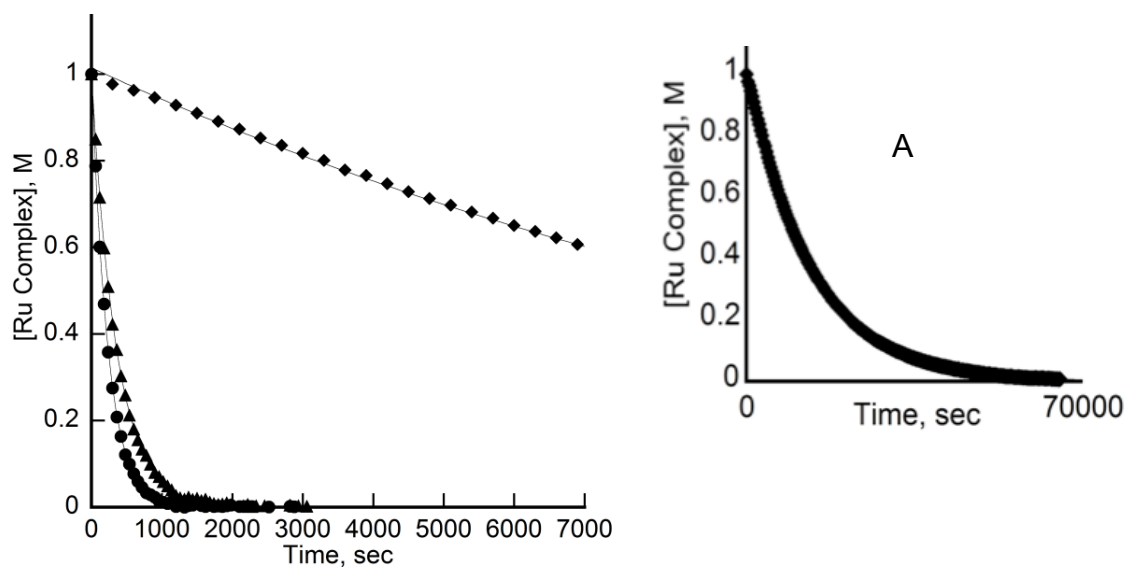


Figure 2.22. Representative kinetic plots for the exchange reaction of L in $(\eta^6\text{-}p\text{-cymene})\text{Ru}(\text{L})\text{Cl}_2$ [$\text{L} = \text{P}(\text{OCH}_2)_2(\text{OCCH}_3)$, $\text{P}(\text{OCH}_2)_3\text{CEt}$ or PPh_3] complexes with $\text{P}(\text{OMe})_3$ (40 equivalents relevant to concentration of Ru complex) in CDCl_3 at 60°C [$\text{L} = \blacktriangle \text{P}(\text{OCH}_2)_2(\text{OCCH}_3)$ (**13**) [$k_{\text{obs}} = 0.0030(1) \text{ s}^{-1}$, $R^2 = 0.99$], $\bullet \text{PPh}_3$ (**15**) [$k_{\text{obs}} = 0.0045(3) \text{ s}^{-1}$, $R^2 = 0.99$], $\diamond \text{P}(\text{OCH}_2)_3\text{CEt}$ (**12**) [$k_{\text{obs}} = 0.000085(6) \text{ s}^{-1}$, $R^2 = 0.99$]. Plot A represents the exchange reaction for $\text{L} = \text{P}(\text{OCH}_2)_3\text{CEt}$.

Figure 2.23 shows a plot of k_{obs} vs concentration of PPh_3 for the reaction of **15** with P(OMe)_3 . Increasing the concentration of PPh_3 decreases the rate of ligand exchange indicating an inverse rate dependence on concentration of PPh_3 . Figure 2.24 displays a plot of k_{obs} vs concentration of P(OMe)_3 for the reaction of **15** with P(OMe)_3 . The rate of reaction initially increases, and saturation is observed at higher concentrations of P(OMe)_3 . Scheme 2.6 shows a potential reaction pathway for the conversion of **12**, **13** or **15** and P(OMe)_3 to $(\eta^6\text{-}p\text{-cymene})\text{Ru}[\text{P(OMe)}_3]\text{Cl}_2$ that is consistent with the kinetic data for the reaction of **15** and P(OMe)_3 . Since **12**, **13** and **15** are 18-electron complexes, a ligand exchange by a dissociative pathway is reasonable. Under saturation conditions {where $k_2[\text{P(OMe)}_3] > k_{-1}[\text{L}]$ }, the rate law can be reduced to $\text{rate} = k_1[\text{Ru complex}]$ where $k_{\text{obs}} = k_1$, which is the rate constant for dissociation of L (Figure 2.25). Thus, the k_{obs} values derived from the kinetic plots in Figure 2.22 should provide relative rates of dissociation of L from $(\eta^6\text{-}p\text{-cymene})\text{Ru}(\text{L})\text{Cl}_2$ complexes. The k_{obs} values indicate that the rate of dissociation of **1** from $(\eta^6\text{-}p\text{-cymene})\text{Ru}[\text{P}(\overline{\text{OCH}_2})_2(\overline{\text{OCCH}_3})]\text{Cl}_2$ (**13**) is similar to that of PPh_3 from $(\eta^6\text{-}p\text{-cymene})\text{Ru}(\text{PPh}_3)\text{Cl}_2$ (**15**), and that **1** and PPh_3 dissociate more rapidly than $\text{P(OCH}_2)_3\text{CEt}$ from $(\eta^6\text{-}p\text{-cymene})\text{Ru}[\text{P(OCH}_2)_3\text{CEt}]\text{Cl}_2$ (**12**).

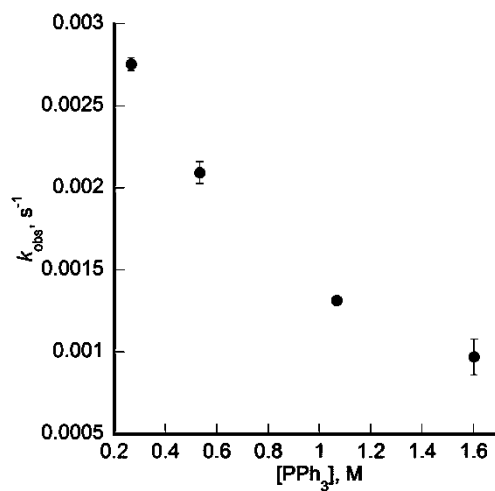


Figure 2.23. Plot of k_{obs} versus concentration of PPh₃ for the exchange of PPh₃ with P(OMe)₃ upon reaction of (η^6 -*p*-cymene)Ru(PPh₃)Cl₂ (**15**) with excess P(OMe)₃ in CDCl₃ at 60 °C.

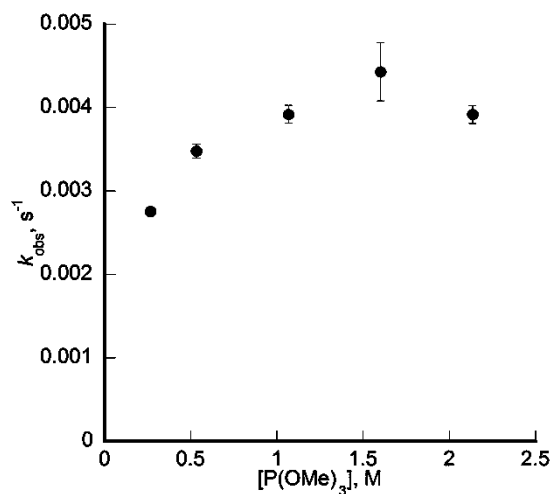
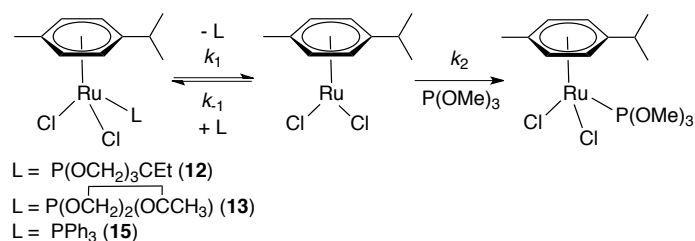


Figure 2.24. Plot of k_{obs} versus concentration of P(OMe)₃ for the exchange of PPh₃ with P(OMe)₃ upon reaction of (η^6 -*p*-cymene)Ru(PPh₃)Cl₂ (**15**) with excess P(OMe)₃ in CDCl₃ at 60 °C.



Scheme 2.6. Proposed mechanism for exchange reaction of L with P(OMe)₃ to form (η⁶-*p*-cymene)Ru[P(OMe)₃]Cl₂ in CDCl₃ at 60 °C.

$$\text{Rate} = \frac{k_1 k_2 [\text{P}(\text{OMe})_3] [\text{Ru-Complex}]}{k_{-1} [\text{L}] + k_2 [\text{P}(\text{OMe})_3]}$$

Figure 2.25. Rate law for exchange reaction of L in (η⁶-*p*-cymene)Ru(L)Cl₂ [L = P(OCH₂)₂(OCCH₃), P(OCH₂)₃CEt or PPh₃] complexes with P(OMe)₃ to form (η⁶-*p*-cymene)Ru[P(OMe)₃]Cl₂ in CDCl₃ at 60 °C.

2.2.5. Calculations: Bicyclic Phosphite π-Acidity

To further understand the bonding between **1** and transition metals, DFT calculations were carried out to compare bonding of **1** to P(OMe)₃, P(OCH₂)₃CEt and PF₃. The calculations were performed by Claire L. McMullin of Tom Cundari's group (University of North Texas). The role of the P–X (X = O, C, halide, etc.) σ* orbitals in π-acidity of phosphorus ligands has been documented.^{9,50,51} The energies of the PX₃ σ* orbitals are a function of the substituent X as well as the X–P–X bond angle.^{1,9} Smaller X–P–X angles are suggested to result in better π-acceptor ligands as σ* LUMOs are

lower in energy due to the reduced overlap between the 3p phosphorus orbitals with σ -orbitals of the X substituents (see Figure 2.2). Thus, the decreased O–P–O bond angles of bicyclic phosphites that result from the cyclic structure are expected to decrease the energy of the P–O σ^* orbitals and, as a result, enhance π -acidity.

Structures were optimized for a linear gold(I) complex $[\text{AuCl(L)}]$ where $\text{L} = \mathbf{1}$, P(OMe)_3 , $\text{P(OCH}_2)_3\text{CEt}$ or PF_3 and for the free ligand L. AuCl(L) is an established organometallic fragment by Fey *et al.* used to parameterize ligand electronic and steric effects.⁵² While the experimental studies herein are focused on Ru(II), the d^{10} configuration of the Au(I) complex allowed for easier delineation of σ -donor and π -acceptor electronic effects without steric influence from *cis* ligands. The free ligand HOMO and LUMO energies (E_{HOMO} and E_{LUMO}) are given in Figure 2.12, along with the Au–P bond length and phosphine substituent angles (X–P–X) from the $[\text{AuCl(L)}]$ complexes.

Care was taken when modeling the conformation of P(OMe)_3 ,⁵³ with the lowest energy conformers in low and high coordinate compounds investigated (ag^+g^+ and ag^-g^+ respectively), as well as the most similar P(OMe)_3 conformation to $\mathbf{1}$, where the OMe groups are all *anti* to the metal–phosphorus bond (*aaa*) (Figure 2.26). Consideration of conformations is important to ensure that possible anomeric effects are not neglected,⁵⁴ as delocalization of the phosphorus lone pair into a C–O σ^* orbital is known to be more favorable if the substituent has an *anti* configuration.⁵⁵ The anomeric effect is lessened when the phosphite is coordinated to a metal center.⁵³

Table 2.7. Data from DFT calculations of $\text{P}(\text{OCH}_2)_2(\text{OCCH}_3)$ (**1**), $\text{P}(\text{OMe})_3$, $\text{P}(\text{OCH}_2)_3\text{CEt}$ and PF_3 .

Ligand	Orientation	E_{HOMO} [hartree]	E_{LUMO} [hartree]	Au–P [Å]	Average X–P–X [°]	Relative Free Energy [kcal mol ⁻¹]
$\text{P}(\text{OCH}_2)_2(\text{OCCH}_3)$ (1)		-0.2343	-0.0428	2.21	97.4	-
$\text{P}(\text{OMe})_3$	ag^+g^+	-0.2190	-0.0235	2.24	102.5	0.0
$\text{P}(\text{OMe})_3$	ag^-g^+	-0.2230	-0.0241	2.24	102.7	1.0
$\text{P}(\text{OMe})_3$	aaa	-0.2215	-0.0118	2.23	105.6	7.6
$\text{P}(\text{OCH}_2)_3\text{CEt}$		-0.2296	-0.0196	2.22	102.2	-
PF_3		-0.3089	-0.0709	2.20	99.5	-

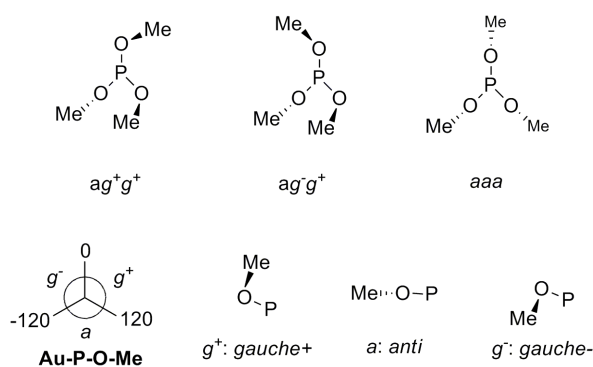


Figure 2.26. Orientations of $\text{P}(\text{OMe})_3$ ligand defined by the torsion Au–P–O–Me (viewed along the Au–P bond) that were modeled using DFT calculations.

The descriptor E_{LUMO} has been shown in Ligand Knowledge Base research to be related to the π -accepting character of a phosphorus ligand.⁵² As the results in Table 2.7 indicate, the energy of the LUMO (E_{LUMO}) is significantly lower for **1** compared to the $\text{P}(\text{OMe})_3$ conformers, which directly correlates to the size of the O–P–O angle. Likewise, the E_{LUMO} of **1** is lower than that calculated for $\text{P}(\text{OCH}_2)_3\text{CEt}$. The calculated X–P–X

angles of **1** and PF₃ are smallest, supporting the hypothesis that small X–P–X angles lower the E_{LUMO} and thereby increase the ligand's π -acidity. The LUMO energy for PF₃ is likely lower than that for **1** as a result of the more strongly withdrawing fluorine substituents of PF₃, which is consistent with the known strong π -acceptor ability of PF₃. Structural parameters from the linear Au(I) calculations also show a clear correlation between the E_{LUMO} and Au–P bond lengths. Again for **1**, Au–P is shorter (~ 0.02 Å) than that observed in the equivalent P(OMe)₃ and P(OCH₂)₃CEt complexes, further corroborating a higher π -acidity character for phosphite **1** than the others included in this study and placing it below PF₃ on the π -acidity scale.

2.3. Conclusions

Crystallographic and cyclic voltammetry data have been used to demarcate the properties of **1** compared with other phosphine and phosphite ligands, as well as carbon monoxide, using three types of ruthenium complexes, TpRu(L)(PPh₃)Cl, (η^6 -C₆H₆)Ru(L)Cl₂ and (η^6 -*p*-cymene)Ru(L)Cl₂. Data clearly indicate that the formal removal of one methylene group from the bicyclic phosphite P(OCH₂)₃CEt, which gives the phosphite P(OCH₂)₂(OCCH₃) (**1**), results in a reduction in electron density at the metal center. For all three types of Ru complexes, redox potentials with **1** in the coordination sphere are shifted positive by 0.11 V to 0.13 V compared to analogous complexes with P(OCH₂)₃CEt. Furthermore, when L = **1**, the metal is less electron-rich (as determined by cyclic voltammetry) than metals coordinated by all other phosphorus ligands studied including P(OMe)₃, PMe₃, PPh₃ and P(OCH₂)₃CEt. It can be concluded that **1** is overall

more weakly donating than the acyclic phosphite $\text{P}(\text{OMe})_3$. The source of these differences is more difficult to pinpoint. Verkade *et al.* have rationalized differences in basicity of cyclic vs acyclic phosphites (and related ligands) with the hinge effect,^{3,23-26} which involves differences in O–P π -overlap as function of O–P–O and P–O–C bond angles (see above). In addition, differences in O–P–O bond angles (for cyclic vs acyclic phosphites) might impact O–P σ -overlap and, hence, the energy of P–O σ^* orbitals, which could influence ligand π -acidity. DFT calculations are consistent with this suggestion and indicate a lower energy LUMO for **1** compared to $\text{P}(\text{OMe})_3$ and $\text{P}(\text{OCH}_2)_3\text{CEt}$.

2.4. Experimental Section

General Methods. Unless otherwise noted, all synthetic procedures were performed under anaerobic conditions in a nitrogen-filled glovebox or by using standard Schlenk techniques. Glovebox purity was maintained by periodic nitrogen purges and was monitored by an oxygen analyzer [$\text{O}_2(\text{g}) < 15$ ppm for all reactions]. Tetrahydrofuran was dried by distillation from sodium/benzophenone. Pentane was distilled over P_2O_5 . Acetonitrile and diethyl ether were dried by distillation from CaH_2 . Hexanes, benzene and methylene chloride were purified by passage through a column of activated alumina. Benzene- d_6 , acetonitrile- d_3 , methylene chloride- d_2 and chloroform- d_1 were stored under a N_2 atmosphere over 4Å molecular sieves. ^1H NMR spectra were recorded on a Varian Mercury Plus 300 MHz Spectrometer or Varian Inova 500 MHz Spectrometer, and ^{13}C NMR spectra were recorded on a Varian Inova 500 MHz Spectrometer (operating

frequency 125 MHz). All ^1H and ^{13}C NMR spectra are referenced against residual proton signals (^1H NMR) or the ^{13}C resonances of the deuterated solvent (^{13}C NMR). ^{31}P NMR spectra were obtained on a Varian 300 MHz (operating frequency 121 MHz) spectrometer and referenced against an external standard of H_3PO_4 ($\delta = 0$). Resonances due to the Tp ligand in ^1H NMR spectra are listed by chemical shift and multiplicity only (all coupling constants for the Tp ligand are ~ 2 Hz).

Electrochemical experiments were performed under a nitrogen atmosphere using a BAS Epsilon Potentiostat. Cyclic voltammograms were recorded in NCMe using a standard three electrode cell from -1700 to 1700 mV at 100 mV/s [with the exception of $(\eta^6\text{-C}_6\text{H}_6)\text{Ru}(\text{CO})\text{Cl}_2$, which was scanned from -1700 to 2500 mV at a scan rate of 100 mV/s] with a glassy carbon working electrode and tetrabutylammonium hexafluorophosphate as electrolyte. All potentials are reported versus NHE (normal hydrogen electrode) using ferrocene as the internal standard.

High-resolution electrospray ionization mass spectrometry (ESI-MS) analyses were obtained on a Bruker BioTOF-Q spectrometer at the University of Richmond. Samples were dissolved in acetonitrile and then mixed 3:1 with 0.1 M aqueous sodium trifluoroacetate (NaTFA) using $[\text{Na}(\text{NaTFA})_x]^+$ clusters as an internal standard. These data are reported using the most intense peaks from the isotopic envelope for $[\text{M} + \text{Na}]^+$. The data are listed as m/z with the intensity relative to the most abundant peak of the isotopic envelope given in parentheses for both the calculated and observed peaks. The difference between calculated and observed peaks is reported in ppm. In all cases, observed isotopic envelopes were consistent with the composition reported.

The preparation, isolation and characterization of $\text{TpRu}[\text{P}(\text{OCH}_2)_3\text{CEt}](\text{PPh}_3)\text{Cl}$ (**3**),³¹ $\text{TpRu}(\text{PMe}_3)(\text{PPh}_3)\text{Cl}$ (**4**),³⁸ $(\eta^6\text{-C}_6\text{H}_6)\text{Ru}(\text{CO})\text{Cl}_2$ (**11**),³⁹ $(\eta^6\text{-C}_6\text{H}_6)\text{Ru}(\text{PPh}_3)\text{Cl}_2$ (**6**),⁴⁰ and $(\eta^6\text{-C}_6\text{H}_6)\text{Ru}[\text{P}(\text{OMe})_3]\text{Cl}$ (**7**)⁴⁰ have been previously reported. $\text{P}(\text{OCH}_2)_3\text{CEt}$ was obtained from a commercial source and purified by reconstitution in hexanes followed by filtration through Celite. The filtrate was concentrated to dryness to yield pure material.

Calculations. DFT calculations were performed using the standard Becke-Perdew (BP86) density functional⁵⁶⁻⁶⁰ in conjunction with the double- ζ 6-31+G(d) basis set for all atoms excluding gold, for which the Los Alamos National Laboratory LANL2DZ⁶¹ basis set, augmented by diffuse and contracted f functions taken from Pyykkö and Mendizabal⁶² and the 6p functions of Couty and Hall,⁶³ was employed. All calculations were performed using the Gaussian 09 suite of programs.⁶⁴

$\text{C}(\text{CH}_3)(\text{OH})(\text{CH}_2\text{OH})_2$. The synthesis of $\text{C}(\text{CH}_3)(\text{OH})(\text{CH}_2\text{OH})_2$ has been previously reported.³⁶ We used an alternate procedure. The reaction was performed in a vented hood. H_2O_2 (30%, 8.51 mL, 0.0826 mol) was added to formic acid (88%, 34.7 mL, 0.808 mol), and the mixture was stirred at room temperature for 5 minutes. The flask was placed in an ice bath, and 2-methyl-2-propen-1-ol (5.0 mL, 0.059 mol) was added slowly using an addition funnel. The reaction was heated at 40 °C for 1 h. The solution was allowed to cool to room temperature. After 16 h at room temperature, the solution was concentrated *in vacuo*, and the residual oil was cooled in an ice bath and treated drop wise with 10 mL of cold NaOH (13.3 M). The resulting mixture was heated for 1 h at 40 °C, which resulted in a yellow solution. After the addition of acetone (~50 mL), the top

layer was removed using a pipette. The acetone addition/extraction was repeated three times, and all extractions were combined. The combined fractions were concentrated under reduced pressure. The remaining pale yellow viscous oil was dissolved in a minimal amount of methanol, and diethyl ether was added to induce precipitation. The mixture was filtered using a fine porosity frit, and the solid was discarded. This step was repeated multiple times until no precipitate was observed upon the addition of diethyl ether. The filtrates were combined and concentrated *in vacuo* to give a brownish-yellow oil. The oil was purified by column chromatography on silica using 1:2 methanol:ethyl acetate as eluent. The solution was concentrated to dryness to yield a brownish-yellow oil (4.206 g, 67%). The sample was dried by azeotropic distillation in benzene. ^1H NMR (D_2O , 300 MHz, δ) 3.47 (s, 4H, CH_2), 1.13 (s, 3H, CH_3). ^{13}C NMR (125 MHz, CD_3OD , δ) 73.8, 67.6 (both s, C and CH_2), 21.3 (s, CH_3).

$\text{P}(\overline{\text{OCH}_2})_2(\overline{\text{OCCH}_3})$ (**1**). The synthesis of $\text{P}(\overline{\text{OCH}_2})_2(\overline{\text{OCCH}_3})$ has been previously reported.³³ We used a modified procedure. $\text{C}(\text{CH}_3)(\text{OH})(\text{CH}_2\text{OH})_2$ (1.032 g, 9.725 mmol) was added to benzene (200 mL) in a 400 mL beaker. NaH (0.695 g, 29.0 mmol) was added to the reaction vessel, and the reaction mixture was stirred at room temperature for 1.25 h. PCl_3 (775 μL , 8.89 mmol) was added slowly via syringe, and the reaction was stirred at room temperature for over night. The heterogeneous mixture was filtered through a fine porosity frit. Attempts to isolate pure **1** lead to decomposition. Thus, for coordination to Ru, **1** was generated as described above and added to the Ru precursor without isolation. $^{31}\text{P}\{^1\text{H}\}$ NMR (121 MHz, C_6D_6 , δ): 115.5 [$\text{P}(\overline{\text{OCH}_2})_2(\overline{\text{OCCH}_3})$].

TpRu[$\overline{\text{P}(\text{OCH}_2)_2(\text{OCCH}_3)}$](PPh₃)Cl (2**).** A benzene solution of phosphite **1** (150 mL, 2.98 mmol) was added to TpRu(PPh₃)₂Cl (0.510 g, 0.564 mmol). The solution was refluxed for 3 h to give a bright yellow solution. The solution was filtered through Celite, and the volatiles were removed from the filtrate *in vacuo*. The resulting solid was dissolved in minimal THF. Hexanes were added to induce precipitation of a yellow solid, which was collected on a fine porosity frit and dried *in vacuo*. The solid was dissolved in CH₂Cl₂ and loaded onto a silica column. The column was washed with hexanes, and the eluent was discarded. The column was then eluted with Et₂O. The eluent was collected and reduced *in vacuo* to ~2 mL. Hexanes were added to induce precipitation of a yellow solid, which was collected on a fine porosity frit and dried *in vacuo* (0.0933 g, 19.5% yield). Crystals of **2** were obtained by slow evaporation of a CH₂Cl₂ solution layered with hexanes. ¹H NMR (500 MHz, CDCl₃, δ): 8.15, 7.65, 7.63, 7.52 (each a d, each 1H, Tp 3 and 5), 7.38–7.15 (overlapping m's, 15H, P(C₆H₅)₃), 6.91, 6.72 (each a d, each 1H, Tp 3 and 5), 6.09 (dt, 1H, ⁵J_{HP} = 1.0 Hz, Tp 4), 5.80 (dt, 1H, ⁵J_{HP} = 1.3 Hz, Tp 4), 5.75 (t, 1H, Tp 4), 3.93 (dd, 2H, ²J_{HH} = 8.0 Hz, ³J_{HP} = 8.0 Hz, $\overline{\text{P}(\text{OCH}_2)_2(\text{OCCH}_3)}$); Note: assignment of coupling constants was based on decoupling experiments), 3.50 (ddd, 1H, ²J_{HH} = 8.0 Hz, ³J_{HP} = 3.6 Hz, ⁴J_{HH} = 1.4 Hz, $\overline{\text{P}(\text{OCH}_2)_2(\text{OCCH}_3)}$), 3.45 (ddd, 1H, ²J_{HH} = 8.0 Hz, ³J_{HP} = 3.6 Hz, ⁴J_{HH} = 1.4 Hz, $\overline{\text{P}(\text{OCH}_2)_2(\text{OCCH}_3)}$), 1.51 (s, 3H, $\overline{\text{P}(\text{OCH}_2)_2(\text{OCCH}_3)}$). ¹³C NMR (125 MHz, CDCl₃, δ): 148.2, 145.3, 143.9, 136.4 (Tp 3 or 5 position), 135.0 (d, J_{CP} = 9.0 Hz, *ortho* or *meta* of PPh₃), 134.7, 134.5 (Tp 3 or 5 or ipso of PPh₃ with one singlet missing presumably due to coincidental overlap), 129.3 (*para* of PPh₃), 127.4 (d,

$J_{CP} = 9.0$ Hz, *ortho* or *meta* of PPh_3), 105.7, 105.5, 105.2 (Tp 4 position), 81.6 [$P(\overline{OCH_2})_2(OCCH_3)$], 74.9-74.7 (overlapping resonances, $P(\overline{OCH_2})_2(OCCH_3)$), 15.6 (d, $J_{CP} = 10$ Hz, $P(\overline{OCH_2})_2(OCCH_3)$). $^{31}P\{^1H\}$ NMR (121 MHz, $CDCl_3$, δ): 162.6 (d, $^2J_{PP} = 55$ Hz, $P(\overline{OCH_2})_2(OCCH_3)$), 44.8 (d, $^2J_{PP} = 55$ Hz, PPh_3). CV (NCMe): $E_{1/2} = 1.08$ V Ru(III/II). Anal. Calcd. for $C_{22}H_{35}BClN_6O_3P_2Ru \cdot CH_2Cl_2$ [NOTE: repeated efforts to dry this sample did not remove residual solvent. Thus, one equivalent of dichloromethane (observed and quantified by 1H NMR spectroscopy) is included in elemental analysis calculations]: C, 46.26; H, 4.12; N, 10.12. Found: C, 46.84; H, 4.19; N, 10.28.

TpRu[P(OMe)₃](PPh₃)Cl (5). TpRu(PPh₃)₂Cl (0.295 g, 0.338 mmol) was added to 20 mL of C_6H_6 , and P(OMe)₃ (0.0460 g, 0.371 mmol) was added. The solution was refluxed for 3 h to give a bright yellow solution. The volatiles were removed *in vacuo*. The resulting solid was dissolved in minimal THF. Hexanes were added, and the solvent was reduced *in vacuo* to induce precipitation of a yellow solid, which was collected on a fine porosity frit and dried *in vacuo* (0.0557 g, 67.0%). 1H NMR (300 MHz, $CDCl_3$, δ) 8.12, 7.65, 7.58, 7.56 (each a d, each 1H, Tp 3 and 5), 7.41–7.11 (overlapping m's, 15H, $P(C_6H_5)_3$), 6.83, 6.66 (each a d, each 1H, Tp 3 and 5), 6.13, 5.75, 5.70 (each a t, each 1H, Tp 4), 3.24 (d, $^3J_{HP} = 10.3$ Hz, 9H, $P(OCH_3)_3$). ^{13}C NMR (125 MHz, $CDCl_3$) δ 148.0, 144.8, 144.1, 136.2, 135.5, 135.2 (Tp 3 or 5 position), 134.9 (d, $J_{CP} = 9$ Hz, *ortho* or *meta* of $P(C_6H_5)_3$), 134.6 (ipso of $P(C_6H_5)_3$), 128.9 (*para* of $P(C_6H_5)_3$), 127.2 (d, $J_{CP} = 9$ Hz, *ortho* or *meta* of $P(C_6H_5)_3$), 105.2 (coincidental overlap of two Tp 4 position), 104.3 (Tp 4 position), 51.8 (d, $^2J_{CP} = 6.3$ Hz, CH_3). ^{31}P NMR (121 MHz, $CDCl_3$, δ): 145.9 (d, $^2J_{PP} =$

54 Hz, $P(\text{OMe})_3$, 46.1 (d, $^2J_{\text{PP}} = 54$ Hz, $P\text{Ph}_3$). CV (NCMe): $E_{1/2} = 0.88$ V Ru(III/II). HRMS: $[\text{M} + \text{Na}]^+$ obsd (%), calcd (%), ppm: 756.091 (38), 756.08845 (31.1), 3.4; 757.09061 (50.3), 757.09029 (53), 0.4; 758.09062 (77), 758.08983 (78.8), 1; 759.08946 (100), 759.08712 (100), 3.1; 760.09086 (56.8), 760.08976 (49.2), 1.4; 761.08919 (73.4), 761.08741 (72.6), 2.3; 762.09149 (26.1), 762.0891 (27.9), 3.1.

$(\eta^6\text{-C}_6\text{H}_6)\text{Ru}(\text{PPh}_3)\text{Cl}_2$ (6). The synthesis and characterization of $(\eta^6\text{-C}_6\text{H}_6)\text{Ru}(\text{PPh}_3)\text{Cl}_2$ have been previously reported.⁴⁰ ^1H NMR spectroscopy revealed pure material and was consistent with previously reported data. CV (NCMe): $E_{1/2} = 1.31$ V Ru(III/II) (quasi-reversible); $E_{\text{p,c}} = -0.85$ V and -1.07 V

$(\eta^6\text{-C}_6\text{H}_6)\text{Ru}[\text{P}(\text{OMe})_3]\text{Cl}$ (7). The synthesis and characterization of $(\eta^6\text{-C}_6\text{H}_6)\text{Ru}[\text{P}(\text{OMe})_3]\text{Cl}_2$ have been previously reported.⁴⁰ ^1H NMR spectroscopy revealed clean material and was consistent with previously reported data. CV (NCMe): $E_{1/2} = 1.30$ V Ru(III/II) (quasi-reversible); $E_{\text{p,c}} = -0.94$ V ($n = 2$).

$(\eta^6\text{-C}_6\text{H}_6)\text{Ru}(\text{PMe}_3)\text{Cl}_2$ (8). The synthesis of $(\eta^6\text{-C}_6\text{H}_6)\text{Ru}(\text{PMe}_3)\text{Cl}_2$ has been previously reported.⁴² We used an alternate procedure. $[(\eta^6\text{-C}_6\text{H}_6)\text{Ru}(\text{Cl})(\text{m-Cl})]_2$ (0.140 g, 0.280 mmol) was stirred in CH_2Cl_2 (~30 mL) at room temperature. PMe_3 (0.0470 g, 0.616 mmol) was added slowly by syringe. The solution was stirred at room temperature for 3 h during which time the heterogeneous solution became a homogeneous red solution. The solution was filtered through a fine porosity frit. The filtrate was reduced *in vacuo* to ~5 mL. Hexanes were added to induce an orange precipitate. The mixture was filtered through a fine porosity fritted funnel. The solid was dried *in vacuo* to yield an

orange solid (0.153 g, 83.8%). Although complex **8** has been previously reported, NMR data were not provided. ^1H NMR (500 MHz, CDCl_3 , δ): 5.58 (s, 6H, C_6H_6), 1.65 (d, 9H, $^2J_{\text{HP}} = 11.4$ Hz, CH_3). ^{13}C NMR (125 MHz, CDCl_3 , δ): 87.2 (s, C_6H_6), 16.6 (d, $^1J_{\text{PC}} = 34.1$ Hz, CH_3) $^{31}\text{P}\{^1\text{H}\}$ NMR (121 MHz, CDCl_3 , δ): 7.5 (s, PMe_3). CV (NCMe): $E_{1/2} = 1.19$ V Ru(III/II) (quasi-reversible); $E_{\text{p,c}} = -1.25$ V.

$(\eta^6\text{-C}_6\text{H}_6)\text{Ru}[\text{P}(\text{OCH}_2)_3\text{CEt}]\text{Cl}_2$ (9**).** $\text{P}(\text{OCH}_2)_3\text{CEt}$ (0.248 g, 1.53 mmol) and $[(\eta^6\text{-C}_6\text{H}_6)\text{Ru}(\text{Cl})(\mu\text{-Cl})]_2$ (0.382 g, 0.764 mmol) were stirred in CH_2Cl_2 (~50 mL) at room temperature overnight to give a heterogeneous mixture. The solid was collected by filtration through a fine porosity frit, washed with CH_2Cl_2 and pentane and dried *in vacuo* to yield a red solid (0.601 g, 95.5%). ^1H NMR (500 MHz, $\text{DMSO-}d_6$, δ): 5.82 (s, 6H, C_6H_6), 4.37 (d, 6H, $^3J_{\text{HP}} = 4.7$ Hz, $\text{P}(\text{OCH}_2)_3\text{CCH}_2\text{CH}_3$), 1.24 (q, 2H, $^3J_{\text{HH}} = 7.7$ Hz, $-\text{CCH}_2\text{CH}_3$), 0.77 (t, 3H, $^3J_{\text{HH}} = 7.6$ Hz, $-\text{CCH}_2\text{CH}_3$). ^{13}C NMR (125 MHz, $\text{DMSO-}d_6$, δ): 90.0 (s, C_6H_6), 87.6 (s, $\text{P}(\text{OCH}_2)_3\text{CCH}_2\text{CH}_3$), 74.8 (s, $\text{P}(\text{OCH}_2)_3\text{CCH}_2\text{CH}_3$), 22.1 (s, $\text{P}(\text{OCH}_2)_3\text{CCH}_2\text{CH}_3$), 6.9 (s, $\text{P}(\text{OCH}_2)_3\text{CCH}_2\text{CH}_3$). $^{31}\text{P}\{^1\text{H}\}$ NMR (121 MHz, $\text{DMSO-}d_6$, δ): 107.5 (s, $\text{P}(\text{OCH}_2)_3\text{CCH}_2\text{CH}_3$). CV (NCMe): $E_{\text{p,a}} = 1.39$ V Ru(III/II); $E_{\text{p,c}} = -1.09$ V Ru(II/I). Anal. Calcd. for $\text{C}_{12}\text{H}_{17}\text{Cl}_2\text{O}_3\text{PRu}\cdot(\text{CH}_2\text{Cl}_2)_{0.25}$ [NOTE: repeated efforts to dry this sample did not remove residual solvent. Thus, 0.25 equivalents of dichloromethane (observed and quantified by ^1H NMR spectroscopy) are included in elemental analysis calculations]: C, 33.94; H, 4.08. Found: C, 34.25; H, 4.18.

$(\eta^6\text{-C}_6\text{H}_6)\text{Ru}[\text{P}(\text{OCH}_2)_2(\text{OCCH}_3)]\text{Cl}_2$ (11**).** Compound **1** [55 mL of **1** in C_6H_6 (~0.0054 M)] was added to $[(\eta^6\text{-C}_6\text{H}_6)\text{Ru}(\text{Cl})(\mu\text{-Cl})]_2$ (0.505 g, 1.01 mmol). The solution

was stirred in CH_2Cl_2 (~100 mL) at room temperature for 2 h to give an orange solution. The mixture was filtered through a fine porosity frit. The filtrate was added to a ¼ inch plug of silica gel on top of ¼ inch of Celite and eluted with CH_2Cl_2 . The volume of the eluent was reduced *in vacuo* to ~3 mL. Hexanes were added to the eluent to yield a red precipitate. The solution was filtered through a fine porosity frit and dried *in vacuo* to give a red solid (0.102 g, 25% based on Ru dimer). Crystals of **4** were obtained by slow evaporation from a chloroform solution. ^1H NMR (500 MHz, CD_2Cl_2 , δ) 5.90 (s, 6H, C_6H_6), 4.26 (m, 2H, $\text{P}(\overline{\text{OCH}_2})_2(\text{OCCH}_3)$), 3.84 (d, 2H, $^2J_{\text{HH}} = 6.5$ Hz CH_2), 1.69 (s, 3H, CH_3). ^{13}C NMR (75 MHz, CDCl_3 , δ): 91.5 (s, C_6H_6), 83.3 (s, $\text{P}(\overline{\text{OCH}_2})_2(\text{OCCH}_3)$), 75.9 (d, $^2J_{\text{CP}} = 5.4$ Hz, $\text{P}(\overline{\text{OCH}_2})_2(\text{OCCH}_3)$), 15.0 (s, $\text{P}(\overline{\text{OCH}_2})_2(\text{OCCH}_3)$). $^{31}\text{P}\{^1\text{H}\}$ NMR (121 MHz, CD_2Cl_2 , δ): 139.7 $\text{P}(\overline{\text{OCH}_2})_2(\text{OCCH}_3)$. HRMS: $[\text{M} + \text{Na}]^+$ obsd (%), calcd (%), ppm: 403.89292 (36.8), 403.8932 (15.2), 0.7; 405.89292 (36.8), 405.89274 (25.3), 0.4; 406.89271 (100), 406.8917 (100), 2.5; 407.89157 (36.8), 407.89134 (12.8), 0.6; 408.88907 (97.7), 408.89079 (28.8), 4.2; 409.89174 (85.5), 409.8919 (84.2), 0.4; 410.88847 (85.5), 410.88871 (84.2), 0.6. CV (NCMe): $E_{\text{p,a}} = 1.50$ V Ru(III/II); $E_{\text{p,c}} = -0.99$ V Ru(II/I).

(η^6 -*p*-cymene)Ru[P(OCH₂)₃CEt]Cl₂ (12**).** The dimeric complex [$(\eta^6$ -*p*-cymene)Ru(Cl)(μ -Cl)]₂ (0.102 g, 0.166 mmol) and P(OCH₂)₃CEt (0.0690 g, 0.436 mmol) were combined in a round bottom flask with 20 mL of CH_2Cl_2 . The reaction mixture was stirred at room temperature for 1 h. The total volume of the solution was reduced *in*

vacuo to ~2 mL. Hexanes were added to yield a red-orange precipitate. The solid was collected by filtration through a fine porosity frit and dried *in vacuo* to yield a red-orange solid (0.3830 g, 83%). ^1H NMR (300 MHz, CDCl_3 , δ) 5.63 (d, 2H, $^3J_{\text{HH}} = 6.0$ Hz, C_6H_4), 5.51 (d, 2H, $^3J_{\text{HH}} = 6.0$ Hz, C_6H_4), 4.37 (d, 6H, $^3J_{\text{HP}} = 5.0$ Hz, $\text{P}(\text{OCH}_2)_3\text{CCH}_2\text{CH}_3$), 2.88 (sept, 1H, $^2J_{\text{HH}} = 7$ Hz, $(\text{CH}_3\text{C}_6\text{H}_4(\text{CH})(\text{CH}_3)_2)$), 2.16 (s, 3H, $\text{C}_6\text{H}_4\text{-CH}_3$), 1.32–1.15 (overlapping m's, 8H, coincidental overlap of $\text{P}(\text{OCH}_2)_3\text{CCH}_2\text{CH}_3$ and $\text{C}_6\text{H}_4\text{-CH}(\text{CH}_3)_2$), 0.84 (t, 3H, $^3J_{\text{HH}} = 8$ Hz, $(\text{P}(\text{OCH}_2)_3\text{CCH}_2\text{CH}_3)$). ^{13}C NMR (75 MHz, CDCl_3) δ 108.9 (s, C_6H_4), 103.3 (s, C_6H_4), 90.1 (d, $^2J_{\text{PC}} = 7.1$ Hz, C_6H_4), 89.3 (d, $^2J_{\text{PC}} = 6.0$ Hz, C_6H_4), 75.5 (d, $^2J_{\text{CP}} = 7.6$ Hz, $\text{P}(\text{OCH}_2)_3\text{CCH}_2\text{CH}_3$), 36.1 ($^3J_{\text{CP}} = 32.2$ Hz, $\text{P}(\text{OCH}_2)_3\text{CCH}_2\text{CH}_3$), 30.5 (s, $\text{C}_6\text{H}_4\text{-CH}(\text{CH}_3)_2$), 23.4 (s, $\text{P}(\text{OCH}_2)_3\text{CCH}_2\text{CH}_3$), 22.1 (s, $\text{C}_6\text{H}_4\text{-(CH}(\text{CH}_3)_2)$), 18.6 (s, $\text{C}_6\text{H}_4\text{-CH}_3$), 7.3 (s, $\text{P}(\text{OCH}_2)_3\text{CCH}_2\text{CH}_3$). $^{31}\text{P}\{^1\text{H}\}$ NMR (121 MHz, CD_2Cl_2 , δ): 111.8 ($\text{P}(\text{OCH}_2)_2\text{CEt}$). HRMS: $[\text{M} + \text{Na}]^+$ obsd (%), calcd (%), ppm: 488.9858 (37.6), 488.98503 (32.9), 1.6; 489.98611 (62.9), 489.98504 (42), 2.2; 490.98525 (100), 490.98445 (100), 1.6; 491.98534 (44.5), 491.98404 (32.9), 2.6; 492.9845 (96.7), 492.98449 (94.8), 0; 493.98643 (85.5), 493.98554 (84.2), 1.8; 494.98312 (85.5), 494.98235 (84.2), 1.6. CV (NCMe): $E_{1/2} = 1.30$ V Ru(III/II) (quasi-reversible); $E_{\text{p,c}} = -1.23$ V Ru(II/I).

$(\eta^6\text{-}p\text{-cymene})\text{Ru}[\overline{\text{P}(\text{OCH}_2)_2(\text{OCCH}_3)}]\text{Cl}_2$ (13). A benzene solution of **1** (0.570 g, 4.25 mmol) was added to $[(\eta^6\text{-}p\text{-cymene})\text{Ru}(\text{Cl})(\mu\text{-Cl})]_2$ (0.369 g, 0.603 mmol) in CH_2Cl_2 (~75 mL). The solution was stirred at room temperature for 30 minutes to give an orange solution. The solvent volume was reduced *in vacuo* to ~25 mL. Hexanes were

added to yield a red precipitate, which formed a red oil. The solution was filtered through Celite. The solid collected on Celite was eluted with CH_2Cl_2 . The solvent was removed *in vacuo*. The resulting solid was washed with pentane. The solid was dried to yield a reddish-orange solid (0.489 g, 92.3%). This crude material was purified on an alumina column with 1:1 CH_2Cl_2 :THF as eluent (0.088 mg, 20%). ^1H NMR (300 MHz, CDCl_3 , δ) 5.76 (d, 2H, C_6H_4 , $^3J_{\text{HH}} = 5.9$ Hz), 5.62 (d, 2H, C_6H_4 , $^3J_{\text{HH}} = 5.9$ Hz), 4.22 (apparent t, 2H, $\text{P}(\overline{\text{OCH}_2})_2(\text{OCCH}_3)$, $^2J_{\text{HH}} = 8$ Hz) 3.83 (d, 2H, $\text{P}(\overline{\text{OCH}_2})_2(\text{OCCH}_3)$, $^2J_{\text{HH}} = 7$ Hz), 2.90 (sept, 1H, $(\text{CH}_3\text{C}_6\text{H}_4(\text{CH})(\text{CH}_3)_2$ $^3J_{\text{HH}} = 7$ Hz), 2.22 (s, 3H, $\text{C}_6\text{H}_4\text{-CH}_3$), 1.68 (s, 3H, $\text{P}(\overline{\text{OCH}_2})_2(\text{OCCH}_3)$), 1.23 (d, 6H, $\text{C}_6\text{H}_4\text{-CH}(\text{CH}_3)_2$, $^3J_{\text{HH}} = 7$ Hz). ^{13}C NMR (75 MHz, CDCl_3 , δ) 110.0 (s, C_6H_4), 106.2 (s, C_6H_4), 90.5 (C_6H_4), 90.4 (C_6H_4), 90.1 (C_6H_4), 90.1 (C_6H_4), 82.9 (s, $\text{P}(\overline{\text{OCH}_2})_2(\text{OCCH}_3)$), 75.7 (s, $\text{P}(\overline{\text{OCH}_2})_2(\text{OCCH}_3)$), 75.6 (s, $\text{P}(\overline{\text{OCH}_2})_2(\text{OCCH}_3)$), 30.9 ($\text{C}_6\text{H}_4\text{-CH}(\text{CH}_3)_2$), 22.3 (s, symm. equivalent $\text{C}_6\text{H}_4\text{-C}(\text{CH}_3)_2$), 18.8 (s, $\text{C}_6\text{H}_4\text{-CH}_3$), 15.3 (d, $^3J_{\text{HH}} = 10.4$ Hz, $\text{P}(\overline{\text{OCH}_2})_2(\text{OCCH}_3)$). $^{31}\text{P}\{^1\text{H}\}$ NMR (121 MHz, CDCl_3 , δ): 143.6 (s, $\text{P}(\overline{\text{OCH}_2})_2(\text{OCCH}_3)$). HRMS: $[\text{M} + \text{Na}]^+$ obsd (%), calcd (%), ppm: 460.95441 (37.4), 460.95328 (46.3), 2.5; 461.95477 (63), 461.95265 (60.9), 4.6; 462.95389 (100), 462.95262 (100), 2.7; 463.95387 (42.9), 463.95148 (48.6), 5.2; 464.95316 (97.1), 464.95168 (91.8), 3.2; 465.95496 (85.5), 465.95309 (84.2), 4; 466.95174 (85.5), 466.95034 (84.2), 3. CV (NCMe): $E_{1/2} = 1.44$ V Ru(III/II) (quasi-reversible); $E_{\text{p,c}} = -1.05$ V.

(η^6 -*p*-cymene)Ru[P(OMe)₃]Cl₂ (14). The synthesis of complex **14** has been previously reported.⁴⁷ We used an alternate procedure, which is given below. [(η^6 -*p*-cymene)Ru(Cl)(μ -Cl)]₂ (0.0517 g, 0.0844 mmol) was stirred at room temperature in CH₂Cl₂ (~15 mL). P(OMe)₃ (0.0232 g, 0.187 mmol) was added by syringe. The solution was stirred at room temperature for 2 h after which time the solution was reduced *in vacuo* to ~3 mL. Hexanes were added to yield an orange precipitate. The solution was filtered through a fine porosity frit. The solid was washed with pentane and dried *in vacuo* to yield an orange solid (0.0553 g, 76.1% yield). ¹H NMR spectroscopy revealed clean material and was consistent with previously reported data.⁴⁷ CV (NCMe): E_{1/2} = 1.25 V Ru(III/II) (quasi-reversible); E_{p,c} = -1.21 V.

(η^6 -*p*-cymene)Ru(PPh₃)Cl₂ (15). The synthesis of complex **15** has been previously reported.⁴⁷ We used an alternate procedure, which is given below. [(η^6 -*p*-cymene)Ru(Cl)(μ -Cl)]₂ (0.400 g, 0.653 mmol) and PPh₃ (0.360 g, 1.37 mmol) were stirred at room temperature for 2 h in CH₂Cl₂ (~15 mL), after which time the solution was reduced *in vacuo* to ~3 mL. Hexanes were added to yield an orange precipitate. The mixture was filtered through a fine porosity frit. The solid was washed with pentane and dried *in vacuo* to yield an orange solid (0.658 g, 88.7% yield). ¹H NMR spectroscopy revealed clean material and was consistent with previously reported data.⁴⁷ CV (NCMe): E_{1/2} = 1.25 V Ru(III/II); E_{p,c} = -1.25 V.

General Procedure for the Measurement of Rates of Exchange. Stock solutions in CDCl₃ were prepared in a volumetric flask. Each kinetic experiment was

performed in triplicate. For each experiment, CDCl_3 solutions of $\text{P}(\text{OMe})_3$ and/or PPh_3 were combined in a screw cap NMR tube with CDCl_3 such that the reaction volume before addition of Ru complex totaled 0.40 mL. Immediately before placing the solution into the NMR probe (equilibrated at 58 °C), 0.20 mL of the Ru complex (**12**, **13** or **15**) (with hexamethyldisiloxane as an internal standard) was added by syringe to give a total volume 0.60 mL. The tube was inverted two times. Reaction progress was monitored by ^1H NMR spectroscopy using automated data acquisition. A single transient was used for each time point with 60 s delay between transients for reactions with solutions of **13** and **15**, and a 600 s between transients for reactions of complex **12**. The rate of the reaction was determined by monitoring the disappearance of starting material [complex **12**: 4.37 ppm [d, $^3J_{\text{HP}} = 5.0$ Hz, $\text{P}(\text{OCH}_2)_3\text{CCH}_2\text{CH}_3$]; complex **15**: 1.87 ppm [s, (*p*-cymene) $\text{C}_6\text{H}_4\text{-CH}_3$], and complex **13**: 1.68 ppm [s, 3H, $\text{P}(\text{OCH}_2)_2(\text{OCCH}_3)$]. Each reaction was monitored through at least 3.5 half-lives. Rates were determined by least squares analyses of a plot of starting material vs time (seconds).

2.5. References

- (1) Crabtree, R. H. *The Organometallic Chemistry of the Transition Metals*; 4th ed.; Wiley-Interscience: USA, 2005.
- (2) Keiter, R. L.; Verkade, J. G. *Inorg. Chem.* **1970**, 9, 404.
- (3) Verkade, J. G.; McCarley, D. G.; Hendricker, D. G.; King, R. W. *Inorg. Chem.* **1965**, 4, 228.
- (4) Meiners, J. H.; Rix, C. J.; Clardy, J. C.; Verkade, J. G. *Inorg. Chem.* **1975**, 14, 705.

- (5) Serron, S.; Nolan, S. P.; Abramov, Y. A.; Brammer, L.; Petersen, J. L. *Organometallics* **1998**, *17*, 104.
- (6) Tolman, C. A. *Chem. Rev.* **1977**, *77*, 313.
- (7) Freixa, Z.; van Leeuwen, P. W. N. M. *Dalton Trans.* **2003**, 1890.
- (8) Buntin, K. A.; Chen, L.; Fernandez, A. L.; Poe, A. J. *Coord. Chem. Rev.* **2002**, *233-234*, 41.
- (9) Leyssens, T.; Peeters, D.; Orpen, A. G.; Harvey, J. N. *Organometallics* **2007**, *26*, 2637.
- (10) Downing, J. H.; Smith, M. B. *Comprehensive Coordination Chemistry II* **2004**, *1*, 253.
- (11) Kuehl, O. *Coord. Chem. Rev.* **2005**, *249*, 693.
- (12) Sasaki, S.; Yoshifuji, M. *Curr. Org. Chem.* **2007**, *11*, 17.
- (13) van Leeuwen, P. W. N. M.; Freixa, Z.; Zuidema, E. *Phosphorus Ligands in Asymmetric Catalysis* **2008**, *3*, 1433.
- (14) Müller, T. E.; Mingos, D. M. P. *Transition Met. Chem.* **1995**, *20*, 553.
- (15) Gilheany, D. G. In *Organophosphorus Compounds*; Hartley, F. R., Ed.; John Wiley & Sons: 1990; Vol. 1, p 9.
- (16) Valentine, D. H.; Hillhouse, J. H. *Synthesis* **2003**, 2437.
- (17) Meiners, J. H.; Clardy, J. C.; Verkade, J. G. *Inorg. Chem.* **1975**, *14*, 632.
- (18) Hartwig, J. F. *Organotransition Metal Chemistry: from Bonding to Catalysis*; University Science Books, 2010.
- (19) Valentine, D. H.; Hillhouse, J. H. *Synthesis* **2003**, 317.
- (20) Kuehl, O. *Can. J. Chem.* **2007**, *85*, 230.
- (21) Cao, M.; Do, L. V.; Hoffman, N. W.; Kwan, M. L.; Little, J. K.; McGilvray, J. M.; Morris, C. B.; Soderberg, B. C.; Wierzbicki, A.; Cundari, T. R.; Lake, C. H.; Valente, E. J. *Organometallics* **2001**, *20*, 2270.
- (22) Fortman, G. C.; Nolan, S. P. *Organometallics* **2010**, *29*, 4579.

- (23) Verkade, J. G.; Hutteman, T. J.; Fung, M. K.; King, R. W. *Inorg. Chem.* **1965**, *4*, 83.
- (24) Heitsch, C. W.; Verkade, J. G. *Inorg. Chem.* **1962**, *1*, 392.
- (25) Rix, C. J.; Verkade, J. G. *Coord. Chem. Rev.* **1975**, *16*, 129.
- (26) Verkade, J. G. *Bioinorg Chem* **1974**, *3*, 165.
- (27) Vande Griend, L. J.; Verkade, J. G.; Pennings, J. F. M.; Buck, H. M. *J. Am. Chem. Soc.* **1977**, *99*, 2459.
- (28) Verkade, J. G. *Coord. Chem. Rev.* **1972**, *9*, 1.
- (29) Milbrath, D. S.; Springer, J. P.; Clardy, J. C.; Verkade, J. G. *J. Am. Chem. Soc.* **1976**, *98*, 5493.
- (30) Huttemann, T. J.; Foxman, B. M.; Sperati, C. R.; Verkade, J. G. *Inorg. Chem.* **1965**, 950.
- (31) Foley, N. A.; Ke, Z. F.; Gunnoe, T. B.; Cundari, T. R.; Petersen, J. L. *Organometallics* **2008**, *27*, 3007.
- (32) Verkade, J. G.; Piper, T. S. *Inorg. Chem.* **1963**, *2*, 944.
- (33) Denny, D. B.; Varga, S. L. *Phosphorus* **1973**, *2*, 245.
- (34) Nifant'ev, E. E.; Koroteev, A. M.; Koroteev, M. P.; Meshkov, S. V.; Belsky, V. K.; Bekker, A. R. *Phosphorus, Sulfur Silicon Relat. Elem.* **1996**, *113*, 1.
- (35) Wadsworth, W. S.; Emmons, W. D. *J. Am. Chem. Soc.* **1962**, 610.
- (36) Wirz, B.; Barner, R.; Hubscher, J. *J. Org. Chem.* **1993**, *58*, 3980.
- (37) Roebuck, A.; Adkins, H. A. *Organic Synthesis*; John Wiley & Sons, Inc. : New York, 1955; Vol. 3.
- (38) Slugovc, C.; Sapunov, V. N.; Wiede, P.; Mereiter, K.; Schmid, R.; Kirchner, K. *J. Chem. Soc., Dalton Trans.* **1997**, 4209.
- (39) Werner, H.; Brauers, G.; Nurnberg, O. *J. Organomet. Chem.* **1993**, *454*, 247.
- (40) Zelonka, R. A.; Baird, M. C. *Can J Chemistry* **1972**, *50*, 3063.

- (41) Bennett, M. A.; Smith, A. K. *J Chem Soc Dalton* **1974**, 233.
- (42) Werner, H.; Werner, R. *Chem Ber-Recl* **1982**, 115, 3766.
- (43) Zelonka, R. A.; Baird, M. C. *J. Organomet. Chem.* **1972**, 35, C43.
- (44) Elsegood, M. R. J.; Tocher, D. A. *Polyhedron* **1995**, 14, 3147.
- (45) Pigge, F. C.; Coniglio, J. J. *Curr. Org. Chem.* **2001**, 5, 757.
- (46) Bard, A. J.; Faulkner, L. R. *Electrochemical Methods: Fundamentals and Applications*; 2nd ed.; John Wiley & Sons: New York, 2001.
- (47) Hodson, E.; Simpson, S. J. *Polyhedron* **2004**, 23, 2695.
- (48) Furstner, A.; Liebl, M.; Lehmann, C. W.; Picquet, M.; Kunz, R.; Bruneau, C.; Touchard, D.; Dixneuf, P. H. *Chem-Eur J* **2000**, 6, 1847.
- (49) Elsegood, M. R. J.; Smith, M. B.; Sanchez-Ballester, N. M. *Acta Crystallogr E* **2006**, 62, M2838.
- (50) Orpen, A. G.; Connelly, N. G. *J. Chem. Soc., Chem. Commun.* **1985**, 1310.
- (51) Dias, P. B.; Depiedade, M. E. M.; Simoes, J. A. M. *Coord. Chem. Rev.* **1994**, 135, 737.
- (52) Jover, J.; Fey, N.; Harvey, J. N.; Lloyd-Jones, G. C.; Orpen, A. G.; Owen-Smith, G. J. J.; Murray, P.; Hose, D. R. J.; Osborne, R.; Purdie, M. *Organometallics* **2010**, 29, 6245.
- (53) Ellis, D. D.; Haddow, M. F.; Orpen, A. G.; Watson, P. J. *Dalton Trans.* **2009**, 10436.
- (54) Taira, K.; Mock, W. L.; Gorenstein, D. G. *J. Am. Chem. Soc.* **1984**, 106, 7831.
- (55) Belyakov, A. V.; Dalhus, B.; Haaland, A.; Shorokhov, D. J.; Volden, H. V. *J Chem Soc Dalton* **2002**, 3756.
- (56) Slater, J. C. *Quantum Theory of Molecules and Solids, Vol. 4: The Self-Consistent Field for Molecules and Solids*; McGraw-Hill: New York, 1974.
- (57) Becke, A. D. *Phys Rev A* **1988**, 38, 3098.
- (58) Perdew, J. P. *Phys Rev B* **1986**, 34, 7406.

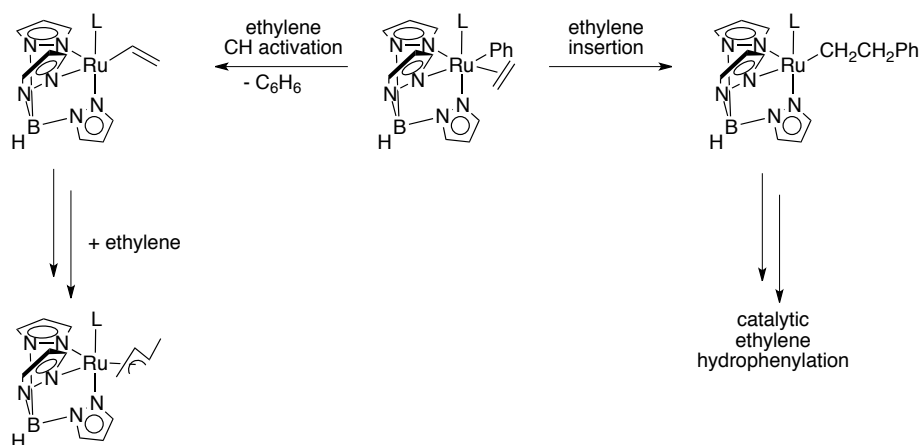
- (59) Perdew, J. P. *Phys Rev B* **1986**, 33, 8822.
- (60) Perdew, J. P.; Zunger, A. *Phys Rev B* **1981**, 23, 5048.
- (61) Hay, P. J.; Wadt, W. R. *J Chem Phys* **1985**, 82, 270.
- (62) Pyykko, P.; Mendizabal, F. *Inorg. Chem.* **1998**, 37, 3018.
- (63) Couty, M.; Hall, M. B. *J Comput Chem* **1996**, 17, 1359.
- (64) M.J. Frisch, G. W. T., H.B. Schlegel, G.E. Scuseria, M.A. Robb, J.R. Cheeseman, G. Scalmani, V.; Barone, B. M., G.A. Petersson, H. Nakatsuji, M. Caricato, X. Li, H.P. Hratchian, A.F. Izmaylov,; J. Bloino, G. Z., J.L. Sonnenberg, M. Hada, M. Ehara, K. Toyota, R. Fukuda, J. Hasegawa, M.; Ishida, T. N., Y. Honda, O. Kitao, H. Nakai, T. Vreven, J.A. Montgomery Jr, J.E. Peralta, F.; Ogliaro, M. B., J.J. Heyd, E. Brothers, K.N. Kudin, V.N. Staroverov, R. Kobayashi, J.; Normand, K. R., A. Rendell, J.C. Burant, S.S. Iyengar, J. Tomasi, M. Cossi, N. Rega, J.M.; Millam, M. K., J.E. Knox, J.B. Cross, V. Bakken, C. Adamo, J. Jaramillo, R. Gomperts, R.E.; Stratmann, O. Y., A.J. Austin, R. Cammi, C. Pomelli, J.W. Ochterski, R.L. Martin, K. Morokuma,; V.G. Zakrzewski, G. A. V., P. Salvador, J.J. Dannenberg, S. Dapprich, A.D. Daniels, O. Farkas, J.B.; Foresman, J. V. O., J. Cioslowski, D.J. Fox. ; Gaussian, Inc.: Willingford, CT, 2009.

3. Aromatic C–H Activation and Catalytic Hydroarylation of Ethylene Using $\text{TpRu}[\text{P}(\text{OCH}_2)_2(\text{OCCH}_3)](\text{NCMe})\text{Ph}$

3.1. Introduction

Previously, our group has demonstrated that $\text{TpRu}(\text{L})(\text{NCMe})\text{Ph}$ [$\text{L} = \text{CO}$, or $\text{P}(\text{OCH}_2)_3\text{CEt}$] complexes are active for olefin hydroarylation.¹⁻⁶ Expanded studies of $\text{TpRu}(\text{L})(\text{NCMe})\text{Ph}$ where $\text{L} = \text{CO}$, $\text{P}(\text{OCH}_2)_3\text{CEt}$, PMe_3 , or $\text{P}(N\text{-pyrrolyl})_3$ revealed important trends.³ It was shown through calculations and experimental data that the rate limiting step of the catalytic cycle is aromatic C–H activation, and the C–H activation step is promoted by more electron rich metal centers. In contrast, olefin insertion is more efficient with less electron rich metal centers. Our explanation of the trend in activation barrier for olefin insertion is based on metal-to-olefin π -backbonding. More electron deficient metals exhibit decreased backbonding into the π^* orbitals of the olefin, making the olefin less tightly bound and, hence, facilitate insertion into the Ru–Ph bond. Thus, a balance has to be struck between the electron richness of the metal center for these two key steps of the olefin hydroarylation catalytic cycle. In the case of electron rich metal centers such as $\text{TpRu}(\text{PMe}_3)(\text{NCMe})\text{Ph}$, olefin C–H activation competes with olefin insertion yielding a Ru–vinyl species, which upon subsequent olefin insertion and isomerization gives a stable $\text{TpRu}(\text{PMe}_3)(\eta^3\text{-C}_4\text{H}_7)$ complex incapable of catalytic olefin hydroarylation (Scheme 3.1).² Even though $\text{TpRu}[\text{P}(\text{OCH}_2)_3\text{CEt}](\text{NCMe})\text{Ph}$ is capable of catalytic olefin hydroarylation leading to approximately 10 TON of ethylbenzene (90 °C, 25 psi of ethylene) before catalytic deactivation, it was found that the metal center was

also too electron rich and olefin C–H activation competes with olefin insertion leading to the deactivation product, $\text{TpRu}[\text{P}(\text{OCH}_2)_3\text{CEt}](\eta^3\text{-C}_4\text{H}_7)$ (Scheme 3.1).



Scheme 3.1. Ethylene C–H activation vs ethylene insertion in olefin hydroarylation cycle.

Therefore, a long-lived catalyst cannot have strong phosphite donor ligands due to the competition between olefin C–H activation and olefin insertion. Additionally, through studies it has been determined that although C–H activation is the rate limiting step in the catalytic cycle, the difference in electron density of the metal center has a greater impact on olefin insertion rather than C–H activation.³ Furthermore, a catalyst with larger steric bulk could potentially bias the olefin orientation upon coordination to the metal center, which could allow us to control linear to branched selectivity when α -olefins are employed. Therefore, our group examined $\text{TpRu}[\text{P}(\text{pyr})_3](\text{NCMe})\text{Ph}$, in hopes to increase linear to branched selectivity. Unfortunately, the $\text{P}(\text{pyr})_3$ ligand was too sterically bulky and olefin coordination was inhibited.

The studies outlined in chapter 2 demonstrated that removing a methylene linker from the bicyclic phosphite $\text{P}(\text{OCH}_2)_3\text{CEt}$ to yield $\text{P}(\text{OCH}_2)_2(\text{OCCH}_3)$ leads to a decrease in donor ability as determined by cyclic voltammetry of $\text{Ru}(\text{II})$ complexes; however, cone angle calculations from crystallographic data showed that steric bulk of the two bicyclic phosphites is similar and significantly less than $\text{P}(\text{pyr})_3$.⁷ The decrease in electron density in P-basicity for $\text{P}(\text{OCH}_2)_2(\text{OCCH}_3)$ related to $\text{P}(\text{OCH}_2)_3\text{CEt}$ has been proposed to result from the “hinge” effect described by John Verkade, which is a consequence of decreased p-orbital overlap between the O and P atom. Alternatively, our group has proposed that changes in O–P–O angles results in lower energy P–O σ^* orbitals for $\text{P}(\text{OCH}_2)_2(\text{OCCH}_3)$ which enhances π -acidity (see chapter 2 for a more detailed discussion).⁷⁻⁹ Hence, we desired to use the ligand $\text{P}(\text{OCH}_2)_2(\text{OCCH}_3)$ to synthesize the catalyst precursor $\text{TpRu}[\text{P}(\text{OCH}_2)_2(\text{OCCH}_3)](\text{NCMe})\text{Ph}$ for olefin hydroarylation.

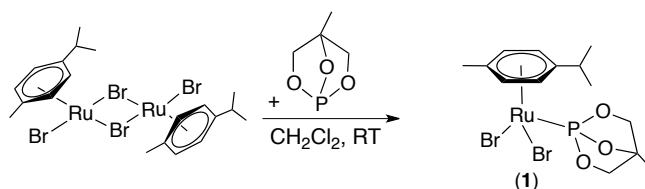
3.2. Results and Discussion

3.2.1. Synthesis of $\text{TpRu}[\text{P}(\text{OCH}_2)_2(\text{OCCH}_3)](\text{NCMe})\text{Ph}$

The initial attempt to synthesize $\text{TpRu}[\text{P}(\text{OCH}_2)_2(\text{OCCH}_3)](\text{NCMe})\text{Ph}$ was by a similar route as the published procedure for $\text{TpRu}[\text{P}(\text{OCH}_2)_3\text{CEt}](\text{NCMe})\text{Ph}$.¹ Refluxing $\text{TpRu}(\text{PPh}_3)_2\text{Cl}$ in benzene with excess $\text{P}(\text{OCH}_2)_2(\text{OCCH}_3)$ led to displacement of one PPh_3 and coordination of $\text{P}(\text{OCH}_2)_2(\text{OCCH}_3)$, yielding $\text{TpRu}(\text{PPh}_3)[\text{P}(\text{OCH}_2)_2(\text{OCCH}_3)]\text{Cl}$. This is evident by the two sets of doublets in the $^{31}\text{P}\{^1\text{H}\}$ NMR spectrum (162.6 and

44.8 ppm) with a $^2J_{\text{PP}} = 55$ Hz (see Chapter 2, Figure 2.3 for NMR spectrum). However, attempts at metathesis reactions with chloride using a variety of triflate or phenyl sources (e.g., AgOTf, TMSOTf, HOTf, $\text{Ph}_2\text{Mg}[\text{THF}]_2$, and PhMgCl) agents were futile. The reactions with triflate sources were not clean and purification was difficult. In addition, attempted reactions of $\text{TpRu}(\text{PPh}_3)[\text{P}(\text{OCH}_2)_2(\text{OCCH}_3)]\text{Cl}$ with phenyl sources lead to no reaction. Therefore, another starting material was sought.

Given previous reports that $[(\eta^6\text{-arene})\text{Ru}(\text{X})(\mu\text{-X})_2]$ ($\text{X} = \text{Cl}$ or Br ; $\eta^6\text{-arene}$ = benzene or cumene) complexes react with neutral two-electron donors to form $(\eta^6\text{-arene})\text{RuX}_2\text{L}$ complexes,¹⁰⁻²¹ we considered the Ru(II) arene complexes as possible precursors to $\text{TpRu}[\text{P}(\text{OCH}_2)_2(\text{OCCH}_3)](\text{NCMe})\text{Ph}$. Stirring $[(\eta^6\text{-}p\text{-cymene})\text{Ru}(\text{Br})(\mu\text{-Br})_2]$ and $\text{P}(\text{OCH}_2)_2(\text{OCCH}_3)$ in CH_2Cl_2 leads to the formation of $[(\eta^6\text{-}p\text{-cymene})\text{Ru}[\text{P}(\text{OCH}_2)_2(\text{OCCH}_3)]\text{Br}_2]$ (**1**) in 91% isolated yield (Scheme 3.2, Figure 3.1, Figure 3.2). The ^1H NMR spectrum shows a symmetric complex with two downfield resonances for the $(\eta^6\text{-}p\text{-cymene})$. The ^{31}P NMR spectrum of **1** shows a resonance at 140 ppm for the $\text{P}(\text{OCH}_2)_2(\text{OCCH}_3)$ ligand.



Scheme 3.2. Synthesis of $[(\eta^6\text{-}p\text{-cymene})\text{Ru}[\text{P}(\text{OCH}_2)_2(\text{OCCH}_3)]\text{Br}_2]$ (**1**).

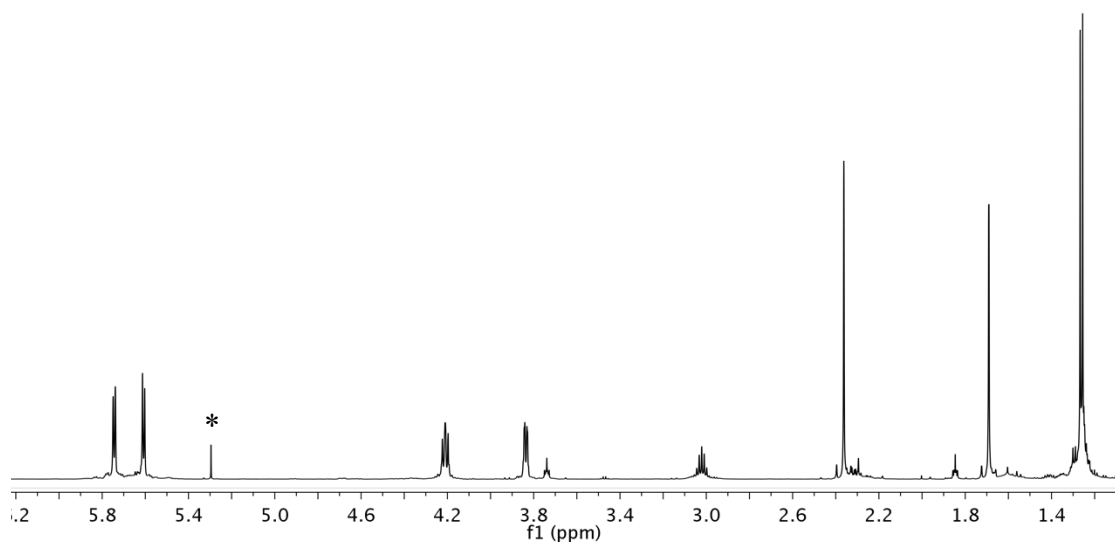


Figure 3.1. ^1H NMR spectrum of $(\eta^6\text{-}p\text{-cymene})\text{Ru}[\text{P}(\text{OCH}_2)_2(\text{OCCH}_3)]\text{Br}_2$ (**1**) in CDCl_3 . (* = residual CH_2Cl_2).

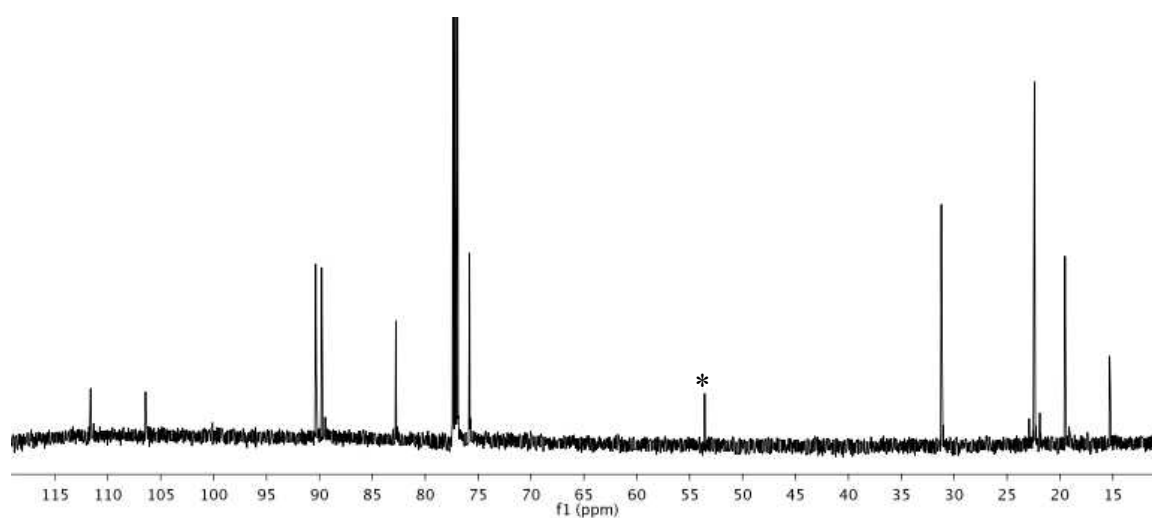
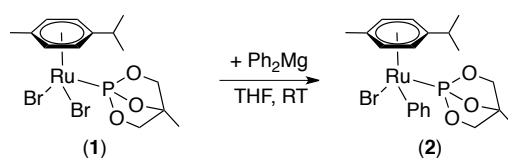


Figure 3.2. ^{13}C NMR spectrum of $(\eta^6\text{-}p\text{-cymene})\text{Ru}[\text{P}(\text{OCH}_2)_2(\text{OCCH}_3)]\text{Br}_2$ (**1**) in CDCl_3 . (* = residual CH_2Cl_2).

Stirring **1** and one equivalent of $\text{Ph}_2\text{Mg}(\text{THF})_2$ at room temperature gives the phenylated species $(\eta^6\text{-}p\text{-cymene})\text{Ru}[\text{P}(\text{OCH}_2)_2(\text{OCCH}_3)](\text{Ph})\text{Br}$ (**2**). Complex **1** is only

partially soluble in THF; however, upon the addition of $\text{Ph}_2\text{Mg}(\text{THF})_2$ to complex **1**, the reaction becomes bright yellow and homogeneous. The formation of **2** is evident by the ^{31}P NMR spectrum, which shows a downfield shift (155.5 ppm) of ~ 15 ppm relative to **1**. Additionally, the ^1H NMR spectrum supports an asymmetric complex with four separate resonances for the aromatic hydrogens of the η^6 -*p*-cymene ligand and the two doublets for the methyl groups of the (η^6 -*p*-cymene) isopropyl with $^3J_{\text{HH}}$ coupling constant of 7 Hz (Scheme 3.3, Figure 3.3, Figure 3.4).



Scheme 3.3. Synthesis of $[(\eta^6\text{-}p\text{-cymene})\text{Ru}[\text{P}(\text{OCH}_2)_2(\text{OCCH}_3)](\text{Ph})\text{Br}]$ (**2**).

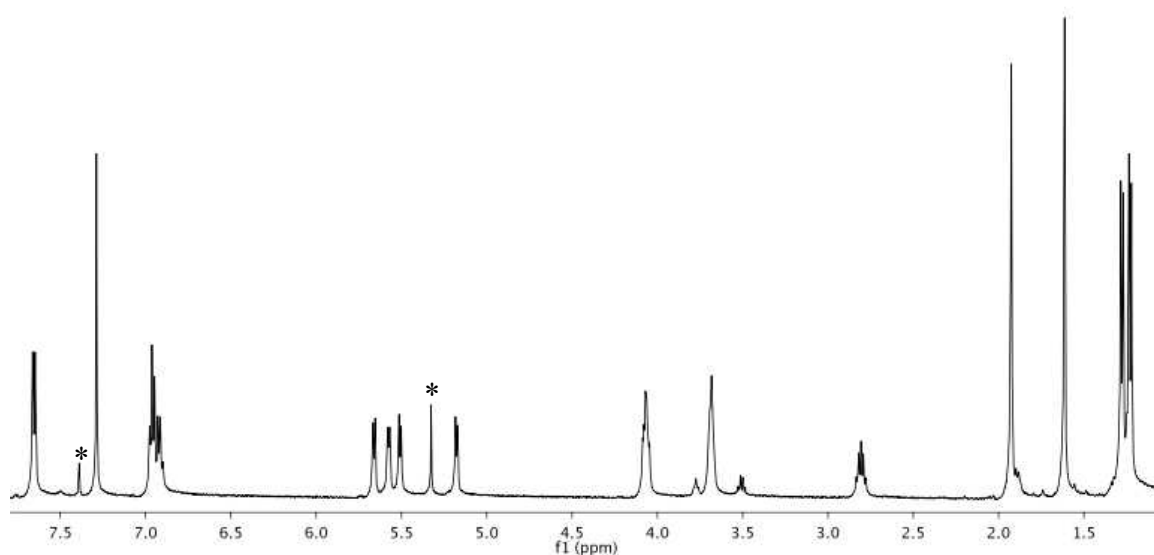


Figure 3.3. ^1H NMR spectrum of $[(\eta^6\text{-}p\text{-cymene})\text{Ru}[\text{P}(\text{OCH}_2)_2(\text{OCCH}_3)](\text{Ph})\text{Br}]$ (**2**) in CDCl_3 . (* = residual C_6H_6 and residual CH_2Cl_2).

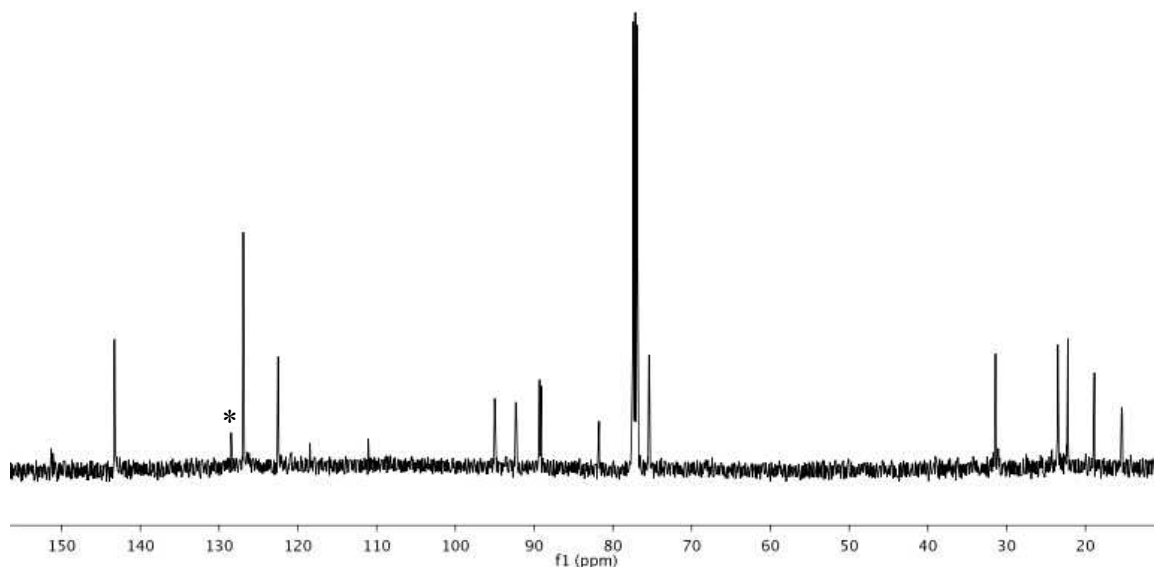
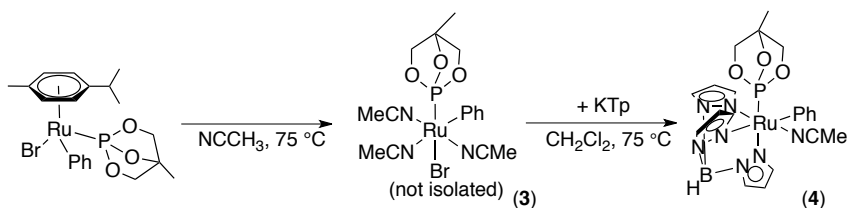


Figure 3.4. ^{13}C NMR spectrum of $(\eta^6\text{-}p\text{-cymene})\text{Ru}[\text{P}(\text{OCH}_2)_2(\text{OCCH}_3)](\text{Ph})\text{Br}$ (**2**) in CDCl_3 . (* = residual C_6H_6).

The *p*-cymene ligand can be displaced upon heating at 75 °C for 4 h in NCMe to yield the putative complex $(\text{NCMe})_3\text{Ru}[\text{P}(\text{OCH}_2)_2(\text{OCCH}_3)](\text{Ph})\text{Br}$ (**3**), whose identity is supported by the distinct disappearance of the 2 doublets for the methyl groups of the η^6 -*p*-cymene isopropyl group and the formation of free *p*-cymene. However, $(\text{NCMe})_3\text{Ru}[\text{P}(\text{OCH}_2)_2(\text{OCCH}_3)](\text{Ph})\text{Br}$ (**3**) has not been characterized beyond *in situ* ^1H NMR spectroscopy (Figure 3.5) due to difficulty in isolation and purification. Heating complex **3** and KTp in CH_2Cl_2 for 4 h at 75 °C produces $\text{TpRu}[\text{P}(\text{OCH}_2)_2(\text{OCCH}_3)](\text{NCMe})\text{Ph}$ (**4**) in 44% isolated yield (Scheme 3.4, Figure 3.6). The ^1H NMR spectrum of **4** is consistent

with an asymmetric complex with the presence of 9 unique Tp peaks. Cyclic voltammetry of complex **4** in NCMe shows a reversible redox couple at $E_{1/2} = 0.69$ V (vs. NHE).



Scheme 3.4. Synthesis of $\text{TpRu}[\text{P}(\text{OCH}_2)_2(\text{OCCH}_3)](\text{NCMe})\text{Ph}$ (**4**).

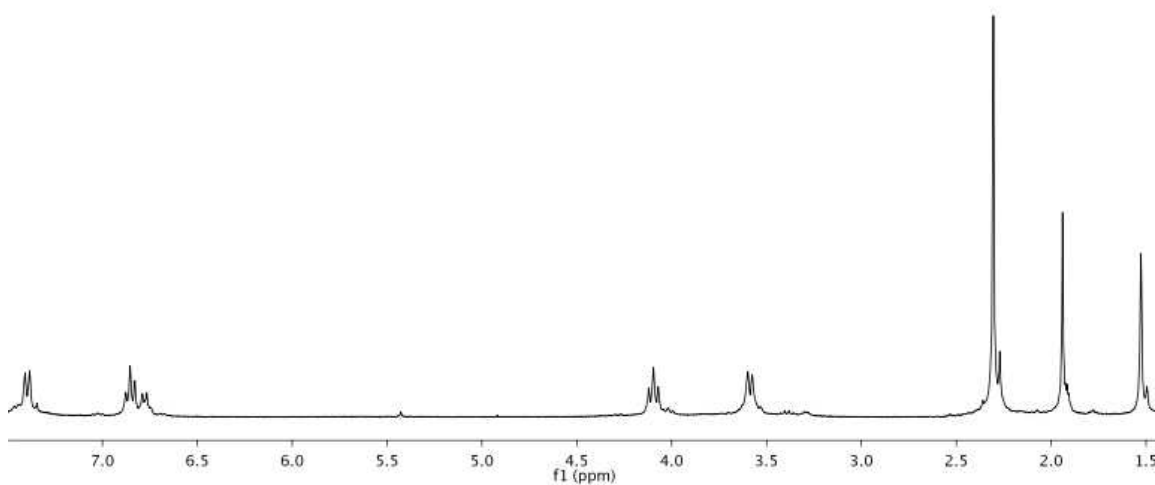


Figure 3.5. ^1H NMR spectrum of $(\text{NCMe})_3\text{Ru}[\text{P}(\text{OCH}_2)_2(\text{OCCH}_3)]\text{PhBr}$ (**3**) in CD_3CN .

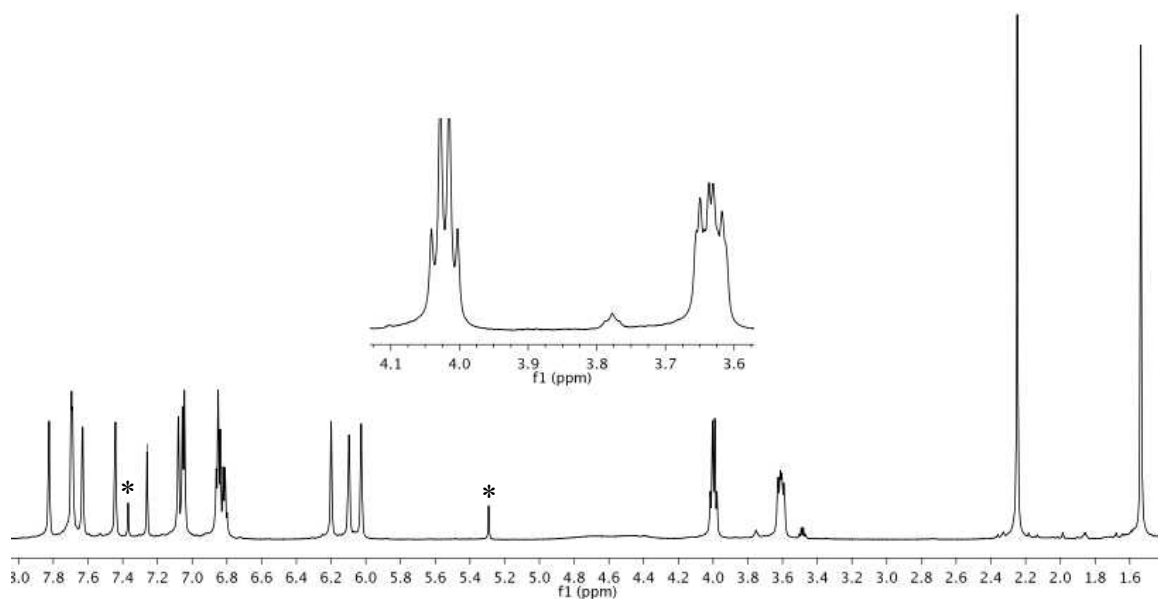


Figure 3.6. ^1H NMR spectrum of $\text{TpRu}[\text{P}(\text{OCH}_2)_2(\text{OCCH}_3)](\text{NCMe})\text{Ph}$ (**4**) in C_6D_6 . (* = residual CH_2Cl_2 and residual C_6H_6).

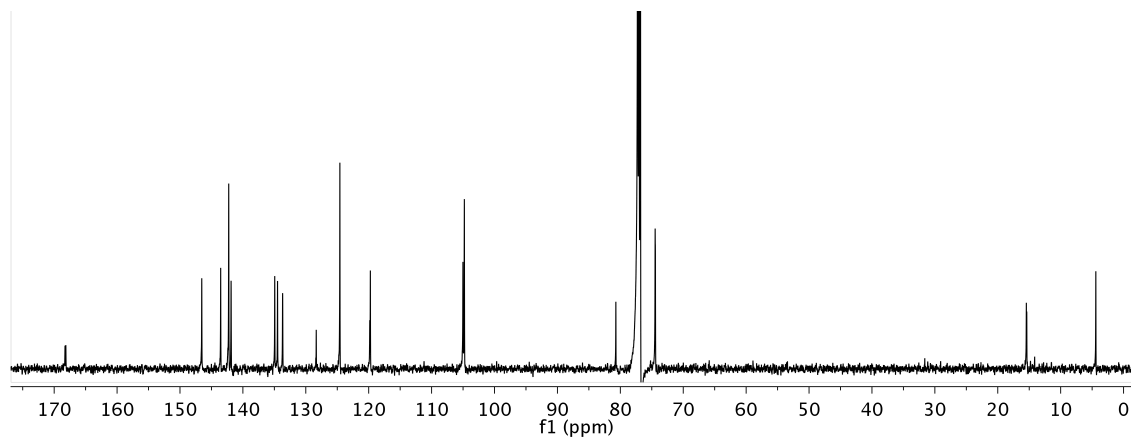


Figure 3.7. ^{13}C NMR spectrum of $\text{TpRu}[\text{P}(\text{OCH}_2)_2(\text{OCCH}_3)](\text{NCMe})\text{Ph}$ (**4**) in C_6D_6 .

A single crystal of **4** suitable for X-ray structure determination was obtained from slow evaporation of a CH_2Cl_2 :pentane ($\sim 1:1$ v:v) solution at room temperature, and the

resulting solid-state structure is shown in Figure 3.8 (Table 3.1). The phosphite has two smaller O–P–O angles of 93.76(1)° and 93.56(1)° and one larger angle at 100.27(2)°. The P–O bond distance for the arm of the phosphite without a CH₂ group is slightly longer at 1.643(2) Å versus 1.628(2) Å and 1.6290(2) Å for TpRu[P(OCH₂)₂(OCCH₃)](NCMe)Ph (4). The C–O–P bond angle is approximately 10° less for the portion of the phosphite lacking the CH₂ whereas the other C–O–P angles are 108.52(2)° and 107.95(2)°.

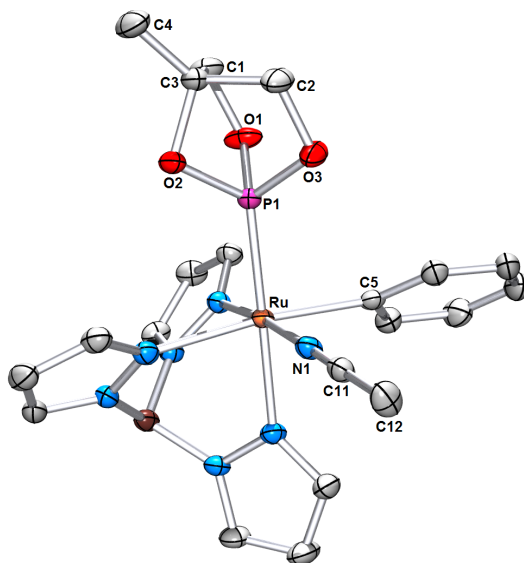


Figure 3.8. ORTEP of TpRu[P(OCH₂)₂(OCCH₃)](NCMe)Ph (4) (50% probability, hydrogen atoms omitted for clarity.) Selected bond lengths (Å): Ru–N1, 2.009(2); Ru–C5, 2.092(2); N1–C11, 1.147(2); C11–C12, 1.445(4); Ru–P1, 2.1602(6); P1–O1, 1.628(2); P1–O2, 1.643(2); P1–O3, 1.629(2). Selected bond angles (°): N1–Ru–C5, 88.55(9); N1–Ru–P1, 92.58(6); C5–Ru–P1, 92.83(6); N1–C11–C12, 178.1(3); O3–P1–O1, 100.27(2); O3–P1–O2, 93.76(1); O1–P1–O2, 93.56(1); O1–P1–Ru, 119.21(7); O3–P1–Ru, 120.47(7); C1–O1–P1, 108.52(2); C3–O2–P1, 98.56(1); C2–O3–P1, 107.95(2).

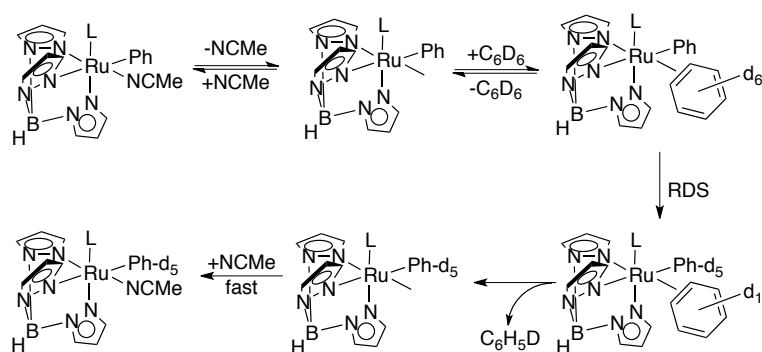
Table 3.1. Selective Crystallographic Data for $\text{TpRu}[\text{P}(\text{OCH}_2)_2(\text{OCCH}_3)](\text{NCMe})\text{Ph}\cdot\text{CH}_2\text{Cl}_2$ (**4**).

empirical formula	$\text{C}_{22}\text{H}_{27}\text{BCl}_2\text{N}_7\text{O}_3\text{PRu}$
Fw	8651.26
cryst syst	Triclinic
space group	P-1
a, Å	7.8849(2)
b, Å	12.4914(3)
c, Å	14.3261(3)
α , deg	81.278(1)
β , deg	88.846(1)
γ , deg	75.726(1)
V, Å ³	1351.43(6)
Z	2
D _{calcd} , mg/m ³	1.600
cryst size (mm)	0.42 x 0.19 x 0.08
R1, wR2 (I > 2(I))	0.0386, 0.1110
GOF	0.898

3.2.2. Stoichiometric Benzene Activation

Based on mechanistic studies, we have suggested that benzene C–H activation by $\text{TpRu}(\text{L})(\text{NCMe})\text{Ph}$ [$\text{L} = \text{CO}, \text{PMe}_3, \text{P}(\text{OCH}_2)_3\text{CEt}$] complexes most likely involves dissociation of NCMe, which gives an open coordination site for C_6D_6 coordination, followed by C–D activation (Scheme 3.5).^{1,2,4,5} The reaction of complex **4** in C_6D_6 under pseudo-first order conditions results in benzene C–D activation as described above for $\text{TpRu}(\text{L})(\text{NCMe})\text{Ph}$ [$\text{L} = \text{CO}, \text{PMe}_3, \text{P}(\text{OCH}_2)_3\text{CEt}$] (Scheme 3.5, Scheme 3.6) Similar to the previously reported $\text{TpRu}(\text{L})(\text{NCMe})\text{Ph}$ complexes,^{1,2,4,5} the addition of NCMe is necessary to inhibit decomposition and allow the C–D activation to proceed in quantitative yield (^1H NMR spectroscopy).² Monitoring a solution of **4** in C_6D_6 at 60 °C by ^1H NMR spectroscopy reveals the formation of benzene ($\text{C}_6\text{H}_5\text{D}$) and the disappearance of resonances for the phenyl ligand of **4**. The addition of one equivalent of

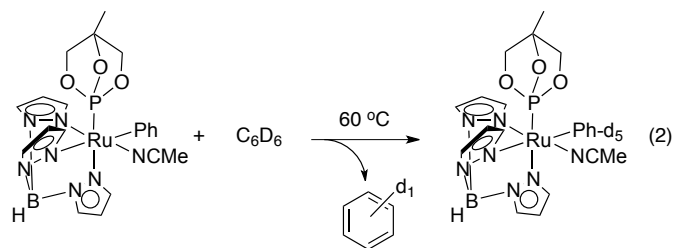
NCMe to the solution results in clean conversion of **4** to **4-d₅** with >90% yield (by ¹H NMR spectroscopy).²² These observations are consistent with C–D activation of C₆D₆ by complex **4**.



Scheme 3.5 Proposed mechanism for benzene C–H activation by TpRu(L)(NCMe)Ph.

In order to compare C₆D₆ activation by complex **4** to other TpRu(L)(NCMe)Ph complexes, the rate of reaction with C₆D₆ was determined under pseudo first order conditions (i.e., large excess of C₆D₆). A k_{obs} of $7.2(5) \times 10^{-6} \text{ s}^{-1}$ (60 °C) was found by fitting the plot concentration of perprotio-**4** versus time to a first-order decay (Figure 3.9). The k_{obs} is an average of four independent kinetic experiments. Thus, the rate of C₆D₆ activation shared good reproducibility. The k_{obs} values for C₆D₆ activation by TpRu(L)(NCMe)Ph (L = CO, PMe₃ or P(OCH₂)₃CET) have been previously determined,³ and a plot of k_{obs} for C₆D₆ activation vs. Ru(III/II) redox potential for the TpRu(L)(NCMe)Ph complexes reveals a clear trend (Table 3.2, Figure 3.10). The rate of C₆D₆ activation decreases as Ru(III/II) potential becomes more positive. The slowest C₆D₆ activation occurs with TpRu(CO)(NCMe)Ph with a $k_{\text{obs}} = 4.62(3) \times 10^{-6} \text{ s}^{-1}$; whereas the most electron-rich metal center, TpRu(PMe₃)(NCMe)Ph, exhibits the fastest rate of

C_6D_6 activation with $k_{\text{obs}} = 1.36(4) \times 10^{-5} \text{ s}^{-1}$ (Table 3.2). The plot of $E_{1/2}$ vs. k_{obs} gives a linear correlation with an R^2 value of 0.92 and a slope of $-1.29 \text{ s}^{-1}\text{V}^{-1}$ (Figure 3.10). However, it is important to note that in these experiments the rate of C–D activation is being determined from $\text{TpRu}(\text{L})(\text{NCMe})\text{Ph}$ rather than the proposed catalyst resting states $\text{TpRu}(\text{L})(\text{CH}_2\text{CH}_2\text{Ph})(\eta^2\text{-C}_2\text{H}_4)$. Since dissociation of ethylene, which is necessary for benzene activation in the catalytic cycle under conditions where $\text{TpRu}(\text{L})(\text{CH}_2\text{CH}_2\text{Ph})(\eta^2\text{-C}_2\text{H}_4)$ complexes are the resting state, might vary differently as a function of the ligand L compared to acetonitrile dissociation, it is not possible to definitively use the comparative rates of benzene activation by $\text{TpRu}(\text{L})(\text{NCMe})\text{Ph}$ to make predictions about relative rates of catalysis.



Scheme 3.6. Stoichiometric C–D benzene of complex 4.

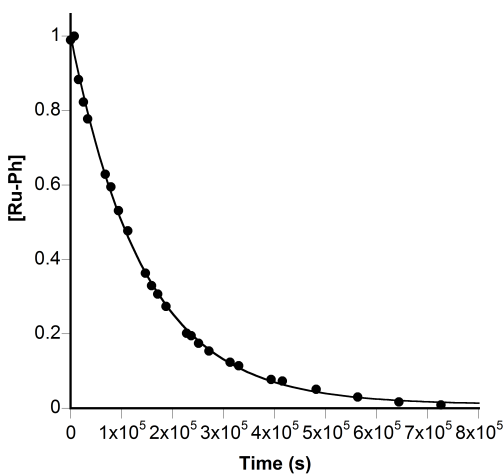


Figure 3.9. Representative plot of C–D activation of C_6D_6 by $TpRu[P(OCH_2)_2(OCCH_3)](NCMe)Ph$ (**4**) in C_6D_6 at 60 °C monitored by 1H NMR spectroscopy ($k_{obs} = 7.0(2) \times 10^{-6} s^{-1}$, $R^2 = 0.99$). The plot shows relative amount of protio-phenyl ligand (integrated against an internal standard) of **4** as a function of time.

Table 3.2. Ru(III/II) Potentials and Rate Constants for the Activation of C_6D_6 at 60 °C by $TpRu(L)(NCMe)Ph$.^a

L	Ru(III/II) Potentials (V vs. NHE)	k_{obs} ($\times 10^{-5}, s^{-1}$) ^a	Relative k_{obs}
PMe_3	0.29	1.36(4)	3.0
$P(OCH_2)_3CEt$	0.54	1.20(2)	2.6
$P(OCH_2)_2(OCCH_3)$	0.69	0.72(5)	1.6
CO	1.03	0.462(3)	1

^a 0.065 mmol of NCMe

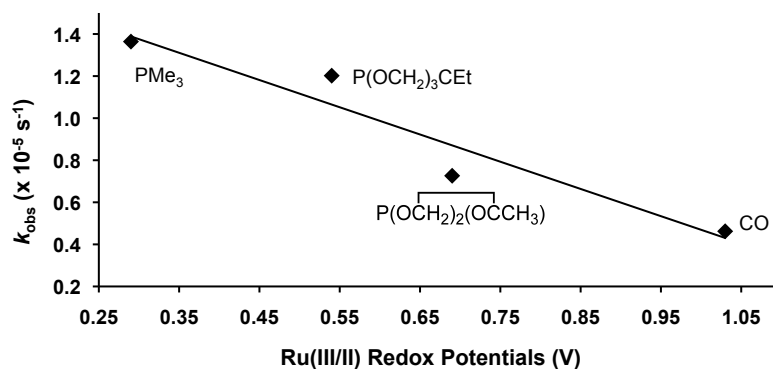
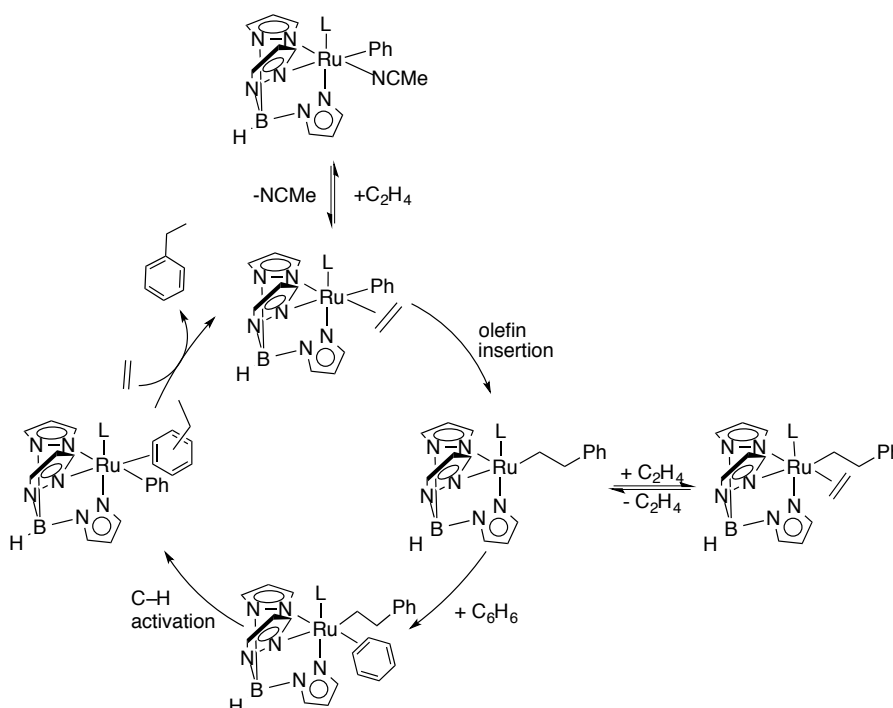


Figure 3.10. Linear fit for plot of k_{obs} ($\times 10^{-5} \text{ s}^{-1}$) values vs. Ru(III/II) potentials (vs. NHE, V) for the C–D activation of C_6D_6 by $\text{TpRu}(\text{L})(\text{NCMe})\text{Ph}$ at 60 °C with 0.065 mmol of added NCMe ($R^2 = 0.92$, $m = -1.29 \text{ s}^{-1}\text{V}^{-1}$).

3.2.3. Catalytic Hydrophenylation of Ethylene by $\text{TpRu}[\text{P}(\text{OCH}_2)_2(\text{OCCH}_3)](\text{NCMe})\text{Ph}$ (4)

Scheme 3.7 shows the proposed catalytic cycle for ethylene hydrophenylation by $\text{TpRu}(\text{L})(\text{NCMe})\text{Ph}$ complexes.^{1-3,5,23} Through experimental and computational mechanistic studies, it has been concluded that the active catalytic species is generated from $\text{TpRu}(\text{L})(\text{NCMe})\text{Ph}$ by dissociation of NCMe. Subsequent coordination of ethylene to Ru followed by olefin insertion into the Ru–Ph bond yields $\text{TpRu}(\text{L})(\text{CH}_2\text{CH}_2\text{Ph})$.⁵ Benzene coordination and C–H activation releases ethylbenzene and regenerates the active catalyst.^{3,1} The catalyst resting state has been identified as $\text{TpRu}(\text{L})(\eta^2\text{-C}_2\text{H}_4)(\text{CH}_2\text{CH}_2\text{Ph})$,³ and the rate-limiting step of the catalytic cycle is likely the aromatic C–H bond activation event as determined by kinetic studies and kinetic isotope effects.



Scheme 3.7. Proposed Catalytic Cycle for the Hydrophenylation of Ethylene using $\text{TpRu(L)(NCMe)}_3\text{Ph}$ [$\text{L} = \text{CO}$, $\text{P(OCH}_2)_3\text{CEt}$ or $\text{P(OCH}_2)_2(\text{OCCH}_3)$].

Complex **4** catalyzes the hydrophenylation of ethylene using 0.025 mol % (relative to benzene) of **4** at with 15 psi of ethylene results in 90 turnovers (TOs) of ethylbenzene after 50 h. Similar to previously reported Ru(II) complexes,²⁵ the catalyst activity is inversely proportional to ethylene concentration (Figure 3.11). The proposed catalyst resting state is $\text{TpRu(L)(}\eta^2\text{-CH}_2\text{CH}_2\text{)(CH}_2\text{CH}_2\text{Ph)}$. Thus, ethylene removes the Ru catalyst from the catalytic cycle, which provides a rationalization for the inhibition of catalyst activity at higher ethylene concentrations. For example, at 90 °C after 8 h, the TOs were 38 (15 psi), 29 (25 psi), 17 (50 psi), 7 (100 psi) and 5 (200 psi). The optimal conditions for catalysis are at 90 °C with 15 psi of ethylene. Under most conditions, no

diethylbenzene or styrene is detected. Increasing the temperature (75 °C, 90 °C and 105 °C) at 15 psi of ethylene increases the rate of ethylbenzene production (Figure 3.13).

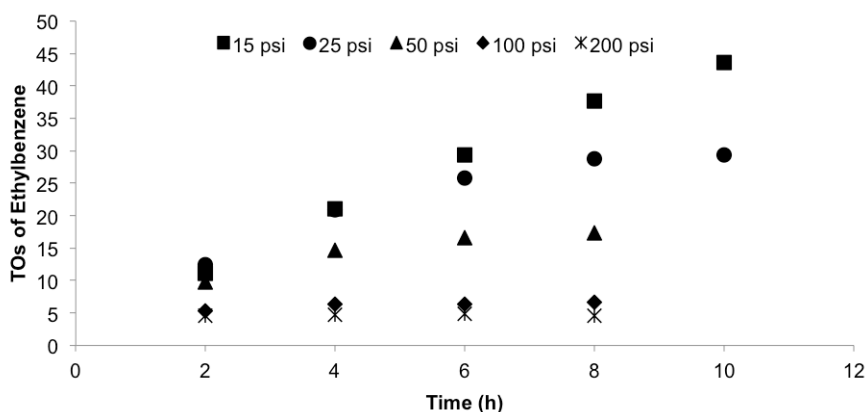


Figure 3.11. Comparison of catalytic hydrophenylation of ethylene by complex **4** (90 °C) at variable ethylene pressures.

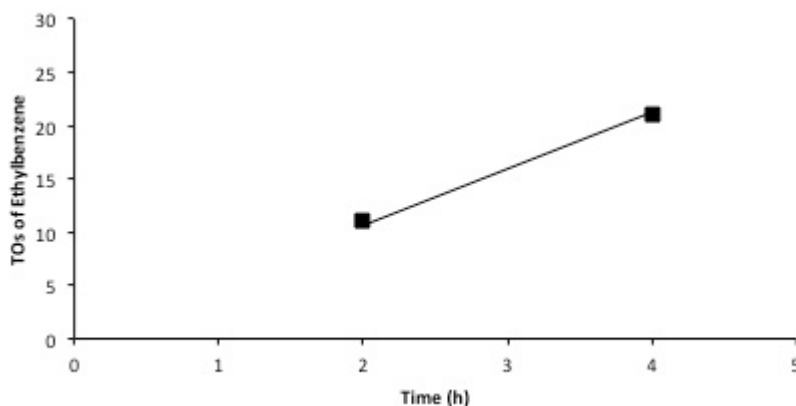


Figure 3.12. Comparison of catalytic hydrophenylation of ethylene by complex **4** (15 psi & 90 °C) through 4 h with minimal decomposition of catalyst present ($R^2 = 0.99$ when trendline is forced through 0,0).

As seen in Figure 3.12, during the first 4 h of catalysis the slope of the change in TO over time is linear (i.e., minimal catalyst deactivation is observed). Therefore initial turnover frequency (TOF) were calculated at 4 h: $\text{TOF} = 2.1 \times 10^{-4} \text{ s}^{-1}$ at 75 °C, 1.5×10^{-3}

s^{-1} at 90°C , and $3.5 \times 10^{-3} \text{ s}^{-1}$ at 105°C . In comparison, the TOF using $\text{TpRu}(\text{CO})(\text{NCMe})\text{Ph}$ (90°C , calculated after 4h of catalysis) is $6.7 \times 10^{-3} \text{ s}^{-1}$ (note: this TOF and the turnover number (TON) are different from previously published data⁵ as a result of different conditions). Thus, at 90°C and 15 psi of ethylene $\text{TpRu}[\text{P}(\text{OCH}_2)_2(\text{OCCH}_3)](\text{NCMe})\text{Ph}$ (**4**) is a less active catalyst than $\text{TpRu}(\text{CO})(\text{NCMe})\text{Ph}$ by a factor of ~ 4.5 .

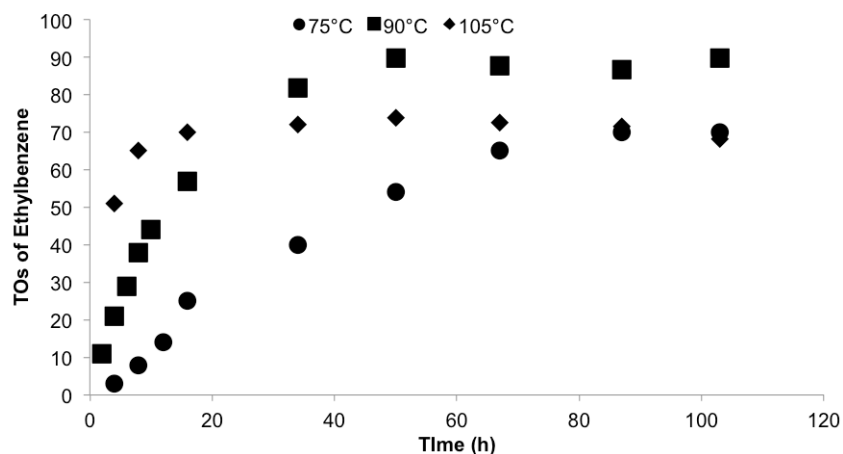
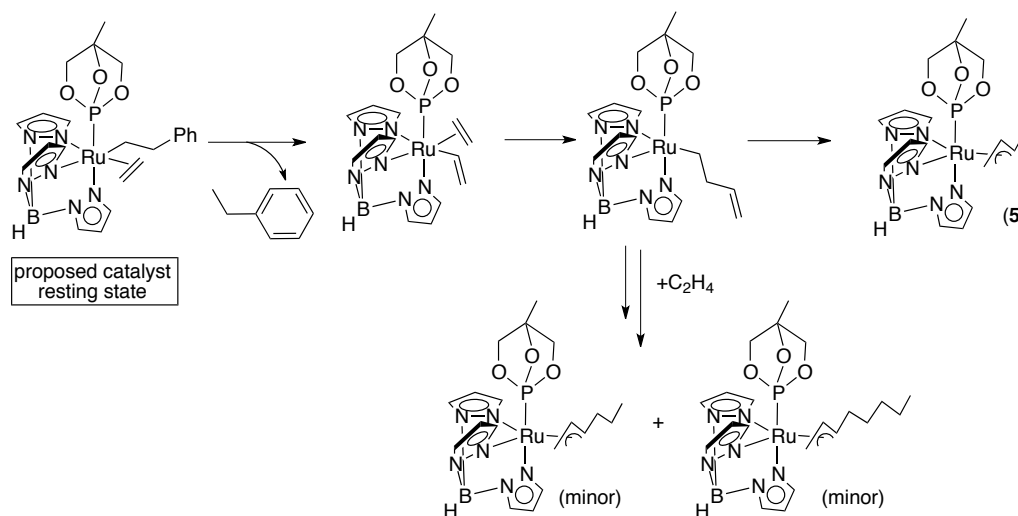


Figure 3.13. Comparison of catalytic hydrophenylation of ethylene by complex **4** at 15 psi of ethylene and variable temperature.

^1H NMR spectroscopy of the non-volatiles after catalyst deactivation indicates that the product of catalyst deactivation is the η^3 -allyl complex $\text{TpRu}[\text{P}(\text{OCH}_2)_2(\text{OCCH}_3)](\eta^3\text{-C}_3\text{H}_4\text{Me})$ (**5**). Complex **5** has been isolated and characterized by ^1H NMR spectroscopy and mass spectrometry (Scheme 3.8, Figure 3.14, Figure 3.15). The ^1H NMR spectrum reveals minor impurities that we were not able to remove. GC-MS analysis of **5** shows the expected parent peak for complex **5** in addition to peaks for

complexes with one and two additional equivalents of ethylene (Figure 3.16). Thus, we speculate that the minor impurities are allyl complexes with propyl and pentyl groups that result from insertion of one or two additional equivalents of ethylene (Scheme 3.8). The deactivation of **4** under catalytic conditions is identical to that observed for $\text{TpRu}(\text{PMe}_3)(\text{NCMe})\text{Ph}$ and $\text{TpRu}[\text{P}(\text{OCH}_2)_3\text{CEt}](\text{NCMe})\text{Ph}$.^{1,2} It has been shown previously that the allyl complex is formed due to an electron-rich Ru center, which results in olefin C–H activation competing with ethylene insertion.³ This ultimately leads to the formation of an η^3 -allyl species due to the formation of a Ru-vinyl species followed by olefin insertion and isomerization.



Scheme 3.8. $\text{TpRu}[\text{P}(\text{OCH}_2)_2(\text{OCCH}_3)](\eta^3\text{-C}_3\text{H}_4\text{Me})$ (**5**) and minor products caused by multiple ethylene insertions.

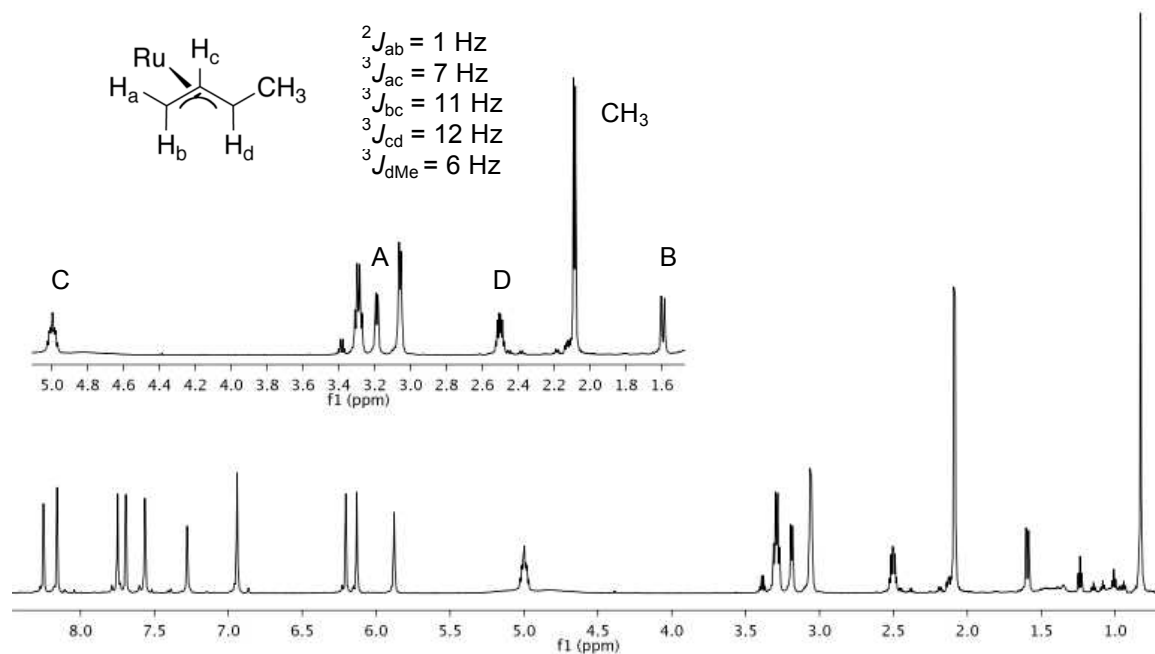


Figure 3.14. ^1H NMR spectrum of $\text{TpRu}[\text{P}(\text{OCH}_2)_2(\text{OCCH}_3)](\eta^3\text{-C}_3\text{H}_4\text{Me})$ (5) in C_6D_6 .

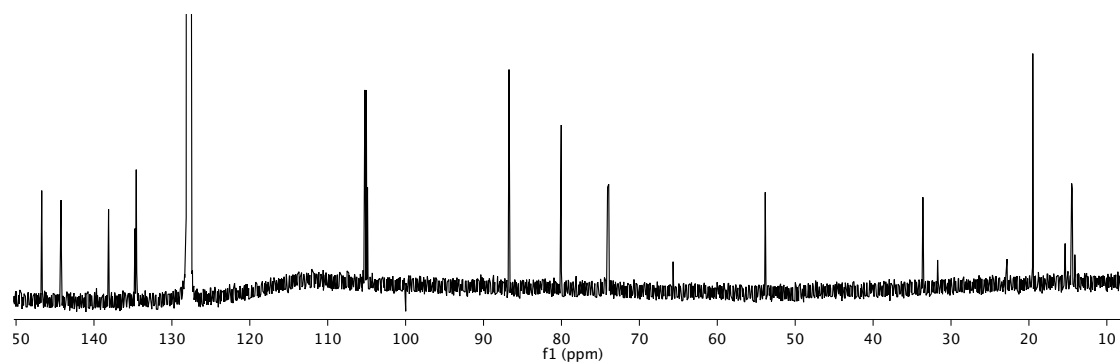


Figure 3.15. ^{13}C NMR spectrum of $\text{TpRu}[\text{P}(\text{OCH}_2)_2(\text{OCCH}_3)](\eta^3\text{-C}_3\text{H}_4\text{Me})$ (5) in C_6D_6 .

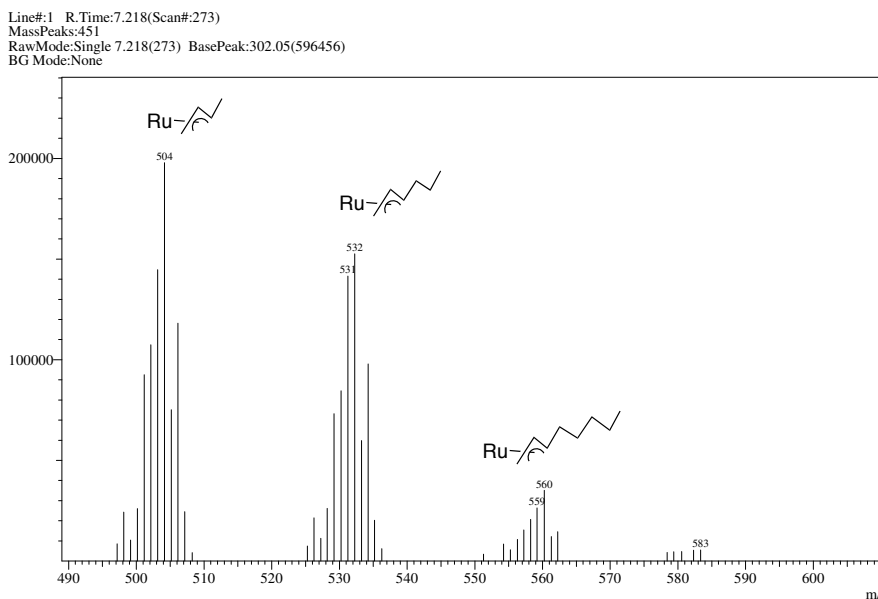
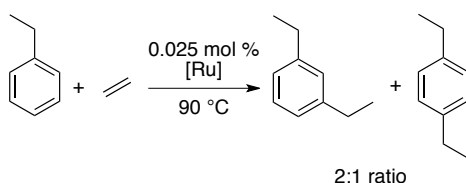


Figure 3.16. Low-Resolution Mass Spectrometry of $\text{TpRu}[\text{P}(\text{OCH}_2)_2(\text{OCCH}_3)](\eta^3\text{-C}_3\text{H}_4\text{Me})$ (**5**) in C_6D_6 from $m/z = 490$ to 600 .

3.2.4. Catalytic Hydroarylation by $\text{TpRu}[\text{P}(\text{OCH}_2)_2(\text{OCCH}_3)](\text{NCMe})\text{Ph}$ (**4**) using Ethylbenzene and Ethylene

Regioselective production of dialkyl benzenes is a challenging reaction. Friedel-Crafts catalysts generally give a mixture of 1,2-, 1,3- and 1,4-dialkyl benzenes.²⁴ To determine if complex **4** exhibits selectivity for the production of diethylbenzene, ethylene hydroarylation studies were performed using ethylbenzene in the presence of ethylene. Upon the reaction of ethylbenzene and ethylene at 90 °C and 15 psi of ethylene with 0.025 mol % of **4**, a 2:1 ratio of 1,3- to 1,4-diethylbenzene (8 and 4 TOs after 4 h, respectively) was observed (Scheme 3.9). No evidence for the formation of 1,2-diethylbenzene was obtained. In the case of $\text{TpRu}(\text{CO})(\text{NCMe})\text{Ph}$, the same 2:1 ratio of 1,3-diethylbenzene to 1,4-diethylbenzene is observed.³⁵ The TOF for the formation of diethylbenzene after 4 h is $8.3 \times 10^{-4} \text{ s}^{-1}$, which is 1.8 times slower than the formation of

ethylbenzene from benzene and ethylene (see above). With Friedel-Crafts catalysts, ethylbenzene is generally more reactive than benzene, which renders selective monoalkylation challenging.³



Scheme 3.9. Formation of 1,3- and 1,4-diethylbenzene.

3.2.5. Attempted Hydrophenylation of Monosubstituted Olefins

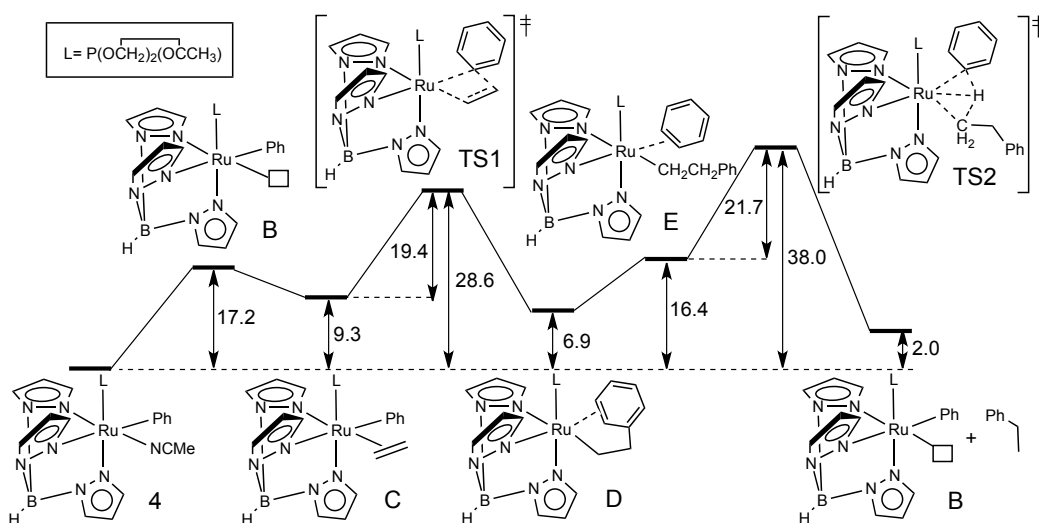
Hydrophenylation of 1-pentene (160 equivalents relative to **4**) was attempted. Only minimal production of 2-phenylpentane (~0.3 TOs) was observed after 8 h. Increasing the amount of 1-pentene did not give increased production of phenylpentane. Additionally, catalytic hydrophenylation was unsuccessful with the substrates methyl acrylate, methyl vinyl ketone and propylene (at pressures from 25 – 150 psi and temperatures of 90 °C or 110 °C).

3.2.6. DFT Calculations of Ethylene Hydrophenylation by $\text{TpRu}[\text{P}(\text{OCH}_2)_2(\text{OCCH}_3)](\text{NCMe})\text{Ph}$

Density Functional Theory (DFT) calculations were used to probe the conversion of $\text{TpRu}[\text{P}(\text{OCH}_2)_2(\text{OCCH}_3)](\text{NCMe})\text{Ph}$ (**4**) and ethylene to ethylbenzene (Scheme 3.10).

Comparison of the free energy surface for $\text{L} = \text{P}(\text{OCH}_2)_2(\text{OCCH}_3)$ with that previously reported for PMe_3 , $\text{P}(\text{pyr})_3$, $\text{P}(\text{OCH}_2)_3\text{CEt}$ and CO shows little variation in the overall

shape and energies of the intermediates and transition states for ethylene insertion (TS1, Scheme 3.10, Scheme 3.11) and benzene C–H activation (TS2, Scheme 3.10, Scheme 3.11).³ As seen for other π -acidic ligands (e.g., $\text{P}(\text{OCH}_2)_3\text{CEt}$ and CO), the coordination mode of benzene in $\text{TpRu}(\text{L})(\text{benzene})(\text{CH}_2\text{CH}_2\text{Ph})$ (E in Scheme 3.10) is $\eta^2\text{-C}=\text{C}$, while for less π -acidic ligands an $\eta^2\text{-C-H}$ coordination mode of benzene was calculated to be most favorable.³ There is very little difference in calculated energetics starting from complex **4** compared to identical calculations for $\text{TpRu}[\text{P}(\text{OCH}_2)_3\text{CEt}](\text{NCMe})\text{Ph}$.¹ In fact, calculated energies for the two phosphites differ by only ~ 1 kcal/mol, which is within the error of these calculations.



Scheme 3.10. Calculated Gibbs free energies (kcal/mol) for hydrophenylation of ethylene by $\text{TpRu}[\text{P}(\text{OCH}_2)_2(\text{OCCH}_3)](\text{NCMe})\text{Ph}$.

Table 3.3 contains key bond distances for the calculated structures of **TS2** (Scheme 3.10 and Table 3.3) for $\text{TpRu}(\text{L})(\text{NCMe})\text{Ph}$ complexes ($\text{L} = \text{PMe}_3$, $\text{P}(\text{OCH}_2)_3\text{CEt}$, $\text{P}(\text{OCH}_2)_2(\text{OCCH}_3)$, CO , $\text{P}(\text{pyr})_3$ or PF_3). Little variation is observed structurally for the

six transition states, and there are no obvious trends in the calculated bond distances relative to donor ability or steric bulk of L. We have previously reported that the calculated Ru–H bond distances (c in Figure 3.17) in the transition state for benzene C–H activation by $\text{TpRu(L)}(\eta^2\text{-C}_6\text{H}_6)\text{Ph}$ complexes are shorter for more strongly donating ligands L; however, a similar trend is not calculated here for benzene C–H activation by $\text{TpRu(L)}(\eta^2\text{-C}_6\text{H}_6)(\text{CH}_2\text{CH}_2\text{Ph})$ complexes. Despite the lack of a straightforward trend, the calculated transition states with the three less donating ligands (i.e., CO, PF_3 and $\text{P}(\text{pyr})_3$) exhibit longer calculated Ru–H bond distances (average = 1.629 Å) than the three complexes with more strongly donating ligands (i.e., PMe_3 , $\text{P}(\text{OCH}_2)_3\text{CEt}$ and $\text{P}(\text{OCH}_2)_2(\text{OCCH}_3)$; average = 1.583 Å).

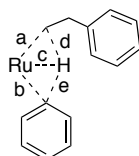


Figure 3.17. Transition state for benzene C–H activation (TS2, Scheme 3.10) by $\text{TpRu(L)}(\text{NCMe})\text{Ph}$. See Table 3.3 for calculated distances.

Table 3.3. Calculated Distances (Å) for C–H Activation Transition State (TS2, Scheme 3.10) for $\text{TpRu(L)}(\text{NCMe})\text{Ph}$ (see Figure 3.17 for labels).

L	Ru–C (a)	Ru–C (b)	Ru–H (c)	C–H (d)	C–H (e)
PMe_3	2.249	2.170	1.584	1.739	1.649
$\text{P}(\text{OCH}_2)_3\text{CEt}$	2.254	2.180	1.579	1.826	1.737
$\text{P}(\text{OCH}_2)_2(\text{OCCH}_3)$	2.262	2.183	1.585	1.787	1.705
$\text{P}(\text{pyr})_3$	2.286	2.215	1.627	1.647	1.525
PF_3	2.288	2.193	1.611	1.690	1.625
CO	2.310	2.194	1.648	1.609	1.549

3.2.7. Comparison of TpRu(L)(NCMe)Ph Catalysts

Based on Ru(III/II) potentials (see Table 3.4), the relative Ru-based electron densities of the complexes TpRu(L)(NCMe)Ph can be assigned as $\text{L} = \text{PMe}_3 > \text{P}(\text{OCH}_2)_3\text{CEt} > \text{P}(\text{OCH}_2)_2(\text{OCCH}_3) > \text{P}(\text{pyr})_3 > \text{CO}$. Table 3.4 provides a comparison of the results from hydrophenylation of ethylene using TpRu(L)(NCMe)Ph complexes.

Table 3.4. Comparison of TON and TOF for Ethylbenzene Production from Catalytic Hydrophenylation of Ethylene by TpRu(L)(NCMe)Ph Complexes.

L	TON	Time	TOF (s^{-1}) ^c	Relative TOF	$E_{1/2}$ (V vs. NHE)
CO	415 ^a	40 h	6.7×10^{-3}	14	1.03
$\text{P}(\text{pyr})_3$	0	---	---	---	0.76
$\text{P}(\text{OCH}_2)_2(\text{OCCH}_3)$	90 ^b	50 h	1.5×10^{-3}	3	0.69
$\text{P}(\text{OCH}_2)_3\text{CEt}$	20 ^b	24 h	4.8×10^{-4}	1	0.54
PMe_3	0 ^b	---	---	---	0.29

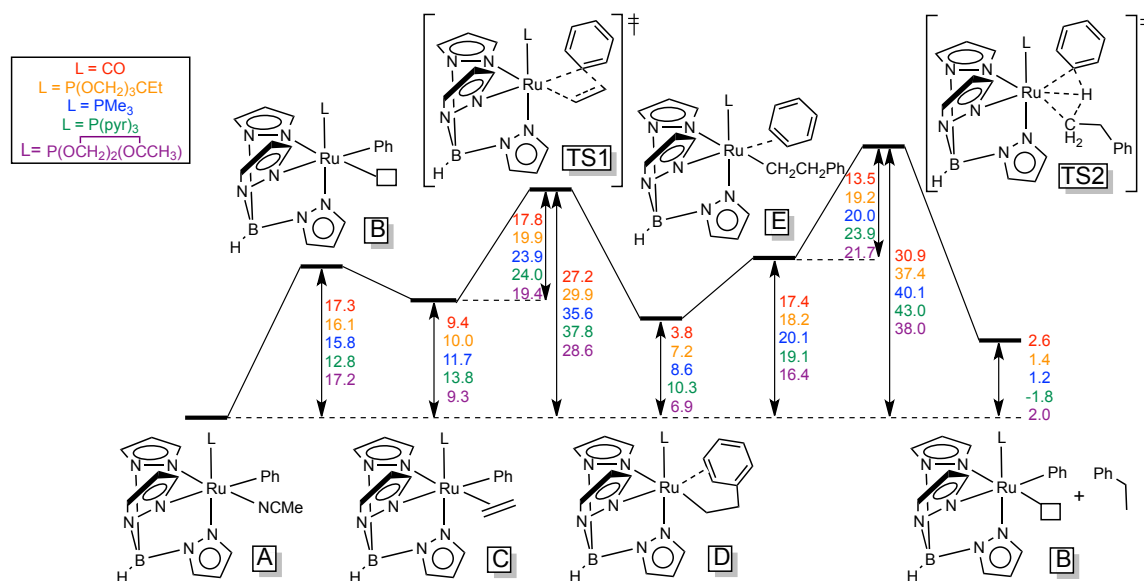
^a Products from catalyst decomposition are unknown, but under most conditions $\text{TpRu(CO)}(\eta^3\text{-C}_3\text{H}_4\text{Me})$ is not formed. ^b Catalyst deactivation occurs by formation of $\text{TpRu(L)}(\eta^3\text{-C}_3\text{H}_4\text{Me})$. ^c Calculated after 4 h at 90 °C with 15 psi ethylene and 0.025 mol % of catalyst.

For the three complexes TpRu(L)(NCMe)Ph ($\text{L} = \text{P}(\text{OCH}_2)_3\text{CEt}$, $\text{P}(\text{OCH}_2)_2(\text{OCCH}_3)$ or CO) that serve as catalysts for the hydrophenylation of ethylene, the catalyst activity and longevity vary as a function of the identity of L. The observed trends in TON and TOF for TpRu(L)(NCMe)Ph catalysts are inverse to the trend in relative rates of benzene activation by TpRu(L)(NCMe)Ph . Our studies provide a clear rationalization for the trends in TON. For TpRu(L)(NCMe)Ph complexes ($\text{L} = \text{P}(\text{OCH}_2)_3\text{CEt}$, $\text{P}(\text{OCH}_2)_2(\text{OCCH}_3)$, CO or PMe_3), a primary factor in the longevity of the

catalyst is the relative rate of olefin insertion versus olefin C–H activation. As previously reported and confirmed again here by our analysis of $\text{TpRu}[\text{P}(\overline{\text{OCH}_2})_2(\text{OCCH}_3)](\text{NCMe})\text{Ph}$, altering the donor ability of L has a relatively minor impact on the ΔG^\ddagger 's for benzene and presumably, also ethylene C–H activation.³ However, the identity of L has a substantial impact on the activation barrier for ethylene insertion into the Ru–Ph bond of $\text{TpRu}(\text{L})(\eta^2\text{-C}_2\text{H}_4)\text{Ph}$ complexes. With the exception of $\text{TpRu}[\text{P}(\text{pyr})_3](\text{NCMe})\text{Ph}$,³ increased donor ability of L results in an increase in the calculated ΔG^\ddagger for olefin insertion from $\text{TpRu}(\text{L})(\eta^2\text{-C}_2\text{H}_4)\text{Ph}$ complexes, which results in competition between ethylene C–H activation and ethylene insertion into the Ru–Ph bond (Scheme 3.1, Scheme 3.11). In the presence of excess ethylene, the C–H activation of ethylene by $\text{TpRu}(\text{L})(\eta^2\text{-C}_2\text{H}_4)\text{Ph}$ results in the formation of η^3 -allyl complexes $\text{TpRu}(\text{L})(\eta^3\text{-C}_3\text{H}_4\text{Me})$ [allyl complexes have been isolated for $\text{L} = \text{CO}$, PMe_3 , $\text{P}(\text{OCH}_2)_3\text{CEt}$ and $\text{P}(\overline{\text{OCH}_2})_2(\text{OCCH}_3)$].³

Table 3.5 shows the calculated ΔG^\ddagger 's for ethylene insertion and the calculated ΔG^\ddagger for ethylene C–H activation from $\text{TpRu}(\text{L})(\eta^2\text{-C}_2\text{H}_4)\text{Ph}$ complexes. The difference in energies ($\Delta\Delta G^\ddagger$) of ethylene insertion vs. ethylene activation demonstrates a clear trend that as the electron density of the metal increases the differences in these two values decreases. Additionally, the calculated $\Delta\Delta G^\ddagger$ for ethylene insertion ($\Delta\Delta G^\ddagger$ of ~ 6.2 kcal/mol) is much larger than the $\Delta\Delta G^\ddagger$ for benzene C–H activation (~ 4.4 kcal/mol) as the ligand L is varied (Scheme 3.11). Therefore, varying the donor ability of L has a greater impact on the rate of olefin insertion compared to the rate of benzene C–H activation. For

$\text{TpRu}(\text{PMe}_3)(\text{NCMe})\text{Ph}$, ethylene insertion does not compete with ethylene C–H activation, and catalytic production of ethylbenzene is not observed (Scheme 3.1).⁴⁵ For $\text{TpRu}[\text{P}(\text{OCH}_2)_3\text{CEt}](\text{NCMe})\text{Ph}$, ethylene insertion is more rapid than ethylene C–H activation, but the $\Delta\Delta G^\ddagger$ between the two processes is sufficiently small that ethylene C–H activation competes and only 20 TON of ethylbenzene are obtained before the catalyst is deactivated to form $\text{TpRu}[\text{P}(\text{OCH}_2)_3\text{CEt}](\eta^3\text{-C}_3\text{H}_4\text{Me})$. This suggests that $k_{\text{ins}}/k_{\text{act}}$ is ~ 20 for $\text{TpRu}[\text{P}(\text{OCH}_2)_3\text{CEt}](\text{NCMe})\text{Ph}$ (k_{ins} is the rate constant for ethylene insertion and k_{act} is the rate constant for ethylene C–H activation).²⁵ For **4**, $k_{\text{ins}}/k_{\text{act}}$ is increased (to ~ 90) relative to the $\text{P}(\text{OCH}_2)_3\text{CEt}$ complex, and multiple TON of ethylbenzene production are observed. Thus, the modulation of ΔG^\ddagger for olefin insertion is a key factor in successful long-lived catalysis using $\text{TpRu}(\text{L})(\text{NCMe})\text{Ph}$ complexes.



Scheme 3.11. Calculated Gibbs free energies (kcal/mol) for ethylene hydrophenylation catalytic cycle by $\text{TpRu}(\text{L})(\text{NCMe})\text{Ph}$ [L = CO, PMe_3 , $\text{P}(\text{OCH}_2)_3\text{CEt}$, $\text{P}(\text{pyr})_3$ and $\text{P}(\text{OCH}_2)_2(\text{OCCH}_3)$].

Table 3.5. Calculated $\Delta G^{\ddagger}_{\text{insertion}}$ (kcal/mol) for ethylene insertion (TS1, Scheme 3.10) and $\Delta G^{\ddagger}_{\text{CH activation}}$ (kcal/mol) of ethylene for $\text{TpRu(L)}(\eta^2\text{-C}_2\text{H}_4)\text{Ph}$ Complexes.

L	$\Delta G^{\ddagger}_{\text{insertion}}$ of C_2H_4	$\Delta G^{\ddagger}_{\text{C-H activation}}$ of C_2H_4	$\Delta\Delta G^{\ddagger}$
PMe_3	23.9	27.0	3.1
P(pyr)_3	23.2	28.6	5.4
$\text{P(OCH}_2)_3\text{CEt}$	20.1	27.3	7.4
$\text{P}(\overline{\text{OCH}_2})_2(\text{OCCH}_3)$	19.4	28.3	8.9
PF_3	18.3	28.0	9.7
CO	17.7	28.9	11.2

The TOF for catalytic hydrophenylation of ethylene by $\text{TpRu(L)}(\text{NCMe})\text{Ph}$ complexes also varies as a function of the identity of L, and a plot of TOF vs. Ru(III/II) potential shows a good linear correlation (Figure 3.18). The TOFs were calculated after 4 h since there is no evidence of catalyst deactivation at this time point for any of the catalysts. Benzene C–H activation is the proposed rate limiting step for the catalytic hydrophenylation of ethylene using $\text{TpRu(L)}(\text{NCMe})\text{Ph}$ complexes.³ Thus, given the relative rates of C_6D_6 activation by $\text{TpRu(L)}(\text{NCMe})\text{Ph}$ complexes, which are opposite to the observed rates for catalytic ethylene hydrophenylation, the trend in TOF is more difficult to rationalize than TON. One potential explanation for the inverse trend for rates of stoichiometric benzene activation and TOF for catalytic hydrophenylation is that the rate of benzene C–H activation from proposed catalyst resting states, $\text{TpRu(L)}(\eta^2\text{-C}_2\text{H}_4)(\text{CH}_2\text{CH}_2\text{Ph})$, might be different from the observed relative rates of C_6D_6 activation by $\text{TpRu(L)}(\text{NCMe})\text{Ph}$ complexes. To probe this possibility, we calculated the energetics for benzene C–H activation starting from $\text{TpRu(L)}(\eta^2\text{-C}_2\text{H}_4)(\text{CH}_2\text{CH}_2\text{Ph})$ for the active catalysts $\text{L} = \text{CO}$, $\text{P(OCH}_2)_3\text{CEt}$ and $\text{P}(\overline{\text{OCH}_2})_2(\text{OCCH}_3)$ (Scheme 3.12).

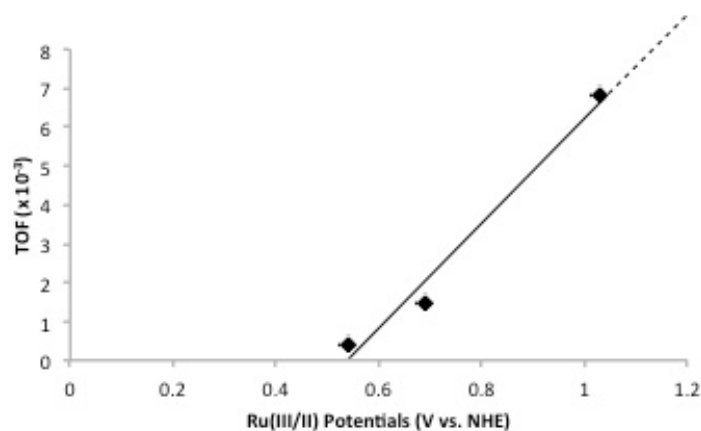
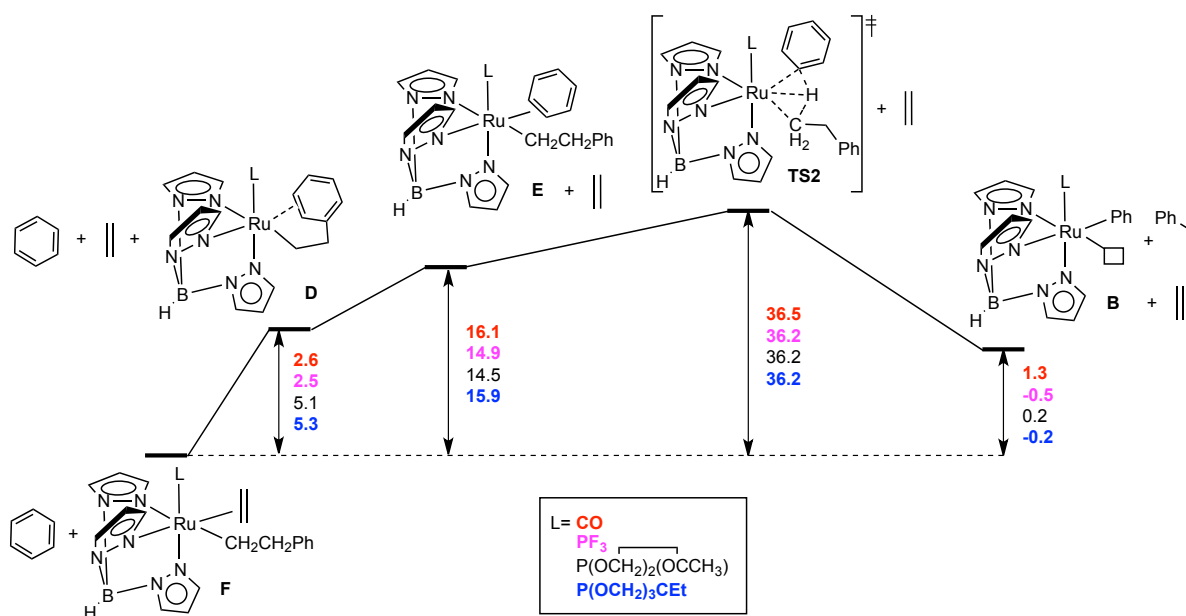


Figure 3.18. Plot of TOF vs. Ru(III/II) potential for catalytic hydrophenylation of ethylene by $\text{TpRu}(\text{L})(\text{NCMe})\text{Ph}$ ($\text{L} = \text{P}(\text{OCH}_2)_3\text{CEt}$, $\text{P}(\text{OCH}_2)_2(\text{OCCH}_3)$ or CO) using 0.025 mol % of catalyst, 15 psi of ethylene at 90 °C. TOF calculated after 4 hours of reaction ($R^2 = 0.97$).



Scheme 3.12. Calculated Gibbs Free Energies (kcal/mol) for benzene C–H activation and formation of ethylbenzene by $\text{TpRu}(\text{L})(\eta^2\text{-C}_2\text{H}_4)(\text{CH}_2\text{CH}_2\text{Ph})$.

As Scheme 3.12 shows, within the anticipated error, the calculations predict identical activation barriers for the production of ethylbenzene from all of the $\text{TpRu(L)}(\eta^2\text{-C}_2\text{H}_4)(\text{CH}_2\text{CH}_2\text{Ph})$ complexes. Although these results do not reproduce the experimental observations, they are not surprising given the small difference in activation barrier of ~ 2 kcal/mol between the most and least active catalysts. Perhaps most informative is a comparison of the ethylene binding energy among the series of $\text{TpRu(L)}(\eta^2\text{-C}_2\text{H}_4)(\text{CH}_2\text{CH}_2\text{Ph})$ complexes. Comparison of the energetics for ethylene dissociation from $\text{TpRu(L)}(\eta^2\text{-C}_2\text{H}_4)(\text{CH}_2\text{CH}_2\text{Ph})$ (**F**) to form $\text{TpRu(L)}(\kappa^3\text{-CH}_2\text{CH}_2\text{Ph})$ (**D**) reveals that the phosphite complexes exhibit stronger binding energies of ethylene than the CO complex by 2.5 and 2.7 kcal/mol, respectively, for $\text{P}(\overline{\text{OCH}_2})_2(\text{OCCH}_3)$ and $\text{P}(\text{OCH}_2)_3\text{CEt}$ (Scheme 3.12). This could be a result of the more strongly donating character of the phosphite ligands compared to CO, which would enhance Ru-to-ethylene π -backbonding. The difference in binding energies might also be due to sterics; however, the calculated binding energy of ethylene for $\text{TpRu}(\text{PF}_3)(\eta^2\text{-C}_2\text{H}_4)(\text{CH}_2\text{CH}_2\text{Ph})$ is identical to the CO complex (given the expected error in calculations), which is consistent with the electronic effect playing a dominant role. We believe that more strongly donating ligands enhance ethylene binding for the proposed resting states $\text{TpRu(L)}(\eta^2\text{-C}_2\text{H}_4)(\text{CH}_2\text{CH}_2\text{Ph})$, which should increase the overall activation barriers for catalytic hydrophenylation of ethylene.

3.3. Summary and Conclusions

$\text{TpRu}[\text{P}(\overline{\text{OCH}_2})_2(\text{OCCH}_3)](\text{NCMe})\text{Ph}$ (**4**) has been shown to catalyze the hydrophenylation of ethylene to yield ~ 90 TOs of ethylbenzene after 50 h at 90 °C with

15 psi of ethylene. Complex **4** does not catalyze the hydrophenylation of propene or 1-pentene. A comparison of catalytic hydrophenylation of ethylene, or in some cases the failure of the complex to catalyze the reaction, by the series of TpRu(II) complexes TpRu(L)(NCMe)Ph [$\text{L} = \text{CO}, \text{PMe}_3, \text{P(pyr)}_3, \text{P(OCH}_2)_3\text{CEt}$ and $\text{P}(\overline{\text{OCH}_2})_2(\overline{\text{OCCH}_3})$] allows some conclusions to be drawn:

- 1) Increasing the donor ability of the ligand L of TpRu(L)(NCMe)Ph complexes increases the overall rate of stoichiometric benzene C–H activation.
- 2) The influence of the donor ability of L on the rate of ethylene insertion into Ru–phenyl bonds appears to be the most important factor that determines the TON for Ru(II) catalysts.
- 3) For TpRu(L)(NCMe)Ph catalysts, the steric profile of L plays an important role. For example, we have published data that suggest ethylene/NCMe exchange with $\text{TpRu[P(pyr)}_3\text{](NCMe)Ph}$ is unfavorable due to sterics.²³
- 4) Although only three data points are available, the TOFs in Table 3.4 suggest that less electron-rich Ru(II) catalysts supported by poly(pyrazolyl) ligands are more active for ethylene hydrophenylation.

3.4. Experimental

General Methods. Unless otherwise noted, all synthetic procedures were performed under anaerobic conditions in a nitrogen-filled glovebox or by using standard Schlenk techniques. Glovebox purity was maintained by periodic nitrogen purges and was monitored by an oxygen analyzer [$\text{O}_2(\text{g}) < 15$ ppm for all reactions]. Tetrahydrofuran was dried by distillation from sodium/benzophenone. Pentane was distilled over P_2O_5 .

Acetonitrile and diethyl ether were dried by distillation from CaH_2 . Hexanes, benzene and methylene chloride were purified by passage through a column of activated alumina. Benzene- d_6 , acetonitrile- d_3 , methylene chloride- d_2 and chloroform- d_1 were stored under a nitrogen atmosphere over 4Å molecular sieves. ^1H NMR spectra were recorded on a Varian Inova 500 MHz or Varian MRS 600 MHz spectrometer, and ^{13}C NMR spectra were recorded on a Varian Inova 500 MHz or Varian MRS 600 MHz spectrometer (operating frequency 126 MHz or 151 MHz, respectively). All ^1H and ^{13}C NMR spectra are referenced against residual proton signals (^1H NMR) or the ^{13}C resonances of the deuterated solvent (^{13}C NMR). ^{31}P NMR spectra were obtained on a Varian Mercury Plus 300 MHz (operating frequency 121 MHz) spectrometer and referenced against an external standard of H_3PO_4 ($\delta = 0$). Resonances due to the Tp ligand in ^1H NMR spectra are listed by chemical shift and multiplicity only (all coupling constants for the Tp ligand are ~ 2 Hz).

Electrochemical experiments were performed under a nitrogen atmosphere using a BAS Epsilon Potentiostat. Cyclic voltammograms were recorded in CH_3CN using a standard three electrode cell from -1700 to 1700 mV at 100 mV/s with a glassy carbon working electrode and tetrabutylammonium hexafluorophosphate as electrolyte. All potentials are reported versus NHE (normal hydrogen electrode) using ferrocene as the internal standard.

High-resolution electrospray ionization mass spectrometry (ESI-MS) analyses were obtained on a Bruker BioTOF-Q spectrometer at the University of Richmond. Samples were dissolved in acetonitrile, then mixed 3:1 with 0.1 M aqueous sodium trifluoroacetate

(NaTFA) using $[\text{Na}(\text{NaTFA})_x]^+$ clusters as an internal standard. These data are reported using the most intense peaks from the isotopic envelope for $[\text{M} + \text{Na}]^+$. The data are listed as m/z with the intensity relative to the most abundant peak of the isotopic envelope given in parentheses for both the calculated and observed peaks. The difference between calculated and observed peaks is reported in ppm. Low-resolution mass spectra were acquired on a Shimadzu G-17A/QP-5050 GC-MS instrument operating in EI-direct-inlet-MS mode. Mass spectra are reported as M^+ for originally neutral samples. In all cases, observed isotopic envelopes were consistent with the molecular composition reported.

The preparation, isolation and characterization of $\text{TpRu}[\text{P}(\text{OCH}_2)_3\text{CEt}](\text{PPh}_3)\text{Cl}$,¹ $\text{TpRu}(\text{CO})\text{Ph}(\text{NCMe})$,⁵ $\text{TpRu}[\text{P}(\text{OCH}_2)_3\text{CEt}]\text{Ph}(\text{NCMe})$,¹ $\text{TpRu}[\text{P}(\text{pyr})_3]\text{Ph}(\text{NCMe})$,²³ $\text{Ph}_2\text{Mg}[\text{THF}]_2$,²⁶ $\text{P}(\overline{\text{OCH}_2})_2(\overline{\text{OCCH}_3})$ ⁷ and $\text{C}(\text{CH}_3)(\text{OH})(\text{CH}_2\text{OH})_2$ ⁷ have been previously reported. $\text{P}(\text{OCH}_2)_3\text{CEt}$ was obtained from a commercial source and purified by reconstitution in hexanes and filtration through Celite. The filtrate was concentrated to dryness to yield a white solid.

Calculations. Density functional theory calculations were performed using the Gaussian 09 suite of programs²⁷ employing the hybrid functional B3LYP with the effective core potential basis set CEP-31G(d).²⁸ Optimized geometries and transition states were confirmed by the presence of zero and one imaginary frequencies, respectively, with thermochemistry determined at 298.15 K and 1 atm.

$(\eta^6\text{-}p\text{-cymene})\text{Ru}[\text{P}(\overline{\text{OCH}_2})_2(\overline{\text{OCCH}_3})]\text{Br}_2$ (1). The complex $[(\eta^6\text{-}p\text{-cymene})\text{Ru}(\text{Br})(\mu\text{-Br})_2]$ ²¹ (1.36 g, 1.73 mmol) was dissolved in 150 mL of methylene

chloride and added to a round bottom flask (500 mL) containing a benzene solution of $\text{P}(\overline{\text{OCH}_2})_2(\overline{\text{OCCH}_3})$ (~1.13 g, 6.90 mmol, 200 mL of C_6H_6). The reaction was stirred for 1 h. The reaction mixture was concentrated to ~20 mL under vacuum. Hexanes were added, and the mixture was stirred for 1 h. The hexanes were decanted through a fine porosity frit with ~1/3 inch of Celite, and the filtrate was discarded. The Celite was washed with methylene chloride, and this second filtrate was placed back into the reaction flask. All solvent was removed under vacuum. The resulting solid was placed on a fine porosity frit, washed with pentane, and dried in vacuo (1.67 g, 91% yield). ^1H NMR (600 MHz, CDCl_3) δ 5.74 (d, $^3J_{\text{HH}} = 6$ Hz, 2H, *p*-cymene: C_6H_4), 5.61 (d, 2H, $^3J_{\text{HH}} = 6$ Hz, *p*-cymene: C_6H_4), 4.21 (dt, 2H, $^2J_{\text{HH}} = 10$ Hz, $^3J_{\text{HP}} = 5$ Hz, $\text{P}(\overline{\text{OCH}_2})_2(\overline{\text{OCCH}_3})$), 3.86 – 3.82 (m, 2H, $\text{P}(\overline{\text{OCH}_2})_2(\overline{\text{OCCH}_3})$), 3.02 (sept, 1H, $^3J_{\text{HH}} = 7$ Hz, *p*-cymene: $\text{CH}(\text{CH}_3)_2$), 2.36 (s, 3H, *p*-cymene: CH_3), 1.69 (s, 3H, $\text{P}(\overline{\text{OCH}_2})_2(\overline{\text{OCCH}_3})$), 1.26 (d, 6H, $^3J_{\text{HH}} = 7$ Hz, *p*-cymene: $\text{CH}(\text{CH}_3)_2$). ^{13}C NMR (151 MHz, CDCl_3) δ 111.6, 106.4, 90.4, 90.3, 89.8, 89.8 (each a singlet, C_6H_4), 82.8 (s, $\text{P}(\overline{\text{OCH}_2})_2(\overline{\text{OCCH}_3})$), 75.86 ($\text{P}(\overline{\text{OCH}_2})_2(\overline{\text{OCCH}_3})$), 75.81 ($\text{P}(\overline{\text{OCH}_2})_2(\overline{\text{OCCH}_3})$), 31.2 (s, $\text{C}_6\text{H}_4\text{-CH}(\text{CH}_3)_2$), 22.4 (s, $\text{C}_6\text{H}_4\text{-CH}(\text{CH}_3)_2$), 19.5 (s, $\text{C}_6\text{H}_4\text{-CH}_3$) 15.3 (d, $^3J_{\text{CP}} = 11$ Hz, $\text{P}(\overline{\text{OCH}_2})_2(\overline{\text{OCCH}_3})$). $^{31}\text{P}\{^1\text{H}\}$ NMR (121 MHz, CDCl_3) δ 140.5. HRMS: $[\text{M}+\text{Na}^+]$ obs'd (%), calc'd (%), ppm: 548.85142 (20.2), 548.85313 (23.7), -3.1; 549.85263 (40.7), 549.85355 (45.5), -1.7; 550.85317 (57.1), 550.85257 (64.7), 1.1; 551.85322 (46.3), 551.85251 (55), 1.3; 552.85149 (100), 552.85172 (100), -0.4; 553.85181 (29.1), 553.85252 (31.3), -1.3; 554.84983 (49.9), 554.85096 (70.3), -2.

(η^6 -*p*-cymene)Ru[$\overline{\text{P}(\text{OCH}_2)_2(\text{OCCH}_3)}$](Ph)Br (**2**). The complex (η^6 -*p*-cymene)Ru[$\overline{\text{P}(\text{OCH}_2)_2(\text{OCCH}_3)}$] Br_2 (**1**) (0.543 g, 1.10 mmol) in 75 mL of THF and $\text{Ph}_2\text{Mg}[\text{THF}]_2$ (0.331 g, 1.10 mmol) in 50 mL of THF were combined to give a red solution. Over a period of 45 minutes the red solution turned yellow with formation of a light pink precipitate. The mixture was filtered through Celite. The filtrate was concentrated to dryness, reconstituted in benzene and filtered through Celite. The filtrate was loaded onto a ½ inch plug of silica and washed with THF to elute a bright yellow band. The filtrate was reduced to ~10 mL, hexanes were added, and the mixture was reduced to dryness. The resulting yellow solid was collected, washed with pentane, and dried under vacuum. (0.228 g, 42% yield). ^1H NMR (500 MHz, CDCl_3) δ 7.62 (dd, 2H, $^3J_{\text{HH}} = 8$ Hz, $^4J_{\text{HH}} = 1$ Hz, ortho phenyl), 6.98 – 6.85 (m, 3H, para and meta phenyl), 5.63 (dd, 1H, $^3J_{\text{HH}} = 6$ Hz, $^4J_{\text{HH}} = 1$ Hz, *p*-cymene: C_6H_4 , fine coupling is observed for this resonance but other *p*-cymene resonances are too broad for resolution of fine coupling), 5.54 (d, 1H, $^3J_{\text{HH}} = 6$ Hz, *p*-cymene: C_6H_4), 5.48 (d, 1H, $^3J_{\text{HH}} = 6$ Hz, *p*-cymene: C_6H_4), 5.15 (d, $^3J_{\text{HH}} = 6$ Hz, 1H, *p*-cymene: C_6H_4), 4.04 (td, $^2J_{\text{HH}} = 8$ Hz, $^3J_{\text{HP}} = 4$ Hz, 2H, $\overline{\text{P}(\text{OCH}_2)_2(\text{OCCH}_3)}$), 3.70 – 3.61 (m, 2H, $\overline{\text{P}(\text{OCH}_2)_2(\text{OCCH}_3)}$), 2.78 (sept, 1H, $^3J_{\text{HH}} = 7$ Hz, *p*-cymene: $\text{CH}(\text{CH}_3)_2$), 1.89 (s, 3H, *p*-cymene: CH_3), 1.58 (s, 3H, $\overline{\text{P}(\text{OCH}_2)_2(\text{OCCH}_3)}$), 1.25 (d, 3H, $^3J_{\text{HH}} = 7$ Hz, *p*-cymene: $\text{CH}(\text{CH}_3)_2$), 1.20 (d, 3H, $^3J_{\text{HH}} = 7$ Hz, *p*-cymene: $\text{CH}(\text{CH}_3)_2$). ^{13}C NMR (126 MHz, CDCl_3) δ 151.3 (s, ipso of phenyl), 143.3, 126.9, 122.5 (each a singlet, phenyl), 118.4 (s, Cy- C_{quat}), 111.1 (s, *p*-cymene: C_{quat}), 95.0 (s, *p*-cymene: C_6H_4), 92.3 (d, $^2J_{\text{PC}} = 9$ Hz, *p*-cymene: C_6H_4), 89.3, 89.1 (each a singlet, *p*-cymene: C_6H_4), 81.7 (

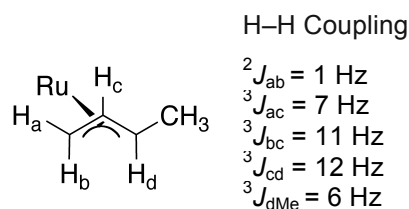
$\text{P}(\overline{\text{OCH}_2)_2(\text{OCCH}_3)}$), 75.4 ($\text{P}(\overline{\text{OCH}_2)_2(\text{OCCH}_3)}$), 75.4 (s, $\text{P}(\overline{\text{OCH}_2)_2(\text{OCCH}_3)}$), 31.4 (s, *p*-cymene: $\text{CH}(\text{CH}_3)_2$), 23.5 (s, *p*-cymene: $\text{CH}(\text{CH}_3)_2$), 22.2 (s, *p*-cymene: $\text{CH}(\text{CH}_3)_2$), 18.9 (s, *p*-cymene: CH_3), 15.35 (d, $^3J_{\text{CP}} = 10.7$ Hz, $\text{P}(\overline{\text{OCH}_2)_2(\text{OCCH}_3)}$). ^{31}P NMR (121 MHz, CD_2Cl_2) δ 155.5. HRMS: $[\text{M}+\text{Na}^+]$ obs'd (%), calc'd (%), ppm: 546.97455 (34.4), 546.97431 (34.6), 0.4; 547.97473 (65.1), 547.97492 (66), 0.3; 548.9739 (100), 548.97344 (100), 0.8; 549.97459 (53.5), 549.97293 (47.9), 3; 550.9734 (107.1), 550.97294 (104.5), 0.8; 551.97659 (85.5), 551.9763 (84.2), 0.5; 552.9734 (85.5), 552.97181 (84.2), 2.9.

TpRu[$\text{P}(\overline{\text{OCH}_2)_2(\text{OCCH}_3)}$](NCMe)Ph (4). The complex $(\eta^6\text{-}p\text{-cymene})\text{Ru}[\text{P}(\overline{\text{OCH}_2)_2(\text{OCCH}_3)}](\text{Ph})\text{Br}$ (**2**) (0.228 g, 0.434 mmol) was taken up in approximately 15 mL of NCMe, added to a pressure tube and heated overnight at 75 °C. The reaction was brought into the glovebox and allowed to cool to room temperature. The mixture was filtered through Celite, and the filtrate was concentrated to dryness yielding $(\text{NCMe})_3\text{Ru}[\text{P}(\overline{\text{OCH}_2)_2(\text{OCCH}_3)}](\text{Ph})\text{Br}$ (**3**). Without any purification, the resulting solid was taken up in ~10 mL of methylene chloride and added to a pressure tube along with a 5 mL solution of KTp (0.109 g, 0.434 mmol) in methylene chloride. The reaction was heated to 75 °C for 4 hours. The reaction was brought into the glovebox and filtered through Celite. The filtrate was concentrated to dryness and then reconstituted in diethyl ether (partially soluble). The mixture was loaded onto an ½ inch plug of silica and washed with 50 mL of diethyl ether. Methylene chloride (~100 mL) was used to elute a light yellow solution. The eluent was concentrated to ~5 mL and added to a stirring flask of hexanes. The mixture was concentrated to ~5 mL of solvent, and the resulting solid was collected on a

fine porosity frit. The solid was washed with pentane and dried in vacuo to yield an off-white solid (0.109 g, 44%). ^1H NMR (600 MHz, C_6D_6) δ 8.27, 8.00, 7.55, 7.38 (each a d, each 1H, Tp 3 and 5 positions), 7.70 (dd, 2H, $^3J_{\text{HH}} = 8$ Hz, $^4J_{\text{HH}} = 1$ Hz, ortho phenyl), 7.62 – 7.61 (m, 1H, Tp 3 or 5 position), 7.58, (s, 1H, Tp 3 or 5 position), 7.31 (t, 2H, $^3J_{\text{HH}} = 8$ Hz, meta of phenyl), 7.20 – 7.16 (m, 2H, para phenyl), 6.20 – 6.17 (m, 1H, Tp 4 position), 6.03 (s, 1H, Tp 4 position), 5.96 – 5.95 (m, 1H, Tp 4 position), 3.41 (td, 2H, $^2J_{\text{HH}} = 7$ Hz, $^2J_{\text{HP}} = 3$ Hz, $\text{P}(\overline{\text{OCH}_2})_2(\text{OCCH}_3)$), 3.24 (dd, 1H, $^2J_{\text{HH}} = 7$ Hz, $^3J_{\text{HP}} = 3$ Hz), 3.17 (dd, 1H, $^2J_{\text{HH}} = 7$ Hz, $^3J_{\text{HP}} = 3$ Hz, $\text{P}(\overline{\text{OCH}_2})_2(\text{OCCH}_3)$), 0.82 (s, 3H, $\text{P}(\overline{\text{OCH}_2})_2(\text{OCCH}_3)$), 0.62 (s, 3H, CH_3CN). ^{13}C NMR (151 MHz, CDCl_3) δ 168.4 (d, $^2J_{\text{CP}} = 19$ Hz, ipso phenyl), 146.7, 128.5, 124.7 (each a singlet, phenyl), 143.7, 142.4, 142.0, 135.1, 134.6, 133.8 (each a singlet, Tp 3 and 5 positions), 119.9 (NCCH_3), 105.2 (Tp 4 position), 104.9 (2C, overlapping Tp 4 positions), 80.8 ($\text{P}(\overline{\text{OCH}_2})_2(\text{OCCH}_3)$), 74.6 (d, $^2J_{\text{CP}} = 2$ Hz, $\text{P}(\overline{\text{OCH}_2})_2(\text{OCCH}_3)$), 74.6 (d, $^2J_{\text{CP}} = 2$ Hz, $\text{P}(\overline{\text{OCH}_2})_2(\text{OCCH}_3)$), 15.6 (d, $J_{\text{CP}} = 10$ Hz, $\text{P}(\overline{\text{OCH}_2})_2(\text{OCCH}_3)$), 4.5 (NCCH_3). ^{31}P NMR (121 MHz, CDCl_3 , δ): 164.6. HRMS: $[\text{M}+\text{Na}^+]$ obs'd (%), calc'd (%), ppm: 587.08142 (42.6), 587.08084 (44.6), 1; 588.07974 (51.1), 588.08042 (54.7), -1.2; 589.07966 (73.8), 589.0809 (77.2), -2.1; 590.07876 (100), 590.07943 (100), -1.1; 591.08134 (40.4), 591.08228 (35.6), -1.6; 592.07975 (63.8), 592.08025 (54.6), -0.8; 593.08074 (10.6), 593.08269 (13.2), -3.3. Anal. Calcd. for $\text{C}_{21}\text{H}_{25}\text{BN}_7\text{O}_3\text{PRu}$. C, 44.54; H, 4.45; N, 17.31. Found C, 44.10; H, 4.52; N, 16.56. CV (NCMe): $E_{1/2} = 0.69$ V Ru(III/II).

$\text{TpRu}[\text{P}(\overline{\text{OCH}_2})_2(\overline{\text{OCCH}_3})](\eta^3\text{-C}_3\text{H}_4\text{Me})$ (5). $\text{TpRu}[\text{P}(\overline{\text{OCH}_2})_2(\overline{\text{OCCH}_3})](\text{NCMe})\text{Ph}$ (4) (0.0384 g, 0.0678 mmol) was dissolved in 12 mL of benzene and placed in a stainless steel pressure reactor. The reactor was charged with 50 psi of ethylene and heated to 90 °C for 20 h. The volatiles were removed in vacuo. The residue was taken up in diethyl ether and loaded on a plug of silica gel and eluted with a 1:1 mixture of diethyl ether and pentane. The solvent was removed from the pale yellow filtrate in vacuo to give a beige solid (0.0162 g, 47% yield). ^1H NMR (600 MHz, C_6D_6) δ 8.23, 8.14, 7.73, 7.67, 7.55, 6.92 (each a d, each 1H, Tp 3 and 5 positions), 6.19, 6.11 (each a t, each 1H, Tp 4 position), 5.86 (s, 1H, Tp 4 position), 4.98 (m, 2H, H_c in Table 3.6), 3.27 (dd, 2H, $^3J_{\text{HP}} = 8$ Hz, $^2J_{\text{HH}} = 6$ Hz, $\text{P}(\overline{\text{OCH}_2})_2(\overline{\text{OCCH}_3})$), 3.17 (d, 1H, $^3J_{\text{AC}} = 7$ Hz, H_a in Table 3.6), 3.04 (d, 2H, $^2J_{\text{HH}} = 6$ Hz, 3H, $\text{P}(\overline{\text{OCH}_2})_2(\overline{\text{OCCH}_3})$), 2.48 (dq, 1H, $^3J_{\text{DC}} = 12$ Hz, $^3J_{\text{DMe}} = 6$ Hz, H_d in Table 3.6), 2.07 (d, 3H, $^3J_{\text{MeD}} = 6$ Hz, CH_3 in Table 3.6), 1.57 (d, 1H, $^3J_{\text{AB}} = 1$ Hz, $^3J_{\text{BC}} = 11$ Hz, H_b in Table 3.6), 0.81 (s, 3H, $\text{P}(\overline{\text{OCH}_2})_2(\overline{\text{OCCH}_3})$). ^{13}C NMR (151 MHz, C_6D_6) δ 147.0, 144.5, 138.4, 135.0, 134.8, 134.8 (each a singlet, Tp 3 and 5 positions), 105.5, 105.3, 105.1 (each a singlet, Tp 4 positions), 87.0 (allyl- $\text{CH}_2\text{CHCHCH}_3$), 80.3 ($\text{P}(\overline{\text{OCH}_2})_2(\overline{\text{OCCH}_3})$), 74.3 (d, $^2J_{\text{CP}} = 7$ Hz, $\text{P}(\overline{\text{OCH}_2})_2(\overline{\text{OCCH}_3})$), 74.2 (d, $^2J_{\text{CP}} = 7$ Hz, $\text{P}(\overline{\text{OCH}_2})_2(\overline{\text{OCCH}_3})$), 54.1 (d, $^2J_{\text{CP}} = 3$ Hz, allyl- $\text{CH}_2\text{CHCHCH}_3$), 33.8 (d, $^2J_{\text{CP}} = 4$ Hz, allyl- $\text{CH}_2\text{CHCHCH}_3$), 19.8 (s, allyl- $\text{CH}_2\text{CHCHCH}_3$), 14.7 (d, $^3J_{\text{CP}} = 10$ Hz, $\text{P}(\overline{\text{OCH}_2})_2(\overline{\text{OCCH}_3})$). ^{31}P NMR (121 MHz, C_6D_6) δ 171.7. LRMS: obs'd m/z (obs'd %)/calc'd %: 501 (42.6/45.5); 502 (53.6/54.5); 503 (71.9/77.5); 504 (100/100); 505 (33.8/32.1); 506 (58.5/55.0).

Table 3.6. Allyl Coupling Diagram for $\text{TpRu}[\text{P}(\text{OCH}_2)_2(\text{OCCH}_3)](\eta^3\text{-C}_3\text{H}_4\text{Me})$ (**5**).



Kinetic Studies: Rate Determination for Activation of C_6D_6 by $\text{TpRu}[\text{P}(\text{OCH}_2)_2(\text{OCCH}_3)](\text{NCMe})\text{Ph}$ (4**).** A solution of $\text{TpRu}[\text{P}(\text{OCH}_2)_2(\text{OCCH}_3)](\text{NCMe})\text{Ph}$ (**4**) (0.0115 g, 0.0203 mmol), acetonitrile (3.4 μL , 0.070 mmol), and a crystal of hexamethylbenzene (as an internal standard) in 2 mL of C_6D_6 (22.6 mmol) was equally divided and transferred into four J. Young NMR tubes. The solutions were heated to 60 $^\circ\text{C}$ in a temperature-regulated oil bath. ^1H NMR spectra were periodically acquired through 3 half-lives (using a pulse delay of 5 s). Relative to the internal standard hexamethylbenzene, the rates of $\text{Ru-Ph/Ru-Ph-}d_5$ exchange were followed by integration of the ortho phenyl resonance at 7.69 ppm.

Representative Catalytic Reaction. $\text{TpRu}[\text{P}(\text{OCH}_2)_2(\text{OCCH}_3)](\text{NCMe})\text{Ph}$ (**4**) (0.0048 g, 0.0085 mmol) was dissolved in 3 mL benzene (with hexamethylbenzene as an internal standard). The homogeneous reaction mixture was transferred to a stainless steel pressure reactor, charged with 15 psi of ethylene followed by pressurization with nitrogen to give a total pressure of 120 psi. The reactor was heated to 90 $^\circ\text{C}$. After 2 h, 4 h, 6 h, 8 h and 10 h, the reaction was analyzed by GC/MS using peak areas of the products and the internal standard to calculate product yields. Ethylbenzene production was quantified using linear regression analysis of gas chromatograms of standard samples. A set of five known standards were prepared consisting of 2:1, 3:1, 4:1, 5:1 and 6:1 molar ratios of

ethylbenzene to hexamethylbenzene in methylene chloride. A plot of peak area ratios versus molar ratios gave a regression line. For the GC/MS system, the slope and correlation coefficient for ethylbenzene were 0.68 and 0.99, respectively.

3.5. References

- (1) Foley, N. A.; Ke, Z. F.; Gunnoe, T. B.; Cundari, T. R.; Petersen, J. L. *Organometallics* **2008**, *27*, 3007.
- (2) Foley, N. A.; Lail, M.; Lee, J. P.; Gunnoe, T. B.; Cundari, T. R.; Petersen, J. L. *J. Am. Chem. Soc.* **2007**, *129*, 6765.
- (3) Foley, N. A.; Lee, J. P.; Ke, Z. F.; Gunnoe, T. B.; Cundari, T. R. *Acc. Chem. Res.* **2009**, *42*, 585.
- (4) Lail, M.; Arrowood, B. N.; Gunnoe, T. B. *J. Am. Chem. Soc.* **2003**, *125*, 7506.
- (5) Lail, M.; Bell, C. M.; Conner, D.; Cundari, T. R.; Gunnoe, T. B.; Petersen, J. L. *Organometallics* **2004**, *23*, 5007.
- (6) Andreatta, J. R.; McKeown, B. A.; Gunnoe, T. B. *J. Organomet. Chem.* **2011**, *696*, 305.
- (7) Joslin, E. E.; McMullin, C. L.; Gunnoe, T. B.; Cundari, T. R.; Sabat, M.; Myers, W. H. *Inorg. Chem.* **2012**, *51*, 4791.
- (8) Vande Griend, L. J.; Verkade, J. G.; Pennings, J. F. M.; Buck, H. M. *J. Am. Chem. Soc.* **1977**, *99*, 2459.
- (9) Verkade, J. G. *Coord. Chem. Rev.* **1972**, *9*, 1.
- (10) Werner, H.; Brauers, G.; Nurnberg, O. *J. Organomet. Chem.* **1993**, *454*, 247.
- (11) Zelonka, R. A.; Baird, M. C. *Can J Chemistry* **1972**, *50*, 3063.
- (12) Bennett, M. A.; Smith, A. K. *J Chem Soc Dalton* **1974**, 233.
- (13) Werner, H.; Werner, R. *Chem Ber-Recl* **1982**, *115*, 3766.
- (14) Zelonka, R. A.; Baird, M. C. *J. Organomet. Chem.* **1972**, *35*, C43.

- (15) Elsegood, M. R. J.; Tocher, D. A. *Polyhedron* **1995**, *14*, 3147.
- (16) Pigge, F. C.; Coniglio, J. J. *Curr. Org. Chem.* **2001**, *5*, 757.
- (17) Serron, S.; Nolan, S. P.; Abramov, Y. A.; Brammer, L.; Petersen, J. L. *Organometallics* **1998**, *17*, 104.
- (18) Hodson, E.; Simpson, S. J. *Polyhedron* **2004**, *23*, 2695.
- (19) Furstner, A.; Liebl, M.; Lehmann, C. W.; Picquet, M.; Kunz, R.; Bruneau, C.; Touchard, D.; Dixneuf, P. H. *Chem-Eur J* **2000**, *6*, 1847.
- (20) Elsegood, M. R. J.; Smith, M. B.; Sanchez-Ballester, N. M. *Acta Crystallogr E* **2006**, *62*, M2838.
- (21) Mendoza-Ferri, M. G.; Hartinger, C. G.; Nazarov, A. A.; Eichinger, R. E.; Jakupec, M. A.; Severin, K.; Keppler, B. K. *Organometallics* **2009**, *28*, 6260.
- (22) *Percent yield was determined using ^1H NMR spectroscopy versus an internal standard.*
- (23) Foley, N. A.; Lail, M.; Gunnoe, T. B.; Cundari, T. R.; Boyle, P. D.; Petersen, J. L. *Organometallics* **2007**, *26*, 5507.
- (24) Olah, G. A.; Molnar, A. *Hydrocarbon Chemistry*; 2nd ed.; Wiley-Interscience: New York, 2003.
- (25) *Relative rates were determined by using experimental TOs.*
- (26) Lühder, K.; Nehls, D.; Madeja, K. *Journal Fur Praktische Chemie* **1983**, *325*, 1027.
- (27) Frisch, M. J., et al.; Gaussian, Inc: Willingford, CT, 2009.
- (28) Stevens, W. J.; Krauss, M.; Basch, H.; Jasien, P. G. *Can J Chem* **1992**, *70*, 612.

4. Catalytic Decomposition Pathway for $\text{TpRu}(\text{CO})(\text{NCMe})\text{Ph}$

4.1. Introduction

Our group has demonstrated that $\text{TpRu}(\text{CO})(\text{NCMe})\text{Ph}$ is one of the most active olefin hydroarylation catalyst.¹⁻⁴ $\text{TpRu}(\text{CO})(\text{NCMe})\text{Ph}$ (0.1 mol % loading) catalyzes the formation of 51 TO of ethylbenzene from benzene and ethylene (25 psi) after 4 h with a turnover frequency (TOF) of $3.5 \times 10^{-3} \text{ s}^{-1}$. This TOF is an estimate since it is calculated using TO after 4 hours and some catalyst decomposition of $\text{TpRu}(\text{CO})(\text{NCMe})\text{Ph}$ could have occurred.¹⁻³ Additionally, it was shown that catalysis with α -olefins (e.g., propylene and hexene) using $\text{TpRu}(\text{CO})(\text{NCMe})\text{Ph}$ is selective for the anti-Markovnikov product (*n*-propylbenzene and *n*-hexylbenzene) over the Markovnikov product (cumene and 2-phenylhexane) in a 1.6:1 ratio. The bias for anti-Markovnikov products supports a non-acid catalyzed process (i.e., Friedel-Crafts alkylation). Through experimental and computation studies, we determined that the mechanism for transition metal catalyzed hydroarylation includes two key steps: olefin insertion in a M–Ar bond and benzene C–H activation (see Chapter 1).⁴ Initial studies suggested that the deactivation product of catalysis with $\text{TpRu}(\text{CO})\text{Ph}(\text{NCMe})$ was a paramagnetic multinuclear Ru species; however, the identity of the product(s) of deactivation have not been definitely determined.¹⁻³

Chapter 3 describes the use of $\text{TpRu}[\overline{\text{P}(\text{OCH}_2)_2(\text{OCCH}_3)}](\text{NCMe})\text{Ph}$ as a catalyst for olefin hydroarylation.⁵ Due to a multiple step synthesis with a 17% overall yield for $\text{TpRu}[\overline{\text{P}(\text{OCH}_2)_2(\text{OCCH}_3)}](\text{NCMe})\text{Ph}$, reactions were performed initially at a lower catalyst loading than we typically used for $\text{TpRu}(\text{L})(\text{NCMe})\text{Ph}$ catalysts (0.025 mol %

rather than 0.1 mol %). The optimal catalytic conditions for $\text{TpRu}[\text{P}(\overline{\text{OCH}_2})_2(\overline{\text{OCCH}_3})](\text{NCMe})\text{Ph}$ are 0.025 mol % Ru, 90 °C, and 1 atm of ethylene yielding 90 TON of ethylbenzene. Therefore, to have a direct comparison for the $\text{TpRu}(\text{L})(\text{NCMe})\text{Ph}$ [$\text{L} = \text{CO}, \text{PMe}_3, \text{P}(\overline{\text{OCH}_2})_2(\overline{\text{OCCH}_3}),$ or $\text{P}(\text{OCH}_2)_3\text{CEt}$] series, these previously reported catalysts were evaluated at the same conditions used for $\text{TpRu}[\text{P}(\overline{\text{OCH}_2})_2(\overline{\text{OCCH}_3})](\text{NCMe})\text{Ph}$ (0.025 mol % Ru, 90 °C and 1 atm ethylene). Decreasing the catalyst loading for $\text{TpRu}[\text{P}(\text{OCH}_2)_3\text{CEt}]\text{Ph}(\text{NCMe})$ (25 psi ethylene) had no influence on the TON; however, an increase of 10 TON was observed at lower ethylene concentration (1 atm vs 10 psi) compared to the previously reported values. A significant change in TON was observed for $\text{TpRu}(\text{CO})(\text{NCMe})\text{Ph}$. $\text{TpRu}(\text{CO})(\text{NCMe})\text{Ph}$ at 0.025 mol % loading yielded 415 TON yet, at 0.1 mol % Ru only 77 TON were observed (Table 4.1). The large increase in turnovers at a lower concentration of $\text{TpRu}(\text{CO})(\text{NCMe})\text{Ph}$ supports the hypothesis that the NMR silent decomposition product is a multinuclear species that forms by a second order process (see below). This chapter will describe the effects of catalyst loading and ethylene pressure on ethylene hydrophenylation catalyzed by $\text{TpRu}(\text{CO})(\text{NCMe})\text{Ph}$ with a focus on routes of deactivation.

Table 4.1. Comparison of TON and TOF for Ethylbenzene Production from Catalytic Hydrophenylation of Ethylene by TpRu(L)(NCMe)Ph Complexes.

L	TON	Time	TOF (s^{-1}) ^a	Relative TOF	$E_{1/2}$ (V vs. NHE)
CO	415	40 h	6.7×10^{-3}	14	1.03
$\text{P}(\text{OCH}_2)_2(\text{OCCH}_3)$	90 ^b	50 h	1.5×10^{-3}	3	0.69
$\text{P}(\text{OCH}_2)_3\text{CEt}$	20 ^b	24 h	4.8×10^{-4}	1	0.54

^a Calculated after 4 h at 90 °C with 1 atm ethylene and 0.025 mol % of catalyst (relative to benzene). ^b Catalyst deactivation occurs by formation of $\text{TpRu(L)}(\eta^3\text{-C}_3\text{H}_4\text{Me})$.

4.2. Results and Discussion

4.2.1. Kinetics of Decomposition of TpRu(CO)(NCMe)Ph in THF

Monitoring the deactivation of TpRu(CO)(NCMe)Ph under catalytic conditions (i.e., in benzene under ethylene pressure) is complicated by competing processes (see below). Thus, we explored the decomposition of TpRu(CO)(NCMe)Ph in the absence of benzene and ethylene. TpRu(CO)(NCMe)Ph (0.03 M) was placed in $\text{THF-}d_8$, heated to 75 °C and monitored by ^1H NMR spectroscopy. As the reaction progressed, resonances for the starting material decreased and the appearance of broad resonances were observed in the ^1H NMR spectra. These broad resonances are consistent with the formation of a paramagnetic species and may be the same as one of the products of catalyst deactivation (see below). Plots of the $\ln([\text{TpRu(CO)(NCMe)Ph}])$ vs time and $[\text{TpRu(CO)(NCMe)Ph}]^{-1}$ vs time (Figure 4.1, Figure 4.2) reveal that the decomposition pathway is likely second order in Ru. The rate of decomposition was determined using only the first 30,000 seconds due to larger error associated with the integrations at the end of the reaction. The rate of decomposition was determined to be $0.007(1) \text{ s}^{-1}\text{M}^{-1}$ at 75 °C.

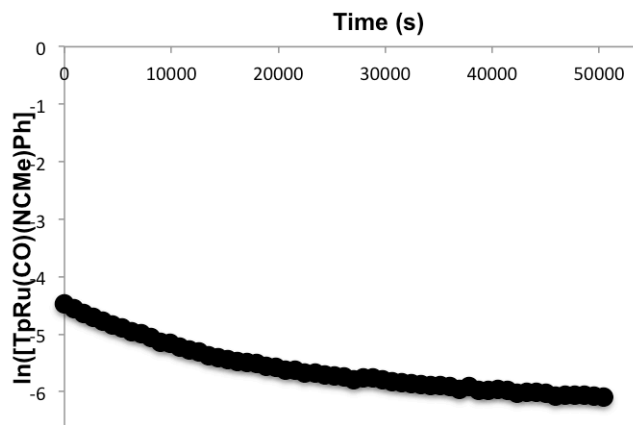


Figure 4.1. First order plot of $\ln([\text{TpRu}(\text{CO})(\text{NCMe})\text{Ph}])$ vs time determined from ^1H NMR spectroscopy (using the internal standard HMDS) for the decomposition of $\text{TpRu}(\text{CO})(\text{NCMe})\text{Ph}$ in $\text{THF-}d_8$ at 75°C .

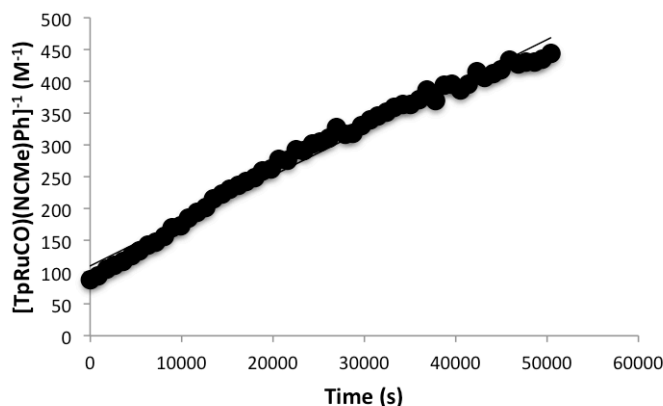
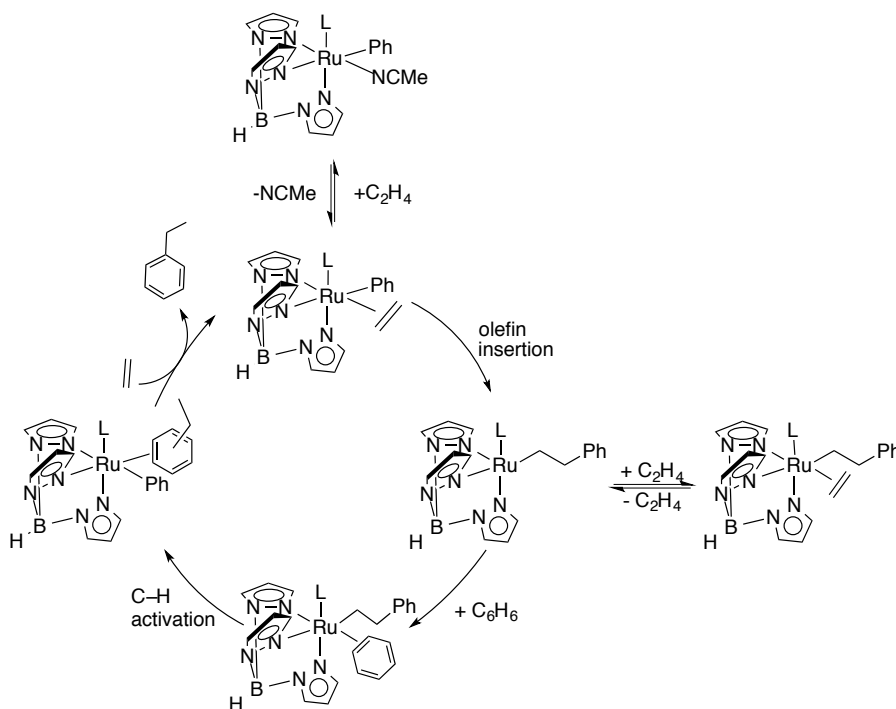


Figure 4.2. Second order plot of the $[\text{TpRu}(\text{CO})(\text{NCMe})\text{Ph}]^{-1}$ vs time ($R^2 = 0.98$) determined from ^1H NMR spectroscopy (using the internal standard HMDS) for the decomposition of $\text{TpRu}(\text{CO})(\text{NCMe})\text{Ph}$ in $\text{THF-}d_8$ at 75°C .

4.2.2. Competing Decomposition Reactions: Dependence on Ethylene Concentration

It has been shown that higher concentrations of ethylene decrease the rate of catalysis for the hydrophenylation of ethylene which has been explained by the resting state $\text{TpRu}(\text{CO})(\eta^2\text{-H}_2\text{C}=\text{CH}_2)(\text{CH}_2\text{CH}_2\text{Ph})$ (Scheme 4.1).² Unlike $\text{TpRu}(\text{L})(\text{NCMe})\text{Ph}$ [$\text{L} = \text{PMe}_3$, $\text{P}(\text{OCH}_2)_2(\text{OCCH}_3)$, or $\text{P}(\text{OCH}_2)_3\text{CEt}$] where catalysis is halted by the

formation of a $\text{TpRu}(\text{L})(\eta^3\text{-C}_4\text{H}_7)$,^{3,5,6} previous analysis of the non-volatiles after deactivation of $\text{TpRu}(\text{CO})(\text{NCMe})\text{Ph}$ revealed potential formation of a paramagnetic species and lack of evidence for the presence of $\text{TpRu}(\text{CO})(\eta^3\text{-C}_4\text{H}_7)$.⁷ $\text{TpRu}(\text{CO})(\eta^3\text{-C}_4\text{H}_7)$ has been synthesized by the reaction of $\text{TpRu}(\text{CO})(\text{NCMe})\text{Ph}$ with ethylene (250 psi) in THF at 70 °C.¹ We anticipate that the pathway of deactivation of $\text{TpRu}(\text{CO})(\text{NCMe})\text{Ph}$ [i.e., formation of paramagnetic complex *or* $\text{TpRu}(\text{CO})(\eta^3\text{-C}_4\text{H}_7)$] might depend on ethylene concentration. To examine the effect of ethylene concentration on catalyst deactivation, catalytic experiments were conducted using 0.01 mol % Ru loading at 90 °C with varied ethylene pressures (1 atm, 25 or 50 psi). Also, if the formation of the paramagnetic deactivation product during catalysis is the same process as decomposition of $\text{TpRu}(\text{CO})(\text{NCMe})\text{Ph}$ in THF (see above), it should be second order in $[\text{TpRu}(\text{CO})(\text{NCMe})\text{Ph}]$.



Scheme 4.1. Proposed catalytic cycle for olefin hydroarylation with $\text{TpRu}(\text{II})$ complexes.

Catalytic reactions at 0.01 mol % $\text{TpRu}(\text{CO})(\text{NCMe})\text{Ph}$ and 1 atm of ethylene show significant increase longevity and an increase in TON of ethylbenzene compared to reactions with higher ethylene pressure (Table 6.2). As ethylene pressure increases the longevity and TON of ethylbenzene decreases due to the increased formation of $\text{TpRu}(\text{CO})(\eta^3\text{-C}_4\text{H}_7)$. At ethylene pressures ≥ 25 psi, the formation of the allyl species $\text{TpRu}(\text{CO})(\eta^3\text{-C}_4\text{H}_7)$ is quantitative (Table 6.2). These results suggest at lower ethylene concentrations, deactivation via formation of the proposed paramagnetic complex (which are presumed to be independent of ethylene) and $\text{TpRu}(\text{CO})(\eta^3\text{-C}_4\text{H}_7)$ complete. But, at increased ethylene concentrations the rate of deactivation to form the ally complex $\text{TpRu}(\text{CO})(\eta^3\text{-C}_4\text{H}_7)$ dominates. Therefore, higher ethylene concentrations lead to more rapid catalyst deactivation. At 0.01 mol % $\text{TpRu}(\text{CO})(\text{NCMe})\text{Ph}$ and 1 atm of ethylene the formation of $\text{TpRu}(\text{CO})(\eta^3\text{-C}_4\text{H}_7)$ is the predominate catalytic deactivation product (62% yield) but the proposed paramagnetic species is also formed.

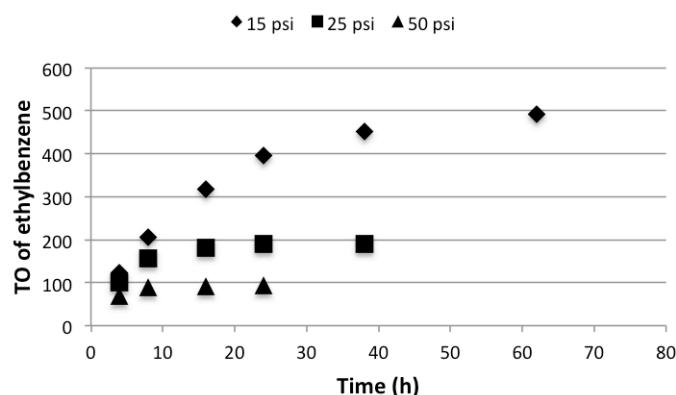


Figure 4.3. Comparison of catalytic hydrophenylation of ethylene at various pressures (1 atm, 25 and 50 psi) by $\text{TpRu}(\text{CO})(\text{NCMe})\text{Ph}$ at 0.01 mol% Ru and 90 °C.

Table 4.2. Comparison of $\text{TpRu}(\text{CO})(\eta^3\text{-C}_3\text{H}_4\text{Me})$ yield during catalysis at 0.01 mol % Ru at varying pressures of ethylene at 90 °C.

Ethylene Pressure	TON	% yield $\text{TpRu}(\text{CO})(\eta^3\text{-C}_3\text{H}_4\text{Me})^a$
1 atm	490	62
25 psi	189	98
50 psi	94	100

^a % yield was determined by ^1H NMR spectroscopy using integrations versus an known concentration of internal standard HMDS.

4.2.3. Competing Deactivation Pathways: Dependence on Catalyst Loading

To further investigate the competition between the formation of $\text{TpRu}(\text{CO})(\eta^3\text{-C}_4\text{H}_7)$ and the proposed paramagnetic Ru species, catalysis was performed with $\text{TpRu}(\text{CO})(\text{NCMe})\text{Ph}$ using catalyst loadings between 0.001 and 0.3 mol %, 1 atm of ethylene and 90 °C. At lower concentrations of catalyst (≤ 0.025 mol % Ru) the TON of the catalyst is significantly increased compared to catalyst loadings greater than 0.05 mol %. At lower catalyst loadings (≤ 0.025 mol % Ru), activity is generally maintained through approximately 40 h and the $\text{TpRu}(\text{CO})(\eta^3\text{-C}_4\text{H}_7)$ is formed in ~60% yield. Higher Ru loadings increase the time during which activity is observed (~90 h) but overall TON of ethylbenzene is decreased significantly. At higher concentration of Ru the proposed paramagnetic species dominates deactivation with only of 22% and 12% of $\text{TpRu}(\text{CO})(\eta^3\text{-C}_4\text{H}_7)$ observed at 0.1 mol % and 0.2 mol % Ru, respectively (Table 4.3).

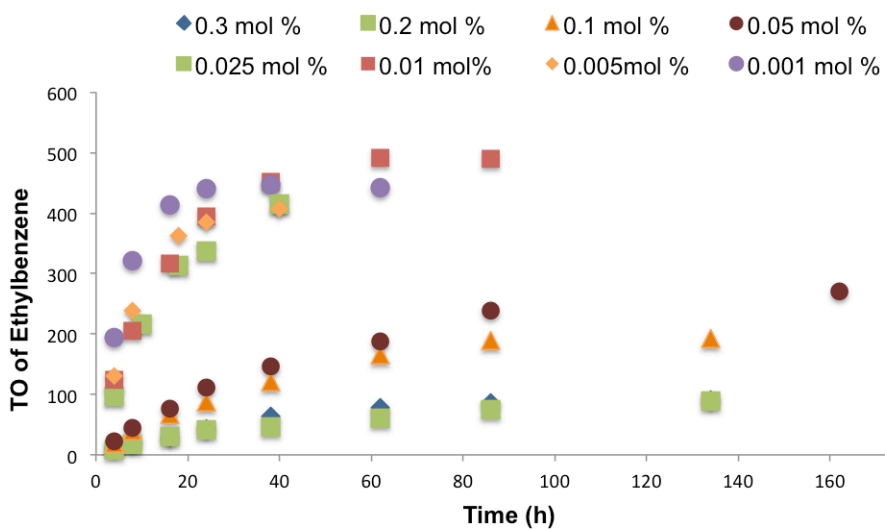


Figure 4.4. Comparison of catalytic hydrophenylation of ethylene at various Ru mol % loadings (0.001 – 0.3 mol %) by TpRu(CO)Ph(NCMe) at 1 atm and 90 °C.

Table 4.3. Comparison of TpRu(CO)(η^3 -C₃H₄Me) concentration during catalysis as a function of catalyst loading^a

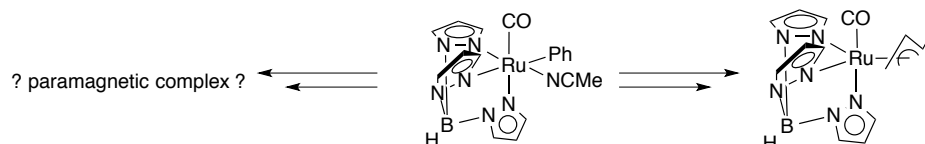
Mol % Ru	% yield TpRu(CO)(η^3 -C ₃ H ₄ Me) ^b
0.2	12
0.1	22
0.025	60
0.01	62
0.005	59
0.001	52

^a Reactions conducted at 1 atm of ethylene and 90 °C ^b % yield was determined by ¹H NMR spectroscopy using integrations versus a known concentration of internal standard, HMDS.

4.3. Conclusions

TpRu(CO)(NCMe)Ph has been observed to be an effective catalyst for ethylene hydrophenylation. Studies of the impact of catalyst loading and ethylene pressure were examined. Two competing deactivation pathways have been proposed based on these studies (Scheme 4.2). It was determined that ethylene concentration influences the catalyst longevity and the pathway to deactivation. At higher ethylene concentrations (i.e,

25 or 50 psi and 0.01 mol % Ru) the total TON was decreased compared to 1 atm of ethylene. Additionally, the only deactivation pathway observed was formation of $\text{TpRu}(\text{CO})(\eta^3\text{-C}_3\text{H}_4\text{Me})$ for 25 or 50 psi of ethylene. At lower catalyst loadings (≤ 0.025 mol % Ru) approximately 60% yield of $\text{TpRu}(\text{CO})(\eta^3\text{-C}_3\text{H}_4\text{Me})$ is observed. However, at higher catalyst loadings (e.g., 0.1 and 0.2 mol % Ru) the main decomposition product is a proposed paramagnetic Ru species with significantly less $\text{TpRu}(\text{CO})(\eta^3\text{-C}_3\text{H}_4\text{Me})$. It is surmised that immobilizing $\text{TpRu}(\text{CO})(\text{NCMe})\text{Ph}$ on a solid support could eliminate the formation of the paramagnetic Ru species, and could improve catalyst longevity.



Scheme 4.2. Competing deactivation pathways during catalysis for $\text{TpRu}(\text{CO})(\text{NCMe})\text{Ph}$.

4.4. Experimental

General Methods. The preparation, isolation and characterization of $\text{TpRu}(\text{CO})\text{Ph}(\text{NCMe})$ have been previously reported.² Benzene was purified by passage through a column of activated alumina. $\text{THF-}d_8$ was stored under a nitrogen atmosphere over 4Å molecular sieves. ^1H NMR spectra were recorded on a Varian MRS 600 MHz spectrometer.

Kinetic Studies: Determination of Order of Deactivation for $\text{TpRu}(\text{CO})(\text{NCMe})\text{Ph}$. A $\text{THF-}d_8$ solution of $\text{TpRu}(\text{CO})(\text{NCMe})\text{Ph}$ (0.0125 g, 0.0272 mmol) and hexamethyldisilane (as an internal standard) was made in a 1 mL volumetric

flask. The solution was equally divided (300 μ L) and transferred into three J. Young NMR tubes. The NMR tube was placed into the temperature calibrated NMR probe (equilibrated at 76 $^{\circ}$ C). The temperature was determined using a 80% Ethylene Glycol in DMSO- d_6 and the following equation provided by Bruker Instruments, Inc. VT-Calibration Manual: $T(K) = (4.218 - \Delta)/0.009132$, where Δ is the shift difference (ppm) between CH₂ and OH peaks of the ethylene glycol. Reaction progress was monitored by ¹H NMR spectroscopy using automated data acquisition. A single transient was used for each time point with 900 s delay between transients. The rate of the reaction was determined by monitoring the disappearance of the most upfield Tp resonance (6.02 ppm) of the starting material. Each reaction was monitored through at least 3 half-lives.

Representative Catalytic Reaction. TpRu(CO)(NCMe)Ph (0.0103 g, 0.0224 mmol, 0.1 mol % Ru relative to benzene) was dissolved in 2 mL of benzene. In a 25 mL volumetric flask decane (0.199 g, 0.273 mL, 0.5 mol % decane relative to benzene) was added to benzene solution. To generate 6 mL of a 0.025 mol % Ru catalyst solution: 1.5 mL of [0.1 mol %] Ru solution, 1.5 mL of [0.5 mol %] decane solution and 3 mL of benzene were transferred to a stainless steel pressure reactor. The reactor was charged with 15 psi of ethylene, degassed to reach a final pressure of 1 atm, pressurized with dinitrogen to a total pressure of 120 psi, and heated to 90 $^{\circ}$ C. After a given duration the reactor was cooled to room temperature and an aliquot of the reaction mixture was removed. The reaction mixture was analyzed by GC/MS using peak areas of the products and the internal standard to calculate product yields. Ethylbenzene production was quantified using linear regression analysis of gas chromatograms of standard samples. A

set of eight known standards were prepared consisting of 1:5, 3:5, 5:5, 7.5:5, 10:5, 50:5, 100:5 and 150:5 molar ratios of ethylbenzene to decane in methylene chloride. A plot of peak area ratios versus molar ratios gave a regression line. For the GC/MS system, the slope and correlation coefficient for ethylbenzene were 0.18 and 0.99, respectively.

Determination of Percent $\text{TpRu}(\text{CO})(\eta^3\text{-C}_3\text{H}_4\text{Me})$ Formation During Catalysis. A catalytic reaction was performed as stated above. After completion of catalysis, the reactor was brought into the glovebox, the volume of the solution was determined, and the volatiles were removed *in vacuo*. The non-volatiles were dissolved in C_6D_6 (0.4 mL) and placed in an NMR tube with 20 μL of the 0.0049 M HMDS solution. A ^1H NMR spectrum was collected ($n_t = 8$ and a pulse delay of 20 sec) and an allyl resonance corresponding to $\text{TpRu}(\text{CO})(\eta^3\text{-C}_3\text{H}_4\text{Me})$ (4.4 ppm) was integrated relative to the HMDS standard to calculate the percent yield of $\text{TpRu}(\text{CO})(\eta^3\text{-C}_3\text{H}_4\text{Me})$.

4.5. References

- (1) Lail, M.; Arrowood, B. N.; Gunnoe, T. B. *J. Am. Chem. Soc.* **2003**, *125*, 7506.
- (2) Lail, M.; Bell, C. M.; Conner, D.; Cundari, T. R.; Gunnoe, T. B.; Petersen, J. L. *Organometallics* **2004**, *23*, 5007.
- (3) Foley, N. A.; Lail, M.; Lee, J. P.; Gunnoe, T. B.; Cundari, T. R.; Petersen, J. L. *J. Am. Chem. Soc.* **2007**, *129*, 6765.
- (4) Foley, N. A.; Lee, J. P.; Ke, Z. F.; Gunnoe, T. B.; Cundari, T. R. *Acc. Chem. Res.* **2009**, *42*, 585.
- (5) Joslin, E. E.; McMullin, C. L.; Gunnoe, T. B.; Cundari, T. R.; Sabat, M.; Myers, W. H. *Organometallics* **2012**, *31*, 6851.
- (6) Foley, N. A.; Ke, Z. F.; Gunnoe, T. B.; Cundari, T. R.; Petersen, J. L. *Organometallics* **2008**, *27*, 3007.
- (7) Lail, M., Thesis: Synthesis and Reactivity of Ruthenium Alkyl and Aryl Complexes and Their Applications towards Aromatic C-H Bond Activation and Olefin Hydroarylation, North Carolina State University, 2006.

5. Synthesis and Characterization of (L)Ru(II) complexes (L = neutral 6-electron donor) for Olefin Hydroarylation

5.1. Introduction

Tris(pyrazolyl)borate ligands, which are often called scorpionates were first reported by Trofimenko in the late 1960s.¹⁻³ Poly(pyrazolyl)borate ligands have been extensively studied, and more than 2,000 papers have been published containing this class of ligand.⁴ Their utility stems from the ease of altering electronic properties and steric profile by decorating the 3, 4, and/or 5-position of the pyrazolyl rings, adding substituents to boron, and replacing boron with carbon, silicon, phosphorous or gallium (Figure 5.1).^{3,5-9}

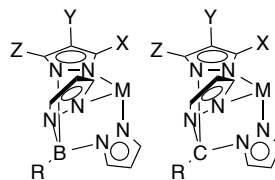


Figure 5.1. Examples of some scorpionate ligands

Our group has studied the use of tris(pyrazolyl)borate ligands on Ru(II) with the motif TpRu(L)(NCMe)Ph [$\text{L} = \text{CO}, \text{PMe}_3, \text{P}(\text{OCH}_2)_3\text{CEt}, \text{P}(\text{pyr})_3$ and $\text{P}(\text{OCH}_2)_2(\text{OCCH}_3)$].¹⁰⁻¹⁴ The best catalyst developed from our studies on TpRu(L)(NCMe)Ph motif is TpRu(CO)Ph(NCMe) , which yields with 415 TO of ethylbenzene at 90 °C (0.025 mol % Ru relative to benzene) with 15 psi of ethylene after 40 h.¹⁵ This catalyst functions by a mechanism that includes two key steps, olefin insertion into a Ru–Ph bond and benzene C–H activation. These two steps require a fine balance of electronics at the metal center.

Whereas olefin insertion requires a less electron rich metal center, which decreases metal-to-olefin backbonding, benzene C–H activation is promoted by more electron-rich metal centers. Experimental studies have found that the electron density of the metal center has a larger impact on the activation barrier for olefin insertion than the activation barrier for benzene C–H activation. Results from catalysis demonstrate these effects. While $\text{TpRu}(\text{PMe}_3)\text{Ph}(\text{NCMe})$ activates benzene C–H bonds most rapidly among the $\text{TpRu}(\text{L})(\text{NCMe})\text{Ph}$ [$\text{L} = \text{CO}, \text{PMe}_3, \text{P}(\text{OCH}_2)_3\text{CEt}, \text{P}(\text{pyr})_3$ and $\text{P}(\overline{\text{OCH}_2)_2(\text{OCCH}_3)}$] series it is not a catalyst for olefin hydroarylation.¹⁰⁻¹⁴ The slow rate of ethylene insertion into the Ru–Ph of $\text{TpRu}(\text{PMe}_3)(\eta^2\text{-C}_2\text{H}_4)\text{Ph}$ allows ethylene C–H activation to compete with catalytic turnover. Although benzene C–H activation by $\text{TpRu}(\text{CO})(\text{NCMe})\text{Ph}$ is slower than $\text{TpRu}(\text{PMe}_3)(\text{NCMe})\text{Ph}$, the CO complex is a catalyst for olefin hydroarylation. $\text{TpRu}[\text{P}(\overline{\text{OCH}_2)_2(\text{OCCH}_3)}]\text{Ph}(\text{NCMe})$ gives approximately 90 TON with 15 psi of ethylene at 90 °C. However, the metal center is still too electron rich, and olefin C–H activation competes with olefin insertion, which reduces catalyst longevity.^{15,16} Thus, we sought an octahedral Ru(II) complex with similar electron density (or less) as $\text{TpRu}(\text{CO})(\text{NCMe})\text{Ph}$ but without the CO ligand. Our goals were to improve selectivity for linear alkyl arenes (for olefin hydroarylation using α -olefins) and to enhance catalyst stability (the CO ligand, which can bridge two Ru metals, might accelerate catalyst decomposition). Modulating the ligand set from the anionic tris(pyrazolyl)borates to the neutral poly(pyrazolyl)alkanes should provide us with a similar steric profile as our previously studied $\text{TpRu}(\text{L})(\text{NCMe})\text{Ph}$ catalyst but would be less donating to the metal.

The less donating poly(pyrazolyl)alkane allows the incorporation of more donating ligands but remain less electron rich than $\text{TpRu}(\text{CO})\text{Ph}(\text{NCMe})$.

Our group has used Ru(III/II) potentials (from cyclic voltammetry) to estimate electron density. We have previously shown that by replacing the Tp ligand in $\text{TpRu}(\text{CO})(\text{NCMe})\text{Ph}$ with Ep (Ep = tris(pyrazolyl)ethane) shifts Ru(III/II) potentials positive approximately 0.38 V (Figure 5.2).^{17,18} Using the predicted 0.38 V shift, $\text{EpRu}[\text{P}(\text{OCH}_2)_3\text{CEt}]\text{Ph}(\text{NCMe})$ should exhibit a Ru(III/II) potential of ~ 0.92 V, which is similar to $\text{TpRu}(\text{CO})\text{Ph}(\text{NCMe})$ (1.02 V). This chapter describes the synthesis of a variety of Ru(II) complexes with neutral 6-electron donor ligands such as η^6 -*p*-cymene, $\text{HC}(\text{pz}')_3$ ($\text{pz}' = 3,5$ dimethylpyrazolyl) and $\text{C}(\text{pz})_4$ ($\text{pz} = \text{pyrazolyl}$)methane) and their ability to catalyze olefin hydrophenylation.

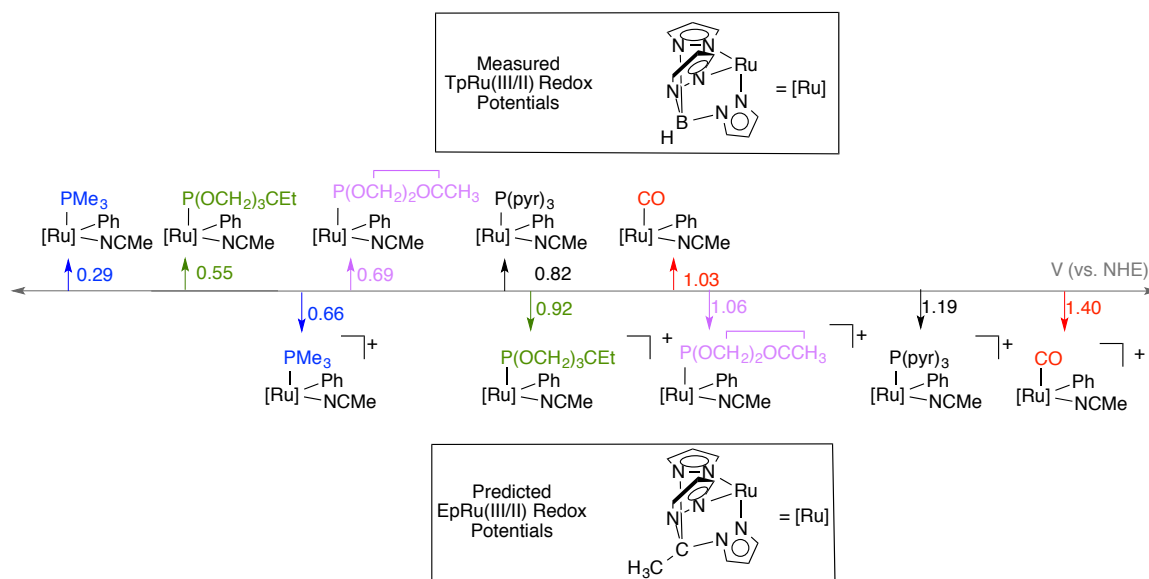
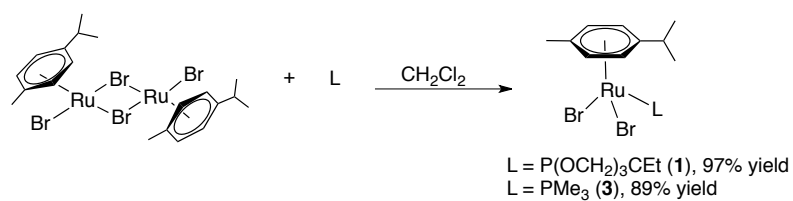


Figure 5.2. Comparison of experimental Ru(III/II) (V vs NHE) potentials for $\text{TpRu}(\text{L})\text{Ph}(\text{NCMe})$ to predicted Ru(III/II) (V vs NHE) potentials for $\text{EpRu}(\text{L})\text{Ph}(\text{NCMe})$.

5.2. Results and Discussion

5.2.1. Synthesis of $(\eta^6\text{-}p\text{-cymene})\text{Ru}(\text{L})\text{PhBr}$

The synthesis of $[(\eta^6\text{-}p\text{-cymene})\text{Ru}[\text{P}(\text{OCH}_2)_2(\text{OCCH}_3)]\text{Br}_2]$ and $[(\eta^6\text{-}p\text{-cymene})\text{Ru}[\text{P}(\text{OCH}_2)_2(\text{OCCH}_3)]\text{PhBr}]$ were described in Chapter 3.¹⁵ The complexes $(\eta^6\text{-}p\text{-cymene})\text{Ru}[\text{P}(\text{OCH}_2)_3\text{CEt}]\text{Br}_2$ (**1**), $(\eta^6\text{-}p\text{-cymene})\text{Ru}[\text{P}(\text{OCH}_2)_3\text{CEt}]\text{PhBr}$ (**2**), $(\eta^6\text{-}p\text{-cymene})\text{Ru}(\text{PMe}_3)\text{Cl}_2$ (**3**) and $(\eta^6\text{-}p\text{-cymene})\text{Ru}(\text{PMe}_3)\text{Br}_2$ (**4**), were synthesized using a similar procedure. Complexes **1** and **3** were synthesized by the reaction of $[(\eta^6\text{-}p\text{-cymene})\text{Ru}(\text{Br})(\mu\text{-Br})_2]$ with excess $\text{P}(\text{OCH}_2)_3\text{CEt}$ or PMe_3 , respectively, in methylene chloride (Scheme 5.1). The ^1H NMR spectra for both **1** and **3** are consistent with the presence of a mirror plane with two downfield resonances for the $(\eta^6\text{-}p\text{-cymene})$ (Figure 5.3, Figure 5.5). The bicyclic phosphite ligand gives rise to a doublet for the methylene hydrogens and a quartet and triplet upfield for the ethyl group of the phosphite (Figure 5.3, Figure 5.5). The ^{31}P NMR spectrum of **1** shows a resonance at 110 ppm for the $\text{P}(\text{OCH}_2)_3\text{CEt}$ ligand. The ^1H NMR spectrum for complex **3** has a doublet with a $^2J_{\text{HP}} = 11$ Hz for the phosphine group, and the ^{31}P NMR spectrum shows a downfield shift to -2.0 ppm for the phosphine (Figure 5.5, Figure 5.6.)



Scheme 5.1. Synthesis of $(\eta^6\text{-}p\text{-cymene})\text{Ru}(\text{L})\text{Br}_2$ [$\text{L} = \text{P}(\text{OCH}_2)_3\text{CEt}$ (**1**) or PMe_3 (**3**)].

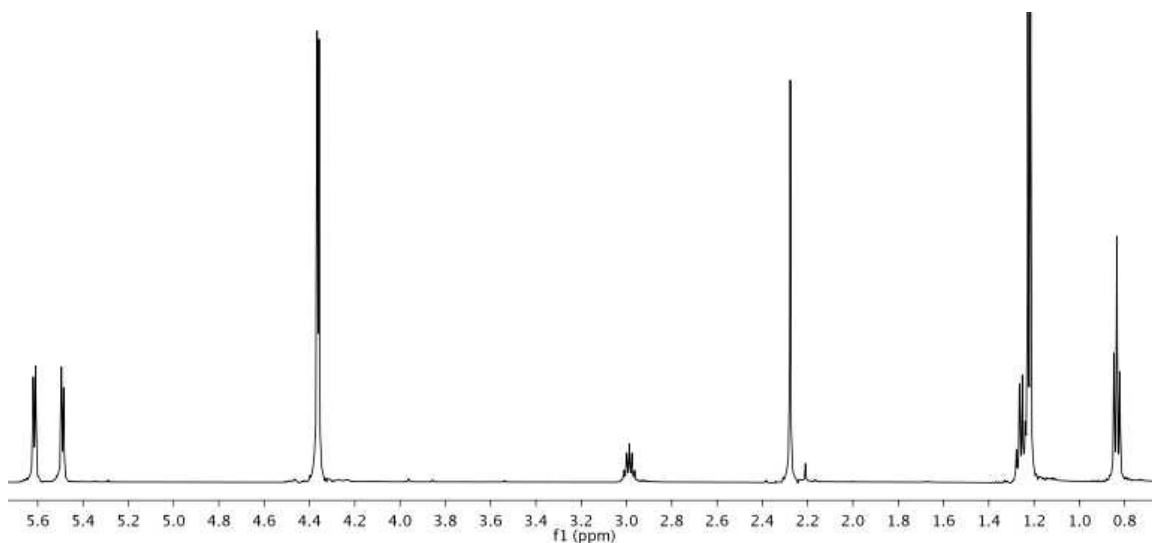


Figure 5.3. ^1H NMR spectrum of $(\eta^6\text{-}p\text{-cymene})\text{Ru}[\text{P}(\text{OCH}_2)_3\text{CEt}]\text{Br}_2$ (**1**) in CDCl_3 .

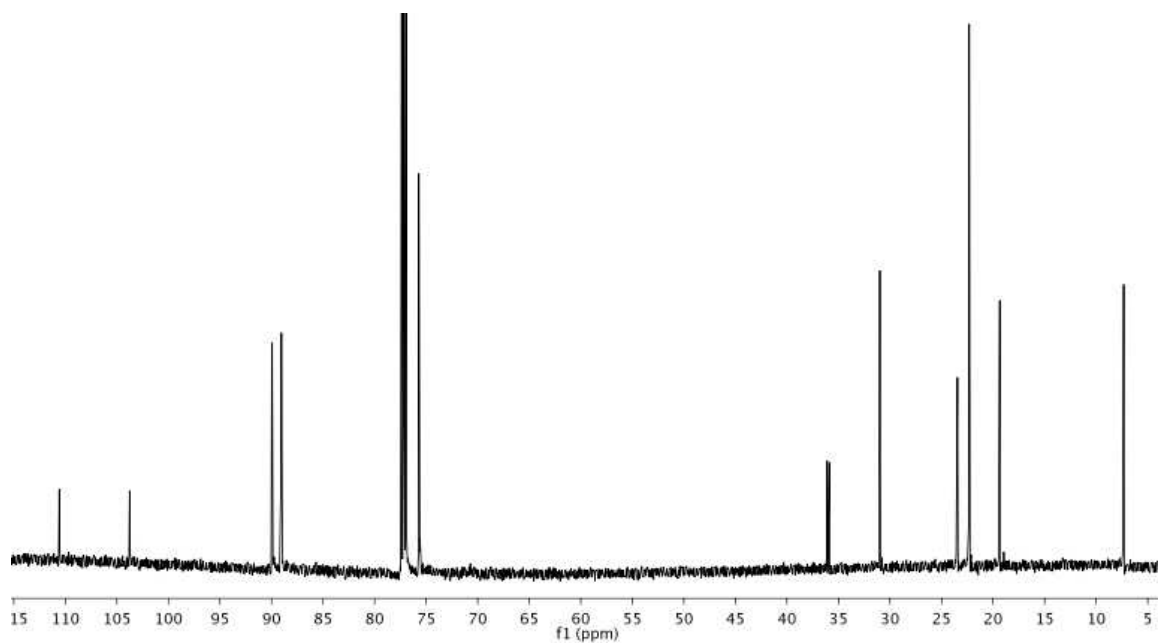


Figure 5.4. ^{13}C NMR spectrum of $(\eta^6\text{-}p\text{-cymene})\text{Ru}[\text{P}(\text{OCH}_2)_3\text{CEt}]\text{Br}_2$ (**1**) in CDCl_3 .

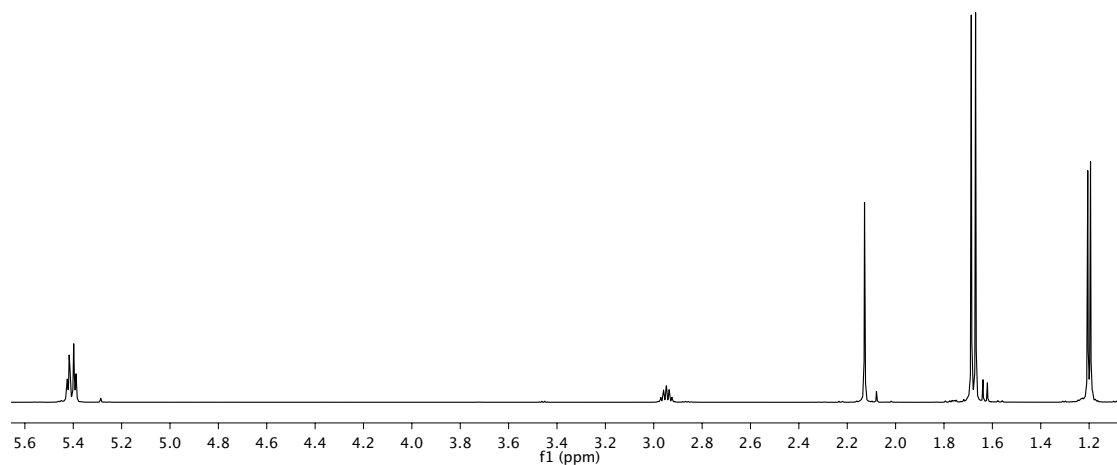


Figure 5.5. ^1H NMR spectrum of $(\eta^6\text{-}p\text{-cymene})\text{Ru}(\text{PMe}_3)\text{Br}_2$ (**3**) in CDCl_3 .

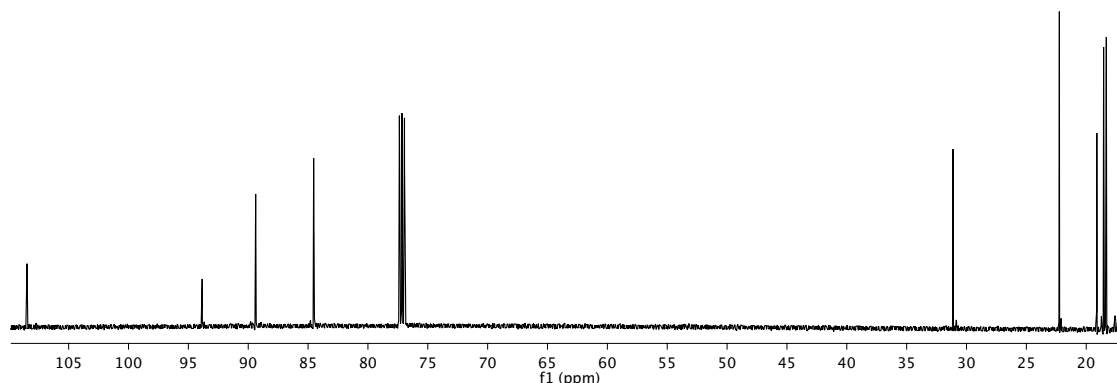
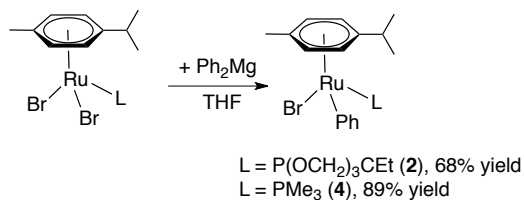


Figure 5.6. ^{13}C NMR spectrum of $(\eta^6\text{-}p\text{-cymene})\text{Ru}(\text{PMe}_3)\text{Br}_2$ (**3**) in CDCl_3

Complexes **1** and **3** can be phenylated using $\text{Ph}_2\text{Mg}[\text{THF}]_2$ in THF. Both reactions begin as heterogeneous mixtures and as the product is formed, $(\eta^6\text{-}p\text{-cymene})\text{Ru}[\text{P}(\text{OCH}_2)_3\text{CEt}](\text{Ph})\text{Br}$ (**2**) (Figure 5.7, Figure 5.8, Figure 5.9) or $(\eta^6\text{-}p\text{-cymene})\text{Ru}(\text{PMe}_3)(\text{Ph})\text{Br}$ (**4**), (Figure 5.10, Figure 5.11, Figure 5.12), the reaction mixture becomes bright yellow and homogeneous (Scheme 5.2). The formation of the asymmetric complex **2** is apparent in the ^1H NMR spectrum with the appearance of 4 downfield resonances (1H each) due to the *p*-cymene ligands and three resonances due to the phenyl ligands between 6.8 and 7.7 ppm. Additionally, the ^{31}P NMR spectrum shows a resonance at 124 ppm, which is a downfield shift of 13 ppm compared to complex **1**. Similar characteristics are observed in the ^1H NMR spectrum of complex **4**, and the phosphine peak in the ^{31}P NMR spectrum is shifted downfield by ~6.6 ppm to 4.5 ppm. Single crystals for both **2** and **4** suitable for X-ray structure determination were obtained by slow diffusion of Et_2O into a THF solution of the complex (Table 5.1). The Ru–P bond length [2.3105(3) Å] of $(\eta^6\text{-}p\text{-cymene})\text{Ru}(\text{PMe}_3)\text{PhBr}$ (**4**) is longer than for $(\eta^6\text{-}p\text{-cymene})\text{Ru}([\text{P}(\text{OCH}_2)_3\text{CEt}]\text{PhBr}$ (**2**) [2.2144(3) Å]; this could potentially be caused by

the difference in back-bonding, with the phosphite, $\text{P}(\text{OCH}_2)_3\text{CEt}$, being a stronger π -acid than PMe_3 . Additionally, sterics could also contribute to the longer Ru–P bond distance of **4** since PMe_3 has a Tolman's cone angle of 118° and $\text{P}(\text{OCH}_2)_3\text{CEt}$ has a smaller cone angle of 101° .¹⁹



Scheme 5.2. Synthesis of $(\eta^6\text{-}p\text{-cymene})\text{Ru}(\text{L})\text{PhBr}$ [$\text{L} = \text{P}(\text{OCH}_2)_3\text{CEt}$ (**2**) or PMe_3 (**4**)].

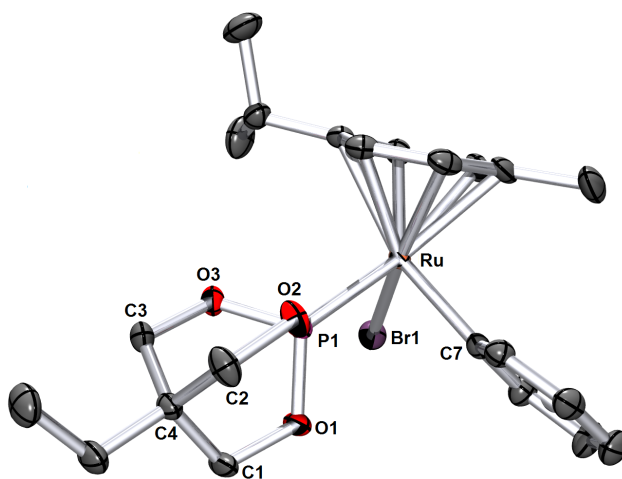


Figure 5.7. ORTEP of $(\eta^6\text{-}p\text{-cymene})\text{Ru}[\text{P}(\text{OCH}_2)_3\text{CEt}]\text{PhBr}$ (**2**) (35% probability with hydrogen atoms omitted.). Selected bond lengths (\AA): Ru–P1, 2.2144(3); P–O1, 1.6003(11); P–O2, 1.602(1); P–O3, 1.6029(1). Selected bond angles ($^\circ$): O3–P1–O2, 102.31(6); O1–P1–O2, 101.88(6); O1–P1–O3, 101.89(6); O1–P1–Ru, 120.62(4); O2–P1–Ru, 112.98(4); O3–P1–Ru, 114.78(4).

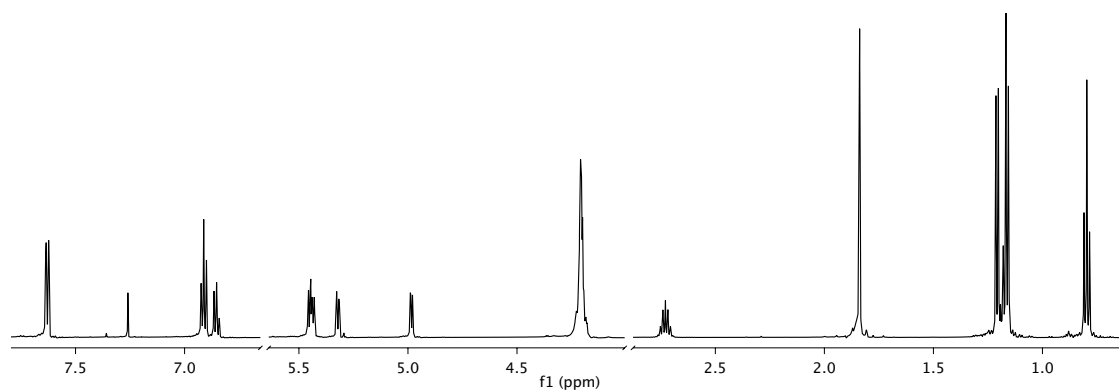


Figure 5.8. ^1H NMR spectrum of $(\eta^6\text{-}p\text{-cymene})\text{Ru}[\text{P}(\text{OCH}_2)_3\text{CEt}]\text{PhBr}$ (**2**) in CDCl_3 .

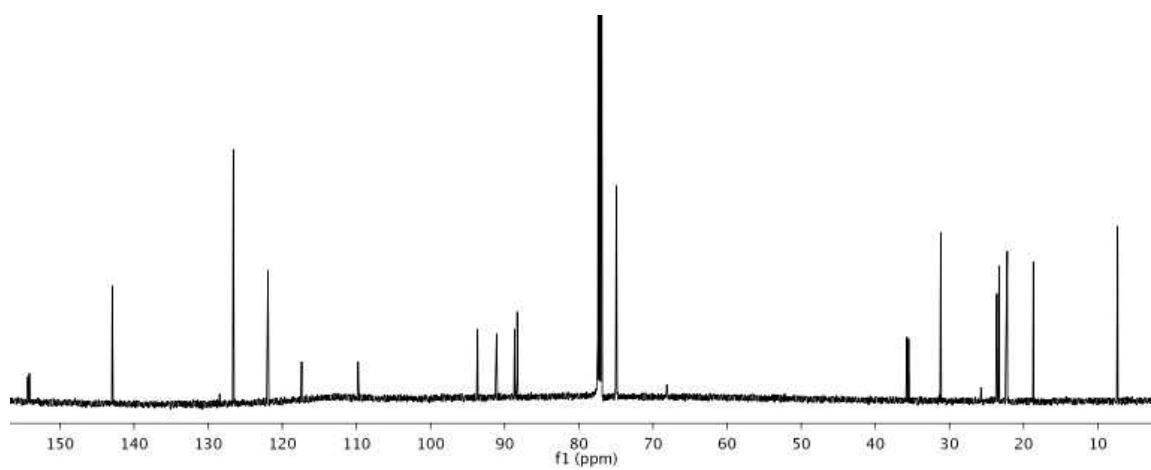


Figure 5.9. ^{13}C NMR spectrum of $(\eta^6\text{-}p\text{-cymene})\text{Ru}[\text{P}(\text{OCH}_2)_3\text{CEt}]\text{PhBr}$ (**2**) in CDCl_3 .

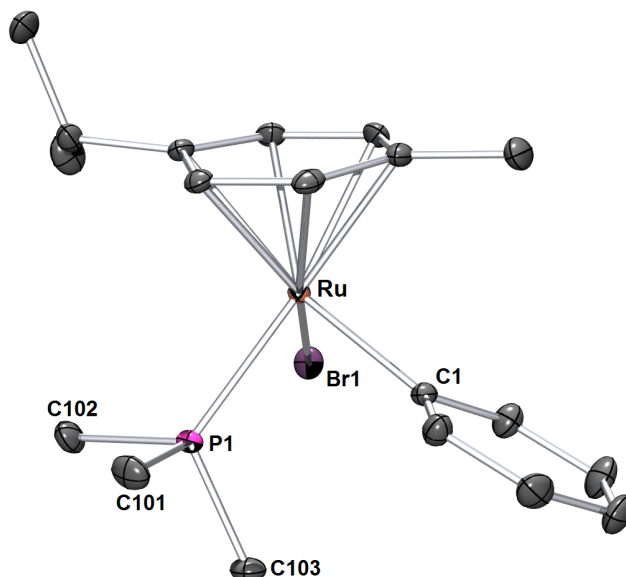


Figure 5.10. ORTEP of $(\eta^6\text{-}p\text{-cymene})\text{Ru}(\text{PMe}_3)\text{PhBr}$ (**4**) (35% probability with hydrogen atoms omitted.). Selected bond lengths (Å): Ru–P1, 2.3105(5). Selected bond angles (°): C101–P1–Ru, 118.19(8); C103–P1–Ru, 116.33(8); C102–P1–Ru, 114.28(8).

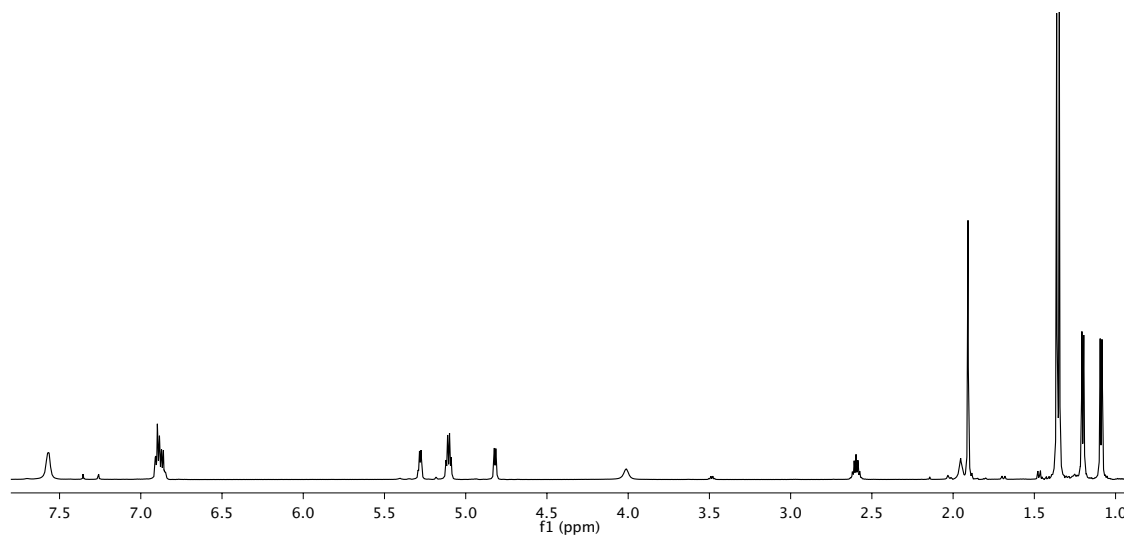


Figure 5.11. ^1H NMR spectrum of $(\eta^6\text{-}p\text{-cymene})\text{Ru}(\text{PMe}_3)\text{PhBr}$ (**4**) in CDCl_3 .

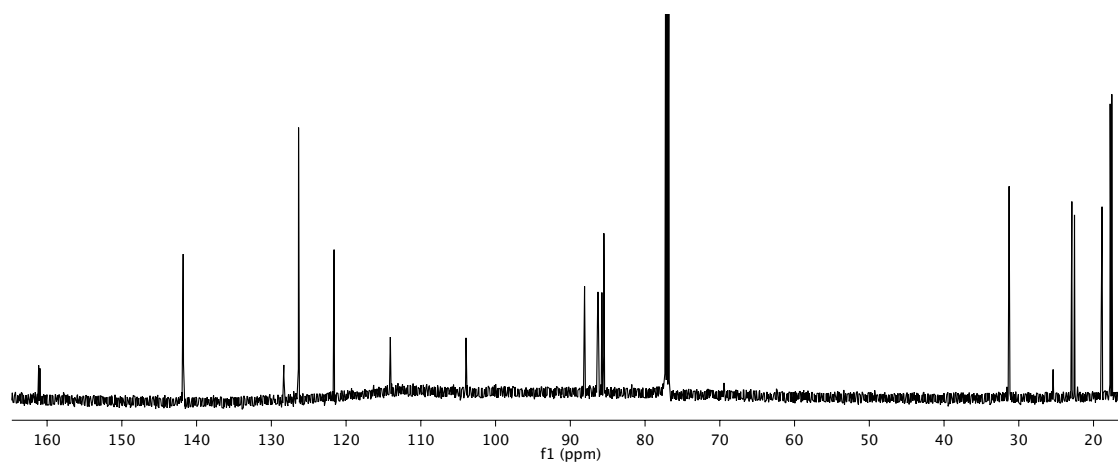


Figure 5.12. ^{13}C NMR spectrum of $(\eta^6\text{-}p\text{-cymene})\text{Ru}(\text{PMe}_3)\text{PhBr}$ (**4**) in CDCl_3 .

Table 5.1. Selected Crystallographic Data for $(\eta^6\text{-}p\text{-cymene})\text{Ru}[\text{P}(\text{OCH}_2)_3\text{CEt}]\text{PhBr}$ (**2**), and $(\eta^6\text{-}p\text{-cymene})\text{Ru}(\text{PMe}_3)\text{PhBr}$ (**4**)

	complex 2	complex 4
empirical formula	$\text{C}_{22}\text{H}_{30}\text{BrO}_3\text{PRu}$	$\text{C}_{19}\text{H}_{28}\text{BrPRu}$
Fw	554.41	458.36
cryst syst	monoclinic	monoclinic
space group	$P2_1/n$	$P2_1/n$
a, Å	7.1218(2)	7.2196(4)
b, Å	13.8532(4)	27.801(1)
c, Å	23.3707(7)	9.6591(5)
β , deg	94.316(1) $^\circ$	92.812(1)
V, Å ³	2299.2(1)	1936.4(2)
Z	4	4
D_{calcd} , mg/m ³	1.602	1.607
cryst size (mm)	0.42 x 0.18 x 0.18	0.440 x 0.340 x 0.250
R1, wR2 ($I > 2\sigma(I)$)	0.0272, 0.0598	0.0192, 0.0441
GOF	1.036	1.336

5.2.2. Olefin hydrophenylation using $(\eta^6\text{-}p\text{-cymene})\text{Ru}(\text{L})\text{PhBr}$

Initial attempts to isolate the cationic Ru(II) complexes $(\eta^6\text{-}p\text{-cymene})\text{Ru}(\text{L})\text{Ph}(\text{L}')[\text{BAR}'_4]$ and $(\eta^6\text{-}p\text{-cymene})\text{Ru}(\text{L})\text{Ph}(\text{OTf})$ [$\text{L} = \text{P}(\text{OCH}_2)_3\text{CEt}$ or

PMe_3 , $\text{Ar}'_4 = 3,5\text{-(CF}_3)_2\text{-C}_6\text{H}_3$ and $\text{L}' = \text{NCMe}$ or THF] were unsuccessful. For example, reactions were run with complex **2** and a range of halide abstractors (e.g., NaBAR'_4 , AgBAR'_4 , NaOTf , TiOTf , KOTf) in THF or NCMe ; however, all conditions lead to no reaction. This was due to being unable to abstract the halide under conditions that would not displace the $(\eta^6\text{-}p\text{-cymene})$ ligand and cause decomposition. Therefore, ethylene hydrophenylation was attempted under catalytic conditions using complexes **2** or **4** in the presence of a halide abstractor (e.g., NaBAR'_4 , AgOTf or AgBAR'_4). Both complexes gave irreproducible results with all of the halide abstractors. For example, four separate catalysis runs at 0.025 mol % complex **2**, 25 psi of ethylene, and <1 equiv. NaBAR'_4 at 90 °C gave an average of 13(\pm 16) TO of ethylbenzene. NMR scale reactions showed that free $p\text{-cymene}$ is formed under conditions of catalysis. The lability of the $p\text{-cymene}$ ligand has been shown with a similar species described in Chapter 3. In the presence of NCMe the $p\text{-cymene}$ ligand of $[(\eta^6\text{-}p\text{-cymene})\text{Ru}[\text{P}(\text{OCH}_2)_2(\text{OCCH}_3)]\text{PhBr}]$ is displaced and $(\text{NCMe})_3\text{Ru}[\text{P}(\text{OCH}_2)_2(\text{OCCH}_3)](\text{Ph})\text{Br}$ is formed. Moreover, addition of free $p\text{-cymene}$ does slow the rate of decomposition, but no catalysis was observed.

5.2.3. Synthesis of $\{[\text{C}(\text{pz})_4]\text{Ru}[\text{P}(\text{OCH}_2)_3\text{CEt}]\text{Ph}(\text{NCMe})\}[\text{Y}]$ Complexes

In order to study the effect of having a charge neutral ligand similar to Tp , we sought to synthesize $\text{C}(\text{pz})_4\text{Ru(II)}$ complexes where $\text{C}(\text{pz})_4 = \kappa^3\text{-}N,N,N\text{-tetrakis(1-pyrazolyl) methane}$. A potential synthetic route to the desired precatalyst, $[\text{C}(\text{pz})_4]\text{Ru}[\text{P}(\text{OCH}_2)_3\text{CEt}]\text{Ph}(\text{NCMe})[\text{BAR}'_4]$, is similar to the synthesis discussed in Chapter 3 for $\text{TpRu}[\text{P}(\text{OCH}_2)_2(\text{OCCH}_3)](\text{Ph})(\text{NCMe})$. The reaction of $(\eta^6\text{-}p\text{-cymene})$

cymene)Ru[(P(OCH₂)₃CEt]PhBr with NCMe leads to the displacement of *p*-cymene and coordination of NCMe to form the tris-acetonitrile species (NCMe)₃Ru[P(OCH₂)₃CEt]PhBr (**5**) (Scheme 5.3, Figure 5.13).

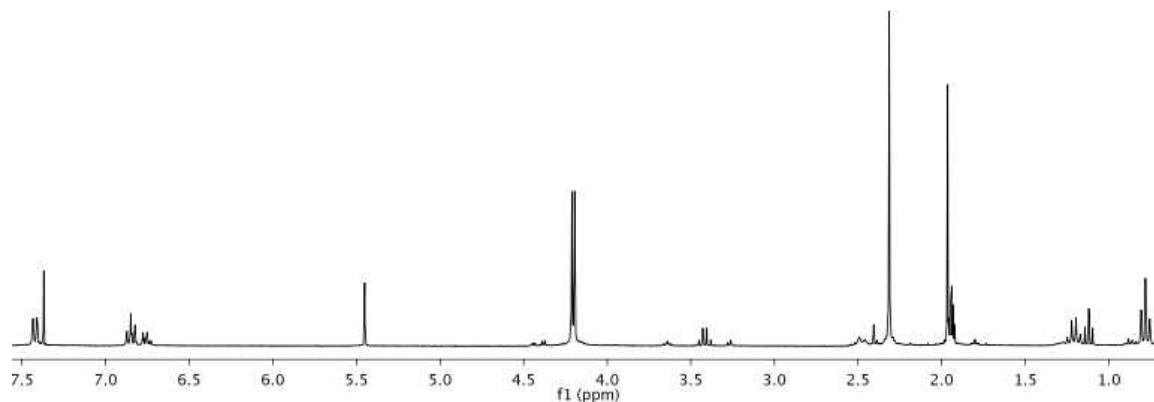


Figure 5.13. ¹H NMR spectrum of (NCMe)₃Ru[P(OCH₂)₃CEt]PhBr (**5**) in CD₃CN.

The reaction of complex **3** or complex **5** with C(pz)₄ in NCMe leads to the formation of a new species. Following the reaction of complex **3** and C(pz)₄ by ¹H NMR spectroscopy reveals the formation of free *p*-cymene; however, the formation of free benzene and disappearance of the phenyl resonances were also observed (Figure 5.14).

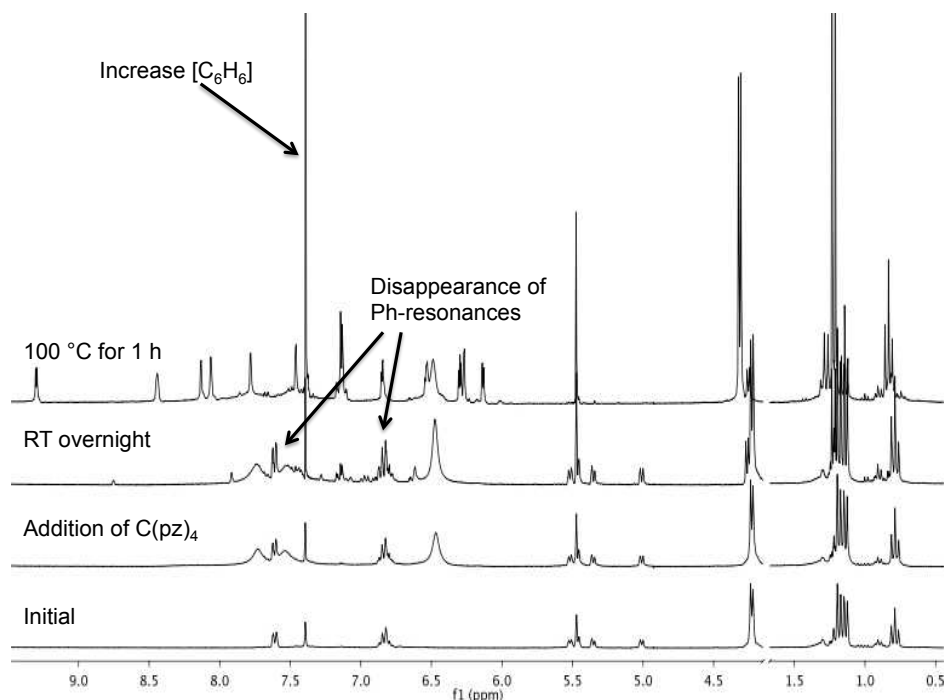
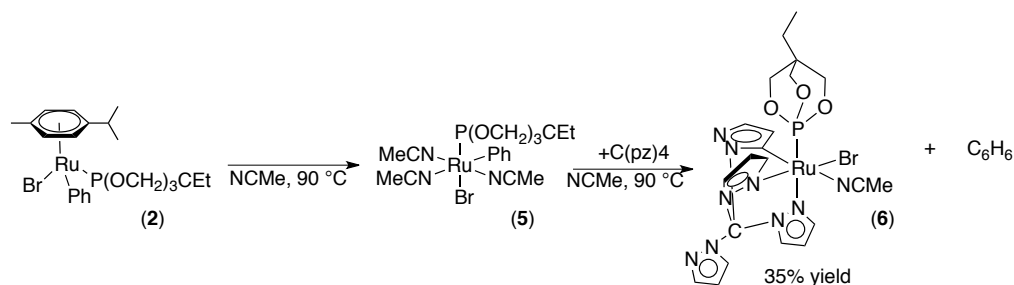


Figure 5.14. The reaction of (η^6 -*p*-cymene)Ru[P(OCH₂)₃CEt]PhBr (**2**) and C(pz)₄ in NCMe at 90 °C.

The formation of benzene upon reaction of **2** with C(pz)₄ is clear evidence of a C–H activation process. ¹H NMR of the Ru product revealed only 11 resonances for the C(pz)₄, yet 12 resonances were observed in ¹³C NMR spectrum, with one of the pyrazolyl resonances split into a doublet with a ²J_{CP} = 18 Hz. These data are consistent with C–H activation of the 5-position of the pyrazolyl ring leading to the displacement of free benzene and the formation of a (κ^3 -*N*,*C*⁵,*N*)C(pz)₄Ru[P(OCH₂)₃CEt](NCMe)Br (**6**) (Scheme 5.3, Figure 5.15, and Figure 5.16). There are at least two previous examples of C–H activation of the 5-position of the pyrazolyl ring. TpIr(PPh₃)(C₂H₄) and HC(pz)₃Ir(PPh₃)(C₂H₄)[BF₄] in the presence of PPh₃ in methylene chloride yield the

cyclometalated species, $(N,C^5,N)\text{TpIr}(\text{PPh}_3)_2\text{H}$ and $(N,C^5,N)\text{HC}(\text{pz})_3\text{Ir}(\text{PPh}_3)_2\text{H}[\text{BF}_4]$, respectively (Scheme 5.4).^{19,20}



Scheme 5.3. Synthesis of $(\kappa^3\text{-}N,C^5,N)\text{C}(\text{pz})_4\text{Ru}[\text{P}(\text{OCH}_2)_3\text{CEt}](\text{NCMe})\text{Br}$ (**6**).

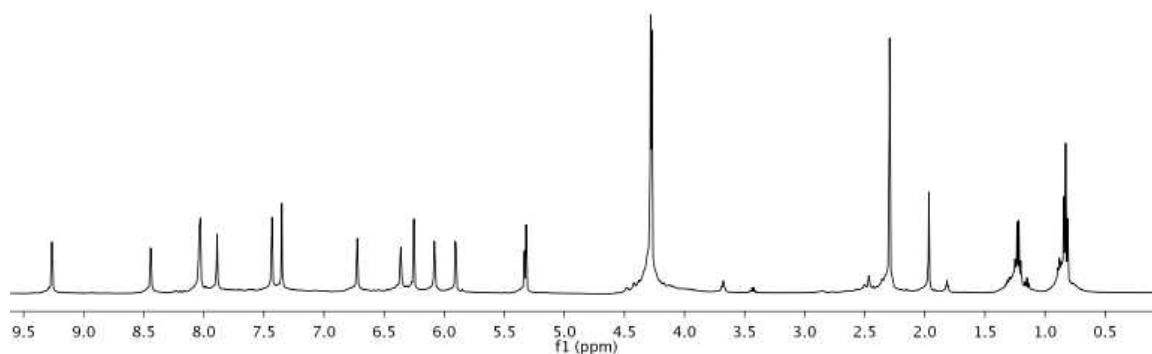


Figure 5.15. ^1H NMR spectrum of $(\kappa^3\text{-}N,C^5,N)\text{C}(\text{pz})_4\text{Ru}[\text{P}(\text{OCH}_2)_3\text{CEt}](\text{NCMe})\text{Br}$ (**6**) in CD_2Cl_2 .

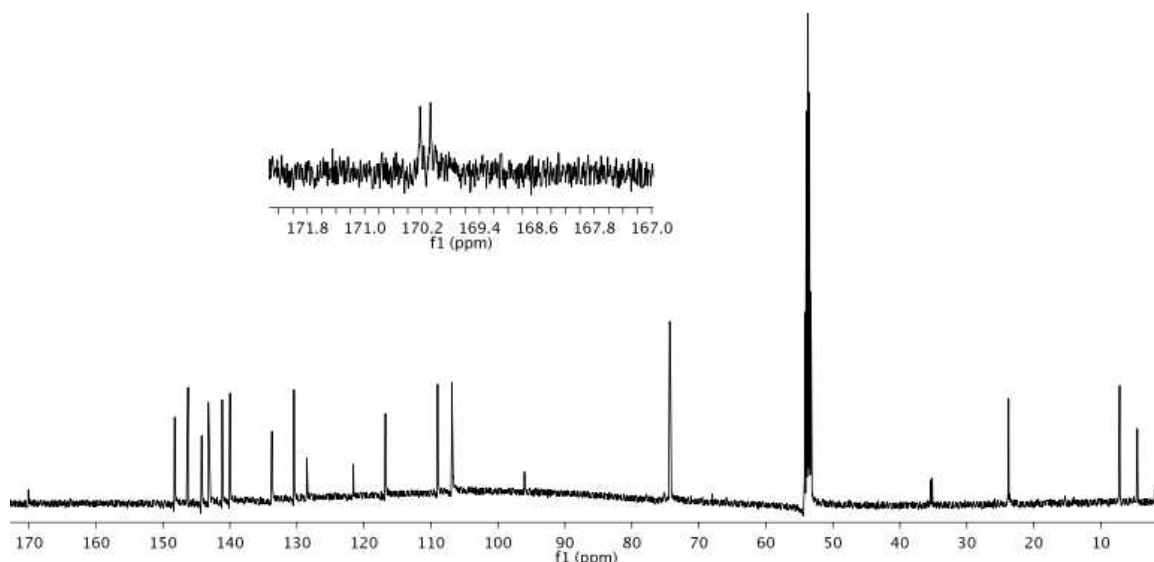
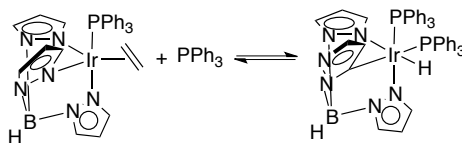


Figure 5.16. ^{13}C NMR spectrum of $(\kappa^3\text{-}N, C^5, N)\text{C}(\text{pz})_4\text{Ru}[\text{P}(\text{OCH}_2)_3\text{CEt}](\text{NCMe})\text{Br}$ (**6**) in CD_2Cl_2 .



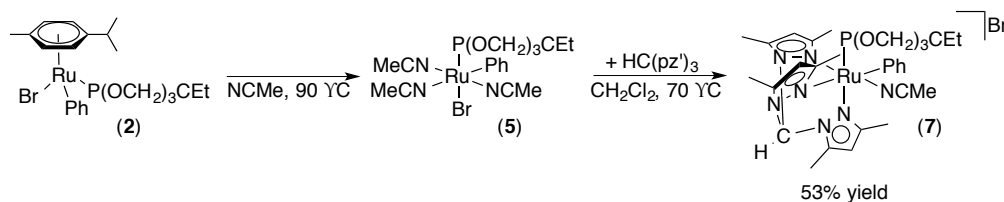
Scheme 5.4. C–H activation of 5-position of the Tp pyrazolyl ring in $\text{TpIr}(\text{PPh}_3)(\text{C}_2\text{H}_4)$.¹⁹

Attempts to replace the bromide ligand of **6** with a phenyl or a triflate ($\text{Ph}_2\text{Mg}[\text{THF}]_2$, PhMgBr , PhLi , MeLi , AgOTf , TiOTf , and TMSOTf) under a variety of reaction conditions did not proceed cleanly or, in some cases, only starting material was recovered. Therefore, another synthetic route or an analogous complex of another neutral tris(pyrazoly)alkane was sought.

5.2.4. Synthesis of $\{[\text{HC}(\text{pz}')_3]\text{Ru}[\text{P}(\text{OCH}_2)_3\text{CEt}]\text{Ph}(\text{NCMe})\}[\text{Y}]$ Complexes ($\text{pz}' = 3,5\text{-dimethyl-pyrazolyl}$ and $\text{Y} = \text{Br}, \text{BAr}'_4, \text{BF}_4$ or PF_6)

Due to the undesirable C–H activation of the 5-position on the pyrazolyl ring upon the reaction of **2** with $\text{C}(\text{pz})_4$, we targeted replacement of the hydrogen in the 5-

position with a methyl group. Therefore, reactions were run using $\text{HC}(\text{pz}')_3$ ($\text{pz}' = 3,5$ -dimethyl-pyrazolyl) as a neutral tridentate ligand. As stated above, refluxing complex **2** in NCMe yields $(\text{NCMe})_3\text{Ru}[\text{P}(\text{OCH}_2)_3\text{CEt}]\text{PhBr}$ (**5**). Heating complex **5** in methylene chloride in a sealed pressure tube with 1.2 equivalent of $\text{HC}(\text{pz}')_3$ for 1.5 hours leads to clean formation of $\{[\text{HC}(\text{pz}')_3]\text{Ru}[\text{P}(\text{OCH}_2)_3\text{CEt}]\text{Ph}(\text{NCMe})\}[\text{Br}]$ (**7**). Heating complex **7** in deuterated acetonitrile results in the disappearance of the resonance at 1.41 ppm, which is assigned as coordinated NCMe. The product can be purified by removal of methylene chloride, washing the remaining solid with benzene, the solid was dissolved in methylene chloride and precipitating with pentane to yield a tan solid in 53% yield (Scheme 5.5, Figure 5.17, Figure 5.18).



Scheme 5.5. Synthesis of $\{[\text{HC}(\text{pz}')_3]\text{Ru}[\text{P}(\text{OCH}_2)_3\text{CEt}]\text{Ph}(\text{NCMe})\}[\text{Br}]$ (**7**).

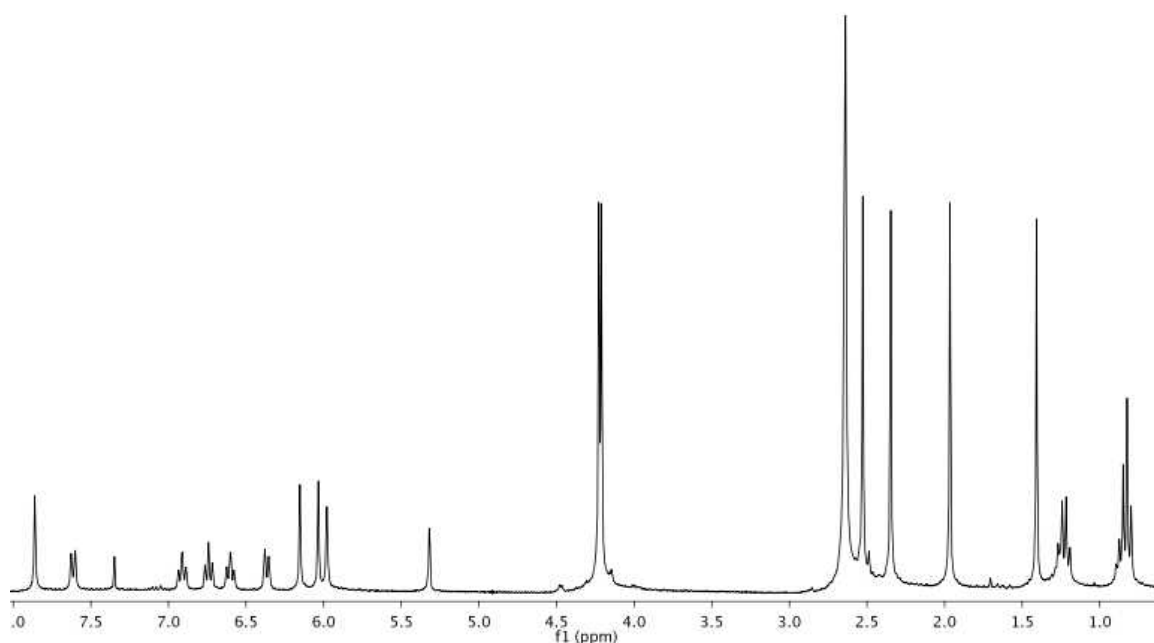


Figure 5.17. ^1H NMR spectrum of $\{[\text{HC}(\text{pz}')_3]\text{Ru}[\text{P}(\text{OCH}_2)_3\text{CEt}]\text{Ph}(\text{NCMe})\}[\text{Br}]$ (**7**) in CD_2Cl_2 .

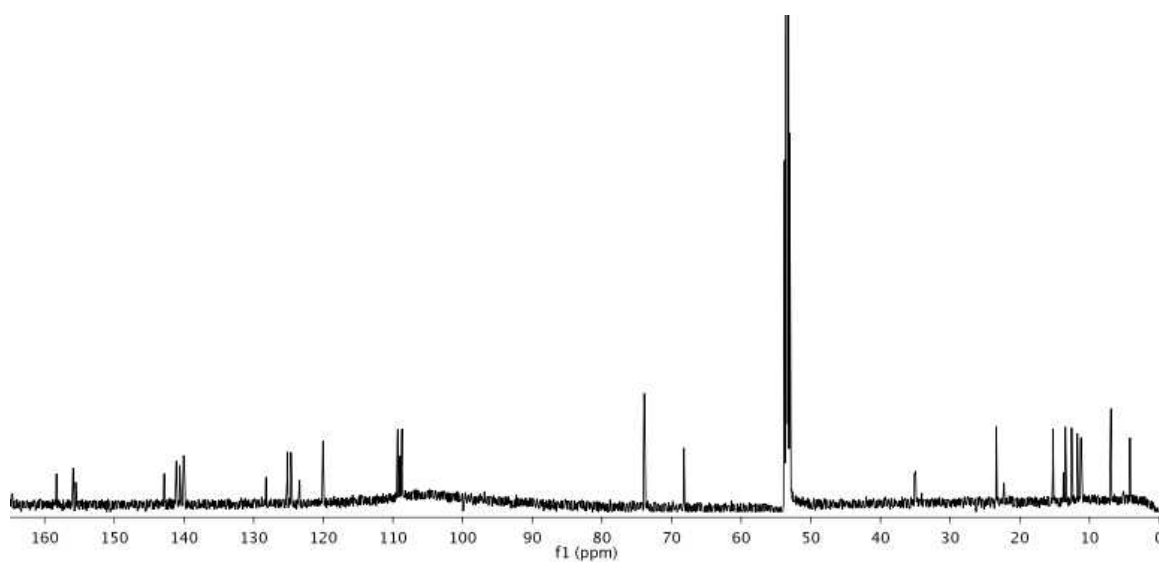
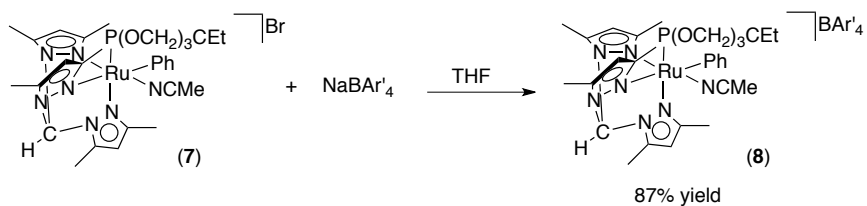


Figure 5.18. ^{13}C NMR spectrum for $\{[\text{HC}(\text{pz}')_3]\text{Ru}[\text{P}(\text{OCH}_2)_3\text{CEt}]\text{Ph}(\text{NCMe})\}[\text{Br}]$ (**7**) in CD_2Cl_2 .

The lack of solubility of complex **7** in benzene inhibited catalytic olefin hydroarylation. Therefore, the bromide counter-ion was replaced using NaBAR'₄ to increase the complex's solubility in benzene. Complex **7** in the presence of 1 equivalent of NaBAR'₄ in THF results in clean conversion to {[HC(pz')₃]Ru[P(OCH₂)₃CET]Ph(NCMe)}[BAR'₄] (**8**) (Scheme 5.7, Figure 5.19, Figure 5.20). Complex **8** gives a Ru(III/II) E_{1/2} potential of 0.82 V vs NHE, which is close to the Ru(III/II) potential (1.02 V) of TpRu(CO)(NCMe)Ph and is approximately a 0.13 V positive shift compared to TpRu[P(OCH₂)₃CET]Ph(NCMe) (0.69 V vs NHE).¹² Although this is not as significant of a decrease in electron density as we expected (see above), this does provide a catalyst that is electronically identical to TpRu[P(pyr)₃]Ph(NCMe)¹⁰ but with a less sterically bulky two electron donor ligand (albeit, with a more bulky poly(pyrazolyl)ligand). Complex **8** demonstrated significantly increased solubility in benzene compared to complex **7**. Therefore, ethylene hydrophenylation was attempted at 90 °C with both 15 and 25 psi of ethylene. Unfortunately, no production of ethylbenzene or styrene was observed. During attempted catalysis, complex **8** was observed to oil out of solution. Increasing the temperature to 105 °C with 25 psi of ethylene or propylene yielded minimal TON of ethylbenzene and no *n*-propylbenzene or cumene, respectively.

Similar to the reaction with NaBAR'₄, the bromide counter-ion from complex **7** can be abstracted using NaBF₄ or NaPF₆ to yield {[HC(pz')₃]Ru[P(OCH₂)₃CET]Ph(NCMe)}[BF₄] and {[HC(pz')₃]Ru[P(OCH₂)₃CET]Ph(NCMe)}[PF₆], respectively (Scheme 5.7). However,

both complexes are insoluble in benzene. Therefore, the complexes could not be used for olefin hydrophenylation.



Scheme 5.6. Synthesis of {[HC(pz')₃]Ru[P(OCH₂)₃CEt]Ph(NCMe)}[BAR'₄] (**8**).

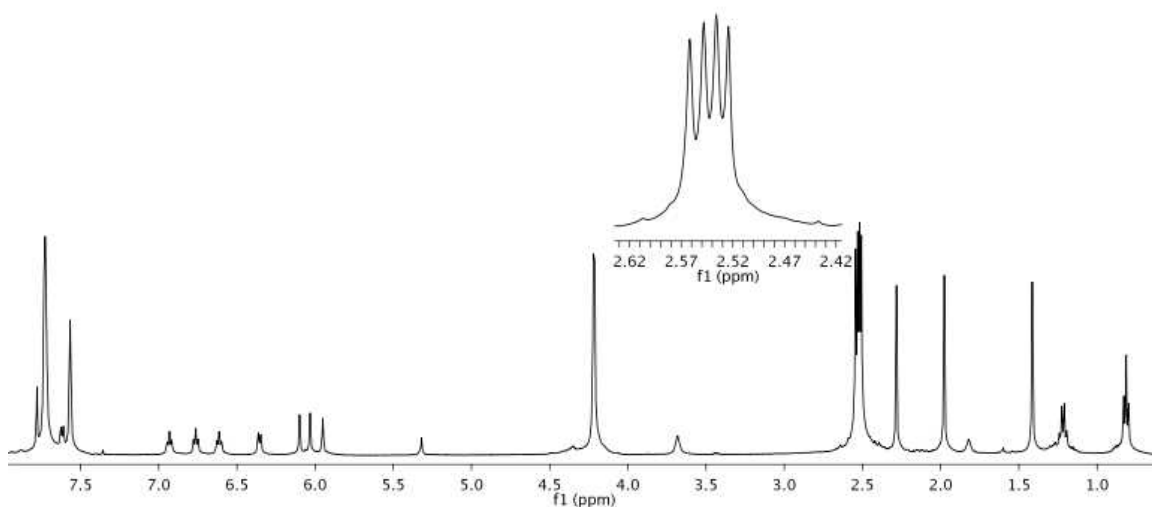


Figure 5.19. ¹H NMR spectrum of {[HC(pz')₃]Ru[P(OCH₂)₃CEt]Ph(NCMe)}[BAR'₄] (**8**) in CD₂Cl₂.

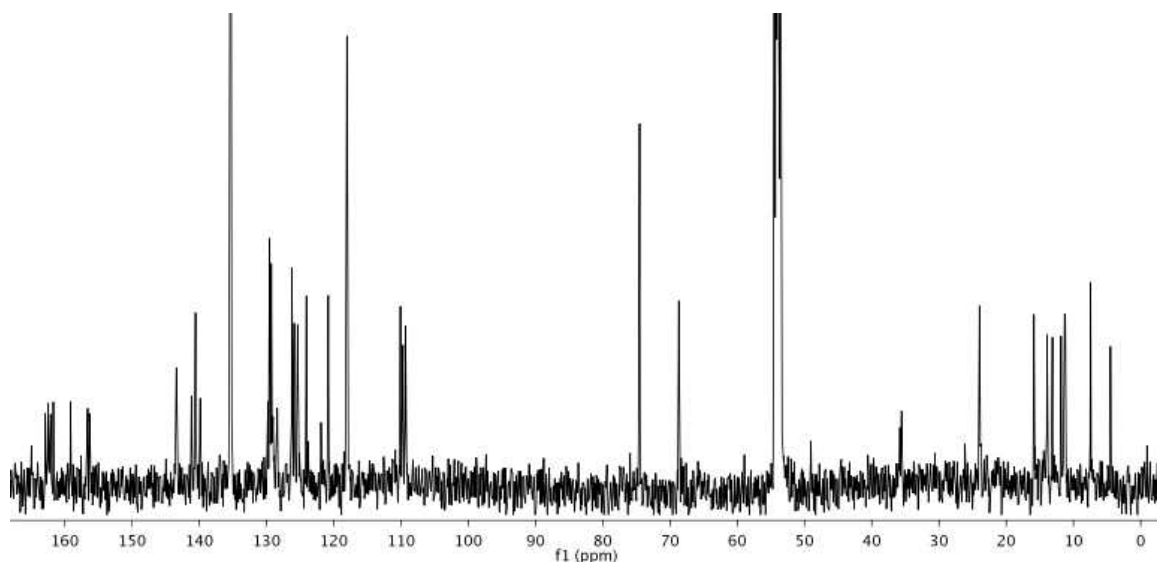


Figure 5.20. ^{13}C NMR spectrum of $\{[\text{HC}(\text{pz}')_3]\text{Ru}[\text{P}(\text{OCH}_2)_3\text{CEt}]\text{Ph}(\text{NCMe})\}[\text{BAr}'_4]$ (**8**) in CD_2Cl_2 .

5.2.5. Attempted Synthesis of $\{[\text{C}(\text{pz})_4]\text{Ru}[\text{P}(\text{OCH}_2)_3\text{CEt}]\text{Ph}(\text{NCMe})\}[\text{BAr}'_4]$

As stated above, the 5-position on the $\text{C}(\text{pz})_4$ pyrazolyl rings is susceptible to intramolecular C–H activation. Therefore, an alternative synthetic route was attempted by adding the $\text{C}(\text{pz})_4$ ligand to a Ru complex which lacks an alkyl group. Refluxing $\text{C}(\text{pz})_4$ in the presence of $\text{RuCl}_2(\text{PPh}_3)_4$ in toluene overnight lead to the formation of $[\text{C}(\text{pz})_4]\text{Ru}(\text{PPh}_3)\text{Cl}_2$ (**9**). Complex **9** precipitates out of toluene and to give a green-yellow solid in 79% yield. The presence of mirror symmetry is evident by the presence of nine $\text{C}(\text{pz})_4$ resonances in the downfield region with an integration of 1:1:1:1:1:2:2:1:2 (Scheme 5.7, Figure 5.21, Figure 5.22).



Scheme 5.7. Synthesis of $[\text{C}(\text{pz})_4]\text{Ru}(\text{PPh}_3)\text{Cl}_2$ (**9**).

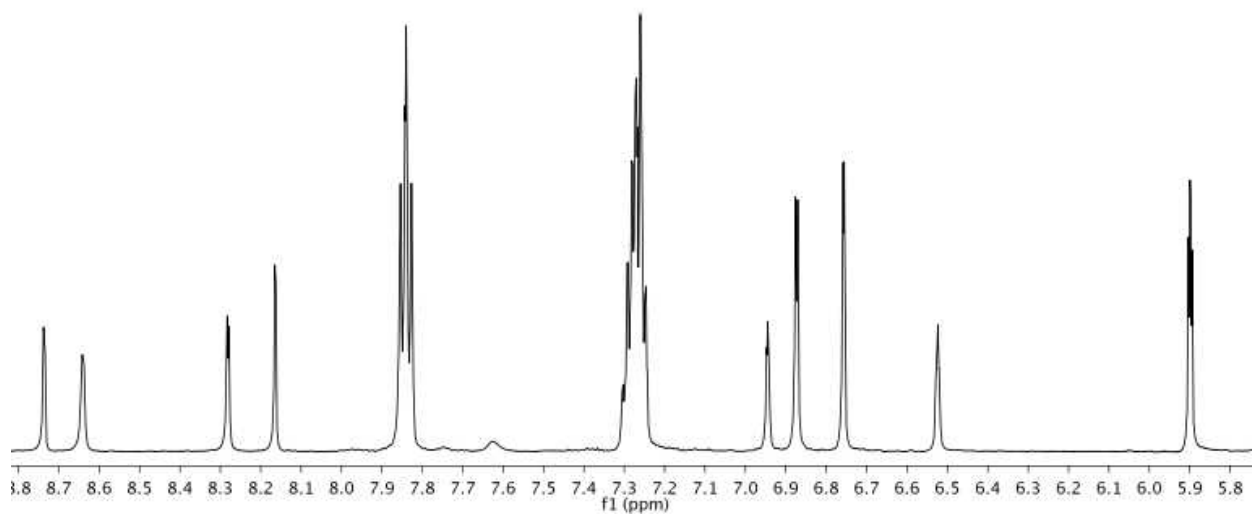


Figure 5.21. ^1H NMR spectrum of $[\text{C}(\text{pz})_4]\text{Ru}(\text{PPh}_3)\text{Cl}_2$ (**9**) in CDCl_3 .

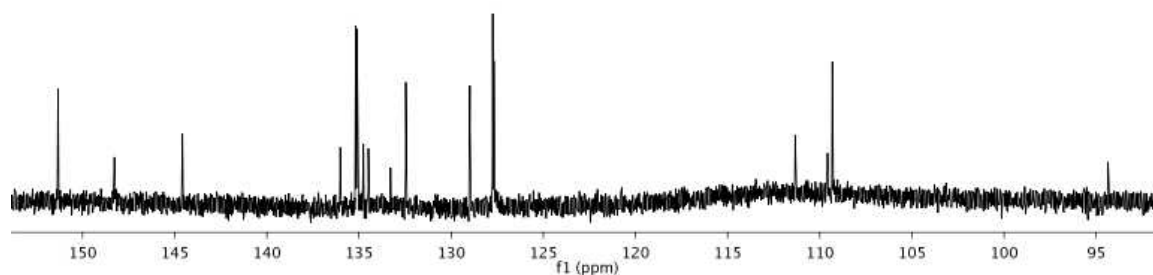
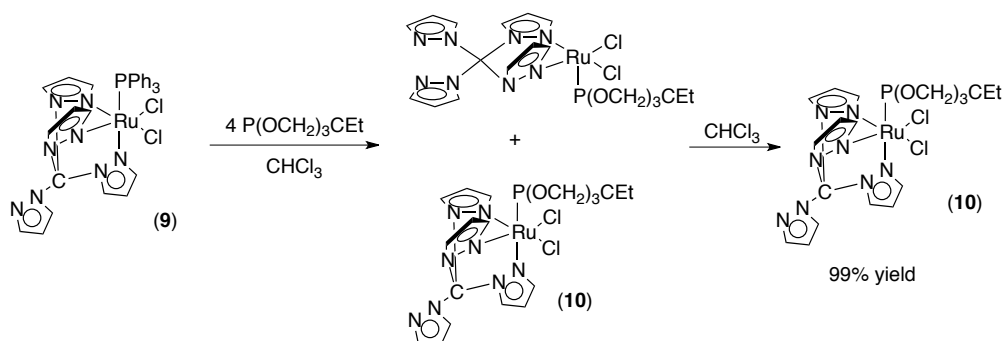


Figure 5.22. ^{13}C NMR spectrum of $[\text{C}(\text{pz})_4]\text{Ru}(\text{PPh}_3)\text{Cl}_2$ (**9**) in CDCl_3 .

The PPh_3 ligand can then be displaced by refluxing **9** in chloroform in the presence of excess $\text{P}(\text{OCH}_2)_3\text{CEt}$. Initially, both $[\kappa^2\text{-C}(\text{pz})_4]\text{Ru}[\text{P}(\text{OCH}_2)_3\text{CEt}]\text{Cl}_2$ and $[\kappa^3\text{-C}(\text{pz})_4]\text{Ru}[\text{P}(\text{OCH}_2)_3\text{CEt}]\text{Cl}_2$ species are observed. The addition of hexanes to the reaction mixture, isolation of the precipitate, followed by multiple rinses with hexanes to remove any free PPh_3 , and subsequent reconstitution in fresh chloroform and refluxing overnight yields $[\kappa^3\text{-C}(\text{pz})_4]\text{Ru}[\text{P}(\text{OCH}_2)_3\text{CEt}]\text{Cl}_2$ (**10**) as a yellow solid. The coordination of the $\text{P}(\text{OCH}_2)_3\text{CEt}$ is apparent the disappearance of the resonance for coordinated PPh_3 at 52 ppm and the appearance of a downfield resonance at 128 ppm (^{31}P NMR). Additionally, a phosphite resonance in the ^1H NMR spectrum is observed as a doublet for the methylene hydrogens and a triplet and quartet for the ethyl tail of the ligand (Scheme 5.8, Figure 5.24, Figure 5.25).



Scheme 5.8. Synthesis of $[\kappa^2\text{-C}(\text{pz})_4]\text{Ru}[\text{P}(\text{OCH}_2)_3\text{CEt}]\text{Cl}_2$ and $[\kappa^3\text{-C}(\text{pz})_4]\text{Ru}[\text{P}(\text{OCH}_2)_3\text{CEt}]\text{Cl}_2$ (**10**).

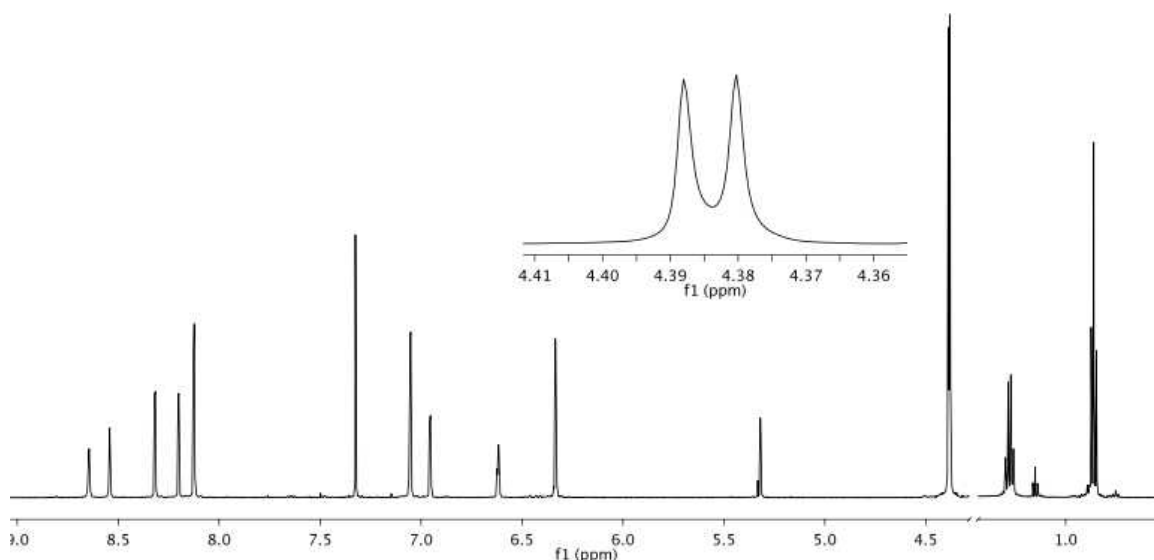


Figure 5.23. ^1H NMR spectrum of $[\text{C}(\text{pz})_4]\text{Ru}[\text{P}(\text{OCH}_2)_3\text{CEt}]\text{Cl}_2$ (**10**) in CD_2Cl_2 .

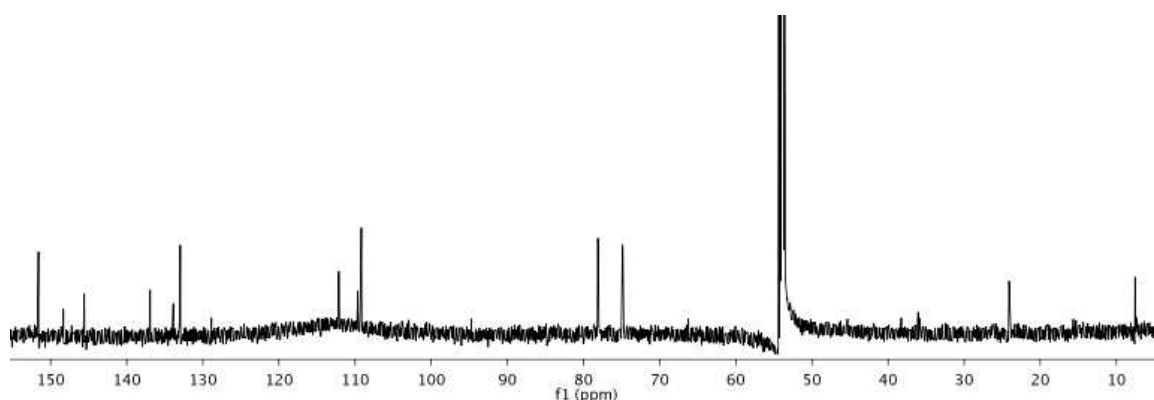
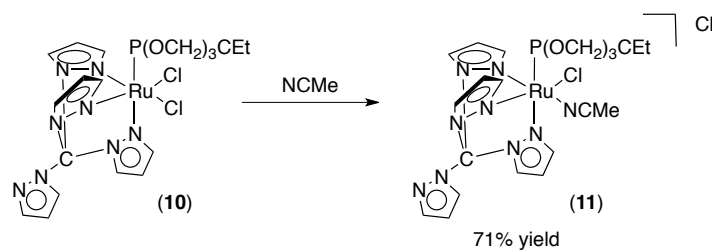


Figure 5.24. ^{13}C NMR spectrum of $[\text{C}(\text{pz})_4]\text{Ru}[\text{P}(\text{OCH}_2)_3\text{CEt}]\text{Cl}_2$ (**10**) in CD_2Cl_2 .

Refluxing complex **10** in acetonitrile overnight leads to conversion to the asymmetric $[\text{C}(\text{pz})_4]\text{Ru}[\text{P}(\text{OCH}_2)_3\text{CEt}]\text{Cl}(\text{NCMe})[\text{Cl}]$ (**11**) in approximately 71% yield. The coordination of NCMe is evident by a singlet at 2.59 ppm in the ^1H NMR spectrum. The ^1H NMR spectrum demonstrates that complex **11** is asymmetric since twelve $\text{C}(\text{pz})_4$ resonances are observed. The reaction leads to one predominate product; however, there

are some minor impurities, which are removed in the next step (Scheme 5.9, Figure 5.25, Figure 5.26).



Scheme 5.9. Synthesis of $\{[\text{C}(\text{pz})_4]\text{Ru}[\text{P}(\text{OCH}_2)_3\text{CEt}]\text{Cl}(\text{NCMe})\}[\text{Cl}]$ (**11**).

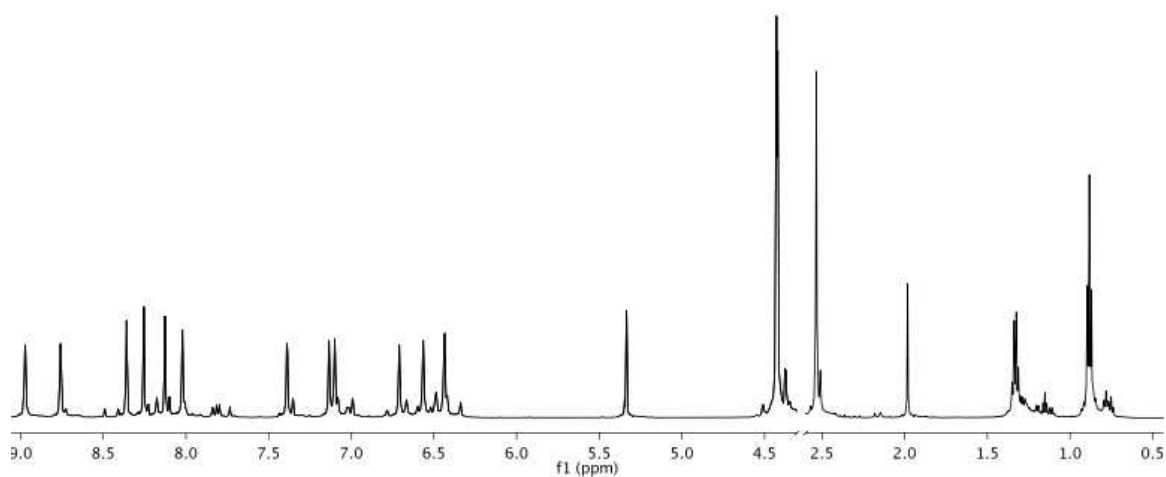


Figure 5.25. ^1H NMR spectrum of $\{[\text{C}(\text{pz})_4]\text{Ru}[\text{P}(\text{OCH}_2)_3\text{CEt}]\text{Cl}(\text{NCMe})\}[\text{Cl}]$ (**11**) in CD_2Cl_2 .

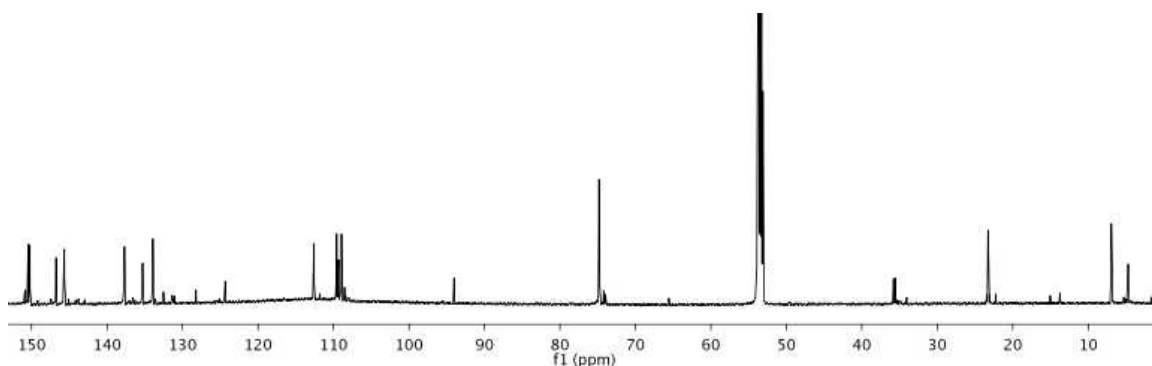
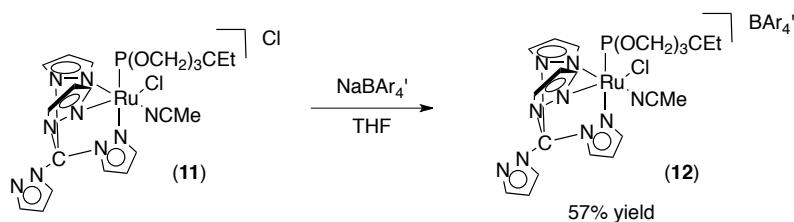


Figure 5.26. ^{13}C NMR spectrum of $\{[\text{C}(\text{pz})_4]\text{Ru}[\text{P}(\text{OCH}_2)_3\text{CEt}]\text{Cl}(\text{NCMe})\}[\text{Cl}]$ (**11**) in CD_2Cl_2 .

The reaction of NaBAR'_4 to a THF solution of complex **11** at room temperature, leads to the displacement of a chloride with BAR'_4 yielding $\{[\text{C}(\text{pz})_4]\text{Ru}[\text{P}(\text{OCH}_2)_3\text{CEt}]\text{Cl}(\text{NCMe})\}[\text{BAR}'_4]$ (**12**). The presence of the BAR'_4 is evident in the ^1H NMR spectrum by two singlets in the downfield region and a singlet in the ^{19}F NMR spectrum at -63 ppm. Complex **12** can be purified on neutral alumina by first washing the plug with diethyl ether to remove the impurities followed by 1:1 mixture of $\text{Et}_2\text{O}:\text{CH}_2\text{Cl}_2$ to give the purified product in 57% yield (Scheme 5.10, Figure 5.28, Figure 5.29). A single crystal of complex **12** was obtained by hexanes diffusion into a THF solution of complex **12** at $-30\text{ }^\circ\text{C}$ by Dr. Brandon Quillian (Figure 5.27, Table 5.2).



Scheme 5.10. Synthesis of $\{[\text{C}(\text{pz})_4]\text{Ru}[\text{P}(\text{OCH}_2)_3\text{CEt}]\text{Cl}(\text{NCMe})\}[\text{BAR}'_4]$ (**12**).

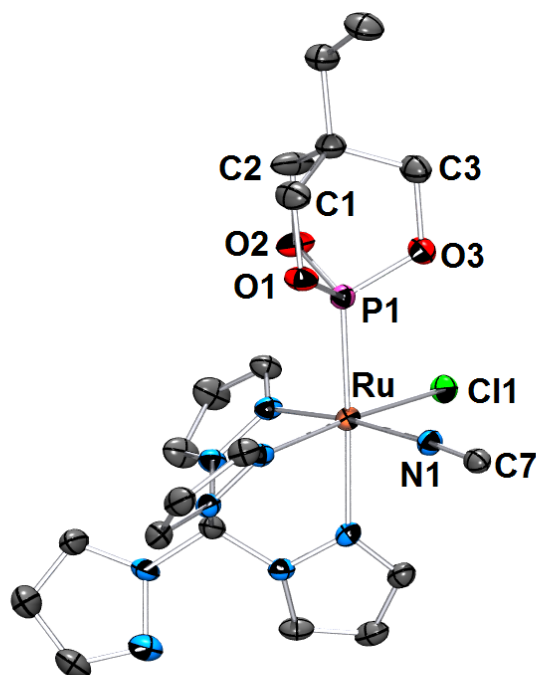


Figure 5.27. ORTEP of $\{[C(pz)_4]Ru[P(OCH_2)_3Cet]Cl(NCMe)\}[BAr'_4]$ (**12**) (35% probability with hydrogen atoms and BAr'_4 omitted.). Selected bond lengths (Å): Ru–P1, 2.2053(15); P–O1, 1.594(4); P–O2, 1.599(5); P–O3, 1.595(4); Ru–Cl1, 2.397(2); Ru–N1, 2.023(6). Selected bond angles (°): O3–P1–O2, 102.2(2); O1–P1–O2, 101.7(2); O1–P1–O3, 101.8(2); O1–P1–Ru, 115.12(15); O2–P1–Ru, 118.32(16); O3–P1–Ru, 115.35(17).

Table 5.2. Selected Crystallographic Data for $\{[C(pz)_4]Ru[P(OCH_2)_3Cet]Cl(NCMe)\}[BAr'_4]$ (**12**).

	complex 12 •2THF
empirical formula	$C_{61}H_{46}BClF_{24}N_9O_5PRu$
Fw	1619.37
cryst syst	monoclinic
space group	$P2_1/c$
a, Å	11.5204(2)
b, Å	35.9819(7)
c, Å	16.6646(3)
β , deg	99.818(1)
V, Å ³	6806.7(2)
Z	4
D _{calcd} , mg/m ³	1.580
cryst size (mm)	0.44 x 0.16 x 0.12
R1, wR2 ($I > 2\sigma(I)$)	0.0583, 0.1721
GOF	1.415

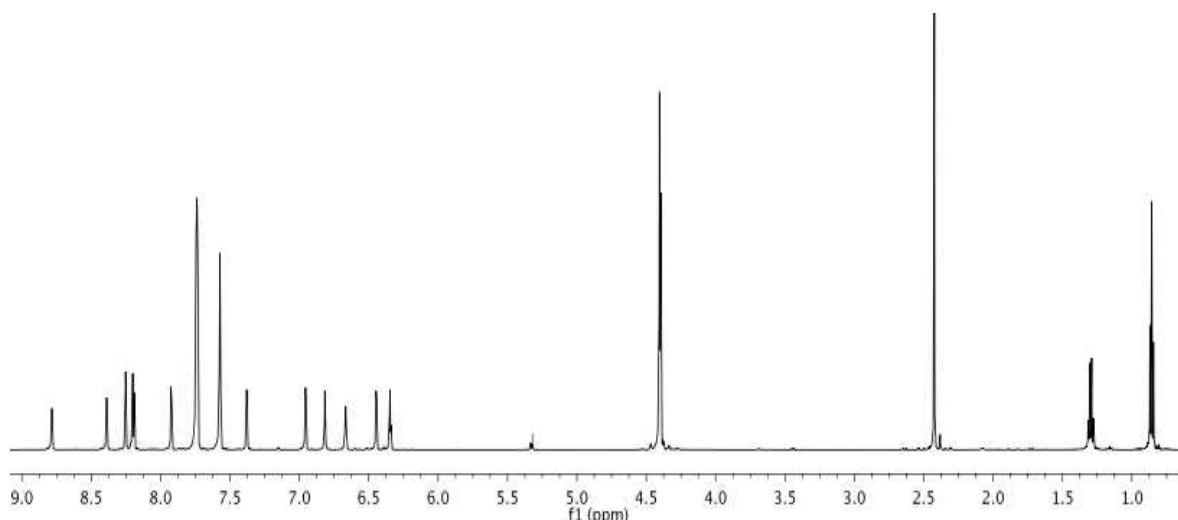


Figure 5.28. ^1H NMR spectrum of $\{[\text{C}(\text{pz})_4]\text{Ru}[\text{P}(\text{OCH}_2)_3\text{CEt}]\text{Cl}(\text{NCMe})\}[\text{BAr}'_4]$ (**12**) in CD_2Cl_2 .

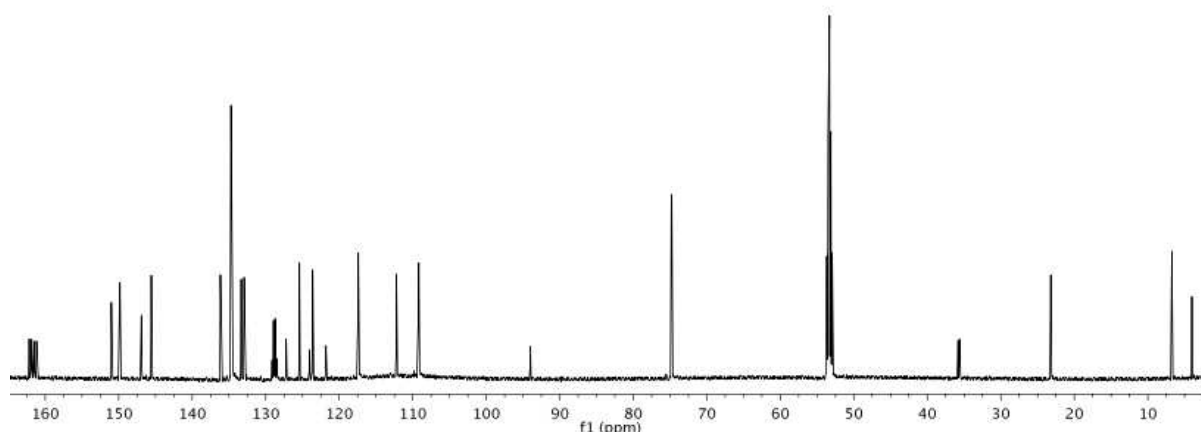


Figure 5.29. ^{13}C NMR spectrum of $\{[\text{C}(\text{pz})_4]\text{Ru}[\text{P}(\text{OCH}_2)_3\text{CEt}]\text{Cl}(\text{NCMe})\}[\text{BAr}'_4]$ (**12**) in CD_2Cl_2 .

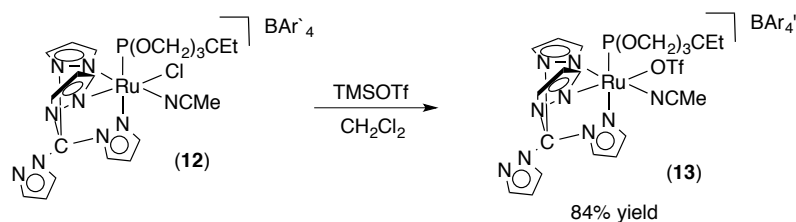
Direct alkylation of complex **12** was attempted with a range of reagents, temperatures and solvents (Table 5.3). However, all attempts led to no reaction or decomposition. Therefore, due to the better leaving ability of a triflate group, the chloride was replaced with a triflate group via a salt metathesis reaction. The removal of the chloride proved to

be more difficult than expected. Multiple different triflate reagents were tested, and the only one that proved to be successful was TMSOTf in methylene chloride. The reaction of **12** and TMSOTf must be heated overnight at 100 °C to yield $\{[C(pz)_4]Ru[P(OCH_2)_3CEt](OTf)(NCMe)\}[BAR'_4]$ (**13**) in an 84% isolated yield (Scheme 5.11, Figure 5.30, Figure 5.31). The coordination of triflate is evident by the singlet in the ^{19}F NMR spectrum at -79 ppm. Additionally, even in the presence of excess TMSOTf at high temperatures, the NCMe ligand appears to be tightly bound since an asymmetric complex was still observed with 12 $C(pz)_4$ resonances and a coordinated NCMe resonance in the 1H NMR spectrum.

Table 5.3. Attempted alkylation of $\{[C(pz)_4]Ru[P(OCH_2)_3CEt]Cl(NCMe)\}[BAR'_4]$ (**12**).

Reagent	Solvent	Temperature (°C)	Result
1 Me ₂ Mg	THF	-78 → RT	Decomposition
2 Me ₂ Mg	THF	-78 → RT	Decomposition
1.05 MeMgBr	THF	-78 → 0 → RT	No Reaction
1.05 PhMgBr	THF	-78 → 0 → RT	No Reaction
1.05 MeLi	THF	-78 → RT	Decomposition
1.05 PhLi	THF	-78 → RT	Decomposition
1.3 PhSn(n-Bu) ₃ 0.65 CuOTf	THF	Reflux	Multiple Products
1 Me ₂ Cu	THF	-78 → RT	No Reaction
0.75 Me ₃ Al	C ₆ D ₆	RT	Decomposition

*RT = room temperature



Scheme 5.11. Synthesis of $\{[C(pz)_4]Ru[P(OCH_2)_3CEt](OTf)(NCMe)\}[BAR'_4]$ (**13**).

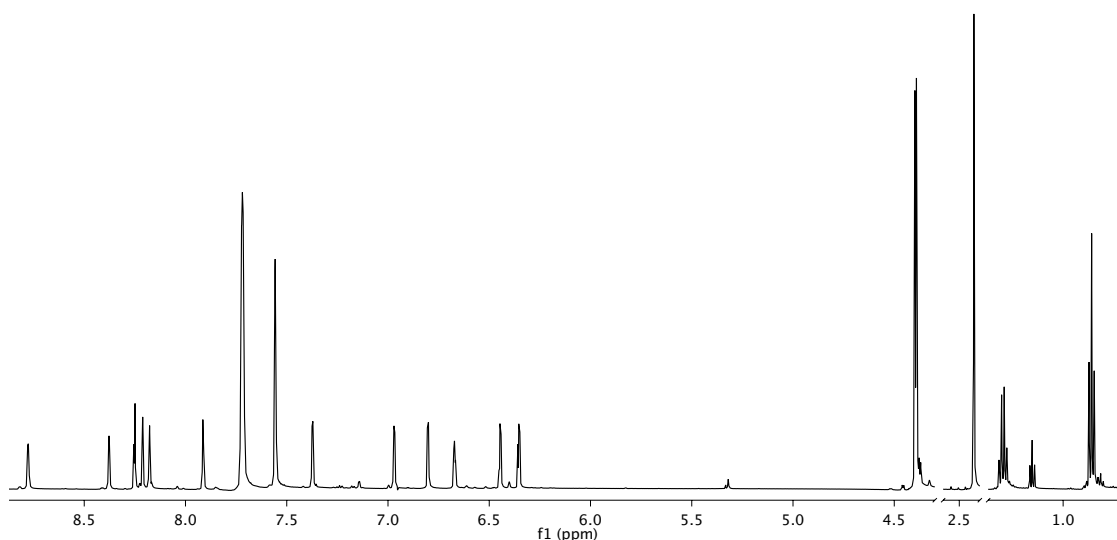


Figure 5.30. ^1H NMR spectrum of $\{[\text{C}(\text{pz})_4]\text{Ru}[\text{P}(\text{OCH}_2)_3\text{CEt}](\text{OTf})(\text{NCMe})\}[\text{BAr}'_4]$ (**13**) in CD_2Cl_2 .

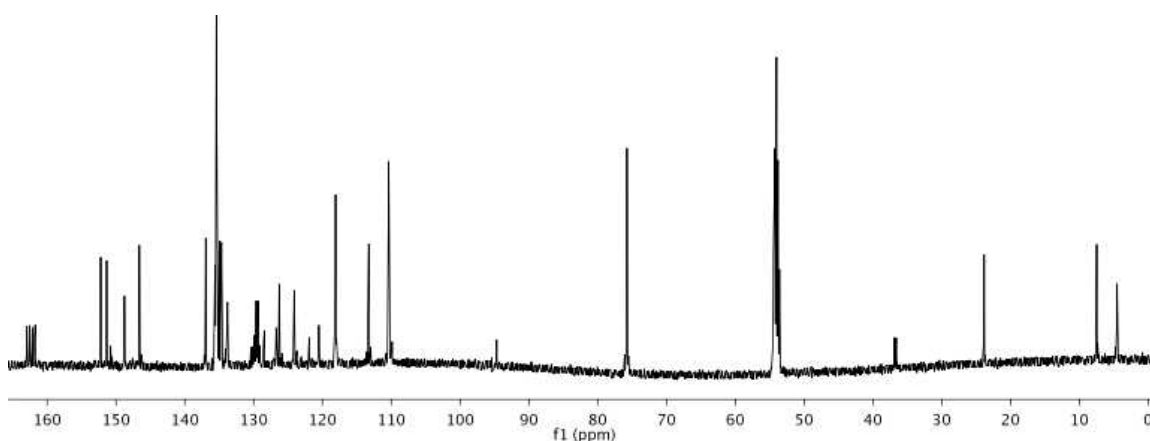


Figure 5.31. ^{13}C NMR spectrum of $\{[\text{C}(\text{pz})_4]\text{Ru}[\text{P}(\text{OCH}_2)_3\text{CEt}](\text{OTf})(\text{NCMe})\}[\text{BAr}'_4]$ (**13**) in CD_2Cl_2 .

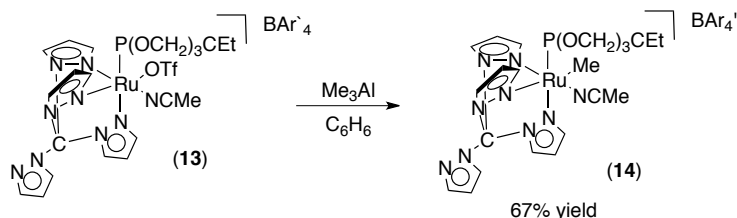
The phenylation or methylation of complex **13** was attempted with a range of reagents, temperatures and solvent (Table 5.4). Most attempts led to decomposition except in the case of PhLi (in Et_2O), and $\text{PhSn}(n\text{-Bu})_3$ with CuOTf in THF which yielded no reaction. However, methylation of complex **13** was accomplished with 1.5

equivalents of Me_3Al in benzene or diethyl ether to yield $\{[\text{C}(\text{pz})_4]\text{Ru}[\text{P}(\text{OCH}_2)_3\text{CEt}](\text{Me})(\text{NCMe})\}[\text{BAr}'_4]$ (**14**) in 67% yield. Complex **13** is sparingly soluble in benzene; however, methylation to give **14** improves solubility. The ^1H NMR spectrum of **14** is consistent with an asymmetric species with twelve resonances due to the $\text{C}(\text{pz})_4$ ligand. A doublet for the methyl group is observed at 0.79 ppm with a $^3J_{\text{HP}} = 1.7$ Hz. Additional evidence of a Ru–Me moiety was provided by treating complex **14** with one equivalent of $\text{HCl}\cdot\text{Et}_2\text{O}$, which gave an insoluble complex identified as $\{[\text{C}(\text{pz})_4]\text{Ru}[\text{P}(\text{OCH}_2)_3\text{CEt}]\text{Cl}(\text{NCMe})\}[\text{BAr}'_4]$ (**12**). Moreover the production of CH_4 was observed in ^1H NMR spectroscopy and GCMS.

Table 5.4. Attempted alkylation of $\{[\text{C}(\text{pz})_4]\text{Ru}[\text{P}(\text{OCH}_2)_3\text{CEt}](\text{OTf})(\text{NCMe})\}[\text{BAr}'_4]$ (**13**).

Reagent	Solvent	Temperature (°C)	Result
1.1 Me_2Mg	THF	-78 \rightarrow RT	Decomposition
1.1 Ph_2Mg	THF	-78 \rightarrow RT \rightarrow 50	Decomposition
2 Ph_2Mg	THF	RT	Decomposition
1.1 Ph_2Mg	C_6D_6	RT	Decomposition
1 PhMgBr	THF	-78 \rightarrow 0 \rightarrow RT	Decomposition
Excess PhMgBr	THF	-78 \rightarrow RT	Decomposition
1 PhLi	THF	-78 \rightarrow RT	Decomposition
1.3 $\text{PhSn}(\text{n-Bu})_3$ 0.65 CuOTf	THF	Reflux	No Reaction
1 Me_2Cu	THF	-78 \rightarrow RT	Multiple Products
1.05 PhLi	Et_2O	-78 \rightarrow RT	No Reaction
1 Ph_3Al	C_6H_6	RT	Decomposition
1 Me_3Al	C_6H_6	RT	Product
1.5 Me_3Al	Et_2O	-78 \rightarrow RT	Product

*RT = room temperature



Scheme 5.12. Synthesis of $\{[\text{C}(\text{pz})_4]\text{Ru}[\text{P}(\text{OCH}_2)_3\text{CEt}](\text{Me})(\text{NCMe})\}[\text{BAR}'_4]$ (**14**).

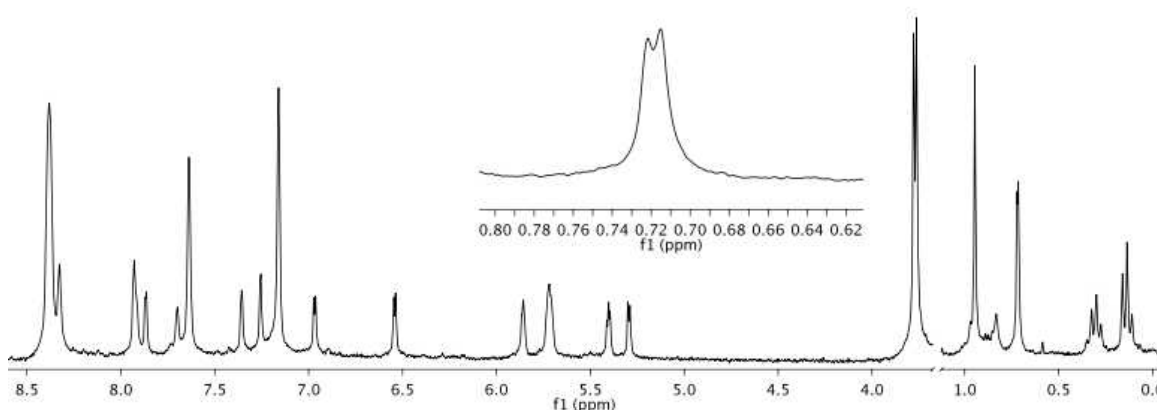
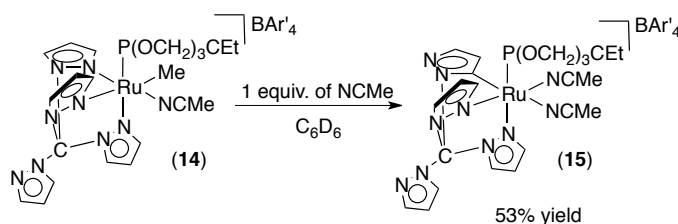


Figure 5.32. ^1H NMR spectrum of $\{[\text{C}(\text{pz})_4]\text{Ru}[\text{P}(\text{OCH}_2)_3\text{CEt}](\text{Me})(\text{NCMe})\}[\text{BAR}'_4]$ (**14**) in C_6D_6 .

Heating $\text{TpRu}(\text{CO})(\text{NCMe})\text{Me}$ in benzene results in C–H activation to yield methane and $\text{TpRu}(\text{CO})(\text{NCMe})\text{Ph}$.^{13,14} Unfortunately, heating complex **14** in benzene at 90 °C did not result in benzene C–H activation. Due to lack of solubility, the complex oiled out of solution, and analysis of the oil did not show the phenylated complex. The same reaction was then attempted with a small amount of added NCMe, since it has been shown with $\text{TpRu}(\text{CO})(\text{NCMe})\text{Me}$ that small amounts of NCMe does eliminate decomposition and increase the yield of the phenylated complex. When complex **14** is placed in benzene with one or more equivalents of NCMe conversion to a new product is observed. Unfortunately, intramolecular C–H activation of the 5-position of the

pyrazolyl ring occurs with release of CH_4 to yield $\{[(N,C^5,N)\text{C}(\text{pz})_4\text{Ru}[\text{P}(\text{OCH}_2)_3\text{CEt}[(\text{NCMe})_2][\text{BAr}'_4]]\}$ (**15**) (Scheme 5.13, Figure 5.33, Figure 5.34). The ^1H NMR spectrum in benzene shows two inequivalent NCMe groups, which indicates that one NCMe is *trans* to carbon-bound pyrazolyl ring while the other NCMe is *trans* to an *N*-bound pyrazolyl ring. Only eleven resonances due to the pyrazolyl hydrogens are observed. However, the ^{13}C NMR spectrum displays twelve peaks for the pyrazolyl rings with one of them resonating as a doublet with a $^3J_{\text{CP}} = 19.6$ Hz at 164.9 ppm. Ethylene hydrophenylation was attempted with complex **14** and complex **15**, but due to poor solubility and poor stability upon heating in benzene there was no evidence for the production of ethylbenzene or styrene.



Scheme 5.13. Synthesis of $\{[(N,C^5,N)\text{C}(\text{pz})_4\text{Ru}[\text{P}(\text{OCH}_2)_3\text{CEt}[(\text{NCMe})_2][\text{BAr}'_4]]\}$ (**15**).

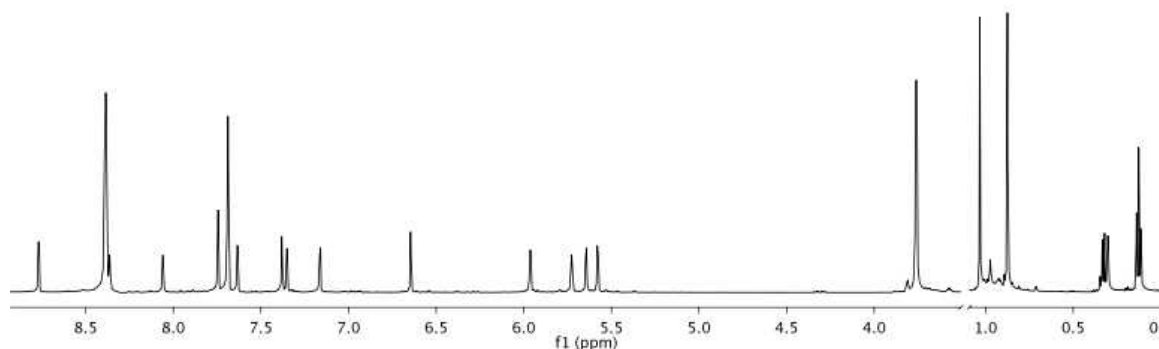


Figure 5.33. ^1H NMR spectrum of $\{[(N,C^5,N)\text{C}(\text{pz})_4\text{Ru}[\text{P}(\text{OCH}_2)_3\text{CEt}[(\text{NCMe})_2][\text{BAr}'_4]]\}$ (**15**) in C_6D_6 .

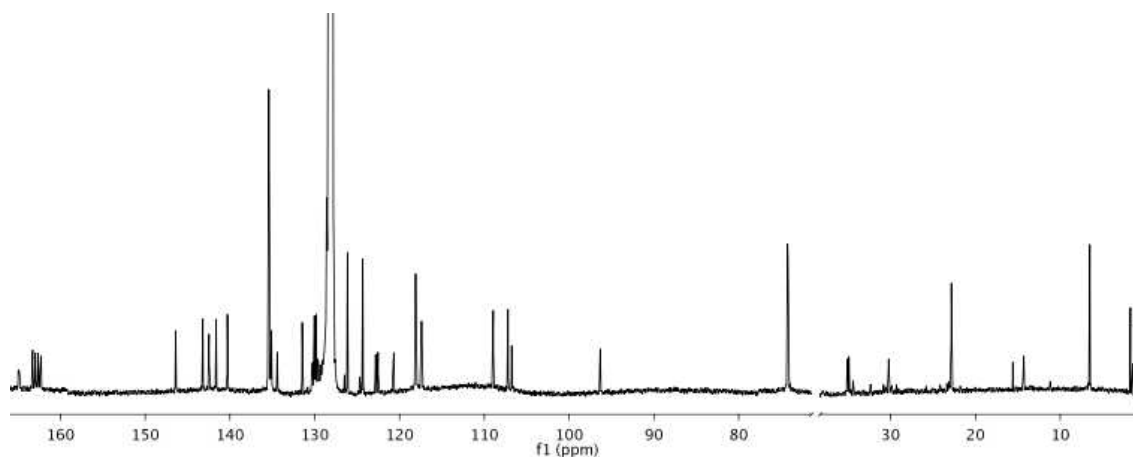


Figure 5.34. ^{13}C NMR spectrum of $\{(N,C^5,N)\text{C}(\text{pz})_4\}\text{Ru}[\text{P}(\text{OCH}_2)_3\text{Cet}[(\text{NCMe})_2]\text{[BAR}'_4]\text{ (15)}$ in C_6D_6 .

5.3. Conclusions

A variety of Ru(II) complexes with neutral 6-electron donor ligands [e.g., (η^6 -*p*-cymene, $\text{C}(\text{pz})_4$, and $\text{HC}(\text{pz}')_3$] were synthesized and characterized. These complexes were tested for olefin hydroarylation and were either unsuccessful or produced only minimal amounts of alkyl arenes. Additionally, it was found that Ru(II) complexes containing the $\text{C}(\text{pz})_4$ ligand are susceptible to intramolecular C–H activation of the 5-position on one of the pyrazolyl rings to produce an anionic 6-electron donor as observed in the formation of $\{(N,C^5,N)\text{C}(\text{pz})_4\}\text{Ru}[\text{P}(\text{OCH}_2)_3\text{Cet}](\text{NCMe})_2\text{[BAR}'_4]$ from $\{\text{C}(\text{pz})_4\}\text{Ru}[\text{P}(\text{OCH}_2)_3\text{Cet}](\text{Me})(\text{NCMe})\text{[BAR}'_4]$ with the release of methane in C_6H_6 . Using cyclic voltammetry, it was found that replacement of the anionic Tp ligand with a neutral tris(pyrazolyl)alkane ligand in the case of $\{\text{HC}(\text{pz}')_3\}\text{Ru}[\text{P}(\text{OCH}_2)_3\text{Cet}]\text{Ph}(\text{NCMe})\text{[BAR}'_4]$ yields a less electron rich metal center than $\text{TpRu}[\text{P}(\text{OCH}_2)_3\text{Cet}]\text{Ph}(\text{NCMe})$.

5.4. Experimental Section

General Methods. Unless otherwise noted, all synthetic procedures were performed under anaerobic conditions in a nitrogen-filled glovebox or by using standard Schlenk techniques. Glovebox purity was maintained by periodic nitrogen purges and was monitored by an oxygen analyzer [$\text{O}_2(\text{g}) < 15$ ppm for all reactions]. Tetrahydrofuran was dried by distillation from sodium/benzophenone. Pentane was distilled over P_2O_5 . Acetonitrile and diethyl ether were dried by distillation from CaH_2 . Hexanes, benzene and methylene chloride were purified by passage through a column of activated alumina. Benzene- d_6 , acetonitrile- d_3 , methylene chloride- d_2 and chloroform- d_1 were stored under a N_2 atmosphere over 4Å molecular sieves. ^1H NMR spectra were recorded on a Varian Mercury Plus 300 MHz Spectrometer, a Varian Inova 500 MHz Spectrometer, or a Bruker Avance DRX 600 MHz spectrometer and ^{13}C NMR spectra were recorded on a Varian Inova 500 MHz Spectrometer (operating frequency 125 MHz), a Bruker Avance DRX 600 MHz spectrometer (operating frequency 201 MHz). All ^1H and ^{13}C NMR spectra are referenced against residual proton signals (^1H NMR) or the ^{13}C resonances of the deuterated solvent (^{13}C NMR). ^{31}P NMR spectra were obtained on a Varian 300 MHz (operating frequency 121 MHz) spectrometer and referenced against an external standard of H_3PO_4 ($\delta = 0$ ppm). ^{19}F NMR spectra were obtained on a Varian 300 MHz (operating frequency 282 MHz) spectrometer and referenced against an external standard of hexafluorobenzene ($\delta = -164.9$ ppm).

Electrochemical experiments were performed under a nitrogen atmosphere using a BAS Epsilon Potentiostat. Cyclic voltammograms were recorded in NCCH_3 using a

standard three electrode cell from -1700 to 1700 mV at 100 mV/s with a glassy carbon working electrode and tetrabutylammonium hexafluorophosphate as electrolyte. All potentials are reported versus NHE (normal hydrogen electrode) using ferrocene as the internal standard. High resolution mass spectra were acquired in ESI mode, from samples dissolved in a 3:1 acetonitrile/water solution containing sodium trifluoroacetate (NaTFA). Mass spectra are reported for M^+ for monocationic complexes, or for $[M+H^+]$ or $[M+Na^+]$ for neutral complexes, using $[Na(NaTFA)_x]^+$ clusters as an internal standard. In all cases, observed isotopic envelopes were consistent with the molecular composition reported. For organic products, the monoisotopic ion is reported; for complexes, the major peaks in the isotopic envelope are reported. Spectra were collected on either a Bruker BioTOF-Q, a PerkinElmer Axion2 TOF, a Shimadzu IT-TOF, a Bruker MaXis Impact, an Agilent 6230 TOF, or a Waters Xevo G2Qtof. Elemental Analysis was performed by Atlantic Microlabs, Inc. Ethylene and propylene were used as received. The preparation, isolation and characterization of $[(\eta^6\text{-}p\text{-cymene})Ru(Br)(\mu\text{-}Br)]_2$ ²¹, $NaBAr'_4$ ²², $Ph_2Mg[THF]_2$ ²³ and $HC(pz')_3$ ²⁴ have been previously reported. $P(OCH_2)_3CEt$ was obtained from a commercial source and purified by dissolution in hexanes and filtration through Celite. The filtrate was concentrated to dryness to yield a white solid. All other reagents were used as purchased from commercial sources.

$(\eta^6\text{-}p\text{-cymene})Ru[P(OCH_2)_3CEt]Br_2$ (1). The binuclear complex $[(\eta^6\text{-}p\text{-cymene})Ru(Br)(\mu\text{-}Br)]_2$ (2.726 g, 3.450 mmol) and $P(OCH_2)_3CEt$ (1.4111 g, 8.692 mmol) were combined in a 1 L round bottom flask with 400 mL of methylene chloride. The reaction mixture was stirred at room temperature for 2 h. The volume of the solution

was reduced *in vacuo* to ~50 mL. Hexanes were added to yield a reddish-orange precipitate. The solid was collected by filtration through a fine porosity frit and dried *in vacuo* to yield a reddish-orange solid (3.7293 g, 97%). ^1H NMR (600 MHz, CDCl_3) δ 5.62 (d, 2H, $^3J_{\text{HH}} = 6$ Hz, Cy- C_{Ar}), 5.49 (d, 2H, $^3J_{\text{HH}} = 6$ Hz, Cy- C_{Ar}), 4.36 (d, 2H, $^3J_{\text{HH}} = 5$ Hz, $\text{P}(\text{OCH}_2)_3\text{CCH}_2\text{CH}_3$), 3.00 (sept, 1H, Cy- $\text{CH}(\text{CH}_3)_2$), 2.28 (s, 3H, Cy- CH_3), 1.26 (q, $^3J_{\text{HH}} = 8$ Hz, $\text{P}(\text{OCH}_2)_3\text{CCH}_2\text{CH}_3$), 1.22 (d, $^3J_{\text{HH}} = 7$ Hz, 6H, Cy- $\text{CH}(\text{CH}_3)_2$), 0.83 (t, $^3J_{\text{HH}} = 8$ Hz, 3H, $\text{P}(\text{OCH}_2)_3\text{CCH}_2\text{CH}_3$). ^{13}C NMR (151 MHz, CDCl_3) δ 110.6, 103.8 (each a s, Cy- C_{Ar}), 89.9 (d, $^2J_{\text{CP}} = 8$ Hz, Cy- C_{Ar}), 89.1 (d, $^2J_{\text{CP}} = 6$ Hz, Cy- C_{Ar}), 75.7 (d, $J_{\text{HP}} = 8$ Hz, $\text{P}(\text{OCH}_2)_3\text{CCH}_2\text{CH}_3$), 36.0 (d, $J = 32$ Hz, $\text{P}(\text{OCH}_2)_3\text{CCH}_2\text{CH}_3$), 30.98 (s, Cy- $\text{CH}(\text{CH}_3)_2$), 23.4 (s, $\text{P}(\text{OCH}_2)_3\text{CCH}_2\text{CH}_3$), 22.3 (s), 19.3 (s), 7.3 (s, $\text{P}(\text{OCH}_2)_3\text{CCH}_2\text{CH}_3$). ^{31}P NMR (121 MHz, CDCl_3) δ 110.5. Anal. Calcd. for $\text{C}_{16}\text{H}_{25}\text{Br}_2\text{O}_3\text{PRu}$. C, 34.49; H, 4.53; Found C, 34.48; H, 4.57.



cymene) $\text{Ru}[\text{P}(\text{OCH}_2)_3\text{CEt}]\text{Br}_2$ (0.3551 g, 0.6373 mmol) was placed in 20 mL of THF in a round bottom flask yielding a heterogeneous mixture. $\text{Ph}_2\text{Mg}[\text{THF}]_2$ (0.1641 g, 0.5085 mmol) was dissolved in 20 mL of THF. The Ph_2Mg solution was added to the round bottom flask containing the Ru complex. The reaction was stirred at room temperature for 1 h, and the reaction slowly became bright yellow and homogeneous. The THF was removed *in vacuo* and 40 mL of benzene was added to the flask. The reaction was stirred for 15 minutes and then filtered through Celite. The benzene solution was eluted through $\frac{1}{2}$ inch of silica followed by THF washes. All solvent was removed, and ~5 mL of methylene chloride was added, followed by hexanes to induce precipitation. The

precipitate was collected on a fine porosity frit and dried *in vacuo* to yield a bright yellow solid (0.3362 g, 95% yield). ^1H NMR (600 MHz, CDCl_3) δ 7.66 – 7.60 (m, 2H, phenyl), 6.93 – 6.88 (m, 2H, phenyl), 6.88 – 6.83 (m, 1H, phenyl), 5.45 (dd, 1H, $^3J_{\text{HH}} = 6$ Hz, $^3J_{\text{HP}} = 1$ Hz, Cy- C_{Ar}), 5.44 (dd, 1H, $^3J_{\text{HH}} = 6$ Hz, $^3J_{\text{HP}} = 1$ Hz, Cy- C_{Ar}), 5.32 (dd, 1H, $^3J_{\text{HH}} = 6$ Hz, $^3J_{\text{HP}} = 1$ Hz, Cy- C_{Ar}), 4.98 (dd, 1H, $^3J_{\text{HH}} = 6$ Hz, $^3J_{\text{HP}} = 1$ Hz, Cy- C_{Ar}), 4.24 – 4.17 (m, 6H, $\text{P}(\text{OCH}_2)_3\text{CCH}_2\text{CH}_3$), 2.73 (sept, 1H, $^2J_{\text{HH}} = 7$ Hz, $(\text{CH}_3\text{C}_6\text{H}_4(\text{CH})(\text{CH}_3)_2$), 1.84 (s, 3H, $\text{C}_6\text{H}_4\text{-CH}_3$), 1.23 – 1.13 (overlapping m's, 8H, coincidental overlap of $\text{P}(\text{OCH}_2)_3\text{CCH}_2\text{CH}_3$ and $\text{C}_6\text{H}_4\text{-CH}(\text{CH}_3)_2$), 0.80 (t, 3H, $^3J_{\text{HH}} = 8$ Hz, $\text{P}(\text{OCH}_2)_3\text{CCH}_2\text{CH}_3$). ^{13}C NMR (151 MHz, CDCl_3) δ 154.2 (d, $^2J_{\text{CP}} = 30$ Hz, ipso of phenyl), 142.9 (d, $^3J_{\text{PC}} = 5$ Hz, phenyl), 126.6 (s, phenyl), 121.9 (s, phenyl), 117.4 (d, $^3J_{\text{PC}} = 5$ Hz, ipso of Cy- C_{Ar}), 109.8 (d, $^3J_{\text{PC}} = 5$ Hz, ipso of Cy- C_{Ar}), 93.6 (d, $^2J_{\text{CP}} = 4$ Hz, Cy- C_{Ar}), 91.0 (d, $^2J_{\text{CP}} = 10$ Hz, Cy- C_{Ar}), 88.6 (d, $^2J_{\text{CP}} = 3$ Hz, Cy- C_{Ar}), 88.3 (s, Cy- C_{Ar}), 74.9 (d, $^2J_{\text{CP}} = 8$ Hz, $\text{P}(\text{OCH}_2)_3\text{CCH}_2\text{CH}_3$), 35.6 (d, $^3J_{\text{CP}} = 32$ Hz, $\text{P}(\text{OCH}_2)_3\text{CCH}_2\text{CH}_3$), 31.2 (s, $\text{C}_6\text{H}_4\text{-CH}(\text{CH}_3)_2$), 23.6, 23.3, 22.2 (all s, representing Cy- $\text{CH}(\text{CH}_3)_2$ and $\text{P}(\text{OCH}_2)_3\text{CCH}_2\text{CH}_3$), 18.7 (s, Cy- CH_3), 7.3 (s, $\text{P}(\text{OCH}_2)_3\text{CCH}_2\text{CH}_3$). ^{31}P NMR (121 MHz, CDCl_3) δ 123.7. Anal. Calcd. for $\text{C}_{22}\text{H}_{30}\text{BrO}_3\text{PRu}$. C, 47.66; H, 5.45; Found C, 46.62; H, 5.40. HRMS: $[\text{M}+\text{Na}^+]$ obs'd (%), calc'd (%), ppm: 576.0067 (52), 576.0061 (60), 1.1; 577.0058 (92), 577.0053 (94), 0.9; 578.0063 (42), 578.0060 (52.5), 0.5; 579.0054 (100), 579.0048 (100), 1.1.

$(\eta^6\text{-}p\text{-cymene})\text{Ru}(\text{PMe}_3)\text{Br}_2$ (3). $[(\eta^6\text{-}p\text{-cymene})\text{Ru}(\text{Br})(\mu\text{-Br})]_2^{21}$ (0.6352 g, 0.8039 mmol) was dissolved in 20 mL of methylene chloride in a round bottom flask. PMe_3 (0.18347 g, 2.416 mmol) was added to the solution in the round bottom flask via

syringe. The reaction was allowed to stir for 30 minutes. The reaction mixture was concentrated to ~ 5 mL under vacuum with slight warming. Hexanes were added to induce a precipitate. The precipitate was collected on a fine porosity frit and washed with pentane three times and dried under vacuum. (0.6724 g, 89% yield) ^1H NMR (600 MHz, CDCl_3) δ 5.44 – 5.41 (m, 2H, Cy- C_{Ar}), 5.39 (d, 2H, $^3J_{\text{HH}} = 6$ Hz, Cy- C_{Ar}), 2.95 (sept, 1H, $^3J_{\text{HH}} = 7$ Hz, Cy- $\text{CH}(\text{CH}_3)_2$), 2.13 (s, 3H, Cy- CH_3), 1.68 (d, 9H, $^2J_{\text{HP}} = 11$ Hz, PMe_3), 1.20 (d, 6H, $^3J_{\text{HH}} = 7$ Hz, Cy- $\text{CH}(\text{CH}_3)_2$). ^{13}C NMR (151 MHz, CDCl_3) δ 108.5 (s, C_6H_4), 93.8 (s, Cy- C_{Ar}), 89.4 (d, $^2J_{\text{CP}} = 5$ Hz, Cy- C_{Ar}), 84.5 (d, $^2J_{\text{CP}} = 6$ Hz, Cy- C_{Ar}), 31.1 (s, Cy- $\text{CH}(\text{CH}_3)_2$), 22.2 (s, Cy- $\text{CH}(\text{CH}_3)_2$), 19.1 (s, Cy- CH_3), 18.4 (d, $^2J_{\text{CP}} = 34.4$ Hz, PMe_3). $^{31}\text{P}\{^1\text{H}\}$ NMR (121 MHz, CDCl_3) δ -2.0 ppm. HRMS: $[\text{M}+\text{Na}^+]$ obs'd (%), calc'd (%), ppm: 491.8850 (32), 491.8844 (45), 1.2; 492.8842 (52), 492.8834 (65), 1.6; 493.8841 (40), 493.8833 (55), 1.5; 494.8835 (100), 494.8826 (100), 1.9; 495.8839 (18), 495.8833 (30), 1.3; 496.8825 (60), 496.8818 (70), 1.4.

(η^6 -*p*-cymene)Ru(PMe_3)PhBr (4). (η^6 -*p*-cymene)Ru(PMe_3)Br₂ (0.3353 g, 0.7116 mmol) was combined with 20 mL of THF (heterogeneous) and added to a 100 mL round bottom flask. $\text{Ph}_2\text{Mg}[\text{THF}]_2$ (0.1770 g, 0.5485 mmol) was dissolved in 20 mL THF and added to the round bottom flask containing the Ru mixture. The reaction was allowed to stir ~ 1 h during which time the reaction slowly became homogeneous and bright yellow. All the solvent was removed *in vacuo*, and ~ 30 mL of benzene were added to the flask. The solution was filtered through Celite. The filtrate was then eluted on a 1" silica plug; the plug was then washed with copious amounts of THF. The THF eluent was removed *in vacuo* to yield a bright yellow solid, which was collected on a fine

porosity frit and washed with pentane. Dried *in vacuo* to yield a yellow solid (0.2974 g, 89% yield). ^1H NMR (600 MHz, CDCl_3) δ 7.57 (bs, 2H, phenyl), 6.95 – 6.82 (m, 3H, phenyl), 5.28 (d, 1H, $^3J_{\text{HH}} = 5.7$ Hz, Cy- C_{Ar}), 5.11 (m, 2H, Cy- C_{Ar}), 4.82 (d, 1H, $J = 5.7$ Hz, Cy- C_{Ar}), 2.62 (sept, 1H, $^2J_{\text{HH}} = 7$ Hz, $\text{C}_6\text{H}_4\text{-CH}(\text{CH}_3)_2$), 1.91 (s, 3H, Cy- CH_3), 1.35 (d, 9H, $^2J_{\text{HP}} = 10$ Hz, PMe_3), 1.20 (d, 3H, $^3J_{\text{HH}} = 7$ Hz, $\text{CH}(\text{CH}_3)_2$), 1.09 (d, 3H, $^3J_{\text{HH}} = 7$ Hz, $\text{CH}(\text{CH}_3)_2$). ^{13}C NMR (151 MHz, CDCl_3) δ 161.2 (d, $^2J_{\text{CP}} = 25$ Hz, ipso of phenyl), 141.9 (d, $^3J_{\text{PC}} = 93.84$ Hz, phenyl) 126.5 (s, phenyl), 121.7 (s, phenyl), 114.2 (d, $^3J_{\text{PC}} = 4$ Hz, ipso of Cy- C_{Ar}), 104.1 (s, Cy- C_{Ar}), 88.2 (d, $^2J_{\text{CP}} = 3$ Hz, Cy- C_{Ar}), 86.4 (d, $^2J_{\text{CP}} = 6$ Hz, Cy- C_{Ar}), 85.9 (d, $^2J_{\text{CP}} = 4$ Hz, Cy- C_{Ar}), 85.6 (s, Cy- C_{Ar}) 31.4 (s, Cy- $\text{CH}(\text{CH}_3)_2$), 23.0 (s, Cy- $\text{CH}(\text{CH}_3)_2$), 22.7 (s, Cy- $\text{CH}(\text{CH}_3)_2$), 19.0 (s, Cy- CH_3) 17.8 (d, $^2J_{\text{CP}} = 33$ Hz, PMe_3). $^{31}\text{P}\{^1\text{H}\}$ NMR (121 MHz, CDCl_3) δ 4.5. HRMS: $[\text{M}^+\text{Na}^+]$ obs'd (%), calc'd (%), ppm: 490.0054 (65), 490.0056 (61), -0.4; 491.0046 (95), 491.0048 (93.6), -0.4; 492.0053 (50), 492.0054 (49.1), -0.2; 493.0042 (100), 493.0043 (100), -0.2.

Tetrakis(1-pyrazolyl)methane. The synthesis of $\text{C}(\text{pz})_4$ has been previously reported.^{25,26} We used an alternate procedure. Pyrazolyl (13.437 g, 0.19737 mol) and $[\text{Bu}_4\text{N}][\text{HSO}_4]$ (2.795 g, 0.008232 mol) were dissolved in CCl_4 (200 mL) and transferred to a 500 mL round bottom flask. K_2CO_3 (27.90 g, 0.2013 mol) was added in small portions with stirring. KOH flakes (57.810 g, 1.0304 mol) were added to the flask and the reaction was stirred at reflux (under nitrogen) for three days. The reaction was cooled and filtered through Celite (~1/2"). The flask and Celite were washed with methylene chloride, yielding a reddish filtrate. The filtrate was then eluted through approximately 1 inch of silica, and the silica was washed with copious amounts of methylene chloride

until the eluent was almost colorless. The yellow eluent was collected and reduced to dryness under reduced pressure. The yellow oil was reconstituted in diethyl ether and was reduced to dryness under reduced pressure. A minimal amount of diethyl ether was added to the flask, and the flask was placed in the freezer. A white solid precipitated. The solid was collected on a fine porosity frit, washed with a minimal amount of cold diethyl ether followed by pentane and dried under vacuum. A second batch could be isolated by reduction of filtrate, reconstitution in fresh ether and slow evaporate at room temperature (1.504 g, 11% yield).

(κ^3 -N,C⁵,N)C(pz)₄Ru[P(OCH₂)₃CEt](NCMe)Br (6). The complex (η^6 -*p*-cymene)Ru[P(OCH₂)₃CEt](Ph)Br (0.0747 g, 0.134 mmol) was dissolved in ~5 mL of NCMe and added to a pressure tube. The reaction was heated for 19 h at 90 °C. The reaction was brought into the glovebox and allowed to cool to room temperature. The mixture was filtered through Celite, and the yellow filtrate was reduced to dryness. The solid was washed with THF and benzene (both solutions discarded). The remaining solid was reconstituted in a minimal amount of methylene chloride and diethyl ether was added to induce a precipitate. The precipitate was collected on a fine porosity frit, washed with pentane and dried under vacuum to yield a yellow solid (0.0321 g, 35% yield). ¹H NMR (497 MHz, CD₂Cl₂) δ 9.27 (d, 1H, ³J_{HH} = 3 Hz, C(pz)₄), 8.44 (s, 1H, C(pz)₄), 8.04 (m, 2H, overlapping C(pz)₄), 7.89 (s, 1H, C(pz)₄), 7.43 (t, 1H, ³J_{HH} = 1.3 Hz, C(pz)₄), 6.72 (s, 1H, C(pz)₄), 6.36 (dt, 1H, ³J_{HH} = 3.6, ³J_{HH} = 1.6 Hz, C(pz)₄), 6.25 (t, 1H, ³J_{HH} = 1.3 Hz, C(pz)₄), 6.08 (t, 1H, ³J_{HH} = 3 Hz, C(pz)₄), 5.91 (d, 1H, ³J_{HH} = 3 Hz, C(pz)₄), 4.28 (d, 6H, ³J_{HP} = 4.6 Hz, P(OCH₂)₃CCH₂CH₃), 2.29 (s, 3H, NCCH₃), 1.23 (q, 2H, ³J_{HH} = 7.7 Hz,

$\text{P}(\text{OCH}_2)_3\text{CCH}_2\text{CH}_3$), 0.83 (t, 3H, $^3J_{\text{HH}} = 7.7$ Hz, $\text{P}(\text{OCH}_2)_3\text{CCH}_2\text{CH}_3$). ^{13}C NMR (125 MHz, CD_2Cl_2) δ 170.4 (d, $^2J_{\text{CP}} = 18$ Hz Ru-C(pz)₄), 148.5, 146.5, 144.5, 143.5, 141.4, 140.3, 130.7, 121.9, 109.3, 107.2, 107.0 (each a s, C(pz)₄), 96.3 (s, C(pz)₄), 74.6 (d, $^2J_{\text{CP}} = 7.2$ Hz, $\text{P}(\text{OCH}_2)_3\text{CCH}_2\text{CH}_3$), 35.6 (d, $^3J_{\text{CP}} = 31$ Hz, $\text{P}(\text{OCH}_2)_3\text{CCH}_2\text{CH}_3$), 24.0 (s, $\text{P}(\text{OCH}_2)_3\text{CCH}_2\text{CH}_3$), 7.5 (s, $\text{P}(\text{OCH}_2)_3\text{CCH}_2\text{CH}_3$), 4.8 (s, NCCH₃). ^{31}P NMR (121 MHz, CD_2Cl_2) δ 133.4.

$\{\text{[HC(pz')}_3\text{]Ru[P(OCH}_2)_3\text{CEt]Ph(NCMe)}\}\text{[Br]}$ (7). The complex (η^6 -p-cymene)Ru[P(OCH₂)₃CEt](Ph)Br (0.2854 g, 0.5151 mmol) was dissolved in approximately 15 mL of NCMe, added to a pressure tube and heated for 2 h at 70 °C. The reaction was brought into the glovebox and allowed to cool to room temperature. The mixture was filtered through Celite, and the filtrate was concentrated to dryness yielding (NCMe)₃Ru[P(OCH₂)₃CEt](Ph)Br (3). Without any purification, the resulting solid was dissolved in ~10 mL of methylene chloride and added to a pressure tube along with a 5 mL methylene chloride solution of HC(pz')₃ (0.1452 g, 0.4870 mmol). The reaction was heated to 70 °C for 2 h. The reaction was brought into the glovebox and filtered through Celite. The filtrate was concentrated to dryness. Benzene was added, and the mixture was stirred. The mixture was filtered through Celite, and the filtrate was discarded. The remaining solid in the flask was reconstituted in methylene chloride and filtered through Celite, concentrated to ~2 mL, and hexanes were added to induce a precipitate. The precipitate was collected on a fine porosity frit. The solid was washed with pentane and dried *in vacuo* to yield a tan solid (0.2065 g, 53% yield). ^1H NMR (600 MHz, CD_2Cl_2) δ 7.87 (s, 1H, HC(pz')₃), 7.62 (d, 1H, $^3J_{\text{HH}} = 7.6$ Hz, *ortho*-phenyl), 6.91 (t, 1H, $^3J_{\text{HH}} = 7.4$

Hz, *meta*-phenyl), 6.74 (t, 1H, $^3J_{\text{HH}} = 7.2$ Hz, *para*-phenyl), 6.60 (t, 1H, $J = 7.4$ Hz, *meta*-phenyl), 6.37 (d, 1H, $^3J_{\text{HH}} = 7.6$ Hz, *ortho*-phenyl), 6.15, 6.04, 5.98 (each a s, 1H, HC(pz')₃; 4-positions), 4.22 (d, 6H, $^3J_{\text{HP}} = 4.6$ Hz, P(OCH₂)₃CCH₂CH₃), 2.64 (overlapping s, 9H, HC(pz')₃; 3,5-methyl positions), 2.53, 1.97, 1.41 (each a s, 3H, HC(pz')₃; 3,5-methyl positions), 2.35 (s, 3H, NCCH₃), 1.23 (q, 2H, $^3J_{\text{HH}} = 7.6$ Hz, P(OCH₂)₃CCH₂CH₃), 0.83 (t, 3H, $^3J_{\text{HH}} = 7.7$ Hz, P(OCH₂)₃CCH₂CH₃). ¹³C NMR (151 MHz, CD₂Cl₂) δ 165.3 (d, $^2J_{\text{CP}} = 19$ Hz, ipso of phenyl) 158.9, 156.5, 156.1, 141.2, 140.6, 140.5 (each a s, HC(pz')₃-CCH₃), 143.46 (phenyl), 141.7 (phenyl), 125.8 (phenyl), 125.2 (phenyl), 124.0 (s, NCCH₃), 120.6 (phenyl), 109.9, 109.6, 109.3 (each a s, HC(pz')₃-CH group), 74.5 (d, $^2J_{\text{CP}} = 7.2$ Hz, P(OCH₂)₃CCH₂CH₃), 68.8 (s, HC(pz')₃), 35.6 (d, $^3J_{\text{CP}} = 30.8$ Hz, P(OCH₂)₃CCH₂CH₃), 24.0 (s, P(OCH₂)₃CCH₂CH₃) 15.8, 14.0, 13.1, 12.3, 11.9, 11.8 (each a s, HC(pz')₃-CH₃ group), 7.5 (s, P(OCH₂)₃CCH₂CH₃), 4.8 (s, NCCH₃). ³¹P NMR (121 MHz, CD₂Cl₂) δ 137.4.



$\{[\text{HC}(\text{pz}')_3]\text{Ru}[\text{P}(\text{OCH}_2)_3\text{CEt}]\text{Ph}(\text{NCMe})\}[\text{Br}]$ (7) (0.0487 g, 0.0641 mmol) was dissolved in approximately 5 mL of THF (heterogeneous) in a round bottom flask. NaBAr'₄ (0.0569 g, 0.0641 mmol) was dissolved in 2 mL of THF and added to the round bottom flask. The reaction was allowed to stir at room temperature for 2 h. The solution was filtered through Celite, and the filtrate was concentrated to dryness. The solid was reconstituted in methylene chloride and all the volatiles were removed yielding a low-density yellow solid (0.0866 g, 87% yield). ¹H NMR (500 MHz, CD₂Cl₂) δ 7.80 (s, 1H, HC(pz')₃), 7.74 (s, 8H, BAr'₄ *ortho* position), 7.64 (d, 1H, $^3J_{\text{HH}} = 7.6$ Hz, *ortho*-phenyl),

7.58 (s, 4H, BAR'_4 *para* position), 6.95 (t, 1H, $^3J_{\text{HH}} = 7.4$ Hz, *meta*-phenyl), 6.78 (t, 1H, $^3J_{\text{HH}} = 7.2$ Hz, *para*-phenyl), 6.63 (t, 1H, $J = 7.5$ Hz, *meta*-phenyl), 6.37 (d, 1H, $^3J_{\text{HH}} = 7.7$ Hz, *ortho*-phenyl), 6.12, 6.05, 5.97 (each a s, 1H, $\text{HC}(\text{pz}')_3$ - 4 positions), 4.23 (d, 6H, $^3J_{\text{HP}} = 4.7$ Hz, $\text{P}(\text{OCH}_2)_3\text{CCH}_2\text{CH}_3$), 2.56, 2.55, 2.54, 2.52, 2.00, 1.43 (each a s, 3H, $\text{HC}(\text{pz}')_3$ - 3,5 methyl positions), 2.30 (s, 3H, NCCH_3), 1.24 (q, 2H, $^3J_{\text{HH}} = 7.7$ Hz, $\text{P}(\text{OCH}_2)_3\text{CCH}_2\text{CH}_3$), 0.83 (t, 3H, $^3J_{\text{HH}} = 7.6$ Hz, $\text{P}(\text{OCH}_2)_3\text{CCH}_2\text{CH}_3$). ^{13}C NMR (151 MHz, CD_2Cl_2) δ 164.9 (four line pattern, $^2J_{\text{CP}} = 21$ Hz, ipso of phenyl), 162.3 (q, $^1J_{\text{CB}} = 50$ Hz, BAR'_4) 159.1, 156.6, 156.3, 140.6, 140.5, 139.8 (each a s, $\text{HC}(\text{pz}')_3\text{-CCH}_3$), 143.4 (phenyl), 141.1 (phenyl), 135.3 (s, BAR'_4), 129.1 (q, $^1J_{\text{CF}} = 32$ Hz, BAR'_4), 125.1 (q, $^1J_{\text{CF}} = 273$ Hz, BAR'_4), 125.9 (phenyl), 125.4 (phenyl), 123.8 (s, NCCH_3), 120.8 (phenyl), 118.0 (s, BAR'_4) 110.1, 109.7, 109.3 (each a s, $\text{HC}(\text{pz}')_3\text{-CH}$ group), 74.5 (d, $^2J_{\text{CP}} = 7.3$ Hz, $\text{P}(\text{OCH}_2)_3\text{CCH}_2\text{CH}_3$), 68.7 (s, $\text{HC}(\text{pz}')_3$), 35.7 (d, $^3J_{\text{CP}} = 30.9$ Hz, $\text{P}(\text{OCH}_2)_3\text{CCH}_2\text{CH}_3$), 24.0 (s, $\text{P}(\text{OCH}_2)_3\text{CCH}_2\text{CH}_3$) 15.8, 13.9, 13.1, 11.8, 11.3, 11.2 (each a s, $\text{HC}(\text{pz}')_3\text{-CH}_3$ group), 7.4 (s, $\text{P}(\text{OCH}_2)_3\text{CCH}_2\text{CH}_3$), 4.5 (s, NCCH_3). ^{31}P NMR (121 MHz, CD_2Cl_2) δ 134.4. ^{19}F NMR (282 MHz, CD_2Cl_2) δ -63.3. CV (NCMe): $E_{1/2} = 0.82$ V Ru(III/II).

$[\text{C}(\text{pz})_4]\text{Ru}(\text{PPh}_3)\text{Cl}_2$ (9). $\text{C}(\text{pz})_4$ (0.3095 g, 1.104 mmol) and $\text{RuCl}_2(\text{PPh}_3)_3$ (1.001 g, 1.045 mmol) were combined in a 50 mL round bottom flask and dissolved in 25 mL of toluene. The reaction was refluxed overnight. The brown solution gradually turned tan-yellow, and a large quantity of yellow precipitate formed. The flask was removed from heat and allowed to cool to room temperature. Hexanes (10 mL) were added complete precipitation. The yellow solid was collected on a fine porosity frit and washed with a small quantity of toluene (5 mL) followed by washing with pentane. The yellow

solid was dried on the frit to yield a brownish-yellow powder (0.5883 g, 79% yield). ^1H NMR (600 MHz, CDCl_3) δ 8.74 (d, 1H, $^3J_{\text{HH}} = 2$ Hz, C(pz)₄), 8.64 (s, 1H, C(pz)₄), 8.28 (d, 1H, $^3J_{\text{HH}} = 3$ Hz, C(pz)₄), 8.16 (d, 1H, $^3J_{\text{HH}} = 2$ Hz, C(pz)₄), 7.90 – 7.79 (m, 6H, PPh₃, overlapping *ortho* protons), 7.33 – 7.19 (m, 9H, PPh₃, overlapping signals for *meta* and *para* protons), 6.94 (vt, 1H, C(pz)₄), 6.87 (d, 2H, $^3J_{\text{HH}} = 3$ Hz, C(pz)₄), 6.76 (m, 2H, C(pz)₄), 6.52 (d, 1H, $^3J_{\text{HH}} = 2$ Hz, C(pz)₄), 5.90 (dd, 2H, $^3J_{\text{HH}} = 3.0$ Hz, $^3J_{\text{HH}} = 2.3$ Hz, C(pz)₄). ^{13}C NMR (151 MHz, CDCl_3) δ 151.3, 148.3, 144.6, 136.0, 134.8, 134.5, 111.3, 109.6, 109.3 (each a s, C(pz)₄), 135.1 (d, $^2J_{\text{CP}} = 9$ Hz, *ortho*-PPh₃), 132.5 (s, *ipso*-PPh₃), 129.0 (s, *para*-PPh₃), 127.7 (d, $^3J_{\text{CP}} = 9$ Hz, *meta*-PPh₃), 94.4 (s, C(pz)₄). ^{31}P NMR (121 MHz, CD_2Cl_2) δ 52.4.

[C(pz)₄]Ru[P(OCH₂)₃CEt]Cl₂ (10). C(pz)₄Ru(PPh₃)Cl₂ (9) (0.457 g, 0.639 mmol) and P(OCH₂)₃CEt (0.415 g, 2.56 mmol) were combined in a round bottom flask with 20 mL of chloroform. The reaction was refluxed overnight. The solution initially turned dark brown, then upon additional heating a yellow precipitate formed. The reaction mixture was reduced to ~5 mL and hexanes were added to induce a precipitate. The precipitate was collected on a fine frit and washed with hexanes. The yellow precipitate was placed back into a round bottom flask with 10 mL of chloroform and the reaction refluxed for 6 h. After cooling to room temperature, the resulting solid was collected on a fine frit and washed with ~5 mL of chloroform and pentane. The yellow solid was dried under vacuum to yield a yellow solid. (0.392 g, 99% yield) ^1H NMR (600 MHz, CD_2Cl_2) δ 8.65 (dt, 1H, $^3J_{\text{HH}} = 1.8$ Hz, $^4J_{\text{HP}} = 0.7$ Hz, C(pz)₄), 8.54 (dd, 1H, $^3J_{\text{HH}} = 1.9$ Hz, $^4J_{\text{HP}} = 0.7$ Hz, C(pz)₄), 8.32 (d, 1H, $^3J_{\text{HH}} = 2.8$ Hz, C(pz)₄), 8.20 (d, 1H, $^3J_{\text{HH}} = 1.7$

Hz, C(pz)₄), 8.13 (dd, 2H, ³J_{HH} = 2.2 Hz, ⁴J_{HP} = 0.9 Hz, C(pz)₄), 7.06 (dd, 2H, ³J_{HH} = 3.2 Hz, ⁴J_{HP} = 0.9 Hz, C(pz)₄), 6.95 (dd, 1H, ³J_{HH} = 2.9 Hz, ³J_{HH} = 1.8 Hz, C(pz)₄), 6.62 (dt, 1H, ³J_{HH} = 2.8, ³J_{HH} = 1.8 Hz, C(pz)₄), 6.33 (dd, 2H, ³J_{HH} = 3.2, ³J_{HH} = 2.2 Hz, C(pz)₄), 4.38 (d, 6H, ³J_{HP} = 4.5 Hz, P(OCH₂)₃CCH₂CH₃), 1.28 (q, 2H, ³J_{HH} = 7.8 Hz, P(OCH₂)₃CCH₂CH₃), 0.86 (t, 3H, ³J_{HH} = 7.7 Hz, P(OCH₂)₃CCH₂CH₃). ¹³C NMR (151 MHz, CD₂Cl₂) δ 151.6, 148.3, 145.6, 136.9, 133.9, 133.0, 112.1, 109.6, 109.2 (s, C(pz)₄ 4 position), 94.7 (s, C(pz)₄), 74.9 (d, ²J_{CP} = 7 Hz, P(OCH₂)₃CCH₂CH₃), 24.1 (s, P(OCH₂)₃CCH₂CH₃), 7.5 (s, P(OCH₂)₃CCH₂CH₃). ¹³C NMR (75 MHz, CD₃NO₂) δ 152.3, 148.9, 146.7, 138.5, 135.6, 134.7, 112.9, 110.0, 109.7, (each a s, C(pz)₄), 95.6 (s, -C(pz)₄), 75.4 (d, ²J_{CP} = 8 Hz, P(OCH₂)₃CCH₂CH₃), 36.5 (d, ³J_{CP} = 31 Hz, P(OCH₂)₃CCH₂CH₃), 24.3 (s, P(OCH₂)₃CCH₂CH₃), 7.5 (s, P(OCH₂)₃CCH₂CH₃). ³¹P NMR (121 MHz, CD₂Cl₂) δ 128.1. HRMS: [M⁺Na⁺] obs'd (%), calc'd (%), ppm: 635.9969 (61), 635.9951 (64), 2.9; 636.9961 (100), 636.9942 (100), 2.9; 637.9963 (47), 637.9943 (52), 3.1; 638.9954 (94), 638.9935 (94), 3.0.

{[C(pz)₄]Ru[P(OCH₂)₃CEt]Cl(NCMe)][Cl] (11). C(pz)₄Ru[P(OCH₂)₃CEt]Cl₂ (**10**) (0.8550, 1.391 mmol) was dissolved in NCMe (25 mL) (heterogenous) and refluxed overnight. During heating the mixture becomes homogenous. The initial yellow color changed to green-yellow, then brown, and finally back to yellow. The solution was filtered through Celite. The filtrate was reduced *in vacuo* to ~2 mL, and ~2 mL of methylene chloride were added followed by the addition of diethyl ether to induce precipitation. The off-white solid was collected over a fine porosity frit, washed with diethyl ether and pentane and dried on the frit under reduced pressure (0.6486 g, 71%

yield). Note: contains a small amount of a second product; however, in the next step (reaction with NaBAr'₄) the second product is removed. ¹H NMR (600 MHz, CD₂Cl₂) δ 8.96 (d, 1H, ³J_{HH} = 3.2 Hz, C(pz)₄), 8.74, 8.34, 8.24, 8.01 (s, 1H, C(pz)₄), 8.11 (d, 1H, ³J_{HH} = 2.2 Hz, C(pz)₄), 7.37 (d, 1H, ³J_{HH} = 3.2 Hz, C(pz)₄), 7.12 (d, 1H, ³J_{HH} = 3.0 Hz, C(pz)₄), 7.08, 6.69, 6.55, 6.42 (s, 1H, C(pz)₄), 4.41 (d, 6H, ³J_{HP} = 4.4 Hz, P(OCH₂)₃CCH₂CH₃), 2.43 (s, 3H, NCCH₃), 1.32 (q, 2H, ³J_{HH} = 7.7 Hz, P(OCH₂)₃CCH₂CH₃), 0.87 (t, 3H, ³J_{HH} = 7.5 Hz, P(OCH₂)₃CCH₂CH₃). ¹³C NMR (151 MHz, CD₂Cl₂) δ 151.0, 150.8, 147.3, 146.2, 138.2, 135.8, 134.5, 134.4, 113.1, 110.1, 109.9, 109.5 (each a s, C(pz)₄), 124.9 (s, NCCH₃), 94.6 (s, C(pz)₄), 75.3 (d, ²J_{CP} = 7 Hz, P(OCH₂)₃CCH₂CH₃), 36.1 (d, ³J_{CP} = 31.9 Hz, P(OCH₂)₃CCH₂CH₃), 23.8 (s, P(OCH₂)₃CCH₂CH₃), 7.5 (s, P(OCH₂)₃CCH₂CH₃), 5.3 (s, NCCH₃). ³¹P NMR (121 MHz, CD₂Cl₂) δ 128.1. HRMS: [M⁺] obs'd (%), calc'd (%), ppm: 617.0645 (23), 617.0640 (33.5), 0.8; 618.0636 (29), 618.0630 (38.5), 1; 619.0640 (52), 619.0634 (59.5), 1; 620.0633 (100), 620.0625 (100), 1.3; 621.0640 (27), 621.0634 (36), 1; 622.0631 (70), 622.0623 (75), 1.4.



{[C(pz)₄]Ru[P(OCH₂)₃CEt]Cl(NCMe)}[Cl] (11) (0.700 g, 1.06 mmol) and NaBAr'₄ (0.4783 g, 0.5397 mmol) were combined in THF (15 mL). The reaction was stirred at room temperature for 3 h. The solution was filtered through Celite, and the filtrate was reduced to dryness. The solid was reconstituted in diethyl ether and loaded on a plug of neutral alumina. The plug was washed with diethyl ether. This portion was discarded. The plug was then washed with a 50/50 solution of methylene chloride/diethyl ether. The

eluate was collected and dried under reduced pressure to yield a yellow oil. The yellow oil was dissolved in a minimal amount of methylene chloride and placed under vacuum to afford a pale-yellow solid (0.8957 g, 57% yield). ^1H NMR (800 MHz, CD_2Cl_2) δ 8.78, 8.38 (each a s, 1H, $\text{C}(\text{pz})_4$), 8.26 (d, 1H, $^3J_{\text{HH}} = 2.5$ Hz, $\text{C}(\text{pz})_4$), 8.22, 8.18 (each a s, 1H, $\text{C}(\text{pz})_4$), 7.93 (m, 1H, $\text{C}(\text{pz})_4$), 7.72 (s, 8H, BAr'_4 *ortho* position), 7.55 (s, 4H, BAr'_4 *para* position), 7.37 (d, 1H, $^3J_{\text{HH}} = 3.0$ Hz, $\text{C}(\text{pz})_4$), 6.98 (m, 1H, $\text{C}(\text{pz})_4$), 6.80 (d, 1H, $^3J_{\text{HP}} = 3.0$ Hz, $\text{C}(\text{pz})_4$), 6.68 (s, 1H, $\text{C}(\text{pz})_4$), 6.45, 6.36 (each a m, 1H, $\text{C}(\text{pz})_4$), 4.40 (d, 6H, $^3J_{\text{HP}} = 4.0$ Hz, $\text{P}(\text{OCH}_2)_3\text{CCH}_2\text{CH}_3$), 2.43 (s, 3H, NCCH_3), 1.30 (q, 2H, $^3J_{\text{HH}} = 7.7$ Hz, $\text{P}(\text{OCH}_2)_3\text{CCH}_2\text{CH}_3$), 0.87 (t, 3H, $^3J_{\text{HH}} = 7.7$ Hz, $\text{P}(\text{OCH}_2)_3\text{CCH}_2\text{CH}_3$). ^{13}C NMR (201 MHz, CD_2Cl_2) δ 162.3 (four line pattern, $^1J_{\text{CB}} = 50$ Hz, BAr'_4), 151.7, 150.5, 147.6, 146.3, 136.8, 135.1, 134.0, 133.6, 112.9, 110.0, 109.9, 109.8 (s, each a s, $\text{C}(\text{pz})_4$) 135.3 (s, BAr'_4), 129.4 (q, $^1J_{\text{CF}} = 32$ Hz, BAr'_4), 125.1 (q, $^1J_{\text{CP}} = 273$ Hz, BAr'_4), 124.7 (s, NCCH_3), 118.0 (s, BAr'_4), 94.7 (s, $\text{C}(\text{pz})_4$), 75.4 (d, $^2J_{\text{CP}} = 7$ Hz, $\text{P}(\text{OCH}_2)_3\text{CCH}_2\text{CH}_3$), 36.4 (d, $^3J_{\text{CP}} = 32$ Hz, $\text{P}(\text{OCH}_2)_3\text{CCH}_2\text{CH}_3$), 23.9 (s, $\text{P}(\text{OCH}_2)_3\text{CCH}_2\text{CH}_3$), 7.5 (s, $\text{P}(\text{OCH}_2)_3\text{CCH}_2\text{CH}_3$), 4.8 (s, NCCH_3). ^{31}P NMR (121 MHz, CD_2Cl_2) δ 128.3. ^{19}F NMR (282 MHz, CD_2Cl_2) δ -63.7. Anal. Calc'd. for $\text{C}_{53}\text{H}_{38}\text{BClF}_{24}\text{N}_9\text{O}_3\text{PRu}$: C, 42.92; H, 2.58; N, 8.50. Found: C, 42.85; H, 2.70; N, 8.30.



$\{[\text{C}(\text{pz})_4]\text{Ru}[\text{P}(\text{OCH}_2)_3\text{CEt}](\text{Cl})(\text{NCMe})\}[\text{BAr}'_4]$ (**12**) (0.8796 g, 0.5932 mmol) was dissolved in 40 mL of methylene chloride in a thick walled pressure tube, and TMSOTf (1.318 g, 1.07 mL, 5.932 mmol) was added by syringe. The reaction was heated at 100 °C overnight. The reaction was brought back into the glovebox and allowed to cool to

room temperature. The reaction mixture was added to 100 mL of hexanes and allowed to stir for 30 minutes. The desired product oiled out of solution. The hexanes solution was filtered through Celite, and the filtrate was discarded. The Celite was washed with methylene chloride, and the filtrate was placed in the flask with the oil. The methylene chloride was removed *in vacuo* to yield an oil. The oil was dissolved in a minimal amount of methylene chloride and placed in a vial, and the solvent was removed. After removing the solvent *in vacuo*, a minimal amount of diethyl ether was added, followed by removal of the volatiles to yield a yellow solid (0.7976 g, 84% yield). ^1H NMR (600 MHz, CD_2Cl_2) δ 8.82, 8.43 (m, 1H, C(pz)₄), 8.30 (d, 1H, $^3J_{\text{HH}} = 2.9$ Hz, C(pz)₄), 8.26 (d, 1H, $^3J_{\text{HH}} = 1.7$ Hz, C(pz)₄), 8.23 (dd, 1H, $^3J_{\text{HH}} = 2.2$ Hz, $^4J_{\text{HP}} = 0.8$ Hz, C(pz)₄), 7.96 (m, 1H, C(pz)₄), 7.77 (s, 8H, BAr'₄ *ortho* position), 7.60 (s, 4H, BAr'₄ *para* position), 7.42 (dd, 1H, $^3J_{\text{HH}} = 3.2$ Hz, $^4J_{\text{HP}} = 0.8$ Hz, C(pz)₄), 7.02 (dd, 1H, $^3J_{\text{HH}} = 2.8$ Hz, $^4J_{\text{HH}} = 1.8$ Hz, C(pz)₄), 6.85 (dd, 1H, $^3J_{\text{HH}} = 3.4$ Hz, $^4J_{\text{HP}} = 0.9$ Hz, C(pz)₄), 6.72 (dt, 1H, $^3J_{\text{HH}} = 3.5$ Hz, $^4J_{\text{HH}} = 1.9$ Hz, C(pz)₄), 6.49 (dd, 1H, $^3J_{\text{HH}} = 3.4$ Hz, $^4J_{\text{HH}} = 2.2$ Hz, C(pz)₄), 6.40 (dd, 1H, $^3J_{\text{HH}} = 3.2$ Hz, $^4J_{\text{HH}} = 2.2$ Hz, C(pz)₄), 4.45 (d, 6H, $^3J_{\text{HP}} = 4.6$ Hz, P(OCH₂)₃CCH₂CH₃), 2.43 (s, 3H, NCCH₃), 1.34 (q, 2H, $^3J_{\text{HH}} = 7.7$ Hz, P(OCH₂)₃CCH₂CH₃), 0.91 (t, 3H, $^3J_{\text{HH}} = 7.7$ Hz, P(OCH₂)₃CCH₂CH₃). ^{13}C NMR (125 MHz, CD_2Cl_2) δ 162.3 (four lined pattern, $^1J_{\text{CB}} = 50$ Hz, BAr'₄), 152.2, 151.3, 148.7, 146.6, 136.9, 134.9, 134.6, 133.8, 113.2, 110.2 (each a s, C(pz)₄, one resonances missing due to coincidental overlap), 129.5 (q, $^1J_{\text{CF}} = 32$ Hz, BAr'₄), 125.2 (q, $^1J_{\text{CP}} = 273$ Hz, BAr'₄), 135.4 (s, BAr'₄), 126.7 (s, NCCH₃), 118.1 (s, BAr'₄), 94.6 (s, C(pz)₄), 75.7 (d, $^2J_{\text{CP}} = 7$ Hz, P(OCH₂)₃CCH₂CH₃), 36.7 (d, $^3J_{\text{CP}} = 32$ Hz, P(OCH₂)₃CCH₂CH₃), 23.8 (s,

P(OCH₂)₃CCH₂CH₃), 7.5 (s, P(OCH₂)₃CCH₂CH₃), 4.5 (s, NCCH₃). ³¹P NMR (121 MHz, CD₂Cl₂) δ 127.7. ¹⁹F NMR (282 MHz, CD₂Cl₂) δ -63.2 (BAR'4), -78.9 (OTf). Anal. Calc'd. for C₅₄H₃₈BF₂₇N₉O₆PRuS: C, 40.62 H, 2.40; N, 7.89. Found: C, 39.81; H, 2.62; N, 7.79. HRMS: [M⁺] obs'd (%), calc'd (%), ppm: 731.0476 (24), 731.0471 (35), 0.6; 732.0469 (32), 732.0463 (42.5), 0.8; 733.0476 (48), 733.0469 (55), 0.9; 734.0467 (100), 734.046 (100), 1.0; 735.0485 (19), 735.0479 (30), 0.9; 736.0472 (48), 736.0465 (55), 1.0.



{[C(pz)₄]Ru[P(OCH₂)₃CET](OTf)(NCMe)}[BAR'₄] (**13**) (0.1296 g, 0.08118 mmol) was placed in a round bottom flask in 15 mL of benzene (heterogeneous-oil was observed). Me₃Al (0.043 mL, 0.085 mmol) was added by syringe in two portions with 15 minutes stirring between each addition during which the reaction became bright yellow and homogeneous. The reaction was allowed to stir for 30 minutes followed by filtration through a plug of Celite. The benzene filtrate was then concentrated and transferred to a pre-weighed vial. The solvent was removed to yield a yellow low density solid. (0.0801 g, 67% yield). ¹H NMR (500 MHz, C₆D₆) δ 8.38 (br s, 8H, BAR'₄ *ortho* position), 7.95 (d, 1H, ³J_{HH} = 1.9 Hz, C(pz)₄), 7.92 (d, 1H, ³J_{HH} = 3.0 Hz, C(pz)₄), 7.88 (d, 1H, ³J_{HH} = 2.0 Hz, C(pz)₄), 7.65 (s, 4H, BAR'₄ *para* position), 7.38 (d, 1H, ³J_{HH} = 2.1 Hz, C(pz)₄), 7.30 (d, 1H, ³J_{HH} = 1.8 Hz, C(pz)₄), 7.00 (d, 1H, ³J_{HH} = 3.0 Hz, C(pz)₄), 6.57 (d, 1H, ³J_{HH} = 2.9 Hz, C(pz)₄), 5.90 (dd, 1H, ³J_{HH} = 2.8 Hz, ⁴J_{HH} = 1.8 Hz, C(pz)₄), 5.78 (m, 1H, C(pz)₄), 5.74 (d, 1H, ³J_{HH} = 2.6 Hz, C(pz)₄), 5.44 (m, 1H, C(pz)₄), 5.35 (d, 1H, ³J_{HH} = 3.2 Hz, C(pz)₄), 3.79 (d, 6H, ³J_{HP} = 4.3 Hz, P(OCH₂)₃CCH₂CH₃), 0.98 (s, 3H, NCCH₃), 0.71 (d, 3H, ³J_{HP} = 2.0 Hz, CH₃), 0.35 (q, 2H, ³J_{HH} = 7.7 Hz, P(OCH₂)₃CCH₂CH₃), 0.17 (t,

3H, $^3J_{\text{HH}} = 7.7$ Hz, $\text{P}(\text{OCH}_2)_3\text{CCH}_2\text{CH}_3$) ^{13}C NMR (125 MHz, C_6D_6) δ 162.8 (four line pattern, $^1J_{\text{CB}} = 50$ Hz, BAr'_4), 148.2, 147.0, 144.6, 144.0, 136.0, 133.8, 131.9, 131.6, 111.0, 108.8, 108.4, 108.1 (each a s, $\text{C}(\text{pz})_4$), 135.4 (s, BAr'_4), 130.0 (q, $^1J_{\text{CF}} = 32$ Hz, BAr'_4), 126.3 (s, NCCH_3), 118.1 (s, BAr'_4), 94.0 ($\text{C}(\text{pz})_4$), (d, $^2J_{\text{CP}} = 7$ Hz, $\text{P}(\text{OCH}_2)_3\text{CCH}_2\text{CH}_3$), 23.0 (s, $\text{P}(\text{OCH}_2)_3\text{CCH}_2\text{CH}_3$), 6.7 (s, $\text{P}(\text{OCH}_2)_3\text{CCH}_2\text{CH}_3$), 2.2 (s, NCCH_3). Due to solubility some of the resonances could not be resolved. ^{31}P NMR (121 MHz, CD_2Cl_2) δ 135.1. ^{19}F NMR (282 MHz, CD_2Cl_2) δ -62.8. HRMS: $[\text{M}^+]$ obs'd (%), calc'd (%), ppm: 597.1183 (40.7), 597.1186 (39.0), -0.5; 598.1175 (47.7), 598.1178 (44.0), -0.4; 599.1183 (58.1), 599.1185 (56), -0.3; 600.1175 (100), 600.11758 (100), 0.0; 601.1190 (32), 601.1199 (27.5), -1.4; 602.1179 (58.1), 602.1183 (55), -0.6.



$\{[\text{C}(\text{pz})_4]\text{Ru}[\text{P}(\text{OCH}_2)_3\text{CEt}(\text{Me})(\text{NCMe})][\text{BAr}'_4]\} \quad (14)$ (0.055 g, 0.5140 mmol) and NCMe (0.00314 g, 0.0766 mmol, 4 mL) were combined in a pressure tube with 3 mL of benzene. The reaction was heated at 75 °C for 3 hours. The solution was filtered through Celite. The filtrate was reduced to yield an oil to which ~0.5 mL of pentane was added. The solvent was removed *in vacuo* to yield a pale yellow low density solid (0.0271 g, 53% yield). ^1H NMR (600 MHz, C_6D_6) δ 8.77 (d, 1H, $^3J_{\text{HH}} = 2.8$ Hz, $\text{C}(\text{pz})_4$), 8.39 (s, 8H, BAr'_4 *ortho* position), 8.06 (d, 1H, $^3J_{\text{HH}} = 2.9$ Hz, $\text{C}(\text{pz})_4$), 7.75 (d, 1H, $^3J_{\text{HH}} = 1.7$ Hz, $\text{C}(\text{pz})_4$), 7.69 (s, 4H, BAr'_4 *para* position), 7.63 (d, 1H, $^3J_{\text{HH}} = 2.2$ Hz, $\text{C}(\text{pz})_4$), 7.38 (d, 1H, $^3J_{\text{HH}} = 1.7$ Hz, $\text{C}(\text{pz})_4$), 7.35 (d, 1H, $^3J_{\text{HH}} = 2.0$ Hz, $\text{C}(\text{pz})_4$), 6.65 (d, 1H, $^3J_{\text{HH}} = 1.5$ Hz, $\text{C}(\text{pz})_4$), 5.96 (dd, 1H, $^3J_{\text{HH}} = 2.9$ Hz, $^4J_{\text{HP}} = 1.8$ Hz, $\text{C}(\text{pz})_4$), 5.73 (t, 1H, $^3J_{\text{HH}} = 2.5$ Hz, $\text{C}(\text{pz})_4$), 5.64 (m, 1H, $\text{C}(\text{pz})_4$), 5.58 (d, 1H, $^3J_{\text{HH}} = 3.1$ Hz, $\text{C}(\text{pz})_4$), 3.76 (d, 6H, $^3J_{\text{HP}} =$

4.2 Hz, $\text{P}(\text{OCH}_2)_3\text{CCH}_2\text{CH}_3$), 1.03 (s, 3H, NCCH_3), 0.88 (s, 3H, NCCH_3), 0.033 (q, 2H, $^3J_{\text{HH}} = 7.6$ Hz, $\text{P}(\text{OCH}_2)_3\text{CCH}_2\text{CH}_3$), 0.13 (t, 3H, $^3J_{\text{HH}} = 7.7$ Hz, $\text{P}(\text{OCH}_2)_3\text{CCH}_2\text{CH}_3$). ^{13}C NMR (201 MHz, C_6D_6) δ 164.6 (four lined pattern, $^2J_{\text{CP}} = 19.6$ Hz Ru-C(pz)₄), 162.5 (q, $^1J_{\text{CB}} = 50$ Hz, BAr'_4), 146.4, 143.2, 142.5, 141.6, 140.3, 135.1, 131.5, 117.4, 108.9, 107.2, 106.7 (each a s, C(pz)₄) 135.4 (s, BAr'_4), 130.0 (q, $^1J_{\text{CF}} = 32$ Hz, BAr'_4), 126.1 (s, NCCH_3), 124.3 (s, NCCH_3), 118.1 (s, BAr'_4), 75.4 (d, $^2J_{\text{CP}} = 7$ Hz, $\text{P}(\text{OCH}_2)_3\text{CCH}_2\text{CH}_3$), 36.4 (d, $^3J_{\text{CP}} = 32$ Hz, $\text{P}(\text{OCH}_2)_3\text{CCH}_2\text{CH}_3$), 23.9 (s, $\text{P}(\text{OCH}_2)_3\text{CCH}_2\text{CH}_3$), 7.5 (s, $\text{P}(\text{OCH}_2)_3\text{CCH}_2\text{CH}_3$), 4.8 (s, NCCH_3). ^{31}P NMR (121 MHz, CD_2Cl_2) δ 133.8. ^{19}F NMR (282 MHz, CD_2Cl_2) δ -62.4.

5.5. Acknowledgements for High-Resolution Mass Spectroscopy Data

We acknowledge the following with gratitude for help with the acquisition of high-resolution mass spectra on some of the compounds and complexes described: Avinash Dalmia and Nicole Elliott, PerkinElmer, Shelton, CT; Jeffrey Dahl, Shimadzu Scientific Instruments, Columbia, MD; Anjali Alving, Bruker Daltonics, Billerica, MA; Joe Hedrick, Agilent Technologies, Wilmington, DE; and Gordon Fujimoto & Besnik Bajrami, Waters Corporation, Beverly, MA.

5.6. References

- (1) Trofimenko, S. *J. Am. Chem. Soc.* **1967**, 89, 3170.
- (2) Trofimenko, S. *J. Am. Chem. Soc.* **1966**, 88, 1842.
- (3) Trofimenko, S. *Scorpionates: The Coordination Chemistry of Polypyrazolylborate Ligands*; Imperial College Press: London, 1999.
- (4) De Bari, H.; Zimmer, M. *Inorg. Chem.* **2004**, 43, 3344.

- (5) Yoshimoto, S.; Mukai, H.; Kitano, T.; Sohrin, Y. *Anal. Chim. Acta* **2003**, *494*, 207.
- (6) Rheingold, A. L.; Liable-Sands, L. M.; Incarvito, C. L.; Trofimenko, S. *J Chem Soc Dalton* **2002**, 2297.
- (7) Goodman, M. A.; Nazarenko, A. Y.; Casavant, B. J.; Li, Z.; Brennessel, W. W.; DeMarco, M. J.; Long, G.; Goodman, M. S. *Inorg. Chem.* **2011**, *51*, 1084.
- (8) Jayaratna, N. B.; Gerus, I. I.; Mironets, R. V.; Mykhailiuk, P. K.; Yousufuddin, M.; Dias, H. V. R. *Inorg. Chem.* **2013**, *52*, 1691.
- (9) Reger, D. L.; Grattan, T. C.; Brown, K. J.; Little, C. A.; Lamba, J. J. S.; Rheingold, A. L.; Sommer, R. D. *Journal of Organometallic Chemistry* **2000**, *607*, 120.
- (10) Foley, N. A.; Lail, M.; Gunnoe, T. B.; Cundari, T. R.; Boyle, P. D.; Petersen, J. L. *Organometallics* **2007**, *26*, 5507.
- (11) Foley, N. A.; Lail, M.; Lee, J. P.; Gunnoe, T. B.; Cundari, T. R.; Petersen, J. L. *J. Am. Chem. Soc.* **2007**, *129*, 6765.
- (12) Foley, N. A.; Ke, Z. F.; Gunnoe, T. B.; Cundari, T. R.; Petersen, J. L. *Organometallics* **2008**, *27*, 3007.
- (13) Lail, M.; Arrowood, B. N.; Gunnoe, T. B. *J. Am. Chem. Soc.* **2003**, *125*, 7506.
- (14) Lail, M.; Bell, C. M.; Conner, D.; Cundari, T. R.; Gunnoe, T. B.; Petersen, J. L. *Organometallics* **2004**, *23*, 5007.
- (15) Joslin, E. E.; McMullin, C. L.; Gunnoe, T. B.; Cundari, T. R.; Sabat, M.; Myers, W. H. *Organometallics* **2012**, *31*, 6851.
- (16) Joslin, E. E.; McMullin, C. L.; Gunnoe, T. B.; Cundari, T. R.; Sabat, M.; Myers, W. H. *Inorg. Chem.* **2012**, *51*, 4791.
- (17) Foley, N. A., Thesis: Synthesis and Comparative Studies of Ru(II) Complexes for Metal-Mediated C-H Activation and Olefin Hydroarylation Catalysis, North Carolina State University, 2008.
- (18) Fujisawa, K.; Ono, T.; Ishikawa, Y.; Amir, N.; Miyashita, Y.; Okamoto, K.; Lehnert, N. *Inorg. Chem.* **2006**, *45*, 1698.
- (19) Wiley, J. S.; Oldham, W. J., Jr.; Heinekey, D. M. *Organometallics* **2000**, *19*, 1670.

- (20) Heinekey, D. M.; Oldham, W. J., Jr.; Wiley, J. S. *J. Am. Chem. Soc.* **1996**, *118*, 12842.
- (21) Mendoza-Ferri, M. G.; Hartinger, C. G.; Nazarov, A. A.; Eichinger, R. E.; Jakupec, M. A.; Severin, K.; Keppler, B. K. *Organometallics* **2009**, *28*, 6260.
- (22) Yakelis, N. A.; Bergman, R. G. *Organometallics* **2005**, *24*, 3579.
- (23) Lühder, K.; Nehls, D.; Madeja, K. *Journal Fur Praktische Chemie* **1983**, *325*, 1027.
- (24) Neves, P.; Gago, S.; Balula, S. S.; Lopes, A. D.; Valente, A. A.; Cunha-Silva, L.; Paz, F. A. A.; Pillinger, M.; Rocha, J.; Silva, C. M.; Gonçalves, I. S. *Inorg. Chem.* **2011**, *50*, 3490.
- (25) Trofimenko, S. *J. Amer. Chem. Soc.* **1970**, *92*, 5118.
- (26) Julia, S.; Del, M. J. M.; Avila, L.; Elguero, J. *Org. Prep. Proced. Int.* **1984**, *16*, 299.

6. Summary and Future Outlook

6.1. Olefin Hydroarylation with TpRu(L)(NCMe)Ph

Our group has previously demonstrated that TpRu(L)(NCMe)Ph ($\text{L} = \text{CO}$, PMe_3 , P(pyr)_3 , and $\text{P(OCH}_2)_3\text{CEt}$) complexes are capable of olefin hydroarylation with simple olefins (i.e., ethylene and propylene).¹⁻⁶ These experimental studies along with computational studies by Professor Tom Cundari's group at the University of North Texas revealed important aspects and trends to olefin hydroarylation using these complexes. In order for a catalyst to be capable of catalytic olefin hydroarylation it has to be able to perform two key steps, olefin insertion into a M-Ar bond and preference for arene C-H activation over olefin C-H activation. These two key steps require two different electronic properties. C-H activation of benzene, which was determined to be the rate limiting step of the reaction (for the TpRu(CO)NCMe , is promoted by electron rich metal centers (see Chapter 1); alternatively, olefin insertion is more facile with electron poor metal centers. An important trend that was observed when systematically altering the electron density of the metal center from an electron rich metal center ($\text{L} = \text{PMe}_3$) to an electron poor metal center ($\text{L} = \text{CO}$) is that the difference in the electron density of the metal center has a greater impact on the rate of olefin insertion compared to the rate of arene C-H activation.

The most active and longest lived catalyst to date is TpRu(CO)(NCMe)Ph with approximately 415 TO at 90 °C, 15 psi and 0.025 mol% Ru and a TOF of $6.7 \times 10^{-3} \text{ s}^{-1}$ (see Chapter 2). Previously, catalysis was run at 0.1 mol % TpRu(CO)(NCMe)Ph at 90 °C and 25 psi of ethylene which gave a significantly lower TON of 77. The increased

TON supported our hypothesis that lowering the catalyst loading would increase the TON because the route of decomposition is proposed to like to be a binuclear pathway leading to an NMR silent species. Chapter 4, discusses the decomposition and catalysis results through altering the catalyst loadings and ethylene pressure when $\text{TpRu}(\text{CO})(\text{NCMe})\text{Ph}$ is employed as the catalyst. ^1H NMR spectroscopy experiments watching the rate of decomposition of $\text{TpRu}(\text{CO})\text{Ph}(\text{NCMe})$ in $\text{THF-}d_8$ at $90\text{ }^\circ\text{C}$ yielded second order kinetics in Ru which supports a bi-nuclear decomposition pathway. Systematically changing the Ru catalyst loadings demonstrated the presence of competing decomposition pathways. At higher catalyst loadings and lower ethylene pressures the dominate decomposition product is the hypothesized multinuclear Ru species; however, at lower concentrations of Ru, decomposition was observed through the allyl-species $\text{TpRu}(\text{CO})(\eta^3\text{-C}_4\text{H}_7)$. Therefore, it is hypothesized that by attaching $\text{TpRu}(\text{CO})(\text{NCMe})\text{Ph}$ to a solid support (Figure 6.1) the binuclear decomposition pathway could be shutdown and the catalyst longevity and TON of allylbenzenes could increase, similar to what being seen by our group's studies comparing the molecular system to the heterogeneous $(^i\text{bpy})\text{Pt}(\text{Ph})(\text{THF})[\text{BAR}'_4]^7$ system.

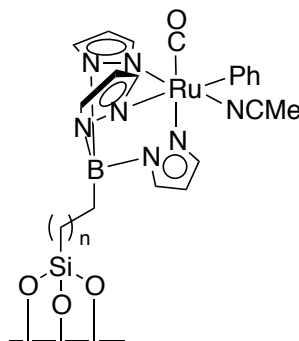


Figure 6.1. MSM supported $\text{TpRu}(\text{CO})\text{Ph}(\text{NCMe})$

In order to shut down the decomposition pathway caused by olefin C–H activation competing with olefin insertion we wanted to investigate a less electron rich metal center than when $L = \text{PMe}_3$ or $\text{P}(\text{OCH}_2)_3\text{CEt}$. We synthesized a phosphite where a methylene group was removed from one of the phosphite tethered arms to yield $\text{P}(\overline{\text{OCH}_2})_2(\overline{\text{OCCH}_3})$. Chapter 2, explores the electronics and structural properties of $\text{P}(\overline{\text{OCH}_2})_2(\overline{\text{OCCH}_3})$ compared to carbon monoxide and a variety of phosphites and phosphines. The Ru(II) complexes studied were of the motif $\text{TpRu}(\text{L})\text{PPh}_3\text{Cl}$, $(\eta^6\text{-C}_6\text{H}_6)\text{Ru}(\text{L})\text{Cl}_2$, $(\eta^6\text{-}p\text{-cymene})\text{Ru}(\text{L})\text{Cl}_2$ where $L =$ neutral two-electron donor). It was hypothesized that removal of a methylene group from one of the phosphite tethered arms would make $\text{P}(\overline{\text{OCH}_2})_2(\overline{\text{OCCH}_3})$ a poor electron donor. Chapter 2 demonstrates that removal of the methylene linker does decrease the electron density of the metal center determined by cyclic voltammetry and crystal data. However, even though $\text{P}(\overline{\text{OCH}_2})_2(\overline{\text{OCCH}_3})$ decreases the electron density at the metal center the metal center is still more electron rich than when $L = \text{CO}$.⁸

Due to decreased electron density at the metal center when $\text{P}(\overline{\text{OCH}_2})_2(\overline{\text{OCCH}_3})$ is employed as the neutral two electron donor, we sought to study this effect on olefin hydroarylation, which is examined in Chapter 3. $\text{TpRu}[\text{P}(\overline{\text{OCH}_2})_2(\overline{\text{OCCH}_3})](\text{NCMe})\text{Ph}$ was synthesized and tested for olefin hydroarylation.⁹ $\text{TpRu}[\text{P}(\overline{\text{OCH}_2})_2(\overline{\text{OCCH}_3})](\text{NCMe})\text{Ph}$ is capable of breaking aromatic C–H bonds but is slower by a factor of two compared to $L = \text{PMe}_3$, which is to be expected since C–H activation is promoted by

more electron rich metal centers. $\text{TpRu}[\text{P}(\text{OCH}_2)_2(\text{OCCH}_3)](\text{NCMe})\text{Ph}$ produces approximately 90 TO of ethylbenzene at 90 °C and 15 psi of ethylene before deactivation. However, the metal center is still too electron rich (similar to $\text{L} = \text{PMe}_3$ and $\text{P}(\text{OCH}_2)_3\text{CEt}$) and olefin C–H activation completes with olefin insertion leading to a $\text{TpRu}[\text{P}(\text{OCH}_2)_2(\text{OCCH}_3)](\eta^3\text{-C}_4\text{H}_7)$ complex. Therefore, it is proposed that future work needs to examine a Ru(II) metal center that would have a similar electronic profile as $\text{L} = \text{CO}$. In order to achieve this one should look at neutral 6-electron donors rather than the anionic Tp ligand. This would enable us to vary the catalyst motif without drastic changes to the sterics. Although not as well studied as the tris(pyrazolyl)borates, tris(pyrazolyl)alkanes (Figure 6.2) have been synthesized and shown that the metal center is less electron rich.¹⁰

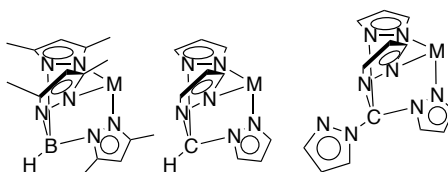


Figure 6.2. Examples of tris(pyrazolyl)alkanes.

6.2. Olefin Hydroarylation with Ru(II) Complex contain neutral 6-electron donor ligands.

Chapter 5 discusses Ru(II) complexes with a variety of neutral 6-electron donors such (η^6 -*p*-cymene), $\text{C}(\text{pz})_4$, and $\text{HC}(\text{pz}')_3$. It was demonstrated that removing the anionic Tp ligand with a neutral ligand does reduce the electron density at the metal center. $\{[\text{HC}(\text{pz}')_3]\text{Ru}[\text{P}(\text{OCH}_2)_3\text{CEt}]\text{Ph}(\text{NCMe})\}[\text{BAr}'_4]$ has a reversible Ru(III/II) potential of 0.82 V where the analogous Tp complexes has a Ru(III/II) potential of 0.69 V.

$\{[\text{HC}(\text{pz}')_3]\text{Ru}[\text{P}(\text{OCH}_2)_3\text{CEt}]\text{Ph}(\text{NCMe})\}[\text{BAR}']$ has an identical Ru(III/II) as $\text{TpRu}[\text{P}(\text{pyr})_3]\text{Ph}(\text{NCMe})$ which was incapable of olefin hydroarylation due to the $\text{P}(\text{pyr})_3$ ligand being too sterically bulky and inhibiting olefin coordination. Therefore, the $\{[\text{HC}(\text{pz}')_3]\text{Ru}[\text{P}(\text{OCH}_2)_3\text{CEt}]\text{Ph}(\text{NCMe})\}[\text{BAR}'_4]$ complex gives us an opportunity to test a Ru(II) catalyst that is of similar electron donor ability as $\text{TpRu}[\text{P}(\text{pyr})_3]\text{Ph}(\text{NCMe})$ but with less steric bulk from the phosphine ligand. $\{[\text{HC}(\text{pz}')_3]\text{Ru}[\text{P}(\text{OCH}_2)_3\text{CEt}]\text{Ph}(\text{NCMe})\}[\text{BAR}'_4]$ was incapable of olefin hydroarylation at 25 psi and 90 °C. This is potentially due to the increase steric bulk caused by the methyl group on the 3-position of the pyrazolyl ring which could inhibit olefin coordination. However, steric bulk of the $\text{HC}(\text{pz}')_3$ ligand still remains problematic, a potential way to eliminate this issue is to replace the 3-position of the pyrazolyl with a less bulky ligand such as a halide. However, the synthesis of a mono, di, or tri-substituted fluorinated or chlorinated pyrazole has only been studied via calculations.⁹ This is potentially due to the experimental hazard of using Cl_2 or F_2 for the synthesis of these complexes. The tris-brominated pyrazole has been synthesized, along with the TpBr_3 ¹⁰ and on going work to synthesis the $\text{HC}(\text{pz}^{\text{Br}_3})_3$ is currently underway. Once the ligand is synthesized and coordinated to the metal center catalytic studies with olefin hydroarylation will be explored.

6.3. Onward to Rhodium

Due to our group's extensive studies with Ru(II) and Pt(II) complexes it is hypothesized that moving to Rh(I) complexes (Figure 6.4) could potential enhance selectivity for olefin hydroarylation.^{1,3-7,11-13} Computation studies by the Cundari group

have predicted that $[(bpy)Rh(Ph)]^+$ will have a lower activated barrier by a $\Delta\Delta G^\ddagger = 7.3$ kcal/mol (Figure 6.3) compared to the analogous Pt system.

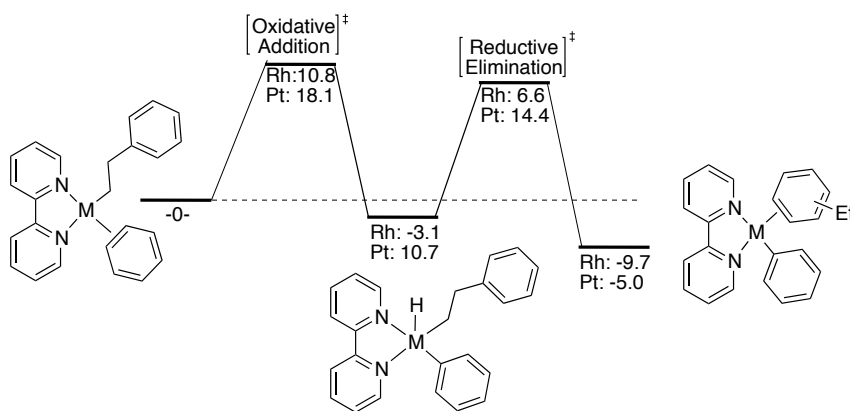


Figure 6.3. Calculated ΔG^\ddagger (kcal/mol) for benzene C-H activation via a two-step reaction for $M = Rh$ or Pt .

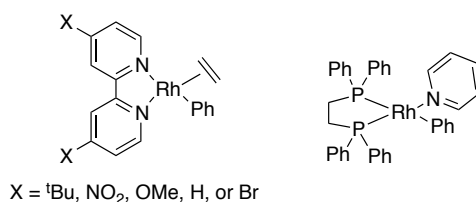


Figure 6.4. Potential Rh(I) catalyst for olefin hydroarylation.

One advantage to using the bpy ligand framework is the ability to do similar studies with Rh as our group has done with Pt.¹³ By varying the 4,4' positions of the bpy the electronics of the metal center can be altered without changing the sterics surrounding the metal center. Hartwig *et al.* has published that a (DPPE)Rh(pyridine)(p-tolyl) [DPPE = 1,2-bis(diphenylphosphino)ethane] is capable of the insertion reaction with electron-poor imines and aldehydes.¹⁴ This is an appealing starting complex since if the pyridine is significantly labile in the presence of ethylene, ethylene could displace the pyridine and

lead to our desired Rh(I)(ethylene)(phenyl) complex. Additionally, it is thought that moving from Ru to Rh the metal center would be less π -basic; therefore, the olefin would be less tightly bound and the olefin would insert more readily into the M–Ph bond which would shut down the decomposition pathway seen with the TpRu(II) complexes where olefin C–H activation is competitive with olefin insertion.

6.4. References

- (1) Lail, M.; Arrowood, B. N.; Gunnoe, T. B. *J. Am. Chem. Soc.* **2003**, *125*, 7506.
- (2) Lail, M.; Bell, C. M.; Conner, D.; Cundari, T. R.; Gunnoe, T. B.; Petersen, J. L. *Organometallics* **2004**, *23*, 5007.
- (3) Foley, N. A.; Lail, M.; Gunnoe, T. B.; Cundari, T. R.; Boyle, P. D.; Petersen, J. L. *Organometallics* **2007**, *26*, 5507.
- (4) Foley, N. A.; Lail, M.; Lee, J. P.; Gunnoe, T. B.; Cundari, T. R.; Petersen, J. L. *J. Am. Chem. Soc.* **2007**, *129*, 6765.
- (5) Foley, N. A.; Ke, Z. F.; Gunnoe, T. B.; Cundari, T. R.; Petersen, J. L. *Organometallics* **2008**, *27*, 3007.
- (6) Foley, N. A.; Lee, J. P.; Ke, Z. F.; Gunnoe, T. B.; Cundari, T. R. *Acc. Chem. Res.* **2009**, *42*, 585.
- (7) McKeown, B. A.; Foley, N. A.; Lee, J. P.; Gunnoe, T. B. *Organometallics* **2008**, *27*, 4031.
- (8) Joslin, E. E.; McMullin, C. L.; Gunnoe, T. B.; Cundari, T. R.; Sabat, M.; Myers, W. H. *Inorg. Chem.* **2012**, *51*, 4791.
- (9) Aullon, G.; Gorun, S. M.; Alvarez, S. *Inorg. Chem.* **2006**, *45*, 3594.
- (10) Rheingold, A. L.; Liabe-Sands, L. M.; Incarvito, C. L.; Trofimenko, S. *J. Chem Soc Dalton* **2002**, 2297.
- (11) Andreatta, J. R.; McKeown, B. A.; Gunnoe, T. B. *J. Organomet. Chem.* **2011**, *696*, 305.

- (12) McKeown, B. A.; Gonzalez, H. E.; Friedfeld, M. R.; Gunnoe, T. B.; Cundari, T. R.; Sabat, M. *J. Am. Chem. Soc.* **2011**, *133*, 19131.
- (13) McKeown, B. A.; Gonzalez, H. E.; Friedfeld, M. R.; Brosnahan, A. M.; Gunnoe, T. B.; Cundari, T. R.; Sabat, M. *Organometallics* **2013**, *32*, 2857.
- (14) Krug, C.; Hartwig, J. F. *Organometallics* **2004**, *23*, 4594.